**UNIVERSIDAD COMPLUTENSE DE MADRID**
FACULTAD DE CIENCIAS QUIMICAS


# TESIS DOCTORAL

## Bioquímica de sistemas de interacciones macromoleculares implicadas en la regulación de la estabilidad del anillo de división en bacterias

## Systems biochemistry of macromolecular interactions involved in the regulation of the division ring stability in bacteria

MEMORIA PARA OPTAR AL GRADO DE DOCTOR

PRESENTADA POR

**Miguel Ángel Robles Ramos**

Directores

**Germán Alejandro Rivas Caballero**
**Silvia Zorrilla López**

Madrid

# UNIVERSIDAD COMPLUTENSE DE MADRID

FACULTAD DE CIENCIAS QUÍMICAS



# TESIS DOCTORAL

Bioquímica de Sistemas de Interacciones Macromoleculares Implicadas en la Regulación de la Estabilidad del Anillo de División en Bacterias

Systems Biochemistry of Macromolecular Interactions Involved in the Regulation of the Division Ring Stability in Bacteria

MEMORIA PARA OPTAR AL GRADO DE DOCTOR

PRESENTADA POR


Miguel Ángel Robles Ramos


DIRECTORES


Prof. Germán Alejandro Rivas Caballero
Dra. Silvia Zorrilla López


UNIVERSIDAD
COMPLUTENSE
MADRID

**FACULTAD DE CIENCIAS QUÍMICAS**
DOCTORADO EN BIOQUÍMICA, BIOLOGÍA MOLECULAR Y BIOMEDICINA

# TESIS DOCTORAL

## Systems Biochemistry of Macromolecular Interactions Involved in the Regulation of the Division Ring Stability in Bacteria

Bioquímica de Sistemas de Interacciones Macromoleculares Implicadas en la Regulación de la Estabilidad del Anillo de División en Bacterias

Memoria para optar al grado de doctor presentada por:

**Miguel Ángel Robles Ramos**

Bajo la dirección de:
Prof. Germán Alejandro Rivas Caballero
Dra. Silvia Zorrilla López
Centro de Investigaciones Biológicas Margarita Salas - CSIC

Madrid, 2022

*A mi familia*

# *Agradecimientos*

Estos últimos años de mi vida dedicados a la realización del doctorado han sido sin duda una época de gran crecimiento profesional y personal que, estoy seguro, marcan un antes y un después en mi vida. Este viaje no lo he recorrido solo sino con el apoyo y cariño de muchas personas a las que me gustaría dedicarles unas líneas.

En primer lugar, me gustaría expresar mi más profunda gratitud a mis directores de tesis, Germán y Silvia, por darme la oportunidad de realizar el doctorado bajo su supervisión. De la misma manera, quiero agradecer a Begoña haberse implicado en el desarrollo de mi proyecto de tesis al mismo nivel, una participación esencial sin la que esta tesis doctoral no hubiera podido ser tan completa. Para mí ha sido una gran suerte poder haberme iniciado en la investigación de la mano de científicos tan excelentes de los que he aprendido tantísimo, siempre preocupados de que mi formación fuera lo más completa posible pero también de mi bienestar personal durante estos años, aconsejándome y motivándome de todas las formas posibles. También me gustaría agradecer a mi tutor, Javier Turnay, la recomendación de este grupo de investigación para la realización de la tesis y su ayuda, con un trato siempre tan cercano, con las cuestiones que implicaban a la universidad.

Gracias a Carlos, por su ayuda y consejos con los experimentos, especialmente los de ultracentrifugación analítica, y a Mercedes, por darme la oportunidad de participar en actividades de divulgación científica, una experiencia muy enriquecedora. Gracias a ambos por vuestra cercanía y amabilidad.

Sin duda, esta aventura no hubiera sido tan gratificante sin los momentos que he compartido con mis compañeros de laboratorio. Gracias a Ana, Noelia y Marina que me vieron dar mis primeros pasos y me enseñaron todo lo que necesitaba saber del GRlab. A Gianfranco, Inés, Lorenzo y Pedro por estar siempre dispuestos a echarme una mano con las pequeñas cosas (y no tan pequeñas) del día a día en el labo y por encontrar un ratito para celebrar los éxitos con chocolate o ahogar las penas también con chocolate. Muy especialmente a Marta, mi compañera y amiga, escribiendo estos agradecimientos me doy cuenta, aún más si cabe, de lo importante que ha sido tenerte en el laboratorio todo este tiempo. Gracias por ayudarme desde el principio de la tesis hasta el final, enseñándome todo lo que sabías y apoyándome siempre que hiciera falta. En general, a todos vosotros

muchas gracias por haber llenado todos los días de momentos alegres que han sido mi principal gasolina.

Debo agradecer también a la prof. Petra Schwille el acogerme durante varios meses en un laboratorio tan sobresaliente como el suyo, permitiéndome así avanzar en mi proyecto de tesis y vivir la experiencia de investigar en el extranjero. A Adrián y María, mi refugio español, gracias por aguantarme primero en Madrid y luego en Múnich y por ayudarme a conocer y adaptarme rápidamente al laboratorio. Sin vuestra presencia no hubiera podido disfrutar ni de lejos tanto de la estancia. También a Leon por su ayuda y consejos sobre el proyecto de estancia y al resto del grupo de investigación, gente extremadamente amable que contribuyó a mejorar esta experiencia.

Gracias a todo el personal del CIB que me ha prestado su ayuda y especialmente a los servicios de interacciones moleculares y microscopía confocal de este centro por haberme aconsejado y proporcinado las herramientas necesarias para la realización de muchos de los experimentos incluidos en esta tesis. También agradezco a la Agencia Estatal de Investigación y al Fondo Social Europeo haber financiado la realización del doctorado a través de la beca BES-2017-082003.

Gracias también a Luque, Óscar, Ruth, Mariano y a todo el mundo que ha hecho algún hueco por las mañanas para tomarnos un café todos juntos, un momento en la mejor compañía para renovar las energías y afrontar el resto del día. También a Leti, Aida y Tranque, los mejores compañeros con los que me pude encontrar en los cursos de verano.

Por supuesto, no solo ha sido importante el apoyo de las personas con las que me he encontrado en el laboratorio, sino también el de todas aquellas que, desde fuera del CIB, con su amistad, me han dado las fuerzas necesarias para continuar. A Jorge por haber sido una de las personas más generosas en mi vida, siempre disponible cuando lo necesitaba y a Laura por haberse comportado como una amiga desde el primer día que la conocí. A Patri, Jose, Clara, Miguel, Ana, Adrián y María, mis compañeros de la facultad de Biología, no solo empecé este viaje con vosotros durante la carrera, sino que os habéis mantenido a mi lado durante todo este tiempo, muchas gracias. A Kristin por sus consejos y por las conversaciones tan interesantes que tenemos cada vez que quedamos y a Nico y Alex por ser dos amigos estupendos con los que pasar un rato divertido cada vez que quedamos.

Por último, he de agradecer a mi familia el haber estado toda mi vida respaldándome. Desde muy pequeño uno de mis sueños fue ser científico y

siempre estuvieron ahí creyendo en mí y avanzando conmigo en cada paso para conseguirlo. A mis dos tíos, Toñi y Chema, por hacerme la vida más fácil siempre que podéis, no importa lo que os cueste, y por el inmenso cariño que he recibido siempre de vosotros. A mi padre, por haber hecho todo lo posible desde que nací para darme la mayor cantidad de oportunidades para que pudiera llegar a donde yo quisiera. A mi hermano por ser el amigo que me ha acompañado toda la vida. A los que se han ido pero que claramente han marcado mi vida llevándome hasta el punto en el que me encuentro. A mi abuela Antonia, una de las personas más fuertes y admirables que he conocido, sin duda uno de mis ejemplos a seguir. Finalmente, quiero agradecer muy especialmente a mi madre su amor, paciencia y confianza, un regalo que me hizo todos los días de su vida sin falta, sin duda alguna si he llegado hasta aquí ha sido por ti, gracias.

# TABLE OF CONTENTS

# Summary / Resumen

# SUMMARY

**Systems biochemistry of macromolecular interactions involved in the regulation of the division ring stability in bacteria**

*Escherichia coli* cell division is mediated by the divisome, a contractile ring consisting of a multiprotein complex that accurately assembles at midcell (corresponding to the long axis midpoint of this bacillus) toward the end of the cell cycle. The first step in the formation of this division machinery is the assembly of the so-called Z-ring, a dynamic macromolecular structure involving the polymerization of the conserved protein FtsZ that serves as a scaffold for the recruitment of the rest of division proteins. Correct spatiotemporal assembly of the Z-ring is critical for the generation of viable daughter cells, since deviations in its positioning might result in catastrophic outcomes such as chromosome bisection or generation of anucleate cells. For this reason, *E. coli* relies on dedicated positioning mechanisms to ensure proper formation of the Z-ring at midcell, being the canonical ones the Min system and nucleoid occlusion, which act by blocking the assembly of the Z-ring at undesired locations. The Min system establishes an oscillation pattern that prevents Z-ring formation at the cell poles while allowing its assembly in the cell center. For its part, nucleoid occlusion inhibits Z-ring assembly in the vicinity of the chromosome through direct interaction of the SlmA protein, bound to specific DNA sequences (SBS) in the chromosome, with FtsZ. Besides, the concerted action of these two negative regulatory mechanisms is complemented by the Ter linkage, a protein network comprising ZapA, ZapB and the DNA-binding protein MatP that reinforces the formation of the Z-ring at midcell.

This regulated assembly of the Z-ring takes place in a highly crowded environment, with a large fraction of the cell volume occupied by macromolecules. It is well known that crowding affects the reactivity of biochemical interactions, primarily through the excluded-volume effect, promoting the compaction and association of macromolecules. Moreover, it can lead to the formation of microenvironments with physiological relevance through liquid-liquid phase separation (LLPS). In fact, in the last decade, it has been reported that different macromolecular systems can assemble into biomolecular condensates, dynamic structures formed by LLPS where proteins and nucleic acids accumulate. Biomolecular condensates are emerging as crucial organizers of the intracellular

space, which have important implications especially in prokaryotes since they lack membranous organelles.

Another important actor during cell division is the membrane envelope, which plays fundamental roles in several biochemical processes involved in cytokinesis. Indeed, Z-ring tethering to the membrane at midcell is essential in divisome assembly. Hence, the study of division elements reconstituted in minimal membrane systems can provide valuable information about some aspects of the processes leading to cell division.

The present doctoral thesis aims to contribute to the understanding of the mechanisms involved in the essential process of bacterial division, and particularly in the positioning of the division ring through the coordinated modulation of the assembly, location and distribution of the central division protein FtsZ. Specifically, this thesis intends to analyze the influence of crowding and the presence of membranes and microenvironments on FtsZ and the DNA-binding proteins SlmA and MatP, involved in the regulation of Z-ring assembly. For this purpose, protein-protein, protein-DNA and protein-lipid interactions have been analyzed following an approach involving a combination of biochemical and biophysical methods as well as reconstitution in cell-like environments.

The first two chapters of this thesis describe the formation of phase-separated condensates by FtsZ in the presence (**chapter 1**) or absence (**chapter 2**) of the nucleoid occlusion effector protein, SlmA, under crowding conditions. Reconstitution of FtsZ and SlmA bound to its specific SBS sequence in the absence of GTP and in crowded solutions (**chapter 1**) resulted in their assembly into micrometric structures compatible with liquid condensates, as visualized by confocal microscopy and confirmed by turbidity assays. In addition, the formation of these structures showed to be favored at low ionic strength and with increasing concentrations of protein and crowder agent. These assemblies exhibited dynamism and reversibility, hallmarks of liquid condensates, as evidenced by capture experiments showing their ability to exchange protein with the outer phase and by the fact that FtsZ retains its GTP-dependent assembly/disassembly properties. The effect of the presence of different microenvironments, similar to those found in the cell, was explored using LLPS systems, consisting of two unrelated crowding agents that phase separate at high concentrations generating compartments. Condensates asymmetrically partitioned among these compartments and, when encapsulated inside microfluidic-based microdroplets, they were principally located at the lipid boundary.

Interestingly, examination of conditions, within the physiological ranges described in *E. coli*, revealed that FtsZ can reversibly undergo biomolecular condensation on its own under conditions known to promote its oligomerization tendency (**chapter 2**). Condensates formed by FtsZ in the absence of SlmA were still dynamic and evolved toward fibers after GTP addition. Besides, encapsulation of FtsZ inside cytomimetic containers led to incipient formation of condensates in conditions under which no condensates were detected in bulk, suggesting that confinement and/or the presence of a lipid membrane influence their formation. Finally, experiments with an FtsZ mutant lacking the C-terminal unstructured domain demonstrated that this region of FtsZ was not strictly required for condensation albeit it likely enhances the overall process.

The last two chapters encompass the identification, analysis and discussion of the lipid interaction of the DNA-binding proteins SlmA (**chapter 3**) and MatP (**chapter 4**). These studies were performed using different minimal membrane systems following an orthogonal approach that included biochemical, biophysical and imaging methods. SlmA was found to bind either to the lipid mixture matching the composition in the *E. coli* inner membrane (EcL), which contains negatively charged components, or to phosphatidylcholine (PC), a neutral phospholipid (**chapter 3**). For the two types of compositions, the affinity of the interaction was found to be greatly enhanced at low ionic strength but weakly affected above a certain threshold, suggesting that both electrostatic and hydrophobic forces play a role in the membrane binding activity of SlmA. Evaluation of this interaction in the presence of the specific SBS sequences recognized by the protein showed that they compete with the lipids for binding to SlmA. Intriguingly, the presence of FtsZ radically changed this behavior, promoting the recruitment of SBS sequences to the membrane by SlmA.

Protein-lipid interaction was also observed in experiments involving reconstitution of MatP on biomimetic membranes (**chapter 4**). Interaction of MatP with the EcL mixture was observed at submicromolar concentration, with relative insensitivity to ionic strength. Besides, binding of MatP to PC was also detected, pointing towards hydrophobic interactions as the most likely driving force of lipid recognition by this protein. Finally, inclusion of the DNA sequence recognized by MatP (*matS*) in binding experiments with lipid membranes demonstrated that ternary complexes are not formed but, instead, *matS* competes for binding to MatP. Notably, these results are in good agreement with parallel experiments conducted *in vivo* by our collaborators showing that, during cell division, just before the daughter cells split, MatP seems to localize close to the inner membrane.

Altogether, this thesis reports the possible existence of new mechanisms, observed in cell-like environments, for the regulation of the central division protein FtsZ by two proteins involved in the positioning of the Z-ring. Both the formation of biomolecular condensates by FtsZ, largely favored by the nucleoprotein complexes of SlmA, and the interaction of the DNA-binding proteins SlmA and MatP with lipids, tuned by its binding partners, may entail new ways to regulate the localization and activity of these proteins in the intracellular space.

# RESUMEN

**Bioquímica de sistemas de interacciones macromoleculares implicadas en la regulación de la estabilidad del anillo de división en bacterias**

En *Escherichia coli* la división se encuentra mediada por el divisoma, un anillo contráctil consistente en un complejo multiproteico posicionado con gran precisión en el centro de la célula (correspondiente al punto medio del eje largo de este bacilo) hacia el final del ciclo celular. El primer paso en la formación de esta maquinaria de división es el ensamblaje del denominado anillo Z, una estructura macromolecular dinámica que implica la polimerización de la proteína conservada FtsZ y que actúa como plataforma sobre la que se incorporan el resto de proteínas de división. El correcto posicionamiento espacial y temporal del anillo Z es crítico para la generación de células hijas viables, dado que desviaciones en la adecuada localización del mismo pueden conllevar consecuencias catastróficas para la bacteria como la bisección del cromosoma o la generación de células anucleadas. Por este motivo, *E. coli* cuenta con mecanismos de posicionamiento que aseguran la formación del anillo en el centro celular, de entre los cuales el sistema Min y el sistema de oclusión por nucleoide son los más estudiados. El sistema Min establece un patrón de oscilaciones que impide la formación del anillo en los polos celulares a la vez que permite su ensamblaje en el centro de la célula. Por su parte, el sistema de oclusión por nucleoide inhibe la formación del anillo Z en las proximidades del cromosoma bacteriano a través de la interacción directa de la proteína SlmA, unida a secuencias específicas de ADN (SBS) en el cromosoma, con FtsZ. Además, la acción conjunta de estos dos mecanismos reguladores negativos está complementada por el anclaje Ter, consistente en una red multiproteica en la que participan las proteínas ZapA, ZapB y la proteína de unión a ADN MatP que refuerza la formación del anillo Z en posiciones centrales.

Este ensamblaje regulado del anillo Z tiene lugar en un entorno altamente aglomerado, resultante de la ocupación de una gran fracción del volumen celular por macromoléculas. Es bien conocido que la aglomeración macromolecular afecta a la reactividad de las interacciones bioquímicas principalmente debido al efecto de exclusión de volumen, favoreciendo la compactación y asociación de macromoléculas. Además, la aglomeración macromolecular puede llevar a la formación de microambientes fisiológicamente relevantes a través de un proceso de separación de fases líquido-líquido. De hecho, en la última década se han

descrito diferentes sistemas bioquímicos capaces de formar condensados biomoleculares, consistentes en estructuras dinámicas formadas por separación de fase líquido-líquido donde se acumulan proteínas y ácidos nucleicos. Actualmente los condensados biomoleculares están emergiendo como elementos cruciales en la organización del espacio intracelular, lo que tiene una especial relevancia en procariotas ya que carecen de orgánulos membranosos.

Otro actor fundamental en la división es la membrana citoplasmática, jugando un papel esencial en diversos procesos bioquímicos involucrados en la citocinesis. De hecho, el anclaje del anillo Z a la membrana es un paso imprescindible en el ensamblaje del divisoma. Es por ello que el estudio de los elementos de división reconstituidos en sistemas mínimos de membrana puede proporcionar información muy valiosa sobre algunos aspectos de los procesos implicados en la división.

El objetivo de la presente tesis doctoral es contribuir al conocimiento de los mecanismos involucrados en la división bacteriana y, particularmente, en el posicionamiento del anillo de división a través de la regulación coordinada del ensamblaje, localización y distribución de la proteína central de división FtsZ. Específicamente, el propósito de esta tesis es analizar la influencia de la aglomeración macromolecular y de la presencia de membranas y microambientes sobre FtsZ, así como sobre SlmA y MatP, las proteínas de unión a ADN implicadas en la regulación del ensamblaje del anillo Z. Para ello, se han analizado interacciones proteína-proteína, proteína-ADN y proteína-lípido siguiendo un enfoque que incluye el uso de métodos bioquímicos y biofísicos, así como de reconstitución en ambientes citomiméticos.

En los dos primeros capítulos de esta tesis se describe el ensamblaje mediante separación de fases de condensados formados por FtsZ en presencia (**capítulo 1**) o ausencia (**capítulo 2**) de la proteína efectora del sistema de oclusión por nucleoide, SlmA, bajo condiciones de aglomeración. La reconstitución de FtsZ (en ausencia de GTP) y SlmA, unida a su secuencia específica SBS, resultó en la formación de estructuras micrométricas compatibles con condensados líquidos (**capítulo 1**) que fueron visualizados mediante microscopía confocal. Este hecho fue confirmado a través de ensayos de turbidez. Además, se observó que la formación de estas estructuras se encontraba favorecida a baja fuerza iónica y a concentración creciente de agente aglomerante y de proteína. Se demostró que estos ensamblados eran dinámicos y reversibles, cualidades distintivas de los condensados biomoleculares, dada su capacidad para intercambiar proteína con la

fase externa (comprobada mediante ensayos de captura) y la conservación de las propiedades de polimerización/despolimerización dependiente de GTP de FtsZ. El impacto de la presencia de diferentes microambientes, imitando a los que se encuentran en el interior celular, se exploró mediante el uso de sistemas de separación de fase líquido-líquido formados por dos agentes aglomerantes no relacionados que se separan en dos fases a altas concentraciones, generando compartimentos. Los condensados reconstituidos en estos medios multifásicos se distribuían asimétricamente entre estos compartimentos localizándose principalmente cerca de la superficie lipídica cuando fueron encapsulados en contenedores citomiméticos.

Una exploración más exhaustiva abarcando un mayor número de condiciones, dentro del rango fisiológico descrito para *E. coli*, reveló que FtsZ puede formar reversiblemente condensados biomoleculares por sí misma en condiciones que promueven su oligomerización (**capítulo 2**). Los condensados formados por FtsZ en ausencia de SlmA resultaron ser dinámicos y capaces de evolucionar hacia fibras tras la adición de GTP. Además, se observó que la encapsulación de FtsZ en contenedores citomiméticos daba lugar a la formación incipiente de condensados en condiciones bajo las que no se detectaron en sistemas abiertos, sugiriendo una posible influencia del confinamiento o de la presencia de la membrana lipídica en su formación. Finalmente, ensayos con un mutante de FtsZ que carece del dominio no estructurado C-terminal demostraron que esta región de la proteína no es estrictamente necesaria para la formación de condensados, aunque probablemente participa potenciando el proceso global.

Los dos últimos capítulos de esta tesis comprenden la identificación, análisis y discusión de la interacción de las proteínas de unión a ADN SlmA (**capítulo 3**) y MatP (**capítulo 4**) con lípidos. Estos estudios se realizaron usando diferentes sistemas mínimos de membrana, siguiendo un enfoque ortogonal que incluía métodos bioquímicos, biofísicos y de imagen. Se observó que SlmA es capaz de unirse tanto a la mezcla ternaria de lípidos de *E. coli*, la cual contiene componentes con carga negativa, como a fosfatidilcolina, un fosfolípido neutro (**capítulo 3**). En ambos casos, la afinidad aumentaba significativamente a baja fuerza iónica, pero apenas variaba por encima de un cierto límite, sugiriendo que tanto fuerzas electrostáticas como hidrofóbicas juegan un papel en la interacción. Análisis en presencia de las secuencias específicas SBS reconocidas por la proteína mostraron que éstas compiten con los lípidos por la unión a SlmA. Finalmente, la inclusión de FtsZ originó un cambio radical en este comportamiento, promoviendo el reclutamiento de secuencias SBS a la membrana mediado por SlmA.

La reconstitución de MatP en membranas biomiméticas también derivó en el hallazgo de que esta proteína es capaz de unirse a lípidos (**capítulo 4**). La interacción de MatP con la mezcla de lípidos de *E. coli* se detectó a concentraciones submicromolares de proteína, siendo la interacción relativamente insensible a la fuerza iónica. Además, también se observó unión de MatP a fosfatidilcolina, indicando que probablemente la interacción entre MatP y lípidos se encuentra mediada por fuerzas hidrofóbicas. Finalmente, la inclusión de las secuencias de ADN reconocidas por MatP (*matS*) en los experimentos de unión a membranas lipídicas demostró que no se forman complejos ternarios, sino que *matS* compite por la unión a MatP. Estos resultados, además, son consistentes con experimentos realizados en paralelo por nuestros colaboradores los cuales mostraron que, durante la división, justo antes de que las dos células hijas se separen, MatP parece localizarse próxima a la membrana interna.

En conjunto, esta tesis describe la posible existencia de nuevos mecanismos, observados en entornos citomiméticos, para la regulación de la proteína central de división FtsZ por dos proteínas implicadas en el posicionamiento del anillo Z. Tanto la formación de condensados biomoleculares por FtsZ, altamente favorecida por los complejos nucleoproteicos formados por SlmA, como la interacción de las proteínas de unión a ADN SlmA y MatP con lípidos, modulada por sus ligandos específicos, podrían implicar nuevas vías para la regulación de la localización y actividad de FtsZ dentro del espacio intracelular.

# Abbreviations

# ABBREVIATIONS

| | |
|---|---|
| **A. U.** | Arbitrary Units |
| ***B. subtilis*** | *Bacillus subtilis* |
| **bp** | Base pairs |
| **CCTP** | C-terminal peptide of FtsZ |
| **$c_{sat}$** | Saturation concentration value |
| **Dextran 500** | Dextran with an average molecular weight of 500 kDa |
| ***dif* site** | Deletion-induced filamentation (recombination site in terminus) |
| **DNA** | Deoxyribonucleic Acid |
| **DMPC** | 1,2-dimyristoyl-sn-glycero-3-phosphocholine |
| **EcL** | *Escherichia coli* ternary lipid mixture |
| **EDTA** | Ethylenediaminetetraacetic Acid |
| ***E. coli*** | *Escherichia coli* |
| **Ficoll 70** | Poly(sucrose-co-epichlorhydrin) with average molecular weight of 70 kDa |
| **FRAP** | Fluorescence Recovery after Photobleaching |
| **FtsZ** | Filamenting temperature sensitive mutant Z |
| **FtsZ$\Delta_{Cter}$** | FtsZ mutant lacking residues 315-383 |
| **FtsZ-GDP** | FtsZ bound to GDP nucleotide |
| **FtsZ-GTP** | FtsZ bound to GTP nucleotide |
| **GDP** | Guanosine 5'di-phosphate |
| **GTP** | Guanosine 5'tri-phosphate |
| **GMPCPP** | Guanosine-5'-[(α,β)-methyleno]triphosphate |
| **GUV** | Giant Unilamellar Vesicle |
| **HTH** | Helix-Turn-Helix motif |
| **IDR** | Intrinsically Disordered Region |
| **IPTG** | Isopropyl-β-D-1-thiogalactopyranoside |
| **LB** | Luria-Bertani media |

| | |
|---|---|
| **LLPS** | Liquid-liquid Phase Separation |
| **MatP** | Macrodomain Ter protein |
| ***matS*** | DNA sequence recognized by MatP |
| **MD** | Chromosomal Macrodomain |
| **OD** | Optical Density |
| **PC** | L-α-phosphatidylcholine |
| **PDMS** | Polydimethylsiloxane polymer |
| **PEG 8** | Polyethylene glycol with average molecular weight of 8 kDa |
| **RHH** | Ribbon-Helix-Helix motif |
| **RNA** | Ribonucleic Acid |
| **rpm** | Revolutions Per Minute |
| **SBS** | SlmA Binding Sequence |
| **SD** | Standard Deviation |
| **SDS-PAGE** | Sodium Dodecyl Sulfate Polyacrylamide Gel Electrophoresis |
| **SEC-MALS** | Size Exclusion Chromatography coupled to Multi-Angle Light Scattering |
| **SLB** | Supported Lipid Bilayer |
| **SlmA** | Synthetically lethal with a defective Min system protein A |
| **SUMO** | Small Ubiquitin-related Modifier |
| **SUV** | Small Unilamellar Vesicle |
| **SV** | Sedimentation Velocity |

# Introduction

# *E. COLI* CELL DIVISION

## *E. coli* cell cycle

Since the discovery of FtsZ, considered the central protein in the cytokinesis of the majority of prokaryotic species, the field of bacterial division has experimented an outstanding development in the understanding of the mechanism by which a bacteria splits into two daughter cells (den Blaauwen et al., 2017). Indeed, the bacterial division machinery constitutes an object of strong interest in synthetic biology due to its lower complexity in comparison with eukaryotic cells (Hürtgen et al., 2019). The reconstitution and minimization of this cellular process is a milestone in the generation of synthetic cells that would improve our knowledge about cell reproduction, a fundamental feature common to all living organisms (Ausländer et al., 2017). Moreover, advances in the field of bacterial division also provide attractive insights for the exploration of new antibiotics (Silber et al., 2020), an endeavor of utmost priority since the appearance of resistances to the existing antimicrobials is considered a major threat in our days. Hence, a deeper knowledge of the processes that converge in effective and successful division is of great value for the identification of targets for the synthesis of new antibiotics.

Conventionally, the bacteria cell cycle has been divided into three different stages (B, C and D) (**Figure I.1**). Phase B consists in a gap phase that starts in the newly generated daughter cell, comprising the period between completion of cytokinesis of the mother cell and the beginning of chromosome replication. This stage is of variable duration, heavily dependent on growth conditions and characterized by the absence of any major cell cycle event. Nucleoid segregation and cell division are associated with phases C and D, whose onsets are marked by the beginning and end of chromosome replication, respectively. The period comprising phases C and D, where DNA duplication occurs, cannot be reduced below 40 minutes, although *E. coli* can undergo a complete cell cycle in as short as 20 minutes due to multifork replication, consisting in new rounds of replication before completion of cell division (Dewachter et al., 2018). Interestingly, during the whole cell cycle, the bacterial chromosome remains organized into four macrodomains of ~1 Mb named Ori (that is flanked by two non-structured regions), Right, Left and Ter (Niki et al., 2000, Valens et al., 2004), each one being a dynamic entity that occupies specific subcellular regions during the cell cycle (Espeli et al., 2008). It seems that this organization is important for cell division coordination, since inactivation of DNA organizing factors leads to defects in nucleoid partitioning (Dewachter et al., 2018).

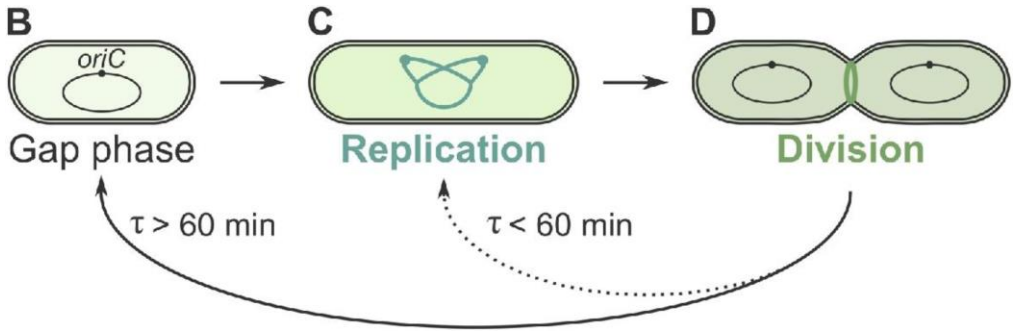


**Figure I.1. Illustrative scheme of the bacterial cell cycle.** The bacterial cell cycle can be divided into three phases. Stage B corresponds to a gap phase characterized by the absence of major events. Replication of the nucleoid occurs during phase C. In period D, completion of division generates two daughter cells. Under conditions in which the generation time (τ) decreases below 60 min, the B period is completely skipped (dotted arrow) and cells are generated with replicating chromosomes. Figure adapted from (Dewachter et al., 2018).

Proper synchronization of fundamental processes for cell reproduction requires exquisite regulation since deviations in the correct timing of these events normally result in catastrophic outcomes for the cell like chromosome guillotining or mini-cell phenotype. One example that illustrates this fine regulation is the formation of the division machinery, accurately positioned at the nascent division site, which in *E. coli* occurs at midcell with remarkable accuracy after bulk chromosome segregation (den Blaauwen et al., 2017). Such precision arises from the combined action of negative regulators that block the assembly of the division machinery at undesired locations, like the Min system comprising MinC, MinD and MinE proteins (Hu and Lutkenhaus, 1999), or the nucleoid occlusion mechanism, exerted by SlmA bound to specific DNA sites (Cho et al., 2011). In addition, the assembly of the division machinery at the cell center is reinforced by a multiprotein network involving ZapA, ZapB and the DNA-binding protein MatP (Buss et al., 2015).

### The Division Machinery of *E. coli*

*E. coli* cell cytokinesis is mediated by the divisome, a contractile ring consisting of a multiprotein complex formed by over 20 different proteins that assemble in the middle of the cell close to the end of the cell cycle (**Figure I.2**). The initial step in the formation of the divisome is the self-assembly of the conserved protein FtsZ into filaments at midcell, resulting in the formation of the so-called Z-ring, which serves as a platform where the rest of proteins are recruited at the division site (Haeusser and Margolin, 2016, Rico et al., 2013, den Blaauwen et al., 2017). Besides, the Z-ring also guides the synthesis of septal peptidoglycan and may provide some of the force necessary for cell constriction (Osawa et al., 2009, Coltharp et al., 2016). Two additional factors, the tether proteins ZipA and FtsA,

are required to anchor the Z-ring to the membrane. Both are membrane-associated proteins that can interact with FtsZ (Rico et al., 2013). The Z-ring fails to form if both proteins are inactivated, although the single presence of either ZipA or FtsA is enough to attach FtsZ to the membrane (Pichoff and Lutkenhaus, 2002). Additionally, other FtsZ associated proteins participate in the stabilization of the Z-ring (Zap proteins) (Huang et al., 2013). After Z-ring formation, followed by a time delay that can represent up to 20% of the cell cycle, the rest of division elements involved in cell wall synthesis and its coordination with cell constriction are recruited (den Blaauwen et al., 2017, Haeusser and Margolin, 2016). Finally, the divisome disassembles in a sequential and coordinated manner that follows a first-in, first-out principle (Söderström and Daley, 2017).

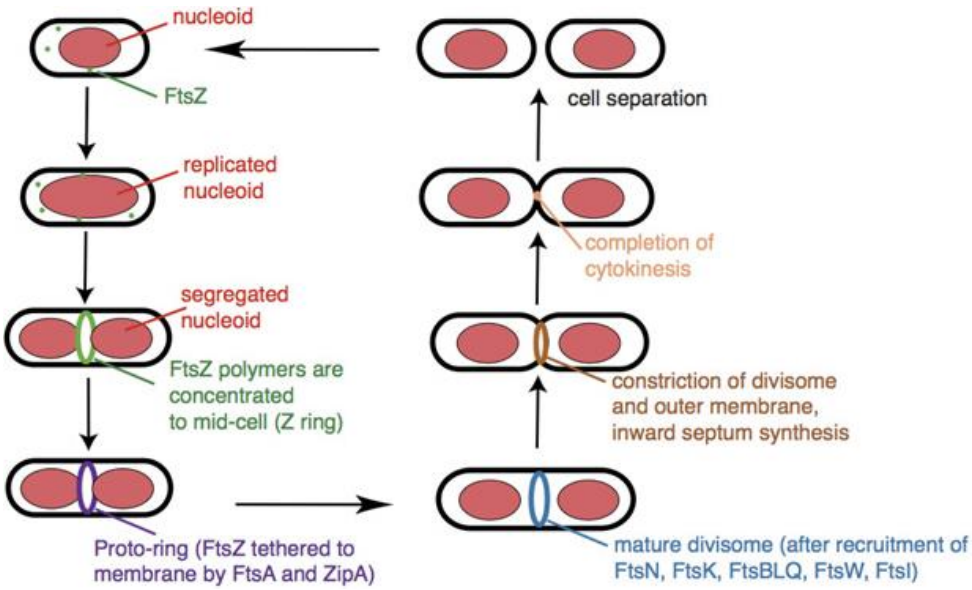


**Figure I.2. Overview of bacterial division.** Starting from the top-left scheme, as the cell cycle progresses, the bacterial chromosome replicates and the nucleoids are segregated into opposite halves. At this point, FtsZ and its membrane anchors are concentrated at midcell and form the Z-ring that, after recruitment of other division partners, progresses into a mature divisome. The divisome coordinates cell constriction with the functions of cell wall hydrolases and synthesis of new peptidoglycan. Finally, after completion of cell division, two daughter cells are born. Figure adapted from (Haeusser and Margolin, 2016).

According to high-resolution imaging experiments, the divisome of *E. coli* is a patchy ring or toroid structure composed of different modules separated in at least three concentric rings (**Figure I.3**): i) the inner layer(s) contains ZapB and MatP proteins and plays a regulatory role, ii) the middle ring corresponds to the Z-ring formed by FtsZ, FtsA and ZipA and iii) the outer ring is related to peptidoglycan synthesis and ingrowth (Söderström and Daley, 2017).

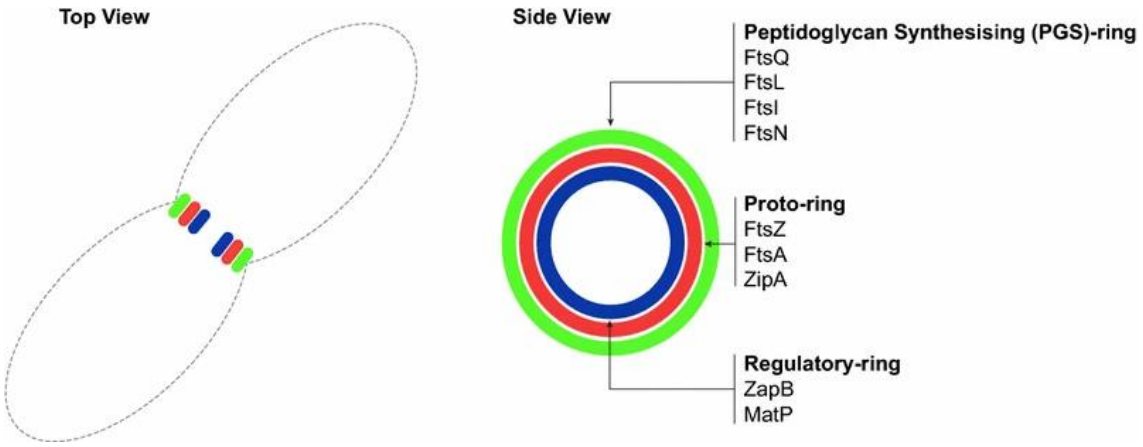


**Figure I.3. Illustration of divisome rings:** Schemes of the top (left) and side (right) views showing the location of the three concentric divisome rings assembled at midcell during cell division. From the membrane inwards, the peptidoglycan synthesis (PGS)-ring, the Z-ring (proto-ring) and the regulatory-ring formed by MatP and ZapB are represented. Figure adapted from (Söderström and Daley, 2017).

### FtsZ, the key protein in bacterial division

FtsZ is a cytoplasmic soluble GTPase of 40.3 kDa widely conserved among bacteria and archaea and is considered the ancestral homolog of eukaryotic tubulins (Hurley et al., 2016). Although both proteins share low sequence homology, FtsZ and tubulin present striking similar protein folds and GTP binding interactions (Romberg and Levin, 2003). A model of the 3D structure of *E. coli* FtsZ has been proposed based on the crystal structure of FtsZ resolved for *Methanococcus jannaschii* **(Figure I.4)**, *Thermotoga maritima*, *Pseudomonas aeruginosa* and *Mycobacterium tuberculosis* (Cordell et al., 2003, Leung et al., 2004, Löwe, 1998, Oliva et al., 2004). FtsZ monomers display a 10-amino acid disordered segment followed by a globular domain, which comprises two independent folded subdomains connected, by a ~50-amino acid unstructured flexible linker, to the conserved C-terminal peptide. The N-terminal globular domain contains the GTP binding site that is formed during filament assembly by the addition of the synergy T7 loop from the incoming subunit. The C-terminal peptide (CCTP), often referred to as the central hub, is highly conserved among bacteria and is involved in the interaction with several division partners such as the associated-membrane proteins FtsA and ZipA and the regulatory inhibitor proteins MinC and SlmA among others (Erickson et al., 2010). The required flexibility to accommodate such diversity of binding proteins is provided by the long intrinsically disordered region that precedes this peptide (Du and Lutkenhaus, 2019).

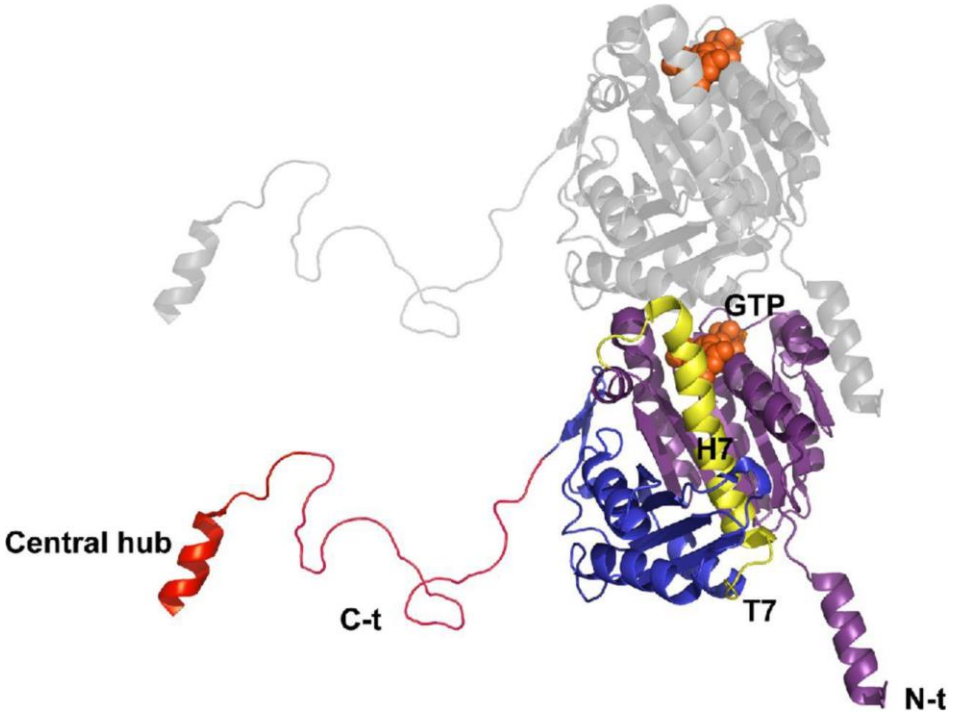


**Figure I.4. Model of FtsZ structure.** FtsZ dimer modeled from the crystal structure of *Methanococcus jannaschii*. The bottom colored monomer displays the N-terminal domain (purple) and the carboxy-terminal domain (blue) connected by the catalytic H7 helix followed by the T7 loop (both in yellow). After GTP coupling to the GTP-binding site, the T7 loop achieves the correct positioning of the phosphate activating the hydrolytic activity. The highly variable flexible C-terminal linker (red) is depicted here as a free-drawn unstructured peptide. The structure of the central hub at the C-terminal end (also colored in red) is based on the structure of the interacting region of the *E. coli* FtsZ protein with the globular domain of ZipA. Figure from (Ortiz et al., 2016).

In the absence of GTP, FtsZ monomers assemble into linear single-stranded oligomers (**Figure I.5A**) following a $Mg^{2+}$ linked non-cooperative indefinite self-association mechanism. The affinity of the interaction of a new subunit of FtsZ with a given oligomer decreases with oligomer length, this step involving the incorporation of an additional $Mg^{2+}$. Besides, the length distribution of the oligomers is modulated by protein, salt and $Mg^{2+}$ concentration (Rivas et al., 2000). FtsZ oligomers are active for the recognition of other division proteins like ZipA and the negative regulators such as MinC and SlmA.

In the presence of GTP and provided the concentration of FtsZ is above a certain concentration threshold, termed critical concentration (variable depending on conditions) (Mukherjee and Lutkenhaus, 1998), the protein polymerizes following a cooperative self-association mechanism (**Figure 1.5A**) (Du and Lutkenhaus, 2019). FtsZ-GTP forms single-stranded protofilaments of one subunit thick through head-to-tail interactions between globular regions of two monomers (Scheffers et al., 2002). These protofilaments are structurally flexible and,

depending on the conditions, can assemble into various types of higher-order structures with different geometries as filaments, ribbons, bundles, spirals or toroids (**Figure I.5B**) (Gonzalez et al., 2003, Erickson et al., 2010). Besides, it has been observed that many proteins can crosslink FtsZ filaments *in vitro* as the FtsZ-associated proteins ZapA, ZapC and ZapD (Du and Lutkenhaus, 2019).

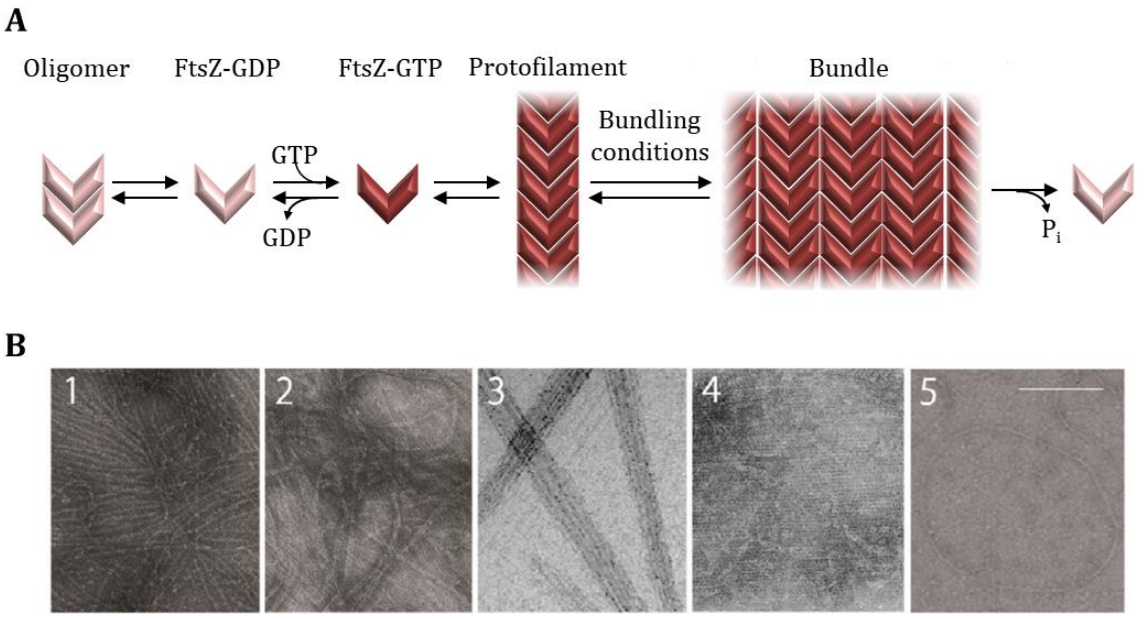


**Figure I.5. Self-assembly of FtsZ.** (A) Scheme of the possible association states of FtsZ depending on the absence or presence of GTP and in conditions promoting bundling. (B) Depending on the conditions, FtsZ can assemble into higher-order structures, such as protofilaments (1), ribbons (2), bundles (3), lamins (4) or toroids (5). Scale bar ~100 nm. Adapted from (Gonzalez et al., 2003, Popp et al., 2009, de Pereda et al., 1996, González et al., 2005, Yu and Margolin, 1997).

FtsZ protofilaments are highly dynamic and rapidly disassemble in solution when the GDP:GTP ratio increases as a consequence of nucleotide hydrolysis. Different strategies have been applied to maintain FtsZ in its polymeric state during experiments in solution involving the use of slowly hydrolyzable analogs of GTP, like GMPCPP (Salvarelli et al., 2011) or the inclusion in the sample of an enzymatic regeneration system that replenishes GTP as a result of the reaction between released GDP and acetyl phosphate catalyzed by the acetate kinase (Gonzalez et al., 2003, Small and Addinall, 2003).

# MECHANISMS INVOLVED IN THE SPATIOTEMPORAL MODULATION OF Z-RING ASSEMBLY

## Z-ring formation is controlled by multiple interactions with division proteins

Correct spatiotemporal assembly of FtsZ is fundamental for cell fitness. In *E. coli*, positioning of the Z-ring is a highly precise process that occurs within ~2 % of the cell's midpoint (den Blaauwen et al., 2017). Since FtsZ is distributed throughout the bacterial cytoplasm, positioning of the Z-ring at midcell requires a tight control by dedicated regulatory mechanisms, in which interactions with other division partners act as positive and negative input signals that mark the center of the cell (Du and Lutkenhaus, 2019).

Among the described mechanisms that modulate the assembly of the Z-ring, the Min system, a highly conserved positioning mechanism that prevents polar septation (**Figure I.6A**), is the best known (Lutkenhaus et al., 2012). Inactivation of this regulator leads to the production of anucleate cells due to aberrant Z-ring formation at the cell poles, where the Min system inhibits polymerization of FtsZ (Rowlett and Margolin, 2013). The system comprises MinC, MinD and MinE proteins that establish pole-to-pole oscillations (Hu and Lutkenhaus, 1999). MinD and MinE are responsible for the oscillatory behavior while MinC (the one directly interacting with FtsZ) is passively transported with the MinDE wave. As a consequence, MinC concentration displays a time-averaged local minimum at midcell, allowing Z ring formation at this position (Kretschmer and Schwille, 2016, Hu and Lutkenhaus, 1999, Meinhardt and Boer, 2001). The inhibitory effect of the Min system in the cell poles is complemented by the nucleoid occlusion mechanism mediated by the DNA-binding protein SlmA, which prevents FtsZ polymerization in the vicinity of the chromosome except at the division site (**Figure I.6B**) (Cho et al., 2011). Besides, *E. coli* cells are endowed with an additional positioning mechanism, the Ter linkage, which acts as a positive signal that promotes the localization of the Z-ring at the cell center by linking it to the terminus of replication of the chromosome (**Figure I.6C**) (Du and Lutkenhaus, 2019). Due to the relevance of the two last regulatory systems in the present doctoral thesis, they are described in more detail in sections below. Remarkably, inactivation of the three regulatory systems does not result in complete random positioning of the Z-ring, suggesting that other mechanism(s) responsible for the localization of the divisome must exist (Bailey et al., 2014).

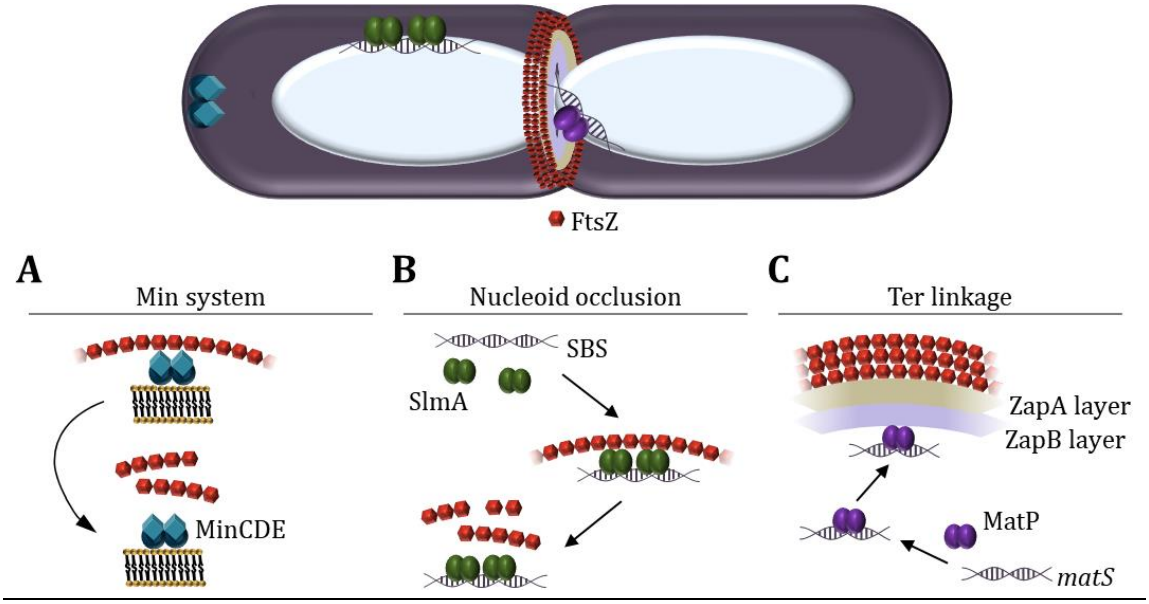


**Figure I.6. Overview of mechanisms involved in Z-ring positioning.** At the center, illustration of a dividing *E. coli* cell showing the Z-ring formed at midcell and its regulatory systems. (A) Pole-to-pole oscillations of the MinCDE system on the inner membrane prevent FtsZ polymerization at the cell poles. (B) SlmA bound to specific SBS sequences within the bacterial chromosome, except in the Ter macrodomain, inhibits FtsZ polymerization, thus protecting the chromosome from aberrant scission. (C) The Ter linkage contributes to Z-ring positioning at midcell. From top to bottom, FtsZ interacts with ZapA, ZapB, and MatP bound to *matS* sequences distributed in the chromosomal Ter macrodomain. Figure adapted from (Zorrilla et al., 2021).

### The nucleoid occlusion system

The nucleoid occlusion theory was initially proposed by Woldring and coworkers after they observed that cell division was inhibited in the vicinity of the nucleoid (Woldringh et al., 1990, Woldringh et al., 1991). More than ten years later, the identification of Noc in *B. subtilis* (Wu and Errington, 2004) and, subsequently, its counterpart in *E. coli*, SlmA (Bernhardt and de Boer, 2005), demonstrated that nucleoid occlusion is mediated, indeed, by protein factors.

SlmA, the nucleoid occlusion effector in *E. coli*, is a double-stranded DNA-binding protein that recognizes a 20-bp palindromic sequence usually referred to as SBS (SlmA Binding Sequence). Over 20 SBS sites are distributed throughout the chromosome except in the Ter macrodomain (the last portion of the chromosome that is segregated containing the replication terminus) (**Figure I.7A**) (Cho et al., 2011, Tonthat et al., 2011). During the cell cycle, SlmA bound to the SBS sites scattered over the bacterial nucleoid prevents the assembly of the Z-ring in the vicinity of the chromosome, hence protecting the DNA from bisection during cell constriction. It is only during cell division, when the Ter macrodomain of the segregating chromosomes occupies the cell center, that the midcell position

becomes available for Z-ring formation due to the lack of SBS sites in this region (**Figure I.7B**) (Ortiz et al., 2016, Tonthat et al., 2011, Cho et al., 2011). It is widely accepted that the inhibitory effect of SlmA should occur also at noncentral regions of the membrane (Mannik and Bailey, 2015, Schumacher, 2017, Tonthat et al., 2013, Du and Lutkenhaus, 2014). However, there is no evidence of direct interaction of SlmA with the membrane, in contrast with the known ability of Noc to interact with lipids (Adams et al., 2015). In this regard, it has been proposed that, due to the presence of SBS sequences close to genes encoding for membrane proteins, transertion (coupled transcription, translation, and insertion) of nascent membrane proteins might act as a mechanism to bring the nucleoprotein complex near the membrane (Tonthat et al., 2013). Nevertheless, experimental evidence is still necessary to shed light on the precise mechanisms that may contribute to localizing the inhibitory effect of SlmA close to membrane regions.

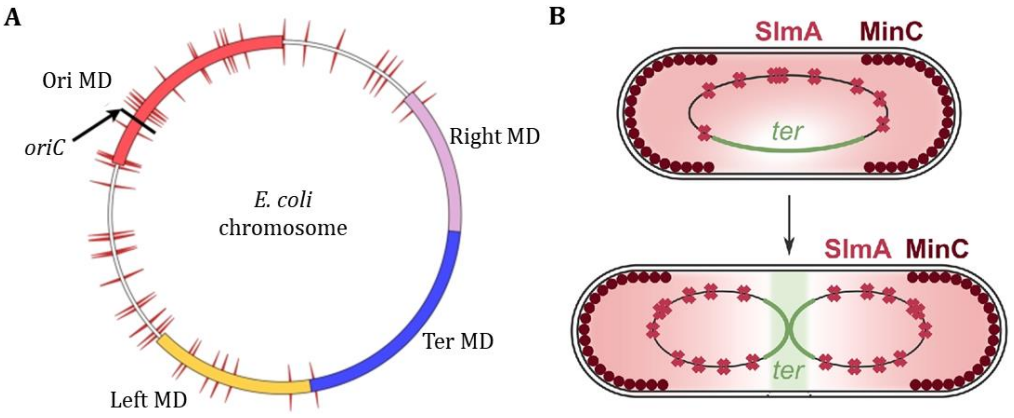


**Figure I.7. Overview of nucleoid occlusion regulation.** (A) Distribution of SBS sequences within the bacterial chromosome macrodomains (MDs) displayed as red ticks. Note that the Ter macrodomain is depleted of SlmA-binding sites. (B) Scheme of inhibitory Min and nucleoid occlusion systems in a bacterial cell before (top) and during division (bottom). Only when the Ter macrodomain is positioned in the center of the cell during chromosome segregation, the midcell position is clear of nucleoprotein complexes allowing Z-ring formation. Figure adapted from (Tonthat et al., 2011) and (Dewachter et al., 2018).

Structurally, SlmA is a TetR-like protein that is widespread among γ- and β-proteobacteria, with some exceptions, and harbors a highly conserved DNA-binding domain suggesting that in these species the consensus SBS sequence might be similar. Interestingly, SlmA was the first identified TetR member that does not play a role in transcription regulation, but instead, its transcription regulator fold has been repurposed for nucleoid occlusion (Schumacher, 2017). The protein interacts with the SBS sites through a helix-turn-helix (HTH) motif located in the N-terminal domain, resulting in the formation of a complex that comprises four

SlmA monomers per SBS site whose affinity is strongly regulated by ionic strength (Cabre et al., 2015, Tonthat et al., 2011, Tonthat et al., 2013). Besides, hydrophobic residues in the C-terminal region of the protein mediate the formation of a dimer that is maintained in the complex with the SBS, hence, the four monomers bound to the SBS are actually a pair of dimers (Tonthat et al., 2011, Tonthat et al., 2013).

Unlike Noc, when bound to its specific DNA sequences, SlmA can directly interact with FtsZ through its C-terminal peptide and a second site that has not been identified yet but that is known to be in the globular domain (Du and Lutkenhaus, 2014). SlmA in the nucleoprotein complex can interact either with the short oligomers formed by GDP-bound FtsZ subunits or with the FtsZ polymers elicited in the presence of GTP. In the latter case, the binding of SlmA to FtsZ filaments accelerates their disassembly into shorter species without modification of the GTPase activity of FtsZ single-stranded protofilaments (Cabre et al., 2015, Tonthat et al., 2013). Besides, this inhibitory effect on FtsZ assembly may be reinforced by a possible ability of SlmA to spread on the DNA adjacent to SBS sites (Tonthat et al., 2013).

**The Ter linkage protein MatP**

*E. coli* division site selection does not rely only on negative mechanisms that act by blocking the formation of the Z-ring. Quite the opposite, the assembly of the Z-ring is specifically guided by the Ter linkage, a physical link between the Z-ring and the Ter macrodomain of the chromosome (Bailey et al., 2014). The search for this additional regulatory mechanism was stimulated by experiments with defective mutants for both nucleoid occlusion and Min systems in *B. subtilis* and *E. coli* in which the Z-ring was still formed at midcell with significant precision in slow growth conditions (Rodrigues and Harry, 2012, Männik et al., 2012). Later, time-lapse microscopy experiments with the double defective mutant showed that the Z-ring correlated with the Ter region of the chromosome (Bailey et al., 2014, Espeli et al., 2012), a result that, combined with super-resolution microscopy imaging, led to the identification of a linkage formed by ZapA, ZapB and the DNA-binding protein MatP (Buss et al., 2015).

MatP is the Ter linkage protein that binds to the chromosome and is considered the main organizing factor of the Ter macrodomain. This DNA-binding protein specifically recognizes a palindromic 13-bp DNA sequence (*matS*) repeated 23 times exclusively within the Ter region (Mercier et al., 2008). After dimerization, binding to *matS* is mediated through the N-terminal domain comprising a four-helix region and a central ribbon-helix-helix (RHH) module (Dupaigne et al., 2012,

Durand et al., 2012). MatP colocalizes, as expected from the distribution of *matS* in the chromosome, with the Ter macrodomain, insulating it from flanking domains and compacting the DNA, as evidenced by the increase in the distance between fluorescent DNA markers located within this region upon deletion of the protein (Mercier et al., 2008, Lioy et al., 2018). Recently, it has been reported that, upon binding to *matS* sites, MatP is also able to displace the chromosome-organizing complex MukBEF from the Ter macrodomain, promoting the formation of a unique chromosomal region (Nolivos et al., 2016). DNA compaction has been proposed to be mediated by a mechanism involving MatP tetramerization through the C-terminal coiled-coil domain between two dimers of MatP bound to *matS*, bridging, thereby, distant *matS* sites (Dupaigne et al., 2012). However, experiments with MatP mutants in which tetramerization was impaired revealed that it is not necessary to maintain the architecture of the Ter macrodomain or for insulating it from flanking domains (Lioy et al., 2018), leaving the precise mechanism for DNA compaction of the Ter region unclear.

As the cell cycle progresses, the Ter macrodomain shifts toward the center of the cell (Espeli et al., 2012) where the interaction network formed by MatP (bound to *matS* sites), ZapB and ZapA (Ter linkage) stabilizes the Z-ring, thus promoting its assembly over the terminus portion of the chromosome (**Figure I.8**) (Buss et al., 2015, Bailey et al., 2014). Once the Ter linkage is fully formed, this anchor also contributes to the extended localization of the Ter region at midcell (Espeli et al., 2012, Mannik and Bailey, 2015).

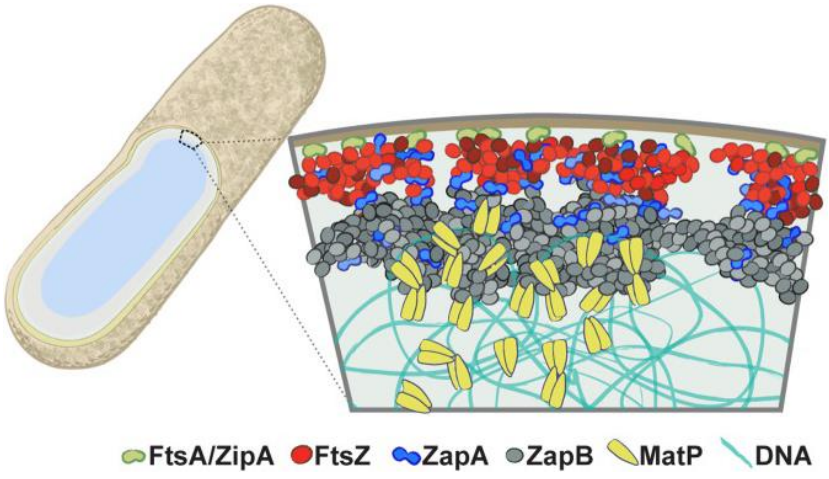


**Figure I.8. Schematic illustration of the Ter linkage.** The Z-ring (tethered to the membrane by ZipA and FtsA) is stabilized by a physical link, the Ter linkage, that connects the Z-ring to the terminus portion of the chromosome through multiple interactions. ZapA can interact with FtsZ and/ or with the network formed by the self-association of ZapB which, in turn, is tethered to the chromosome via its association with DNA-bound MatP. Figure from (Buss et al., 2015).

Finally, upon cell constriction during cell division, the Ter region of the chromosome is segregated into each daughter cell as they separate. This process is assisted by FtsK, a DNA hexameric translocase that moves about 400 bp toward the *dif* sites close to the terminus of the chromosome while displacing MatP from its *matS* sites (Bonne et al., 2009, Graham et al., 2010). The molecular mechanisms by which this last step of chromosome segregation and daughter cell separation are coordinated remain largely unknown.

# SPATIAL ORGANIZATION OF BIOMOLECULES THROUGH PHASE SEPARATION

### The influence of crowding on macromolecular associations

The *E. coli* cell division machinery operates in a highly crowded and heterogeneous environment (**Figure I.9**). Indeed, approximately 25 – 30% of the bacterial volume is occupied by proteins (200 – 300 mg/ml), RNA (100 mg/ml) and DNA (15 mg/ml) (Vendeville et al., 2011). Besides, the intracellular space is characterized by the presence of multiple membrane surfaces and structural fibers that influence those biochemical reactions taking place in their vicinity (Minton, 1990). As a consequence, weak nonspecific interactions with macromolecules arise. These interactions may be individually insignificant but, collectively, they become a factor that must be taken into account in the modulation of the reactivity of biochemical interactions (Rivas and Minton, 2022).

Macromolecular crowding influences biochemical reactions primarily via the excluded volume effect. This term refers to a nonspecific steric repulsion that arises from the mutual impenetrability of macromolecules by which the volume fraction that is occupied by certain macromolecules becomes unavailable to the others (Ellis, 2001). The large impact that excluded volume effects may have on the dynamic and equilibrium properties of biomolecules in solution has been theoretically predicted and experimentally demonstrated (Minton, 2001, Rivas and Minton, 2016). The main outcome derived from the excluded volume effect is the promotion of macromolecules compaction and association (Ellis, 2001, Minton, 2000, Rivas et al., 2001), but it also might increase the rate of slow, transition-state limited association interactions or reduce the rate of fast, diffusion-limited association reactions. Besides, in the limit of high fractional volume occupancy, all association reactions would be diffusion limited and, therefore, slowed by

crowding (Zhou, 2008, Minton, 2001). Since the cell interior is highly occupied, the chemical activity of macromolecules inside the cell is expected to be enhanced.

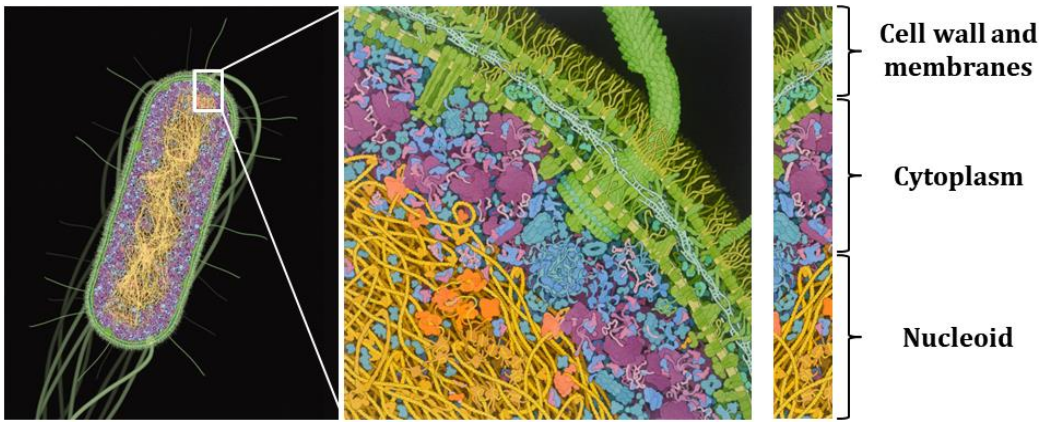


**Figure I.9. Cartoons illustrating crowding inside *E. coli*.** Representation of a cross-section through a whole *E. coli* cell with an amplified image, on the right, of the portion within the white square. The nucleoid, cytoplasm as well as cell wall and membranes can be appreciated. Cartoons adapted from David S. Goodsell gallery https://pdb101.rcsb.org/sci-art/goodsell-gallery.

The impact of macromolecular crowding has been analyzed *in vitro* both on the GDP- and GTP-bound forms of FtsZ. Nonideal tracer sedimentation equilibrium (NITSE) experiments demonstrated that, in the presence of high concentrations of bovine serum albumin and hemoglobin, FtsZ in its GDP-bound state forms larger oligomers (Rivas et al., 2001). The increase in the tendency of FtsZ to associate into higher-order oligomers under crowding conditions observed in this study was in good agreement with the predictions of excluded volume theory. Besides, FtsZ filaments are also sensitive to excluded volume effects. In this case, macromolecular crowding promotes lateral associations between FtsZ protofilaments to form bundles, as observed in the presence of Ficoll 70 or dextran above 100 g/l (Gonzalez et al., 2003). It has been reported that FtsZ can also form toroid structures when polymerized in the presence of methylcellulose or polyvinyl alcohol (Popp et al., 2009). In addition, the self-organization of FtsZ filaments into higher-order structures under crowding conditions decreases the GTPase activity of the protein and retards the dynamics of FtsZ polymers in comparison with diluted conditions (under which FtsZ assembles into protofilaments). This tendency of FtsZ to form higher-order structures is also observed when using homogenous mixtures of macromolecules at high concentration to mimic the crowding and heterogeneity inside the cell, being the extent of the effect dependent on the composition of the mixture (Monterroso et al., 2016a).

## Crowding can drive phase separation leading to the formation of membraneless compartments

Another interesting effect derived from macromolecular crowding is the promotion of phase separation, leading to the spontaneous demixing of macromolecules into two different phases (Walter and Brooks, 1995). Liquid-liquid phase separation (LLPS) is a thermodynamically-driven and reversible process that occurs when a solute concentration threshold is exceeded (Hyman et al., 2014). Interestingly, in the presence of crowding, this threshold can be reduced because of excluded-volume effects (André and Spruijt, 2020). Considering the high levels of occupancy in the bacterial cytoplasm, liquid demixing of cell components can lead to the generation of microenvironments with physiological relevance. In fact, it is believed that the bacterial nucleoid forms a condensed liquid phase similar to a complex coacervate formed by phase separation that contains multivalent cations, DNA-binding proteins and other macromolecules (Cunha et al., 2001, de Vries, 2010, Pelletier et al., 2012). The impact that the presence of compartments formed by this mechanism may have in the cell has been highlighted by studies with LLPS in bacterial cell lysate in which transcription rates are enhanced (Sokolova et al., 2013) or in works showing that the location and activity of enzymes are influenced by LLPS (Cacace et al., 2015, Dominak et al., 2010, Koga et al., 2011, Strulson et al., 2012).

The influence of these microenvironments on the distribution and activity of proteins can be studied *in vitro* by reconstitution of LLPS environments using two crowding agents with predominantly repulsive interaction. While at low concentration the two macromolecules coexist in a single phase, increasing the concentration above the coexistence curve leads to the formation of two separated enriched phases (**Figure I.10**)

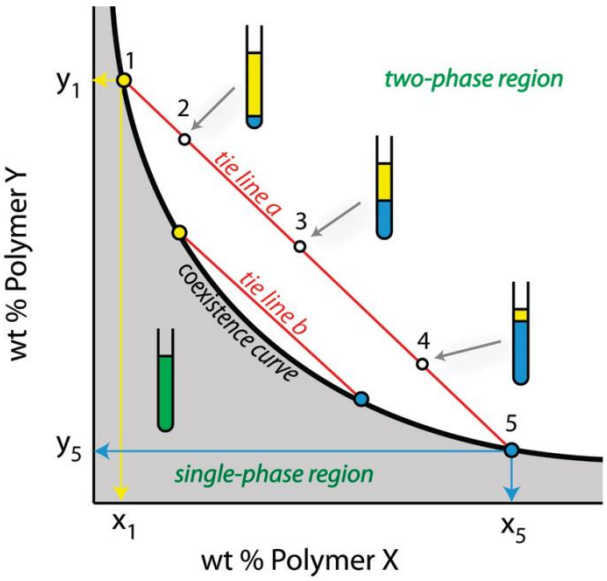


**Figure I.10. Phase separation diagram for two neutral polymers.** The diagram represents the coexistence curve (or binodal) for a generic LLPS system. At concentrations above the coexistence curve, the system separates into two different phases. Tie lines connect the points for which the concentration of polymer in each phase is the same changing only the volume fraction. Figure from (Keating, 2012).

(Albertsson, 1986, Keating, 2012). This sort of system allows the study of the partition of different soluble molecules among both phases and the interface (Walter and Brooks, 1995, Zaslavsky, 1994), a behavior that depends on the properties of the molecule and the particular liquid-liquid phase-separated system (Walter and Brooks, 1995, Zaslavsky et al., 1978). Upon quantification of the concentration of the target molecule in both enriched phases, a partition coefficient can be calculated corresponding to the ratio between the concentration in the top and bottom phases. In addition, binary LLPS systems formed by two inert crowders are susceptible of being encapsulated inside cell-like containers surrounded by a lipid boundary. This approach allows to perform studies in environments that reproduce cellular conditions like compartmentalization, confinement and the presence of biological surfaces (Holthuis and Ungermann, 2013, Sobrinos-Sanguino et al., 2017a).

Microenvironments have been found to modulate the localization and assembly of FtsZ. A study using different LLPS systems formed by a binary mixture of crowders (one of them being PEG 8 and the other dextran 500, Ficoll 70 or DNA) demonstrated that FtsZ asymmetrically distributed within the enriched phases and the interface (**Figure I.11**) (Monterroso et al., 2016b). FtsZ in its GDP-bound state preferentially partitions in the non-PEG phase to a greater or lesser extent depending on the LLPS system composition, with low accumulation at the interface in all cases. Interestingly, assembled FtsZ was more sensitive to the composition of the binary system, with FtsZ polymers localizing in the non-PEG phase and with important fractions at the interface between the two phases (dextran 500), no preference for the interface (Ficoll 70) or even expelled from there (DNA). Therefore, the uneven partition of FtsZ within the LLPS systems was not only largely dependent on their composition, but it was also reversibly regulated by the association state of FtsZ. This differential distribution has potential implications in the spatial regulation of FtsZ polymerization, preventing its assembly in those regions where the concentration decays below the critical threshold for polymerization due to exclusion of the protein. Conversely, accumulation of FtsZ in some microenvironments may help to reach the critical concentration for FtsZ assembly and promote the interaction with biomolecules located in the same region.

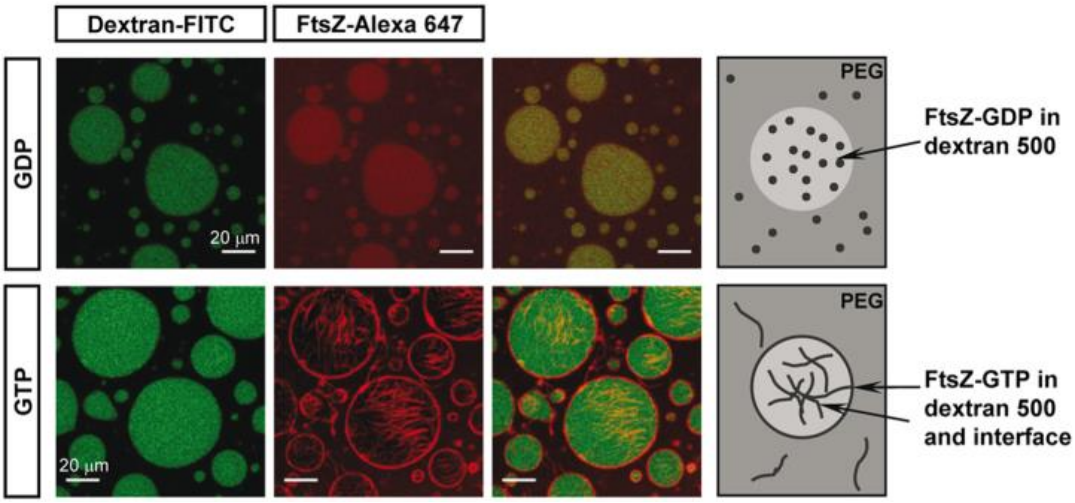


**Figure I.11. Distribution of FtsZ within PEG 8/Dextran 500 LLPS system.** Confocal images of FtsZ in the PEG 8/dextran 500 LLPS system in the absence (top row) and presence (bottom row) of 1 mM GTP with their corresponding illustration, in the right, showing the distribution of FtsZ within the phases and the interface. Figure adapted from (Monterroso et al., 2016b).

## The emergence of biomolecular condensation as an organization mechanism

The first evidence of the existence of membraneless compartments was the description of the nucleolus of neuronal cells in the 1830s. Since then, many other compartments lacking a membrane, physically separated from the rest of the surroundings have been discovered (Banani et al., 2017). The formation mechanism of these compartments remained unclear until a decade ago, when photobleaching experiments demonstrated that proteins inside P granules, in germ cells of *Caenorhabditis elegans*, are highly mobile, suggesting that they are formed through LLPS (Brangwynne et al., 2009). In the last years, the number of subcellular compartments described to exhibit liquid-like properties has rocketed. While these kinds of compartments are highly diverse, the fact that all of them share the ability to concentrate biological molecules led to proposing their aggrupation under the name "biomolecular condensates" (Banani et al., 2017). However, the terminology in the scientific literature is still quite varied (membraneless organelles, cellular bodies, granules, etc.).

Biomolecular condensates are currently considered key organizers of the intracellular space in eukaryotic cells (Boeynaems et al., 2018) and recent investigation points out that they also might have essential functions in prokaryotic organisms (Azaldegui et al., 2021). Moreover, since bacteria lack membranous organelles, they may constitute a mechanism for the spatial regulation of biochemical processes additional to the membrane envelope,

traditionally considered the only organizational element in these organisms. Bacterial condensates have been recently proposed to play roles in RNA degradation (BR-bodies), gene expression (RNAP cluster and PopZ microdomains), DNA protection (Dps protein), DNA replication, repair and recombination (SSB protein), chromosome segregation (ParABS system), stress and starvation (polyphosphate granules), virulence (ATP-binding cassette transporter Rv1747), and photosynthesis (carboxysomes) (Azaldegui et al., 2021). Biomolecular condensates are characterized by several properties that have been suggested as criteria to catalog them as such (Hyman et al., 2014). Because of their liquid nature, biomolecular condensates have spherical shapes due to surface tension (**Figure I.12A**), molecules can diffuse and be exchanged with the outer phase (**Figure I.12B**) and they can undergo fusion upon contact with another condensate (**Figure I.12C**). Additionally, it is characteristic a concentration saturation value ($c_{sat}$) above which phase separation occurs. Above the $c_{sat}$, larger fractions of dense phase are obtained while the concentration in the bulk phase remains equal to the $c_{sat}$ value (**Figure I.12D**) (Banani et al., 2017, Peng and Weber, 2019).

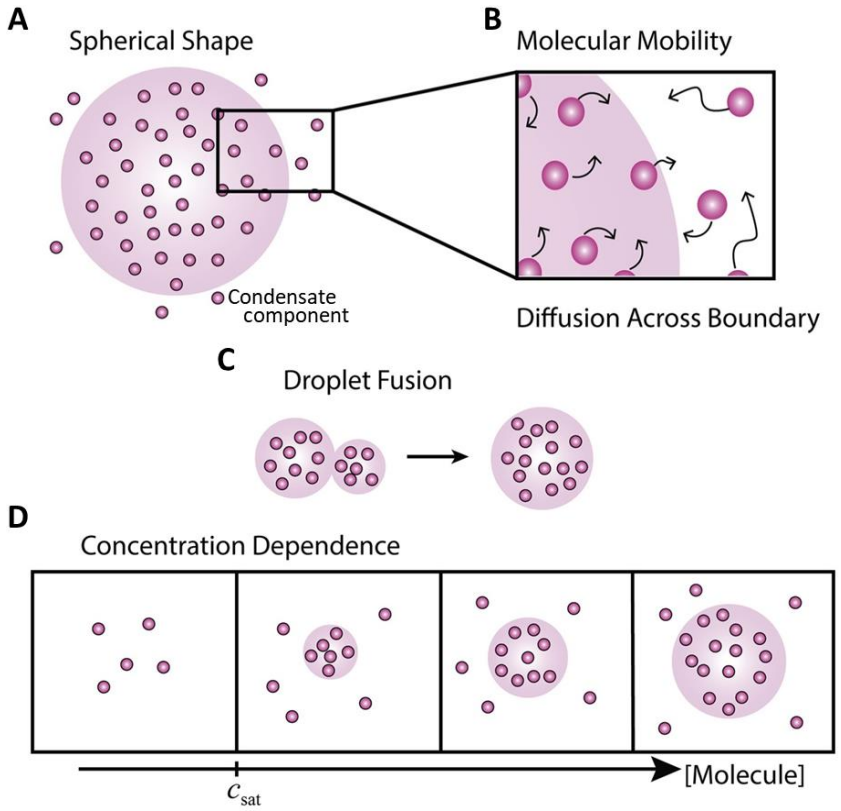


**Figure I.12. Overview of biomolecular condensates properties.** (A) Condensates have spherical shapes due to surface tension. (B) Molecules can diffuse within the condensate and across the boundary. (C) Droplets can undergo fusion upon contact. (D) Condensate formation occurs above $c_{sat}$ and size scales with component concentration. Figure adapted from (Azaldegui et al., 2021).

The dynamic control of the composition of the condensates is still poorly understood. Nevertheless, it seems that their organization can be explained, at least in part, by the presence within the condensates of two types of biomolecules: scaffolds and clients (Banani et al., 2016). Scaffolds are a small subset of macromolecules (sometimes just a single macromolecule) that are fundamental for condensate formation while clients consist of molecules that partition inside the condensates only after they are formed. This simple organization has been observed *in vitro* and in studies in cells showing that changes in the concentration of scaffold proteins dramatically altered the recruitment of client molecules (Banani et al., 2016).

Because biomolecular condensates are formed through a process involving liquid demixing, their composition usually entangles a set of elements that favors a decrease in solubility to reduce the threshold at which they phase separate (Banani et al., 2017). This requirement is commonly satisfied by the presence of proteins with multivalent domains, leading to their association and, thereby, to the mentioned decrease in solubility (Alberti and Dormann, 2019). This is favored in proteins that exhibit modular domains or intrinsically disordered regions (IDRs), which harbor sticker units that provide the attractive interactions separated by spacers, responsible for conformational flexibility (Wang et al., 2018). In addition, other macromolecules such as nucleic acids, especially RNA, can promote the formation of condensates since they are usually an additional source of multivalency (Jain and Vale, 2017).

Biomolecular condensates, therefore, constitute an alternative compartmentalization mechanism to the classic membranous organelles for those processes that require a flexible modulation of the composition, without the need for a specialized transport through a membrane boundary (Banani et al., 2017). Their ability to selectively concentrate different biomolecules makes them excellent platforms to regulate a plethora of vital cellular processes. For instance, by specifically concentrating or excluding different subsets of molecules within the condensate, some interactions or chemical reactions can be potentiated while limiting others (**Figure I.13A**). Interestingly, concentrating reactants does not always lead to enhancing reaction rates, but it depends on the physical properties of the condensate. For example, the viscosity of some condensates can increase with time in a process called maturation, reducing the diffusion and exchange of components with the bulk phase and, therefore, slowing the reaction (**Figure I.13B**). This ability to selectively accumulate molecules can also serve to sequester molecules, reducing their concentration in the outer phase and, hence, inhibiting

their activity there (**Figure I.13C**). Finally, condensates can act as buffering elements since, once they are formed, the concentration of their essential components is maintained in the surroundings equal to the $c_{sat}$ (**Figure I.13D**) (Banani et al., 2017). In view of the myriad of functions that they can exert in the cell, it is not surprising that they are now regarded as fundamental actors in cell physiology. Moreover, the number of publications that relate biomolecular condensates with cell pathology is also growing fast (Alberti and Dormann, 2019, Shin and Brangwynne, 2017).

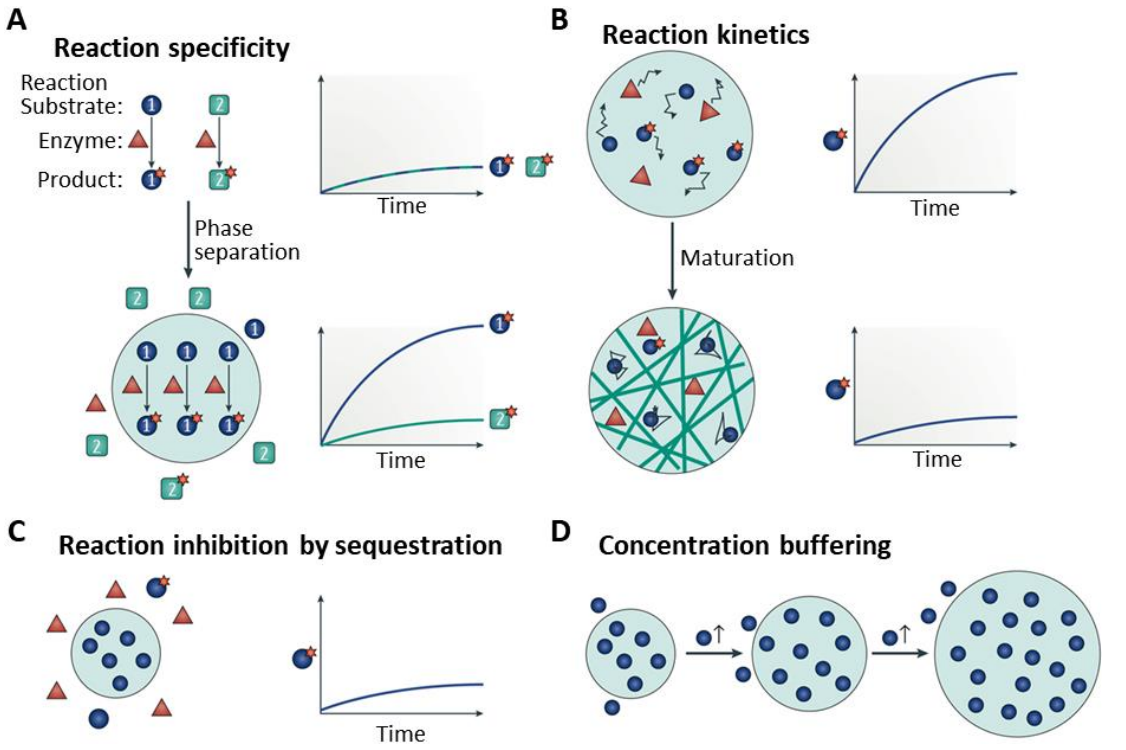


**Figure I.13. Possible functions of biomolecular condensates.** (A) Concentrating reactants inside condensates can increase reaction kinetics and specificities. An enzyme with two alternative substrates is shown. Colocalizing the enzyme with one of its substrates in the condensate increases the rates of reaction with that substrate. Besides, a specific pathway can be selected by excluding the rest of possible substrates. (B) Changes in the physical properties of the condensate can affect the kinetics of reactions. An increase in viscosity may slow the diffusion of molecules, decreasing reaction rates. (C) Sequestering molecules inside condensates can negatively regulate some reactions in the outer phase. (D) The concentration of essential components outside the condensate is maintained at $c_{sat}$ values. Thus, condensates can help to keep constant the concentration of these components in the outer phase. Figure adapted from (Banani et al., 2017).

Interestingly, FtsZ is a protein in which multivalency is undoubtedly present as revealed by its ability to self-associate into oligomers (in the absence of GTP) or in higher-order structures (in the presence of GTP). Besides, FtsZ can interact with multiple division partners, being some of them DNA-binding proteins, and

possesses an unstructured region (the C-terminal linker). Remarkably, there is evidence *in vivo* of relatively rounded patches that contain FtsZ outside and inside the Z-ring (Du and Lutkenhaus, 2019, Lyu et al., 2016, Rowlett and Margolin, 2014). Taking into account all of this, it seems that FtsZ might be a good candidate to be involved in LLPS processes leading to condensate formation.

### Methods to identify biomolecular condensates

Procedures to study biomolecular condensates are far more developed *in vitro* since their study *in vivo* is frequently challenging due to their small size, especially in bacteria (Azaldegui et al., 2021). Condensate formation can be demonstrated by reconstitution from their individual purified components, which allows the identification of the scaffold macromolecules that drive phase separation. If the reconstituted components assemble into a dense phase, its characterization should focus on discerning whether they are formed via LLPS or not (Alberti et al., 2019). Simple visualization of the sample using microscopy techniques may serve to test if the assemblies have a spherical shape and if they are susceptible to undergoing fusion events, properties related with their liquid nature. Since biomolecular condensates are dynamic structures, confirmation of this hallmark is one of the most definitive proofs of formation through LLPS. Dynamism can be verified by demonstrating that components inside the condensate can diffuse and be exchanged with those in the outer phase. In this regard, incorporation of fluorescent-labeled components inside preexisting condensates can be followed by fluorescence microscopy techniques (Woodruff et al., 2017). In addition, fluorescence recovery after photobleaching (FRAP) has been used to demonstrate the mobility of components. However, analysis of the data retrieved using this method is not straightforward, presenting several limitations and challenges. Determination of a $c_{sat}$ constitutes another proof, since the assembly above a certain threshold is a typical behavior of biomolecular condensates (Shin and Brangwynne, 2017, Peng and Weber, 2019). This value can be measured through turbidity measurement of samples, typically at wavelengths ranging between 340 and 400 nm. Importantly, since any kind of large structure increases the turbidity signal, this technique must always be performed in combination with microscopy (Alberti and Dormann, 2019). Additionally, disassembly mediated by 1,6-hexanediol may serve as a complementary indicator, although it is insufficient by itself to demonstrate LLPS (Alberti and Dormann, 2019, Kroschwald et al., 2018).

## RECONSTITUTION OF DIVISION ELEMENTS IN MINIMAL MEMBRANE SYSTEMS AND CYTOMIMETIC CONTAINERS

### Biomimetic membrane systems used to reconstitute protein assemblies

Living organisms are complex entities formed by a large number of components, with redundant functional elements and biomolecular networks. In this context, complexity can be reduced following a bottom-up strategy through the reconstitution of cellular constituents, one by one, increasing the level of complexity with each step forward (Schwille et al., 2018, Ausländer et al., 2017). Following this approach, the properties of individual components of a cellular machinery as well as their interaction and coordination with other elements can be studied in a controlled manner. Thus, the obtained information allows the reconstitution of minimized cellular processes with a plethora of possible applications (production of biosensors, generation of artificial cells, design of new materials, bioremediation, drug discovery, etc.). Ultimately, identification of the minimal set of functional components required to generate a living system would be of great value, improving our knowledge about life and its origin. In the last years, the appearance of novel tools that allow mimicking different components of the bacterial cell has motivated the reconstitution of single elements (or a small subset) in cell-like environments.

During bacterial division, interactions of proteins with the inner membrane of *E. coli* play fundamental roles. Therefore, a significant number of studies in the field of bacterial division have focused on the reconstitution of division elements on biomimetic membranes, particularly FtsZ. This strategy, which allows accurate control of biochemical conditions, has led to important advances in the understanding of the assembly of the Z-ring (Martos et al., 2012a, Rivas et al., 2014). Several membrane systems like nanodiscs, lipid-coated microbeads, supported lipid bilayers (SLBs), microdroplets and giant unilamellar vesicles (GUVs) are among the set of available platforms to investigate the role of lipid surfaces in bacterial division (**Figure I.14**) (Rivas et al., 2014). In this thesis, the behavior of biochemical systems involved in the bacterial division has been studied by encapsulation inside water in oil microdroplets and vesicles mimicking physiological conditions found within the cell. Besides, quantitative measurements on the binding of SlmA and MatP to lipid membranes were conducted using lipid-coated microbeads.

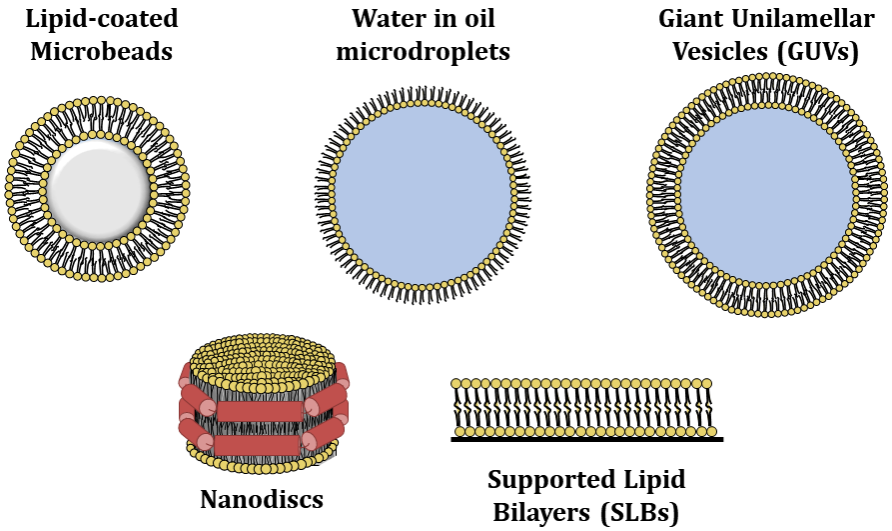


**Figure I.14. Illustration of minimal membrane systems.** Representation of lipid-coated microbeads, water-in-oil microdroplets, Giant Unilamellar Vesicles (GUVs), nanodiscs and supported lipid bilayers (SLBs) as cytomimetic platforms useful for the reconstitution of division elements.

### Reconstitution of division elements inside cytomimetic containers

Reproduction of essential features of the cellular inner environment can be achieved by encapsulation of bacterial elements in droplets dispersed in an oil phase. These droplets can be easily generated by emulsion of an aqueous sample with a larger volume of oil phase containing a surfactant to prevent droplet coalescence (Torre et al., 2014). Droplets produced with this protocol offer valuable information; however, although simple, the heterogeneity in size and composition of droplets obtained with this procedure might be an important limitation. This problem can be overcome by generating the droplets by means of microfluidic techniques, which allow the production of hundreds of identical monodisperse droplets whose composition can be accurately controlled (Theberge et al., 2010).

Microfluidic technology has already been used to study the behavior of FtsZ in confined environments using as surfactant a mixture of *E. coli* lipids matching the composition of those found in the bacterial inner membrane. Initially, FtsZ was encapsulated inside droplets in the presence of GTP in a study in which it was observed that FtsZ bundle distribution was dependent on the geometry of the droplet, conferring specific boundary conditions (Mellouli et al., 2013). Encapsulated FtsZ reversibly assembled with a subunit turnover close to values measured *in vivo*. A forward step in the recreation of cellular conditions was the encapsulation by microfluidics of a binary LLPS system formed by PEG 8 and dextran 500 phases containing FtsZ (Sobrinos-Sanguino et al., 2017a).

Furthermore, generated droplets were transformed into GUVs, following a protocol based on the droplet transfer method (Carrara et al., 2012), that could be permeated by including DMPC in the lipid composition. The behavior of FtsZ could be thus analyzed, before and after inducing its polymerization through external addition of GTP, in biomimetic containers reproducing some of the essential features of the cytoplasm like confinement, macromolecular crowding and the presence of microenvironments and lipid surfaces.

**Lipid-coated microbeads as minimal membrane systems to study lipid-protein interactions**

Lipid-coated microbeads constitute robust systems that provide lipid membranes, of controlled composition, with uniform curvatures for the quantification of lipid-protein interactions (Martos et al., 2012a). Functionalized microbeads are obtained after deposition of lipid vesicles on the surface forming a dynamic and fluid membrane (Nollert et al., 1995). After incubation of the protein with the coated microbeads, the affinity of the interaction can be determined from the depletion of protein in the soluble fraction (due to binding to the lipids), which can be determined after centrifugation to remove the coated particles with the interacting protein. Therefore, this procedure allows direct and unambiguous measurement of the binding.

This kind of assay has been used to study the interaction of elements of the Z-ring with lipids. The binding of FtsA to the mixture of *E. coli* phospholipids was analyzed using lipid-coated microbeads, resulting in an apparent affinity ten-fold lower than that retrieved for experiments in which microbeads were coated with the inner membrane. These results suggest an unknown modulation by proteins of the inner membrane (among other factors) of the binding of FtsA to the inner membrane of *E. coli* (Martos et al., 2012b). In addition, this assay has enabled the analysis of the interaction between FtsZ and ZipA anchored to the lipid membrane (Ahijado-Guzmán et al., 2012) as well as measurements to determine the effect of the nucleotide and receptor density on this interaction (Sobrinos-Sanguino et al., 2017b). The results reported in this study showed that GDP-bound FtsZ can bind to membrane immobilized ZipA with a stoichiometric ratio well above unity because of the ability of FtsZ to oligomerize. Besides, the ability of FtsZ oligomers (assembled in the absence of GTP) to grow indefinitely with concentration leads to lipid-coated microbead unsaturability. Remarkably, this was not observed for FtsZ polymers triggered in the presence of GTP in which microbead saturation was reached, compatible with the formation of narrowly-sized cyclic structures that cannot further grow.

# AIMS

**The general aim of this thesis is to contribute to the understanding of the mechanisms involved in the positioning of the bacterial division ring through the coordinated modulation of the assembly, location and distribution of the central division protein FtsZ.**

The goal in chapters 1 and 2 is addressing the impact of macromolecular crowding and compartmentalization on the modulatory activity of SlmA·SBS nucleoprotein complexes on FtsZ assembly. Previous work has shown that FtsZ reconstituted in crowded LLPS systems, mimicking microenvironments, asymmetrically partitioned among preexisting phases and/ or interfaces. These studies indicated that phase separation may influence the organization and reactivity of FtsZ. Preliminary experiments on the reconstitution of FtsZ with SBS-bound SlmA in cell-like environments led to the observation that, under these conditions, the three elements assemble into structures compatible with liquid droplets. Therefore, we proceeded to characterize these structures and, subsequently, to explore conditions under which FtsZ could phase separate into condensates in the absence of SlmA.

1. **Reconstitution of FtsZ with its nucleoid-associated inhibitor SlmA in crowded cell-like media.** Analysis of the effect of SlmA and SBS-bound SlmA complexes on the behavior of GDP-bound FtsZ in crowded solutions and LLPS systems as well as characterization of the condensates formed by the three elements through turbidity and confocal microscopy. Evaluation of the influence of a lipid boundary and confinement by encapsulation of the condensates, formed by FtsZ and SBS-bound SlmA, inside microfluidics microdroplets containing the LLPS systems.

2. **Exploration of conditions under which FtsZ could phase separate to form biomolecular condensates on its own.** Study on the ability of FtsZ to assemble into biomolecular condensates by itself under conditions promoting oligomerization of the GDP-bound state of the protein, both in bulk and encapsulated inside microfluidic-based containers. Assessment of the formation of FtsZ condensates by turbidity and confocal microscopy as well as the impact of removal of the unstructured C-terminal region of the protein on condensation.

Chapters 3 and 4 are aimed at analyzing the behavior of the DNA-binding proteins SlmA and MatP reconstituted on biomimetic membranes. Considering that assembly of the bacterial cell division machinery takes place at the inner

membrane of *E. coli*, characterization in minimal membrane systems of these two proteins, involved in Z-ring positioning, can help to shed light on their role in cell division. Initial results obtained during the reconstitution in biomimetic membranes showed that both SlmA and MatP proteins are able to interact with lipids. Hence, we conducted the analysis of the interaction for each protein either in the absence and presence of their binding partners.

3. **Analysis of the binding of the nucleoid occlusion protein SlmA to lipid membranes** and the factors modifying this recognition through biochemical, biophysical, and imaging methods following an approach involving the use of different minimal membrane systems. Evaluation of the impact of the two interacting partners of SlmA, FtsZ and its specific double-stranded DNA sequence, on the interaction.

4. **Study of the interaction of the Ter linkage protein MatP with lipid bilayers** through its reconstitution in microfluidics microdroplets and giant unilamellar vesicles (GUVs) complemented with biochemical approaches in the absence and presence of its specific DNA-binding sequence, *matS*.

# METHODS

# MATERIALS

Polar extract of *E. coli* lipids (EcL) and L-α-phosphatidylcholine (PC) from Avanti Polar Lipids (Alabaster, AL, USA) and Sigma, respectively, were stored at 20 g/l in spectroscopy-grade chloroform at −20 °C until use. Silica microbeads with a mean diameter of ~5 μm were purchased from Bangs Laboratories, Inc. (Fishers, IN). Dextran 500 and PEG 8 were from Sigma, Ficoll 70 was from GE Healthcare and Salmon sperm DNA was from Wako Pure Chemical Industries (Japan). Working buffers used are specified in their corresponding chapters in the results section. HiTrap prepacked columns for ionic exchange, size exclusion and $Ni^{2+}$-NTA affinity chromatography were from GE Healthcare. Alexa Fluor 488 and Alexa Fluor 647 carboxylic acid succinimidyl ester dyes were purchased from Molecular Probes/Thermo Fisher Scientific. Analytical grade chemicals and GTP nucleotide were from Merck.

# EXPRESSION, PURIFICATION AND FLUORESCENT LABELING OF PROTEINS

### FtsZ and FtsZ$\Delta_{Cter}$ mutant

Wild-type *E. coli* FtsZ was purified following the procedure described elsewhere (Rivas et al., 2000). FtsZ was overproduced in BL21 cells transformed with the plasmid pMFV56 by induction with 1 mM IPTG at 37 °C for 3 hours. Cells were harvested by centrifugation (10000 ×*g*, 10 min at 4 °C) and stored at -80 °C until use. The pellet corresponding to 2 l of culture was resuspended in 50 mM PIPES pH 6.5, 5 mM $MgCl_2$, 1 mM EDTA, lysed through sonication and centrifuged (120000 ×*g*, 1 h at 4 °C) to obtain the soluble fraction containing FtsZ. The protein was then subjected to two calcium-induced precipitation cycles. Each cycle consisted in the addition of 20 mM $CaCl_2$ and 1 mM GTP and incubation at 30 °C (15 min) followed by centrifugation (13500 ×*g*, 15 min at 4 °C). The pellet with FtsZ was resuspended in the same buffer without calcium and centrifuged as previously to remove any insoluble material. Finally, the protein was further purified by ionic exchange chromatography by loading the solution with the protein in a 5 ml HiTrap Q HP column equilibrated in 50 mM Tris-HCl pH 8.0, 5 mM $MgCl_2$, 0.1 mM EDTA, 10% glycerol. FtsZ was then eluted with a 0 - 100% gradient of the same buffer with 1 M

KCl at a flow rate of 1 ml/min. Collected fractions with the protein (2 ml) were joined and stored in aliquots at -80 °C. FtsZ obtained through this protocol was bound to GDP (Rivas et al., 2000). The FtsZ mutant (FtsZΔ$_{Cter}$) lacking residues 315-383 (i.e., the C-terminal peptide and the unstructured region of FtsZ) was expressed and purified following the protocol described above for wild-type FtsZ. The expression vector pET11b encoding for FtsZΔ$_{Cter}$ was a kind gift of P. Schwille (Max Planck Institute of Biochemistry). Protein purity was verified by SDS-PAGE and its GTPase activity was determined by quantification of the inorganic phosphate released using BIOMOL® GREEN assay. The concentration of both FtsZ and FtsZΔ$_{Cter}$ was calculated from their molar absorption coefficients at 280 nm (14000 $M^{-1}$ $cm^{-1}$ and 7800 $M^{-1}$ $cm^{-1}$, respectively) experimentally determined by quantitative amino acid analysis and colorimetric protein assay using Coomassie Brilliant Blue G-25 reagent (Bio-Rad) as described for FtsZ wild-type (Rivas et al., 2000).

**SlmA**

SlmA was purified essentially as described (Cho et al., 2011). H-SUMO-SlmA was expressed in BL21 cells transformed with the plasmid pTB147, kindly provided by T. Bernhardt (Harvard Medical School, Boston, MA), by addition of 1 mM IPTG and incubation for 3 hours at 37 °C. Cells were harvested by centrifugation (10000 ×*g*, 10 min at 4 °C) and stored at -80 °C until use. The pellet corresponding to 1 l of culture was resuspended in 20 mM Tris-HCl pH 8.0, 500 mM NaCl, 0.1 mM $MgCl_2$ supplemented with 10 µg/ml DNase I, sonicated and centrifuged (120000 ×*g*, 1 h at 4 °C). The resulting soluble fraction containing H-SUMO-SlmA was loaded into a pre-equilibrated 5 ml His-TRAP FF column, washed with 10 ml of 0, 2 and 4% of the same buffer with 1 M imidazole and the protein was eluted with a 4 – 100% gradient at a flow rate of 1 ml/min. Fractions (1 ml) containing the protein were pooled and dialyzed in 50 mM Tris-HCl pH 8.0, 300 mM NaCl, 10% glycerol to remove the imidazole and the H-SUMO tag was subsequently cleaved with 6xHis-tagged SUMO protease. Finally, the untagged protein was separated from the released tag and the protease using a His-bind resin (Novagen) with nickel. Fractions of 0.5 ml corresponding to the flow-through containing SlmA were joined, aliquoted and stored at -80 °C. Protein purity was verified by SDS-PAGE. SlmA concentration was determined from its molar absorption coefficient at 280 nm (9970 $M^{-1}$ $cm^{-1}$) estimated from its sequence.

### MatP

MatP was purified following a previously described method (Dupaigne et al., 2012), with modifications. $His_6$-MatP was expressed from the plasmid kindly provided by M. Schumacher (Duke University). *E. coli* strain BL21 cells transformed with the expression vector (pET15b plasmid with the gene encoding $His_6$-MatP subcloned) were grown in LB media supplemented with 50 µg/ml ampicillin at 37 °C to an $OD_{600}$ of 0.6 and the expression of the protein was induced for 3 hours at the same temperature by addition of 1 mM IPTG. Cells were harvested (1000 ×*g*, 10 min at 4 °C) and stored at -80 °C. The pellet corresponding to 2 l of culture was resuspended in 20 mM Tris-HCl pH 8.0, 500 mM NaCl, 1 mM $MgCl_2$, 5 mM imidazole (supplemented with 10 µg/ml DNase I). Cells were lysed through sonication and centrifuged (120000 ×*g*, 1 hour at 4 °C). The supernatant with the soluble protein was incubated for 30 min with a His-bind resin (Novagen) with nickel and washed stepwise with 20 mM Tris-HCl pH 8.0, 500 mM NaCl buffer with increasing concentrations of imidazole ($His_6$-MatP eluted at 200 mM imidazole). $His_6$-MatP was dialyzed against 20 mM HEPES pH 7.5, 200 mM NaCl, 1 mM EDTA and 10% glycerol, the $His_6$ tag was subsequently removed by cleavage with thrombin (10 U per mg of $His_6$-MatP) during 1 hour at room temperature. The untagged protein was obtained after ion-exchange chromatography using a HiTrap SP HP column with a 0 – 100% gradient of the same buffer with 1 M NaCl at a flow rate of 0.5 ml/min. Fractions (0.5 ml) containing MatP were pooled, dialyzed against 50 mM Tris-HCl pH 7.5, 300 mM KCl, 1 mM EDTA, 10% glycerol, and kept at −80 °C in aliquots. Protein concentration was calculated from its molar absorption coefficient at 280 nm (27960 $M^{-1}cm^{-1}$) estimated from its sequence. Protein purity was confirmed by SDS-PAGE.

### Fluorescent labeling of proteins

FtsZ and $FtsZ\Delta_{Cter}$ were covalently labeled in the amino groups with Alexa Fluor 488 (FtsZ-Alexa 488 and $FtsZ\Delta_{Cter}$-A488) or Alexa Fluor 647 (FtsZ-Alexa 647 and $FtsZ\Delta_{Cter}$-A647) carboxylic acid succinimidyl ester dyes following the protocol described for wild-type FtsZ in (Gonzalez et al., 2003). Polymerization of 75 µM FtsZ or $FtsZ\Delta_{Cter}$ was induced in buffer 20 mM HEPES pH 8.0, 50 mM KCl, 5 mM $MgCl_2$, 1 mM EDTA by addition of 2 mM GTP and 20 mM $CaCl_2$ prior to incubation with the reactive dye (protein:dye ratio of 1:2) to reduce possible interferences of the dye with protein polymerization. The reaction was allowed to proceed for 15 min at 30 °C followed by centrifugation (125000 ×*g*, 15 min at 4 °C). Polymers were resuspended in the same buffer without $CaCl_2$ and the remaining free dye

was removed through size-exclusion chromatography using a 5 ml Hi-Trap desalting column pre-equilibrated in 50 mM Tris-HCl pH 7.5, 500 mM KCl, 5 mM $MgCl_2$. Fractions (0.25 ml) with the labeled protein were pooled and stored at −80 °C in aliquots.

Covalent labeling of SlmA with Alexa Fluor 488 (SlmA-Alexa 488) or Alexa Fluor-647 (SlmA-Alexa 647) carboxylic acid succinimidyl ester dye was conducted as early stated (Cabre et al., 2015). Labeling of MatP with Alexa Fluor 488 (MatP-Alexa 488) was carried out following a similar protocol. The reaction was performed at pH 7.5 (buffer 50 mM HEPES pH 7.5, 300 mM KCl, 1 mM EDTA) to promote selective labeling of the N-terminal residue of the protein (Royer and Scarlata, 2008). SlmA (33 μM) or MatP (58 μM) were incubated with the dye in a protein: dye ratio of 1:5 (SlmA-Alexa 488), 1:7 (SlmA-Alexa 647) or 1:2 (MatP-Alexa-488). The reaction was allowed to proceed for 1 hour (SlmA) or 30 min (MatP) at room temperature. Finally, the free dye was removed by size-exclusion chromatography using a 5 ml Hi-Trap desalting column pre-equilibrated in 50 mM Tris-HCl pH 7.5, 300 mM KCl, 1 mM EDTA and fractions (0.25 ml) with the labeled protein were pooled, aliquoted and stored at −80 °C.

In all cases, the labeling ratio determined from the molar absorption coefficients of the specific protein and the dye ($\varepsilon_{495nm}$ Alexa 488 = 71000 $M^{-1}cm^{-1}$; $\varepsilon_{650nm}$ Alexa 647 = 270000 $M^{-1}cm^{-1}$) was always below 1.0 moles of dye/mole of protein.

## SPECIFIC DNA OLIGONUCLEOTIDES HYBRIDIZATION

Double-stranded DNA containing the binding sequences of SlmA and MatP (5′-AAGTAAGTGAGCGCTCACTTACGT-3′ and 5′-AAAGTGACACTGTCACCTT-3′, SBS (Cho et al., 2011) and *matS* (Mercier et al., 2008) respectively; bases recognized by the proteins are underlined) were obtained after hybridization of complementary oligonucleotides. Shortly, high-performance liquid chromatography (HPLC)-purified oligonucleotides were hybridized in a thermocycler by heating at 85 °C and gradually cooling down to 4 °C and stored at -20 °C until use. Oligonucleotides were purchased from IBA GmbH, Microsynth, Invitrogen or IDT, unlabeled or fluorescently modified with Alexa Fluor 647 or fluorescein attached to the 5' end. Fluorescently labeled sense oligonucleotides were hybridized with a 10% excess of the unlabeled complementary strand.

# PREPARATION OF CROWDERS, PHASES FOR LLPS SYSTEMS AND LABELING OF PEG

### Preparation of dextran 500, PEG 8, Ficoll 70 and fluorescent labeling of PEG 8

Dextran 500, PEG 8 and Ficoll 70 crowder agents were directly dissolved in 50 mM Tris-HCl pH 7.5 with 100 or 300 mM KCl, dialyzed in the same buffer and their concentration estimated from the refractive index increment (dextran 500, 0.142 ml/g; PEG 8, 0.136 ml/g and Ficoll 70, 0.141 ml/g) as earlier described (Monterroso et al., 2016b).

Amino-functionalized PEG 8 ($NH_2$-PEG-$NH_2$ from Nanocs) was covalently labeled in the amino derivate groups with Alexa Fluor 488 (PEG-Alexa 488) or Alexa Fluor 647 (PEG-Alexa 647) carboxylic acid succinimidyl ester. The reaction was conducted in 50 mM sodium borate pH 8.5 for 4 hours at room temperature followed by size-exclusion chromatography using a HiTrap desalting column to remove the free dye. Fractions with labeled PEG 8 were pooled and the concentration of dye determined from its molar absorption coefficient (stated above).

### Unspecific DNA fragmentation and purification

Salmon sperm DNA was fragmented and purified following a method (Monterroso et al., 2016b) based on the phenol:chloroform:isoamyl alcohol extraction procedure described elsewhere (Biswas et al., 2012). Briefly, DNA was dissolved in Milli-Q water and mixed with an equal volume of a phenol:chloroform solution. The mixture was centrifuged and the aqueous phase containing the DNA separated from the organic phase and the material at the interface. Finally, the DNA was subjected to precipitation with ethanol, centrifuged, dried under vacuum and resuspended in 50 mM Tris-HCl pH 7.5, 300 mM KCl. Purified DNA (≤ 300 bp) was stored at -20 °C and its concentration determined from its dry weight after purification.

# BIOPHYSICAL CHARACTERIZATION OF PROTEIN-PROTEIN AND PROTEIN-DNA INTERACTIONS IN SOLUTION

## Sedimentation velocity assays

The self-association of FtsZ$\Delta_{Cter}$ in the absence of GTP (chapter 2) as well as the interaction of SlmA (chapter 3) and MatP (chapter 4) with their respective DNA specific sequences was studied by sedimentation velocity (SV). This technique allows the detection and quantitative analysis of the formation of macromolecular complexes from the distribution of sedimentation coefficients (Howlett et al., 2006). SV experiments were conducted in an Optima XLA equipped with UV-VIS absorbance optics or an Optima XLI with integrated UV-VIS and Raleigh interference optics (Beckman-Coulter Inc.) using an An-50Ti rotor and 12 mm double sector centerpieces. Sedimentation velocity profiles of samples centrifuged at 48000 rpm and 20 °C were recorded at 260 nm or at 230 nm. Sedimentation coefficient distributions were calculated by least squares boundary modeling of sedimentation velocity data using the *c(s)* method with SEDFIT (Schuck, 2000). Calculated sedimentation coefficient values (*s*) were corrected to standard conditions using the program SEDNTERP (Laue, 1992) to obtain the corresponding standard s values ($s_{20,w}$).

## Size exclusion chromatography coupled to multiangle static light scattering (SEC-MALS) measurements

SEC-MALS assays are based on the separation of macromolecular complexes through size exclusion chromatography and parallel measurement of the concentration of, and intensity of light scattered by, the eluting solution, allowing the determination of molecular weights (Folta-Stogniew and Williams, 1999). This method has been used in chapter 4 to calculate the molecular weight of MatP in the presence and absence of *matS*. SEC-MALS experiments were carried out at 20 °C in a DAWN-EOS multiangle laser light scattering photometer (Wyatt Technology Corp) connected to an Optilab rEX differential refractometer configured to collect data simultaneously from the sample eluting from a coupled dextran-agarose column (Superdex 200 10/300 GL, Pharmacia Biotech, flow rate 0.5 ml/min). Loading solutions of MatP with and without *matS* were prepared as detailed

elsewhere (Cabre et al., 2015). The acquired raw data consisted of the scattering intensity at fourteen scattering angles and the differential refractive index of the species fractionated in the column. Recorded data were analyzed using ASTRA (V.4.90, Wyatt Technology) to determine the average molecular masses from the ratio of scattering to concentration at the peak maximum.

**Fluorescence anisotropy binding experiments**

Anisotropy measurements were performed to investigate the binding of MatP to *matS*-Fl in chapter 4. This is a highly sensitive method for the detection and quantification of molecular associations such as those leading to the formation of complexes larger than the free species, as it depends on the rotational diffusion of the fluorescent molecules (Pollard, 2010). Due to its sensitivity, it allows the evaluation of high-affinity interactions under equilibrium conditions. Experiments were conducted in 50 mM Tris-HCl pH 7.5, 5 mM $MgCl_2$ buffer with 300 or 500 mM KCl using a POLARstar Galaxy Plate Reader (BMG Labtech) at 26 °C, equipped with 485 and 520 nm excitation and emission filters, respectively. The concentration of 10 nM fluorescein-labeled *matS* (*matS*-Fl) in the titrations with MatP was selected as a compromise to determine binding parameters under equilibrium conditions while still getting a good signal to noise ratio. The presence of MatP did not alter the emission intensity of fluorescein. Binding isotherms obtained under our experimental conditions were analyzed with BIOEQS software (Royer et al., 1990) assuming a model in which one dimer of MatP binds to one molecule of DNA (according to the stoichiometries determined by SV and SEC-MALS; see chapter 4), in terms of the free energy of formation of the postulated complex from its individual components. Uncertainties associated with the $\Delta G$ values were assessed by rigorous confidence limit testing at 67% with the same software. BIOEQS uses a numerical solver engine based on a Marquardt-Levenberg algorithm, allowing analysis of binding isotherms with no assumption regarding the concentration of any of the species involved in the interaction (Royer et al., 1990, Royer and Beechem, 1992). This is important as, due to instrumental limitations, the concentration of DNA used in the titrations was only slightly lower than the *Kd* retrieved for the interaction, a condition that would have precluded the use, if needed, of simplified analysis models that assume the concentration of free protein equals that of total protein across the titration (Beckett, 2011, Pollard, 2010, Rippe, 1997).

# CHARACTERIZATION OF PROTEIN-MEMBRANE INTERACTIONS

## Binding assays with lipid-coated microbeads

Protein-membrane interactions can be quantitatively analyzed using lipid-coated microbeads. This assay allows unambiguous determination of the fraction of unbound protein remaining in the supernatant (and therefore the fraction of bound protein) after incubation with the lipid-coated microbeads and successive centrifugation to sediment them (**Figure M.1**) (Martos et al., 2012a). Lipid-coated microbeads experiments were performed to study the interaction of SlmA with membranes in the presence and absence of its binding partners (chapter 3) as well as to investigate the binding of MatP with and without *matS* to lipids (chapter 4).

Microbeads coating with *E. coli* lipids or L-α-phosphatidylcholine, binding assessment and theoretical estimation of the accessible lipid concentration were carried out as described (Sobrinos-Sanguino et al., 2017b). Briefly, silica microbeads were washed by centrifugation (1000 ×*g*, 5 min at 4 °C) followed by resuspension in 30% ethanol 3 times. Microbeads were then subjected to a final wash with 1% ethanol (spectroscopic grade) and dried by vacuum centrifugation. The pellet with the microbeads was resuspended in 50 mM Tris-HCl pH 7.5, 300 or 100 mM KCl, 5 mM $MgCl_2$ and incubated with EcL or PC during 90 min at 4 °C with gentle shaking. Finally, the excess of lipid was removed by six successive cycles of centrifugation (1000 ×*g*, 5 min at 4 °C) and resuspension in the same buffer with a sonication step after 3 cycles to get even coating of the microbeads.

In chapter 3, the binding of 0.5 µM SlmA (with 0.25 µM SlmA-Alexa 488 as a tracer) to a variable concentration of coated silica microbeads was explored at different KCl concentrations. Experiments to study the recruitment of SBS sequences by SlmA in the presence of FtsZ were performed at a constant concentration of 150 g/l of microbeads (266 µM accessible lipids) while varying the concentration of FtsZ, SlmA and SBS-Fl (keeping the ratio at 12:5:1, respectively) or varying only FtsZ (at constant 0.5 µM SlmA and 0.125 µM SBS-Fl). Binding measurements of MatP (various concentrations) to lipids in chapter 4 were conducted at various ionic strengths using 0.125 µM of MatP-Alexa 488 as a tracer and 20 g/l microbeads (35 µM accessible lipids). The influence of the specific DNA on the interaction was assessed by addition of *matS* to samples containing 0.25 µM MatP-Alexa 488 prior to or after incubation with the attached lipids. In

addition, experiments were also performed following the signal of fluorescein-labeled *matS* (0.1 μM) in the presence of 0.25 μM MatP. After 20 min incubation with the lipid-coated microbeads, samples were centrifuged, and the concentration of the labeled element remaining in the supernatant was quantified using a fluorescence plate reader (Varioskan Flash, Thermo, or POLARstar Galaxy, BMG Labtech) as described previously (Sobrinos-Sanguino et al., 2017b). In all cases, the linearity of the fluorescence intensity emission of the labeled species with its concentration was verified.

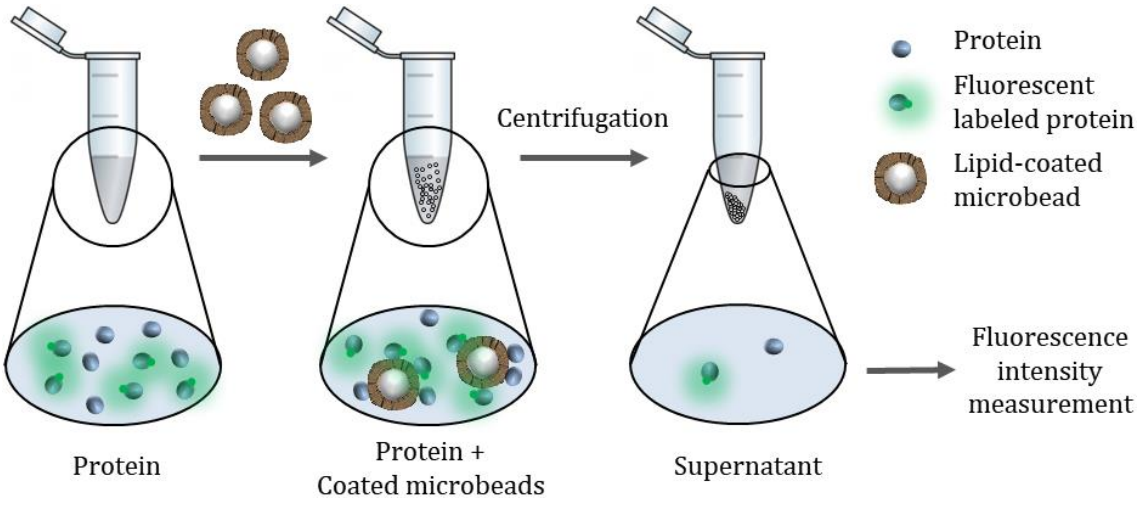


**Figure M.1. Overview of a binding experiment using lipid-coated microbeads.** From left to right, it is represented a solution containing the protein with fluorescently labeled protein as a tracer. Incubation with lipid-coated microbeads allows the protein to interact with the lipids. After centrifugation, the coated-microbeads along with the bound protein sediment and the concentration of unbound protein can be determined from the fluorescence signal in the supernatant.

Binding isotherms were analyzed or simulated, using user-written scripts and functions in MATLAB (ver. 7.10; MathWorks, Natick, MA), by nonlinear least-squares fit of a Langmuir adsorption isotherm to the experimental data:

**Eq.M.1:**
$$y = y_{max}\frac{(c/c_{50})}{1+(c/c_{50})}$$

where $y$ and $y_{max}$ are the response and maximum response recorded upon binding, respectively, $c$ is the concentration of the species that was varied (MatP, or lipids in the case of the binding of SlmA), and $c_{50}$ is the concentration of variable species at which binding is half of the maximum value.

### Fluorescence anisotropy-based competition experiments

The competition of SBS and *matS* with the lipids for their respective binding partners, SlmA and MatP, was analyzed by fluorescence anisotropy measurements coupled to microbead binding assays. The preformed nucleoprotein complexes formed by SlmA and the SBS (chapter 3) or by MatP and *matS* (chapter 4) were incubated at variable concentrations of *E. coli* lipid-coated microbeads. After incubation, the mixture was subjected to low-speed centrifugation and the anisotropy of the supernatant measured in a POLARstar Galaxy Plate Reader (BMG Labtech) at 26 °C. Competition of the lipids with the DNA for the protein increases the fraction of free labeled DNA in the supernatant, rendering lower values of anisotropy (**Figure M.2**). Addition of the protein to a mixture of lipid-coated microbeads with the DNA or addition of the preformed nucleoprotein complexes to the lipids rendered equivalent results. Represented values are the increase in anisotropy due to protein binding to lipids with respect to the measured anisotropy of the free DNA.

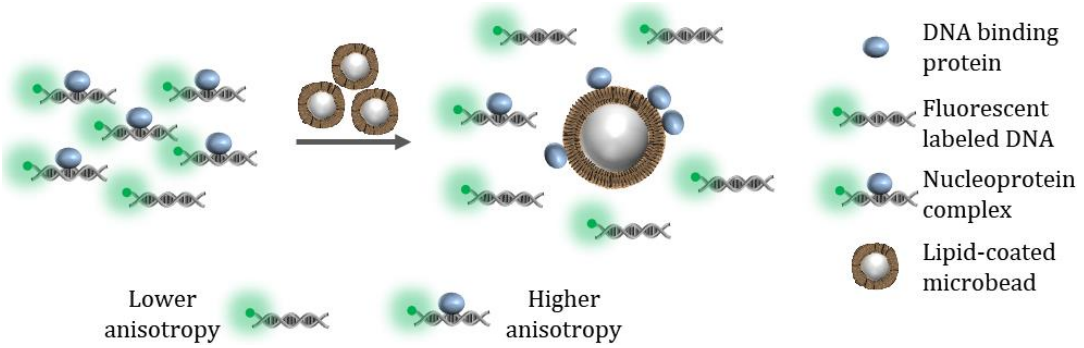


**Figure M.2. Scheme of anisotropy-based competition experiments.** From left to right, DNA-binding proteins are bound to their specific DNA sequences labeled with fluorescein. After addition of coated microbeads, the lipids compete with the specific DNA sequences and the protein can dislodge from the DNA to bind to the lipid-coated microbeads, rendering lower anisotropy values due to the increase in the fraction of free DNA

### Biolayer interferometry measurements

Interaction of proteins with membranes can be measured using biolayer interferometry, in which the change in the refractive index caused by the binding of a protein to an immobilized lipid membrane in a biosensor tip is followed. Interaction of SlmA (chapter 3) and MatP (chapter 4) with lipids was detected by biolayer interferometry using a single-channel BLItz system (ForteBio). Lipids were immobilized on aminopropylsilane biosensor tips by immersion into a 0.5 g/l small unilamellar vesicles (SUVs) solution. SUVs were prepared shortly before the

experiments following a protocol consisting in the sonication of a multilamellar vesicles suspension obtained after rehydration of a dried lipid film to a final concentration of 4 g/l (Martos et al., 2015). SlmA and MatP binding to the immobilized lipids were recorded at the specified protein concentrations at room temperature and with vigorous shaking (2200 rpm). Interaction of MatP with the coated biosensor tip was also followed in the presence of increasing concentrations of *matS*. Binding isotherms in chapter 4 were constructed by representing the experimental binding values at equilibrium versus the MatP total concentration. Analysis was conducted by nonlinear least-squares fit of a Langmuir adsorption isotherm to the experimental data, as described above for lipid-coated microbeads assays.

## CHARACTERIZATION OF PHASE-SEPARATED BIOMOLECULAR CONDENSATES

### Preparation of phases for LLPS systems

Individual enriched phases of PEG/dextran and PEG/DNA LLPS systems were prepared following the protocol described in (Monterroso et al., 2016b). Shortly, a mixture of PEG 8 with dextran 500 or unspecific DNA was thoroughly mixed by vortexing at the nominal concentration rendering phase separation followed by low-speed centrifugation. The enriched phase of each crowder was then separated and stored at -20 °C until use. The concentration of DNA at which it phase-separated from PEG 8 varied slightly among purifications, probably due to differences in the estimation of DNA concentration that did not affect the behavior of the division elements in this LLPS system.

### Preparation of bulk samples

Preparation of bulk samples for confocal microscopy visualization to study the condensates formed by FtsZ and SBS-bound SlmA (chapter 1) or only by FtsZ or the mutant FtsZ$\Delta_{Cter}$ (chapter 2) were prepared by direct addition of the proteins to solutions containing the crowder. For imaging, species labeled with fluorescein (SBS-Fl), Alexa 488 or Alexa 647 (0.5 – 1 μM) were included as tracers. When stated, polymerization of FtsZ was triggered by addition of GTP directly over the mixture. Besides, condensates formed by FtsZ and SlmA (chapter 1) were also studied in biphasic systems to analyze the influence of the presence of different

microenvironments. Proteins were directly added to emulsions containing the PEG/dextran or PEG/DNA LLPS systems, prepared by vigorous mixing of the PEG-rich with the dextran-rich or the DNA-rich phases in a 3:1 volume ratio as described (**Figure M.3**) (Monterroso et al., 2016b). The localization of proteins and the double-stranded SBS oligonucleotide in the LLPS system was assessed from the colocalization with a tracer amount (1 μM) of PEG labeled with Alexa 488 or Alexa 647 depending on the dye attached to the protein or SBS. Images were acquired with different combinations of dyes (FtsZ-Alexa 488, SlmA-Alexa 488, and SBS-Fl with PEG-Alexa 647; FtsZ-Alexa 647 and SlmA-Alexa 647 with PEG-Alexa 488) with equivalent results.

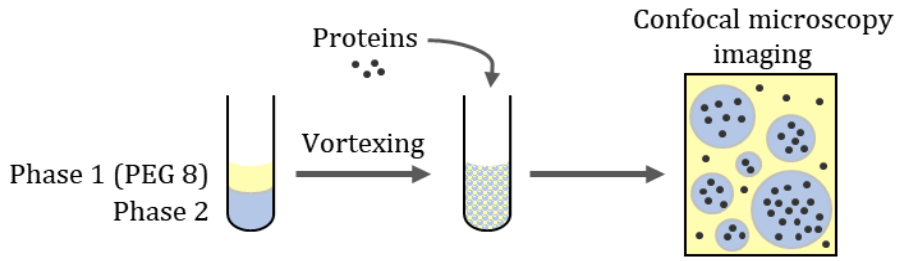


**Figure M.3. Scheme of preparation of bulk LLPS system emulsion for confocal microscopy.** From left to right, the LLPS system formed by two different phases, one being PEG 8, is thoroughly mixed by vortexing. Proteins are added on top of the emulsion and the distribution of the protein within phases is analyzed by visualization with a confocal microscope.

### Determination of the partition of division elements in LLPS systems by fluorescence spectroscopy measurements

Partition of components within the PEG/dextran mixture reported in chapter 1 was determined as described (Monterroso et al., 2016b). Briefly, 0.5 μM of Alexa 488-labeled proteins or fluorescein-labeled SBS (as tracers) and unlabeled species up to the final concentration were gently mixed with the emulsion containing the two phases in a 1:1 volume ratio and the mixture was allowed to equilibrate for 30 min. After centrifugation, phases were isolated and the fluorescence intensity of each phase was measured in a POLARstar Galaxy (BMG Labtech) or Varioskan (Thermo) plate reader (**Figure M.4**). Concentrations of proteins or SBS in the enriched phases were estimated by comparison with samples containing known amounts of tracer in the same phase. Control measurements showed that tracer signals were in all cases linear with total concentration. Data shown correspond to the average of three independent measurements, or six in the case of the samples with the three components, ± SD.

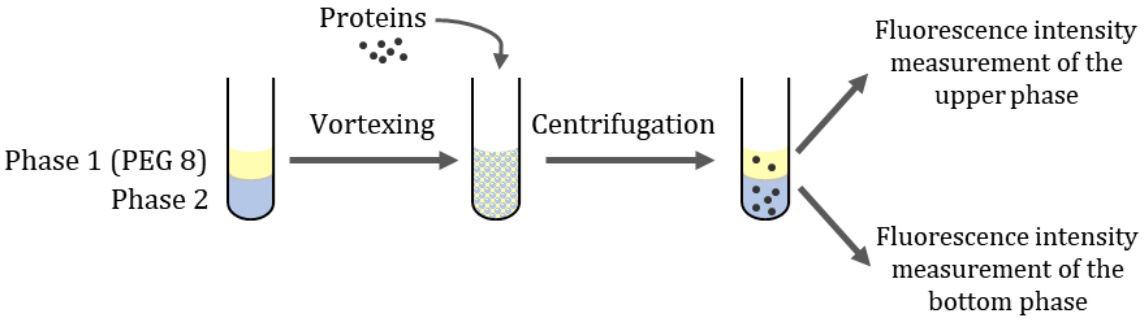


**Figure M.4. Scheme of preparation of bulk LLPS system emulsion.** From left to right, the two phases that form the LLPS system are vigorously mixed and proteins are added over the emulsion formed. After centrifugation, the fluorescence signal in each separated phase can be measured allowing determination of the concentration and, therefore, the partition of elements between phases.

### Characterization of condensate dynamism based on protein capture

To test the dynamism of condensates formed by FtsZ in the presence and absence of SlmA, their ability to capture freshly added FtsZ was studied by confocal microscopy. Samples with FtsZ labeled with Alexa-488 or Alexa-647 in the presence (chapter 1) and absence (chapter 2) of SlmA ± SBS at the specified concentrations and conditions were prepared and imaged before and after addition of FtsZ labeled with the complementary dye (FtsZ-Alexa 647 or FtsZ-Alexa 488, respectively). Diffusion of the added labeled protein into the condensates was followed over time. Assays with the mutant protein ($FtsZ\Delta_{Cter}$) were performed using the same protocol (chapter 2).

### Turbidity measurements

Condensates are large particles that scatter light; hence, their formation under different conditions can be studied following the absorbance signal recorded at 350 nm (Alberti and Dormann, 2019). In chapter 1, turbidity experiments were performed to study the assembly of FtsZ into condensates in the presence of SlmA and its specific SBS sequences. The turbidity of samples (200 µl solutions) containing 12 µM FtsZ, 5 µM SlmA, and 1 µM SBS with and without Ficoll 70 or dextran 500 (150 g/l) or PEG 8 (50 g/l) was determined at room temperature using a Varioskan Flash plate reader (Thermo). The absorbance at 350 nm, measured every 10 min for 140 min, was stable during this time period. To determine the effect of different concentrations of FtsZ, SlmA, and SBS or of KCl (in 150 g/l dextran) or the effect of dextran concentration (at 12 µM FtsZ, 5 µM SlmA, and 1 µM SBS at 300 mM KCl), additional turbidity measurements were conducted.

These samples were incubated at room temperature for 30 min. Absorbance values were stable for, at least, 10 min after incubation.

For the study of the assembly of FtsZ into biomolecular condensates described in chapter 2, turbidity measurements of samples aimed at determining the effect of crowders, salts or FtsZ concentration on condensate formation, and their response to GTP addition, were conducted following a protocol similar to the procedure described above. The absorbance at 350 nm of 125 µl solutions was recorded after 30 min incubation. For time dependence measurements, data were taken every 5 min. Concentration saturation values ($c_{sat}$) corresponding to the concentration of FtsZ above which condensates are formed under the specified conditions were determined from the dependence of the turbidity signal with protein concentration. Data was analyzed by fitting a linear function, rendering a $c_{sat}$ value corresponding to the x-intercept.

# MICROFLUIDIC ENCAPSULATION IN MICRODROPLETS AND GENERATION OF VESICLES

### Microfluidic Chip Preparation

Devices were fabricated using conventional soft lithographic techniques as stated elsewhere (Mellouli et al., 2013) Briefly, polydimethyl siloxane (PDMS) base Sylgard™ 184 and curing agent (Dow Corning GmbH, Germany) were mixed in a 10:1 (w/w) ratio, degassed, decanted onto masters and kept overnight at 65 °C. Design of masters is detailed in (Mellouli et al., 2013) Solid PDMS was peeled from the master, inlet and outlet holes were punched and the channels sealed by a glass slide after surface activation by oxygen plasma (Diener electronic GmbH, Germany). Finally, devices were coated with a hydrophobic layer by treatment with Aquapel (Pittsburgh Glass Works, LLC) directly flushed in the channels and allowed to dry overnight at 65 °C.

### Encapsulation of solutions inside microdroplets

Microfluidics techniques allow the generation of hundreds of monodispersed water-in-oil microdroplets stabilized by a surfactant (Theberge et al., 2010). In the present doctoral thesis, different samples have been encapsulated by means of

microfluidics in microdroplets stabilized by the mixture of *E. coli* lipids to perform studies in environments mimicking inner cell features as confinement and the presence of a lipid surface. Additionally, encapsulation of solutions containing crowders or LLPS systems allowed us to reproduce other conditions found inside the cell as crowding and compartmentalization.

*E. coli* lipids dispersed in mineral oil and aqueous phases were loaded into Hamilton syringes that were connected to inlet holes in the fabricated chip (**Figure M.5A**) and solution flows were controlled using automated syringe pumps (Cetoni GmbH, Germany). *E. coli* lipids (20-25 g/l) in mineral oil were freshly prepared by resuspension (by two cycles of vortex and sonication) of the lipid film formed after evaporation of the chloroform in which lipids were stored with a SpeedVac device. Generation of microdroplets is achieved at the production junction where the oil stream (135-160 µl/h) meets the two aqueous solutions, typically mixed in a 1:1 ratio just before reaching this point (**Figure M.5B**).

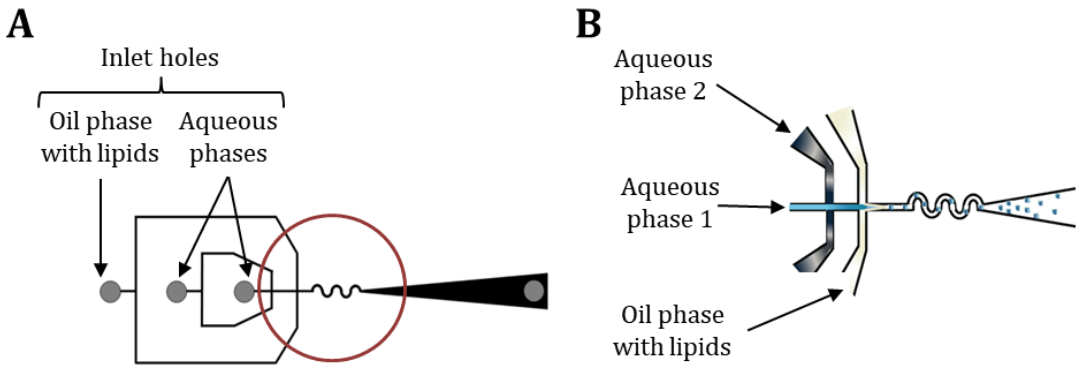


**Figure M.5. Illustration of microdroplet chip design and encapsulation.** (A) Scheme depicting the design imprinted in the PDMS polymer consisting in three inlets for the oil phase (with the mixture of *E. coli* lipids) and the aqueous phases. (B) Amplification of the portion marked with a red circle in (A) corresponding to the production junction. Droplets form at this point when the two aqueous solutions (mixed shortly before) meet the oil phase with *E. coli* lipids. (B) Adapted from (Sobrinos-Sanguino et al., 2017a).

For the encapsulation of homogeneous solutions, either in diluted or crowded conditions, the proteins and the specific DNA (when present) were included in both aqueous phases at the corresponding final concentration or only in one of them at double concentration. When crowder agents were used, they were present in both aqueous streams at final concentration. Production of droplets was conducted at final flow of 20 µl/h for the total aqueous solution yielding uniform droplets. Encapsulation of LLPS systems described in chapter 1 was conducted by mixing the PEG stream and the other one with either dextran or purified salmon

sperm DNA basically as described (Sobrinos-Sanguino et al., 2017a). FtsZ was supplied in one of the aqueous phases and SlmA with or without the SBS was included in the other one. Solutions were delivered at 5 and 7 µl/h (dextran and PEG aqueous phases, respectively), or 6 µl/h (both DNA and PEG aqueous phases). In all cases, protein or DNA labeled with the stated dye were added as tracers (1 - 0.5 µM, final concentration) to the aqueous solutions. In those experiments in which the polymerization of FtsZ was triggered before encapsulation, GTP (2-4 mM) was supplied in the stream that did not contain FtsZ.

### Formation of Giant Unilamellar Vesicles from microdroplets

Giant Unilamellar Vesicles (GUVs) were formed by conversion of microdroplets generated by microfluidics as early stated (**Figure M.6**) (Sobrinos-Sanguino et al., 2017a). Briefly, microdroplets were collected for 30 min into 700 µl of oil phase with the *E. coli* lipids stabilized for at least 1 hour over 400 µl of outer solution (buffer used in the encapsulation supplemented with sucrose at a concentration to render an osmolarity ~25 mOsmol/Kg above the osmolarity of the encapsulated solutions). Collected droplets were centrifuged to force their passage toward the aqueous phase through the coated interface with oriented lipids, the oil phase removed and the droplets washed with outer solution.

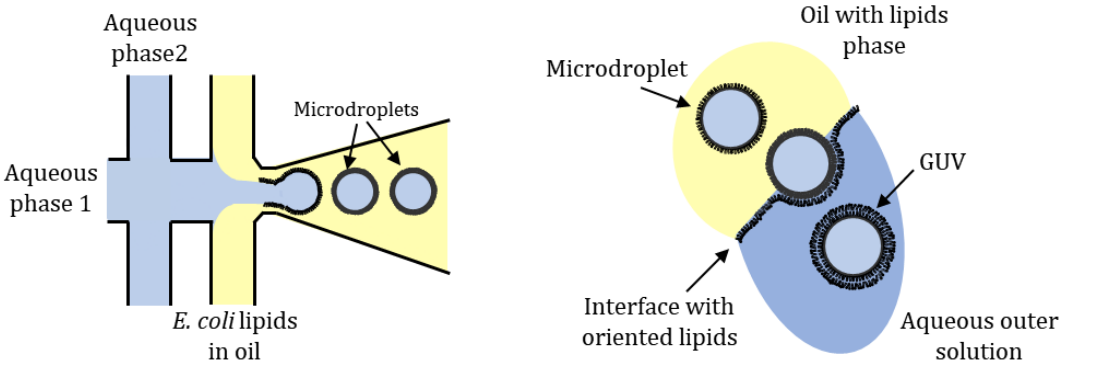


**Figure M.6. Scheme of the procedure to transform microdroplets into GUVs.** Left, scheme showing the encapsulation of two aqueous solutions (depending on the experiment the composition of the aqueous phases can be the same or different) into microdroplets using microfluidic techniques. Right, microdroplets generated by microfluidics acquire the bilayer after passage through the interface with oriented lipids. Figure adapted from (Monterroso et al., 2021).

# CONFOCAL MICROSCOPY MEASUREMENTS AND DATA ANALYSIS

Microdroplets, vesicles and bulk samples were visualized in silicone chambers (Molecular probes/Invitrogen) glued to coverslips. Image acquisition was performed with Leica TCS-SP2 or TCS-SP5 inverted confocal microscopes equipped with a HCX PL APO 63× oil immersion objective (N.A. = 1.4; Leica, Mannheim, Germany). 488 and 633 nm laser excitation lines were used to excite Alexa 488 and Alexa 647 dyes, respectively. Multiple images were registered across each sample, corresponding to different observation fields. Brightfield and fluorescence images were taken simultaneously.

Processing of images and analysis of data were carried out with ImageJ (National Institutes of Health, USA). When necessary, the brightness of the images was enhanced by applying a uniform correction using Microsoft PowerPoint. Production of merged images and data analysis were performed using the original images before brightness correction. Measurements of the distribution of sizes and generation of intensity profiles of the condensates described in chapter 1 were performed by applying the straight-line tool through their equatorial section. The area distribution of the condensates formed by FtsZ (chapter 2) was obtained using the particle analysis tool after noise reduction using a Kuwahara filter and threshold correction by visual inspection. Intensity profiles of microdroplets and GUVs in chapters 3 and 4 were obtained by applying the straight-line tool of the software through their equatorial section. In chapter 3, the intensity ratios were estimated by dividing the mean intensities at the two edges of a droplet by the mean intensity in the lumen.

# CHAPTER 1

# Bacterial FtsZ protein forms phase-separated condensates with its nucleoid-associated inhibitor SlmA

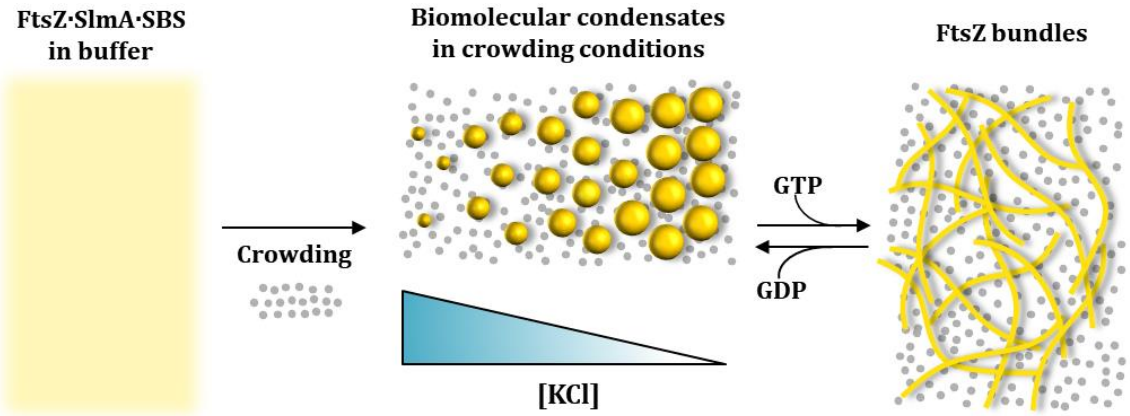


Macromolecular condensation resulting from biologically regulated liquid–liquid phase separation is emerging as a mechanism to organize intracellular space in eukaryotes, with broad implications for cell physiology and pathology. Despite their small size, bacterial cells are also organized by proteins such as FtsZ, a tubulin homolog that assembles into a ring structure precisely at the cell midpoint and is required for cytokinesis. Here, we demonstrate that FtsZ can form crowding-induced condensates, reminiscent of those observed for eukaryotic proteins. Formation of these FtsZ-rich droplets occurs when FtsZ is bound to SlmA, a spatial regulator of FtsZ that antagonizes polymerization, while also binding to specific sites on chromosomal DNA. The resulting condensates are dynamic, allowing FtsZ to undergo GTP-driven assembly to form protein fibers. They are sensitive to compartmentalization and to the presence of a membrane boundary in cell mimetic systems. This is a novel example of a bacterial nucleoprotein complex exhibiting condensation into liquid droplets, suggesting that phase separation may also play a functional role in the spatiotemporal organization of essential bacterial processes.

# RESULTS

## FtsZ from *Escherichia coli* forms biomolecular condensates upon interaction with SlmA in cell-like crowded conditions

FtsZ was found to form round structures compatible with liquid droplets in the presence of SlmA and a 24-bp oligonucleotide containing the consensus sequence targeted by this protein (SBS), in working buffer[1] under crowding conditions, as revealed by confocal microscopy imaging (**Figure 1.1A and B**). Condensates (1–6 µm diameter) were observed in solutions containing FtsZ labeled with Alexa 647 (FtsZ-Alexa 647), unlabeled SlmA, and fluorescein-labeled SBS (SBS-Fl), in which

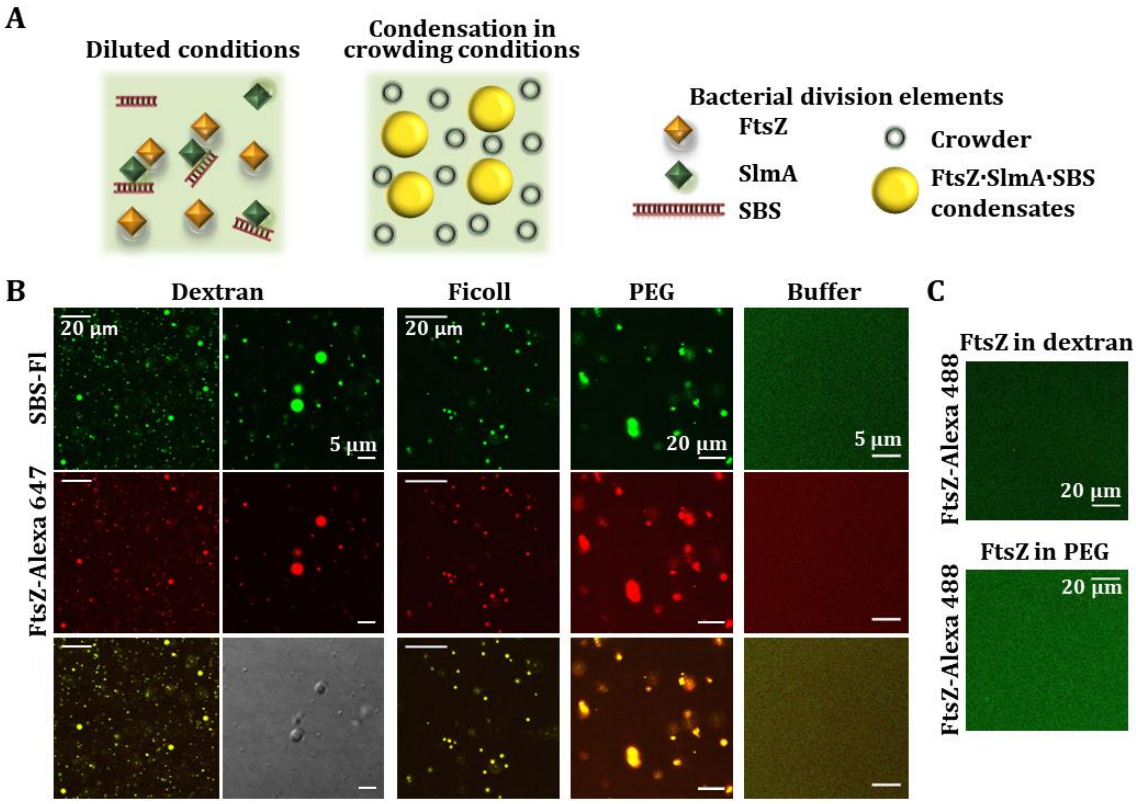


**Figure 1.1. Formation of condensates of FtsZ·SlmA·SBS in crowding conditions.** (A) Scheme of the *Escherichia coli* division elements involved in the formation of condensates. The concentrations of FtsZ, SlmA, and SBS used in this study were 12, 5, and 1 µM, unless indicated otherwise. (B) Representative confocal images of the FtsZ·SlmA·SBS condensates formed in 150 g/l dextran 500, Ficoll 70 or PEG 8, and absence of condensates in diluted solution. (C) Representative confocal images showing the absence of condensates at 40 µM FtsZ with no SlmA·SBS in 150 g/l dextran (top) or in 50 g/l PEG (bottom). All experiments were conducted in working buffer.

[1] Working buffer: 50 mM Tris-HCl, 300 mM KCl, 1 mM $MgCl_2$.

the two dyes colocalized, independently of the macromolecule used to crowd the solution (Ficoll, PEG, dextran; **Figure 1.1B**). These structures were not formed by FtsZ in the absence of SlmA·SBS (**Figure 1.1C**) or by FtsZ·SlmA·SBS complexes in the absence of crowding (**Figure 1.1B**). These findings were confirmed by turbidity experiments done in parallel (**Figure 1.2**).

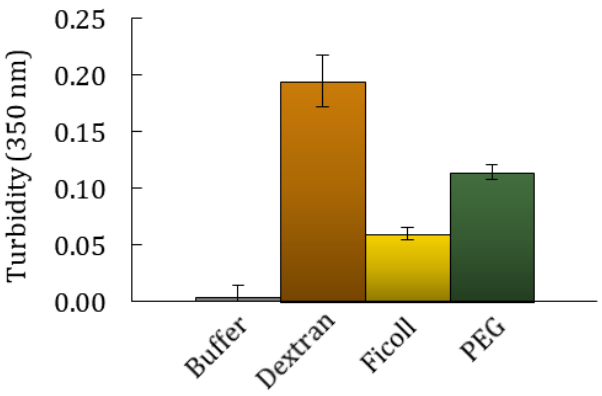


**Figure 1.2. Formation of FtsZ·SlmA·SBS condensates in crowding conditions monitored by turbidity.** Absorbance at 350 nm of FtsZ·SlmA·SBS in buffer (n = 3), in 150 g/l dextran 500 (n = 5) or Ficoll 70 (n = 3), and in 50 g/l PEG 8 (n = 3). Data correspond to the average ± SD. All experiments in working buffer.

To determine the factors influencing the formation of the condensates, confocal imaging and turbidity measurements were conducted on samples containing variable concentrations of the three elements (FtsZ, SlmA, and the SBS oligonucleotide), variable concentration of the crowding agent, and different ionic strengths. Condensation in dextran increased with the concentration of the two proteins and of the SBS oligonucleotide (**Figure 1.3**). When SlmA, but not the SBS, was added to FtsZ, condensates in which the two labeled proteins colocalized were also observed, although in considerably lower amounts (**Figure 1.4A and B**). In the absence of FtsZ, scarce condensates were found in SlmA solutions, with or without the SBS sequence (**Figure 1.4B and C**). Only at high concentrations of SlmA (40 μM), far beyond the physiological concentration, abundant structures with variable morphology (including rounded-like) were observed in the solutions (**Figure 1.4D**).

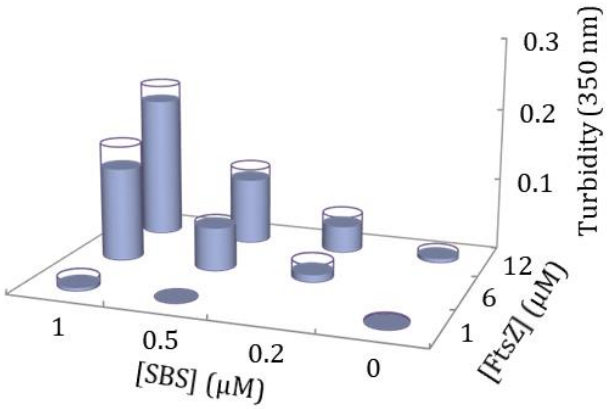


**Figure 1.3. Dependence of the formation of FtsZ·SlmA·SBS condensates on elements concentrations.** Formation of condensates as a function of FtsZ and SlmA·SBS concentration, as measured by turbidity, in working buffer with 150 g/l dextran 500. SlmA concentration was fivefold that of SBS (except at 0.5 μM SBS, where SlmA concentration was 3 μM). Data are the average of two independent measurements. Errors (SD), symmetrical, are depicted as white disks.

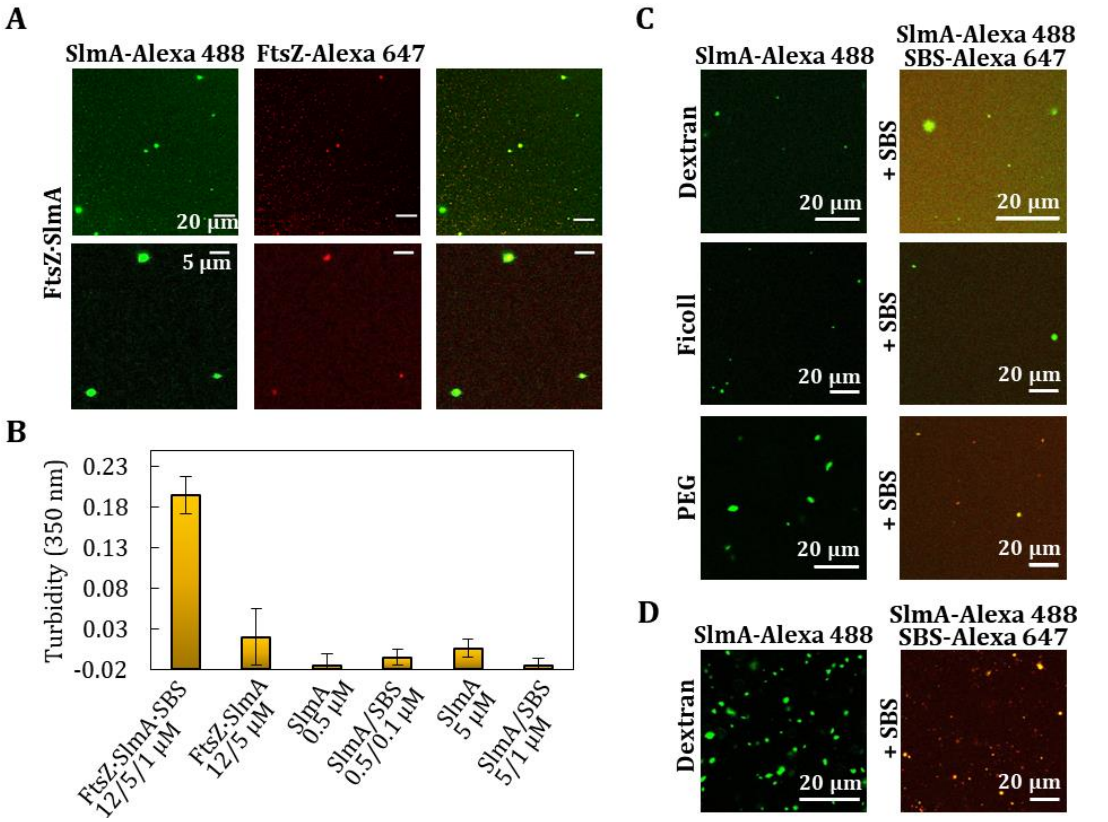


**Figure 1.4. Formation of condensates of SlmA ± FtsZ or SBS in crowding conditions.** (A) Representative confocal images of FtsZ and SlmA at 12 and 5 µM, respectively in 150 g/l dextran. (B) Measurements of turbidity of samples containing SlmA ± SBS in 150 g/l dextran. The samples containing FtsZ·SlmA ± SBS at 12, 5 and 1 µM, respectively, are included as a reference. Data are the average of 2 independent experiments ± SD, except for FtsZ·SlmA·SBS (n = 5). (C) SlmA condensates in the absence and presence of SBS in 150 g/l dextran or Ficoll and in 50 g/l PEG. Concentrations of SlmA and SBS were 5 and 1 µM, respectively. (D) SlmA condensates in the absence and presence of SBS in 150 g/l dextran. Concentrations of SlmA and SBS were 40 and 8 µM, respectively. All experiments were conducted in working buffer. In (A) the brightness of all images was enhanced (40%).

As for other biomolecular condensates (Woodruff et al., 2017), FtsZ·SlmA·SBS condensation increased with the concentration of the crowding agent, being detectable by turbidity above 50 g/l dextran (**Figure 1.5A**). The formation of these condensates was dependent on ionic strength. Reducing the concentration of KCl with respect to that in the working buffer (300 mM KCl) resulted in larger condensates, whereas at 500 mM KCl, small structures were observed, although still abundant (**Figures 1.5B and C**). This is likely related to the impact of ionic strength on the electrostatic interactions among positively charged SlmA and negatively charged FtsZ and SBS.

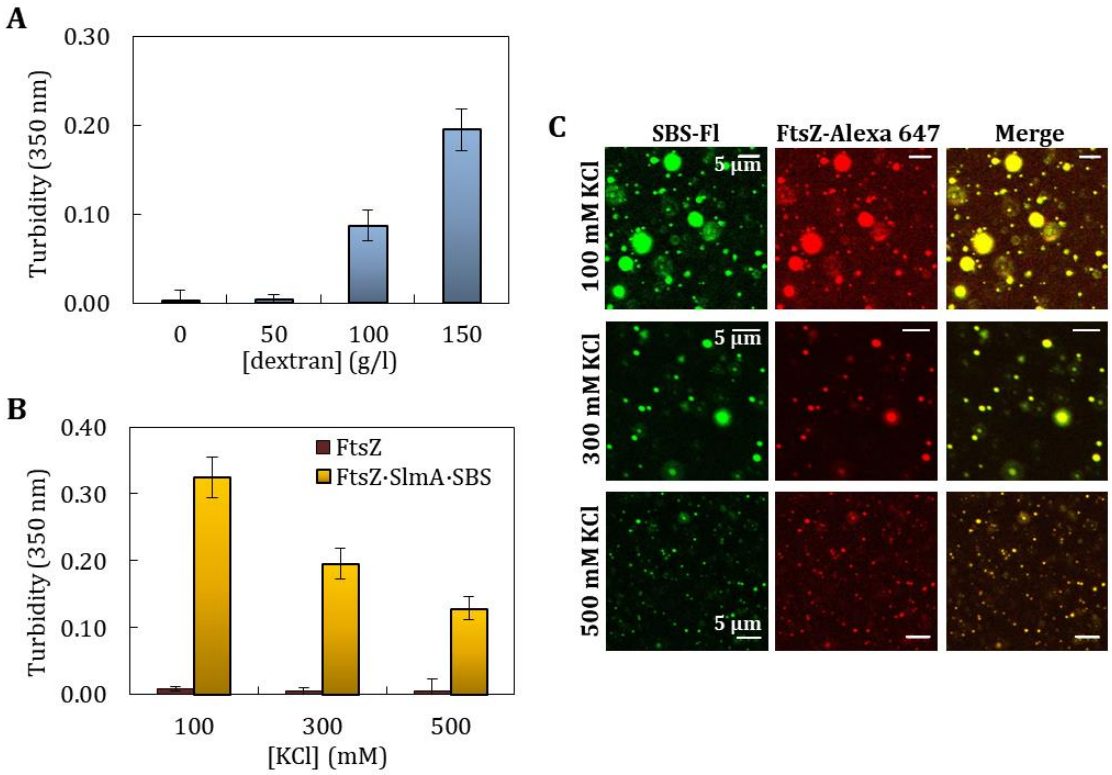


**Figure 1.5. Dependence of the formation of FtsZ·SlmA·SBS condensates on experimental conditions**. (A) Effect of dextran concentration. Data are the average of 2 independent measurements ± SD, except for 150 g/l dextran (n = 5). (B) Effect of KCl concentration in 150 g/l dextran. Data are the average of 3 independent measurements ± SD, except for 300 mM KCl (n = 5). (C) Representative confocal images of the FtsZ·SlmA·SBS condensates at the specified salt concentrations. FtsZ, SlmA and SBS concentrations were 12, 5 and 1 µM, respectively. All experiments in working buffer unless otherwise stated.

Therefore, condensation in this system was strongly favored by the simultaneous presence of the two proteins and the oligonucleotide, probably because this increases multivalency, a feature that has been related to condensation (Banani et al., 2017, Shin and Brangwynne, 2017, Alberti, 2017). Furthermore, crowding, by volume exclusion and/or other unspecific effects, and ionic strength, through modulation of electrostatic interactions, are among the factors determining the formation of these droplet-like condensates.

### FtsZ·SlmA·SBS condensates are dynamic and evolve toward fibers after addition of GTP

The round structures formed by FtsZ·SlmA·SBS were dynamic, a characteristic feature of liquid-like droplets, as revealed by protein capture experiments similar to those carried out recently with other protein systems forming liquid-phase condensates (Woodruff et al., 2017). Images show the final state and temporal

evolution of FtsZ·SlmA·SBS nucleoprotein complexes containing FtsZ-Alexa 647 in dextran, to which FtsZ-Alexa 488 was subsequently added (**Figure 1.6A**). Colocalization of the two dyes indicated that newly added FtsZ was recruited into preformed condensates. These condensates remained dynamic and able to incorporate FtsZ after more than 3 h within similar timescales as the freshly prepared samples (**Figure 1.6B, top**). Analogous behavior and comparable times

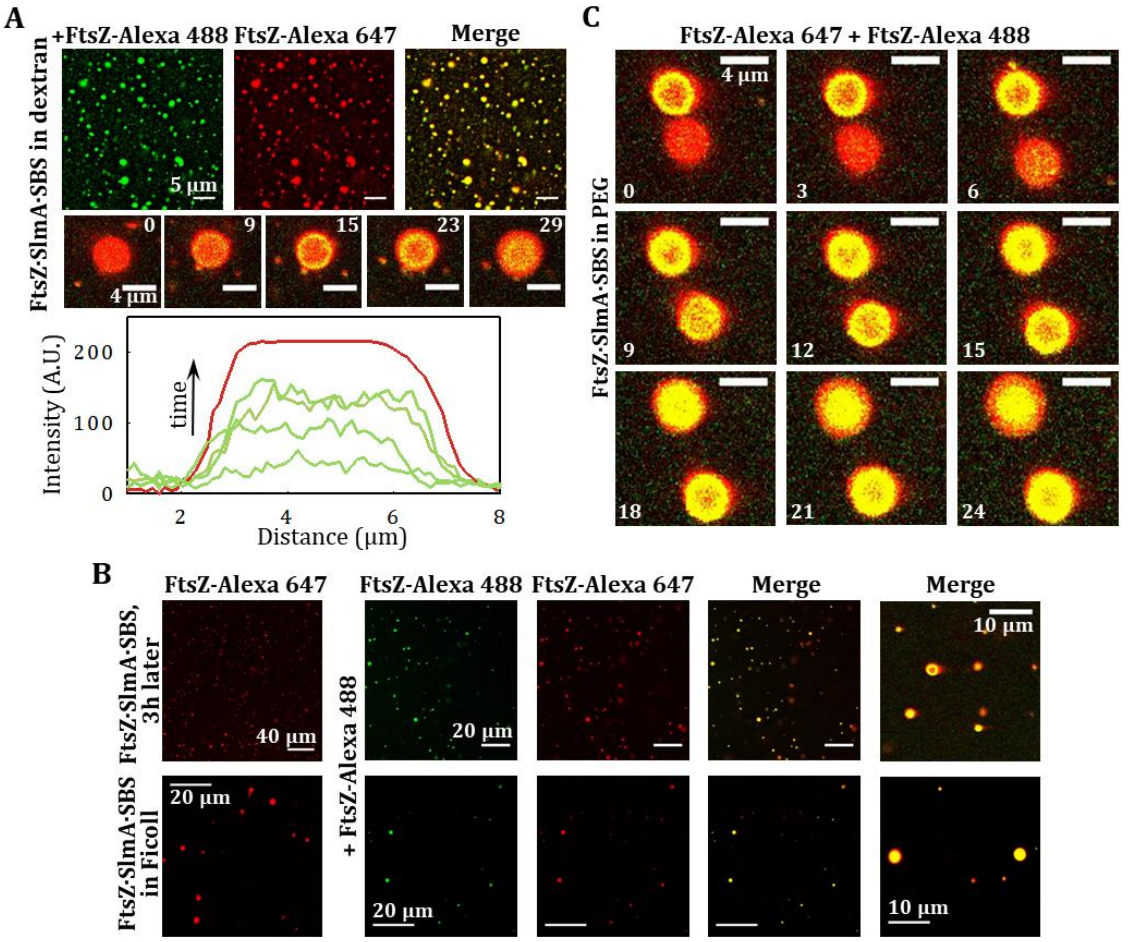


**Figure 1.6. Dynamism of FtsZ·SlmA·SBS condensates.** (A) Representative confocal images showing final state after addition of FtsZ-Alexa 488 to FtsZ·SlmA·SBS complexes (FtsZ labeled with Alexa 647) in 150 g/l dextran. Below, images showing the stepwise diffusion of FtsZ-Alexa 488 into the condensates containing FtsZ-Alexa 647 at the indicated times in seconds (time zero, beginning of visualization for that particular condensate) and corresponding intensity profiles at selected times in the green channel. The profile in the red channel is shown as a reference and varies slightly among images. (B) Initial (far left) and final states after diffusion of FtsZ-Alexa 488 into FtsZ·SlmA·SBS condensates (FtsZ labeled with Alexa 647) in 150 g/l Ficoll (bottom) and 3h after complex formation in 150 g/l dextran (top). Images of the final state (merge) at higher magnification are shown on the right. (C) Stepwise diffusion of FtsZ-Alexa 488 into FtsZ·SlmA·SBS condensates (FtsZ labeled with Alexa 647) at the indicated times in seconds (time zero, beginning of visualization for those particular condensates) in 100 g/l PEG. All experiments were conducted in working buffer.

of FtsZ uptake were found in other crowding solutions (Ficoll and PEG, **Figure 1.6B, bottom and C**). FtsZ·SlmA condensates (i.e., in the absence of the SBS oligonucleotide) behaved as permeable dynamic structures as well, despite the fewer droplets observed (**Figure 1.7**).

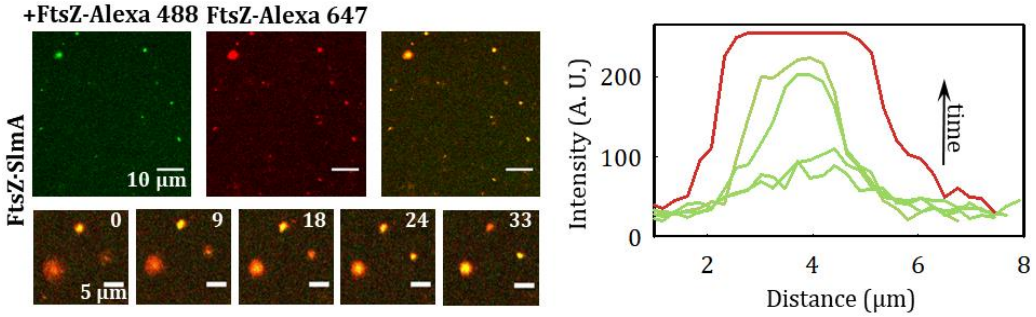


**Figure 1.7. Dynamism of condensates formed by FtsZ·SlmA in 150 g/l dextran.** Left, final state after addition of FtsZ-Alexa 488 to FtsZ·SlmA complexes in working buffer (FtsZ labeled with Alexa 647). Below, images showing the stepwise diffusion of FtsZ-Alexa 488 into the condensates at the indicated times in seconds (time zero, beginning of visualization for those particular condensates). Right, corresponding intensity profiles at selected times in the green channel. The profile in the red channel is shown as a reference and varies slightly among images. FtsZ and SlmA concentrations were 12 and 5 µM, respectively.

Next, we asked whether FtsZ within the condensates was active for assembly into fibers and how the GTP-induced fibers were affected by SlmA·SBS. Addition of GTP on preformed FtsZ·SlmA·SBS condensates induced the formation of FtsZ fibers in which significant colocalization between FtsZ-Alexa 488 and SBS-Alexa 647 was observed (**Figure 1.8A**). Compared with control samples lacking SlmA·SBS (**Figure 1.8B**), the fibers were thinner and their lifetime was appreciably shorter, as previously observed in dilute solution (Cabre et al., 2015). Initially, the fibers coexisted with the round condensates, and then, the amount of fibers increased at the expense of the condensates. Upon GTP depletion, FtsZ fibers disassembled, and afterward, FtsZ, SlmA, and the oligonucleotide incorporated back into condensates larger than their original size (**Figure 1.8A**). FtsZ·SlmA·SBS condensates formed after GTP depletion were still dynamic, as newly added FtsZ rapidly incorporated into them (**Figure 1.8C**). Preassembled GTP-triggered FtsZ filaments were also sensitive to the action of SlmA·SBS. Addition of the nucleoprotein complex resulted in thinner fibers rapidly disassembling compared to the control without SlmA·SBS (**Figure 1.8D**), as observed when eliciting polymerization of FtsZ·SlmA·SBS condensates (**Figure 1.8A**). Large condensates were also found in this case upon GTP exhaustion.

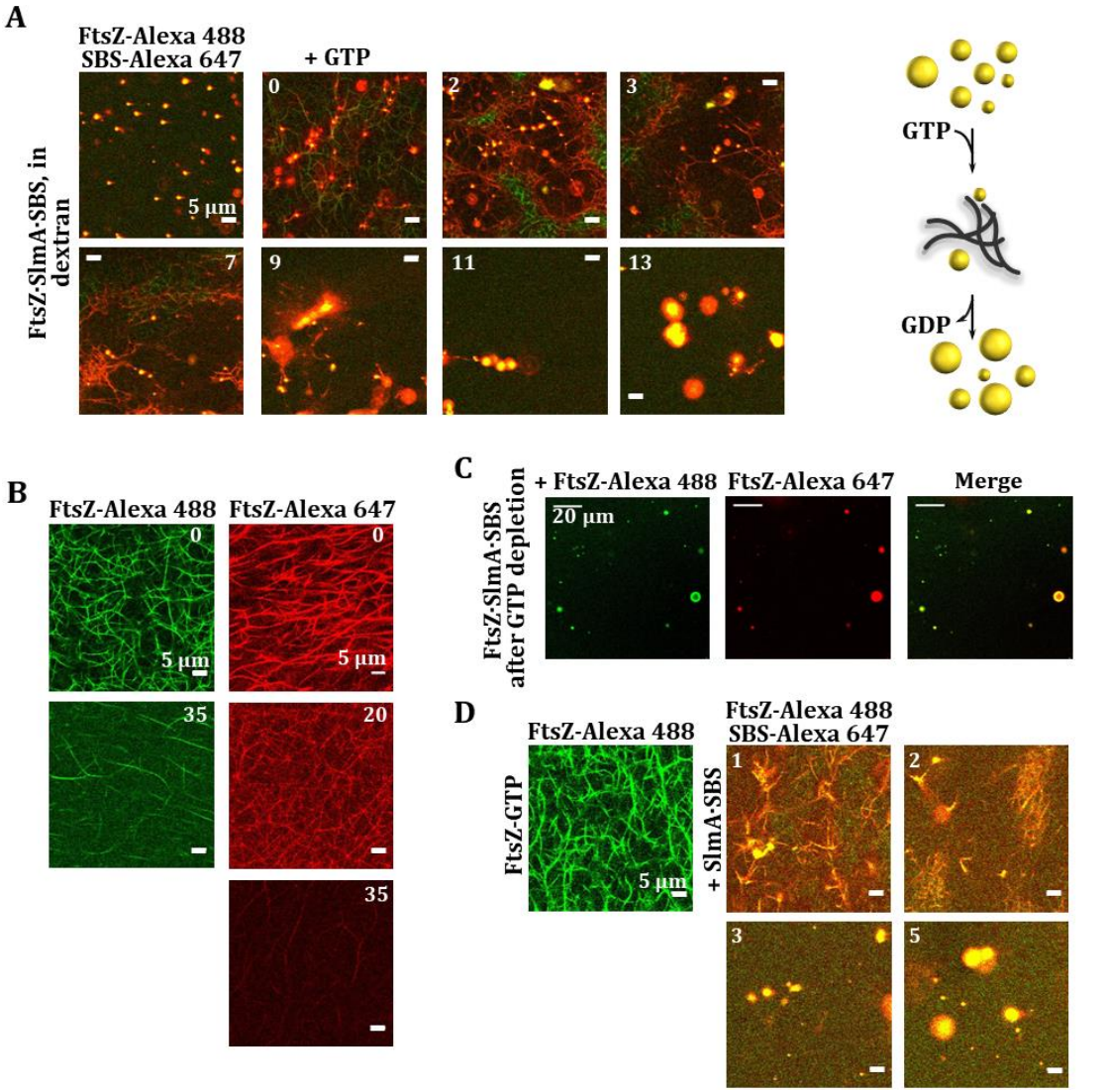


**Figure 1.8. Effect of SlmA·SBS on GTP-triggered FtsZ fibers and dynamism of FtsZ·SlmA·SBS condensates formed after GTP depletion**. (A) Assembly of FtsZ fibers upon GTP addition (0.5 mM) to FtsZ·SlmA·SBS condensates and condensates formed after FtsZ fiber disassembly with time. Scheme of the dynamic process on the right. The number of condensates decreases upon fibers formation, and they rearrange upon GTP depletion and fiber disassembly. (B) Representative confocal images showing depolymerization of FtsZ fibers with time. Two independent experiments are shown in which FtsZ was labeled with either Alexa 647 or Alexa 488. (C) Final state after addition of FtsZ-Alexa 488 on condensates formed by FtsZ·SlmA·SBS (FtsZ-Alexa 647) after FtsZ fibers disassembly due to GTP (0.7 mM) depletion. (D) Effect of SlmA·SBS added on preformed FtsZ fibers induced with GTP on time-dependent disassembly. In all experiments, time indicated in minutes. Time zero, addition of GTP (A and B) or of the inhibitory complex (D). All experiments were performed in working buffer with 150 g/L dextran.

### Compartmentalization affects the distribution and localization of FtsZ·SlmA·SBS condensates in PEG/dextran phase-separated systems

To determine the effect that microenvironments as those found in the cell might have on FtsZ·SlmA·SBS condensation, similar experiments to the ones described above were carried out in PEG/dextran LLPS systems, in which unassembled FtsZ distributes asymmetrically, partitioning preferentially into the dextran-rich phase (Monterroso et al., 2016b). Confocal microscopy images of an emulsion of PEG/dextran containing FtsZ and SlmA·SBS showed abundant condensates of similar size as the ones previously found in homogeneous crowders (see above), in which the two division proteins and SBS colocalized (**Figure 1.9**). In this open, phase-separated system, FtsZ·SlmA·SBS condensates distributed preferentially in

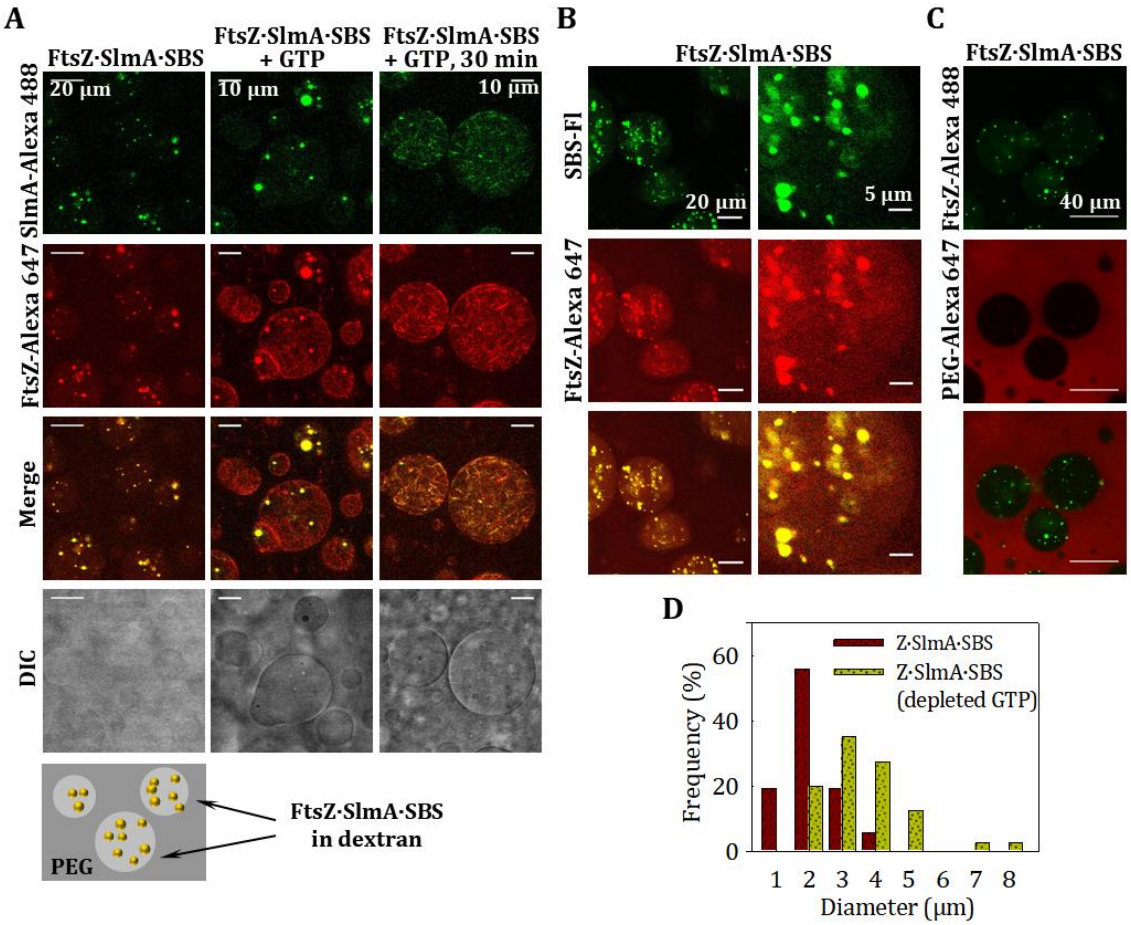


**Figure 1.9. Formation of FtsZ·SlmA·SBS condensates in the PEG/dextran LLPS system and GTP-induced FtsZ assembly into fibers.** (A) Representative confocal and transmitted images of FtsZ·SlmA·SBS complexes with schematic illustration at the bottom. Right, condensates in the presence of GTP (1 mM) at time zero and 30 min after addition of the nucleotide. (B and C) Distribution of condensates formed by FtsZ·SlmA·SBS using different labeling combinations in PEG/dextran LLPS system. Concentrations of FtsZ were 6 µM (C) or 12 µM (A and B). SlmA and SBS, 5 and 1 µM, respectively. (D) Distribution of sizes of FtsZ·SlmA·SBS condensates before (n = 52) and after (n = 40) FtsZ fiber assembly/disassembly cycle. All experiments were conducted in working buffer.

the dextran phase, as shown by the lack of colocalization with labeled PEG (**Figure 1.9C**) and by fluorescence measurements (**Figure 1.10A**). This is likely because of the accumulation of the two proteins and the SBS in this phase (**Figure 1.10A–D**). As in the single crowder solutions, none or very few condensates were observed in this LLPS system for SlmA with or without the SBS (**Figure 1.10B and C**), and for FtsZ either alone (Monterroso et al., 2016b) or in the presence of only SlmA (**Figure 1.10A and 1.11**) or only SBS (**Figure 1.10A and E**). Control experiments showed that these findings were highly reproducible, irrespectively of the fluorescent dyes used and of which element of the condensate was labeled (**Figures 1.9 and 1.10**).

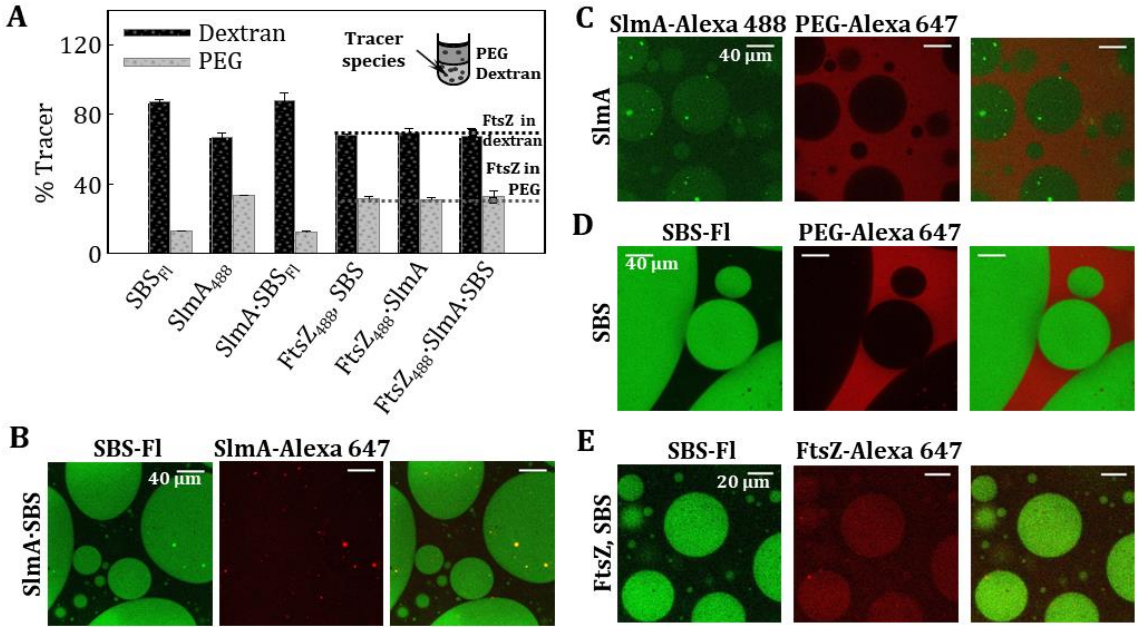


**Figure 1.10. Distribution of division elements in the PEG/dextran LLPS system.** (A) Partition of SlmA, SBS and the complexes with FtsZ within the LLPS mixture as determined by fluorescence, together with an illustration. Horizontal lines depict, for comparison, distribution within these phases of FtsZ alone. Bars represent the percentage of the fluorescently labeled element in each of the phases (dextran-rich or PEG-rich) of the sample. Reported values correspond to the average of 3 independent measurements, 6 in the case of the samples with the three components, ± SD. (B – E) Distribution of (B) SlmA·SBS complex, (C) SlmA, (D) SBS and (E) FtsZ in the presence of SBS. The concentrations of FtsZ, SlmA and SBS, when present, were 12, 5 and 1 µM, respectively. All experiments in working buffer.

The impact of SlmA on the ability of FtsZ to assemble into fibers in the PEG/dextran LLPS system and on the distribution of the fibers was then analyzed. When GTP was added on the FtsZ·SlmA·SBS complexes, FtsZ filaments decorated with SlmA, distributed mostly within the dextran phase, were observed (**Figure**

**1.9A, middle and right columns**). The preference of these filaments for the interface was not as blatant as that of fibers formed solely by FtsZ (**Figure 1.12A, top row**), likely due to their smaller size as a result of the action of SlmA·SBS. Depletion of GTP was found to reverse the process as, upon disassembly, liquid condensates were found again (**Figure 1.12B**). Condensates located within the dextran phase were also found when SlmA·SBS was added to FtsZ fibers, previously elicited by GTP, after nucleotide exhaustion (**Figure 1.12A**).

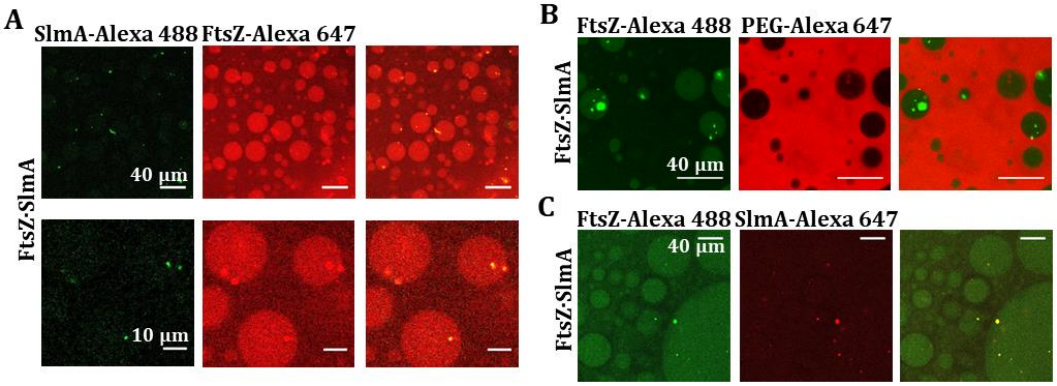


**Figure 1.11. Formation of FtsZ·SlmA condensates in the PEG/dextran LLPS system monitored using different labeling combinations.** Representative confocal images showing the distribution of condensates formed by FtsZ·SlmA in PEG/dextran. FtsZ concentrations were 6 µM (B) or 12 µM (A, C). SlmA, 5 µM. Experiments in working buffer. The brightness of all images was enhanced (40%).

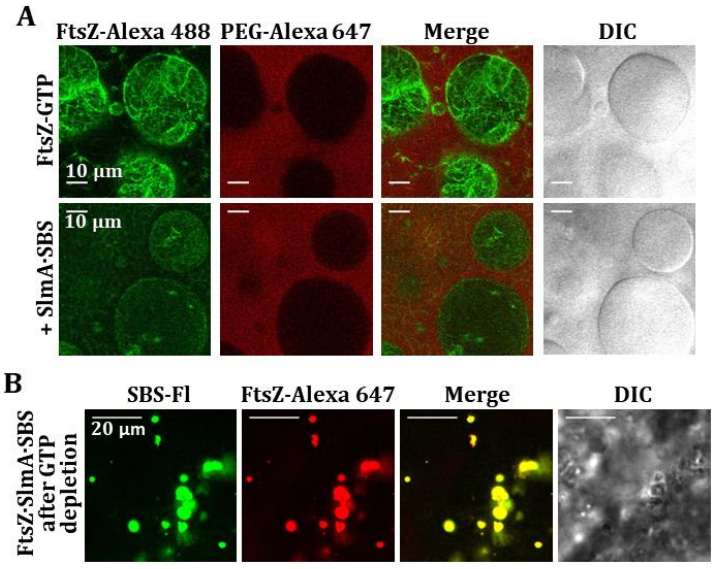


**Figure 1.12. Effect SlmA·SBS on preassembled FtsZ fibers and assembly of condensates after GTP exhaustion in the PEG/dextran LLPS system .** (A) Effect of the addition of SlmA·SBS (bottom row) on preformed FtsZ-GTP fibers induced with 1 mM GTP (top row). (B) FtsZ·SlmA·SBS condensates formed after FtsZ fiber disassembly due to GTP (0.33 mM) depletion. All experiments were conducted in working buffer.

These experiments showed that SlmA bound to its specific nucleic acid sequence modifies the general arrangement and distribution of FtsZ fibers in LLPS systems mimicking compartmentalization. They also suggest that the formation of condensates in dynamic equilibrium with fibers, modulated by GTP binding and hydrolysis, is inherent to the FtsZ·SlmA·SBS system.

### FtsZ·SlmA·SBS condensates contained in microdroplets with PEG/dextran phase-separated systems accumulate at lipid surfaces

To determine how the membrane boundary and confinement in the *E. coli* cells may impact the formation of condensates by FtsZ and SlmA, the two proteins and the SBS sequence were encapsulated within phase-separated microdroplets, picolitre cytomimetic systems surrounded by lipids, using a microfluidics approach optimized in the laboratory (**Figure 1.13A**) (Sobrinos-Sanguino et al., 2017a). Encapsulation of FtsZ (with a tracer amount of FtsZ-Alexa 647) in the stream containing PEG and SlmA·SBS (SBS labeled with fluorescein) in the stream with dextran rendered FtsZ·SlmA·SBS condensates located mostly at the lipid interface of the microdroplets (**Figure 1.13B**). FtsZ outside these condensates was mainly in one of the phases, presumably the dextran, the preference of SBS for this phase being more marked (**Fig 1.13B**).

The same solutions were encapsulated including GTP in the stream with dextran, triggering the formation of FtsZ fibers shortly before encapsulation. Around 30 min after microdroplet production, FtsZ was almost completely disassembled and FtsZ·SlmA·SBS condensates appeared, again mainly at and nearby the lipid interface (**Figure 1.13C**). To observe the fibers, solutions with higher GTP and lower FtsZ and SlmA·SBS concentrations were encapsulated, to increase the lifetime of the fibers (**Figure 1.13D**). FtsZ filaments were observed within the dextran phase, at the interface, and at the lipid boundary. In those areas with a higher local concentration of SlmA·SBS, the presence of the FtsZ filaments was less marked. This is compatible with the previously reported interference of SlmA·SBS with FtsZ filaments bundling (Tonthat et al., 2013), producing thinner structures more difficult to visualize by confocal microscopy. Interestingly enough, the size of the confined condensates, whether formed after depolymerization or not, was smaller (~ 1 μm diameter) than that observed under the same conditions in bulk solution (**Figure 1.9D**).

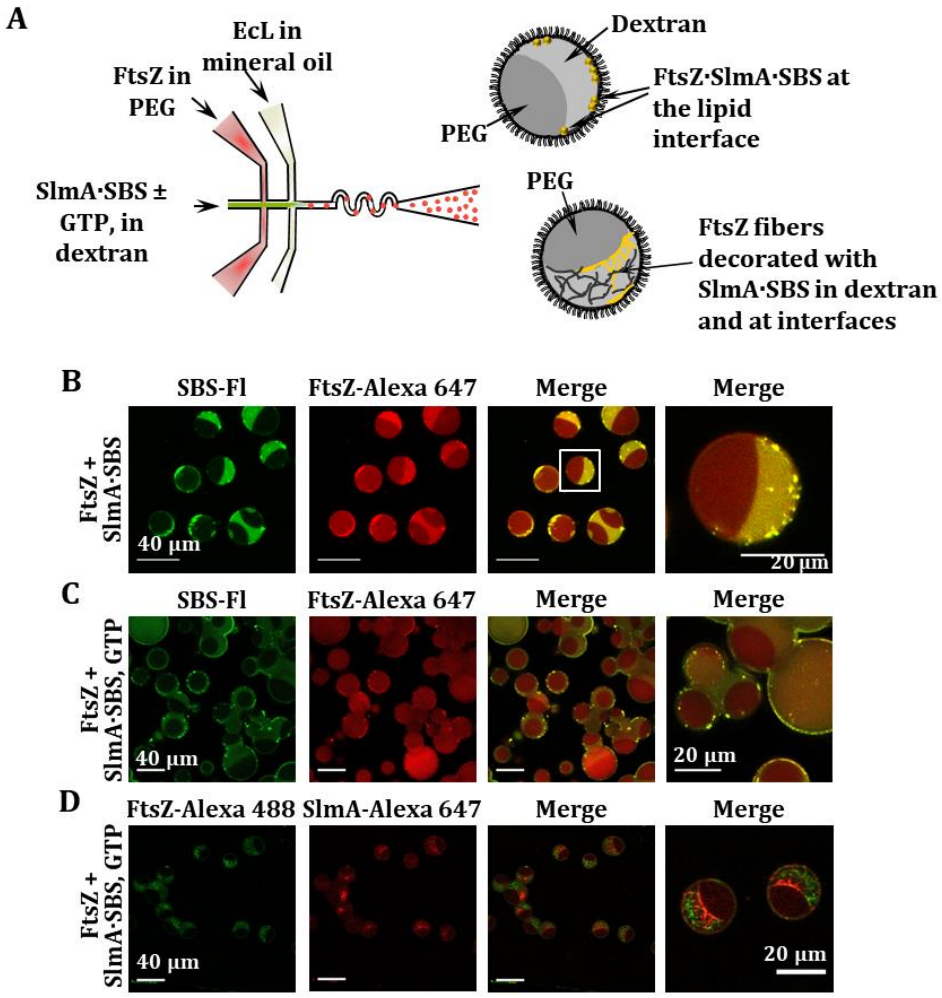


**Figure 1.13. Microfluidic encapsulation of FtsZ·SlmA·SBS in the PEG/dextran LLPS system inside microdroplets stabilized by the *E. coli* lipid mixture.** (A) Scheme of the encapsulation setup and illustration, on the right, of the distribution of species within the encapsulated LLPS system. (B–D) Representative confocal images of the microdroplets without (B) and with GTP (C and D). The concentrations of FtsZ, SlmA, and SBS were 12, 5, and 1 µM, respectively (B and C), or 6, 3, and 0.5 µM, respectively (D). 1 mM (C) or 2 mM GTP (D). Images on the far right are either a magnification of the indicated region in the merged image (B) or independent images at higher magnification (C, D). Encapsulations were conducted in working buffer.

These experiments indicate that the FtsZ·SlmA·SBS system retains the tendency to reversibly form condensates when encapsulated inside micron-sized containers mimicking the compartmentalization of the cytoplasm, and that they display a marked tendency toward the lipid boundary.

### SlmA-driven condensation of FtsZ in PEG/DNA as a model LLPS system closer to an intracellular environment

One LLPS system particularly relevant in the case of the DNA-binding protein SlmA, in which the behavior of FtsZ has been previously studied (Monterroso et al., 2016b), is that comprised by mixtures of PEG and nucleic acid phases. The nucleic acid phase consists of short salmon sperm DNA fragments prepared as previously described (Biswas et al., 2012), allowing to reproduce some of the features of nucleic acid-rich compartments in the bacterial cytoplasm as the charged nature.

In open, phase-separated PEG/DNA systems, abundant FtsZ·SlmA·SBS condensates were found, mostly distributed in the DNA phase (**Figures 1.14A and 1.15A**), probably because of the preferential partition of the individual components (FtsZ, SlmA, and the SBS) into this phase ((Monterroso et al., 2016b) and **Figure 1.15B**). In this LLPS system, FtsZ·SlmA condensation (i.e., in the absence of the SBS sequence) was strongly favored with respect to that previously found in either single or biphasic crowder mixture (cf. **Figures 1.15C, 1.4A and 1.11**), likely because of the unspecific charge effects of the crowder DNA and/or unspecific binding of SlmA to these highly concentrated sequences. The simultaneous presence of SlmA, FtsZ, and DNA was determinant to achieve significant condensation in this LLPS system as no condensates were formed by

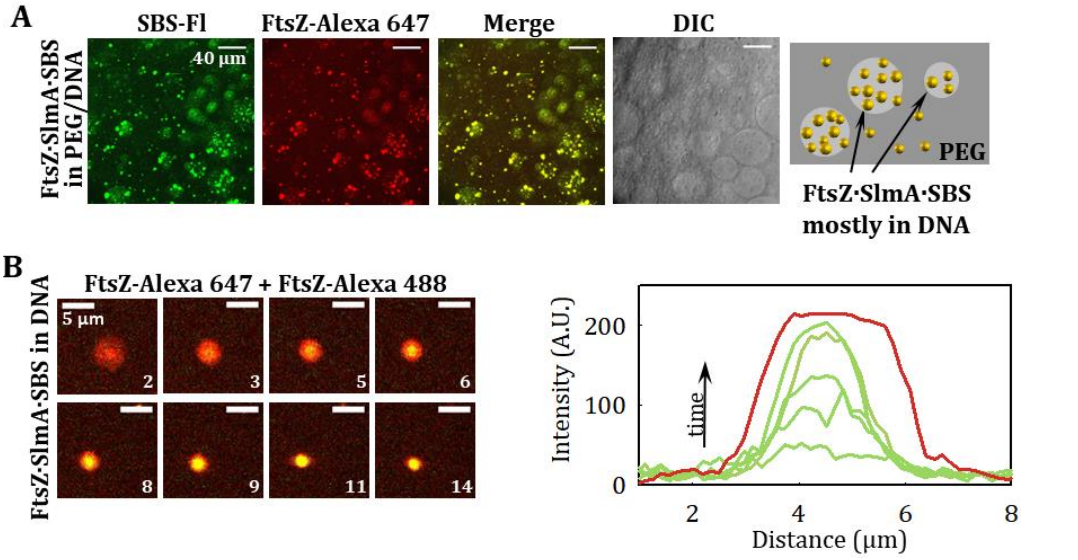


**Figure 1.14. FtsZ·SlmA·SBS condensates in the PEG/DNA LLPS system.** (A) Representative confocal images of FtsZ·SlmA·SBS complexes and schematic illustration of their disposition within the phases on the right. (B) Stepwise diffusion of FtsZ-Alexa 488 added on FtsZ·SlmA·SBS condensates (FtsZ labeled with Alexa 647) at the indicated times in seconds (time zero, beginning of visualization for this particular condensate) in 180 g/l DNA. On the right, representative intensity profiles in the green channel at different times. The profile in the red channel, shown as a reference, varies slightly within the images. All experiments in working buffer

FtsZ on its own (Monterroso et al., 2016b), and a limited number were found for SlmA with or without SBS (**Figure 1.15B**). Like in the crowded systems previously described (see above), FtsZ·SlmA·SBS condensates obtained at high concentrations of the unspecific DNA were dynamic, as they captured FtsZ freshly added to the sample (**Fig 1.14B**). GTP addition to these condensates induced the assembly of FtsZ into fibers coexisting with large liquid droplets (**Figure 1.15D and E**). The fibers appeared mainly distributed within the DNA-rich phase, as previously found for FtsZ fibers in the absence of SlmA (Monterroso et al., 2016b), and also at the interface (**Figure 1.15D and E**).

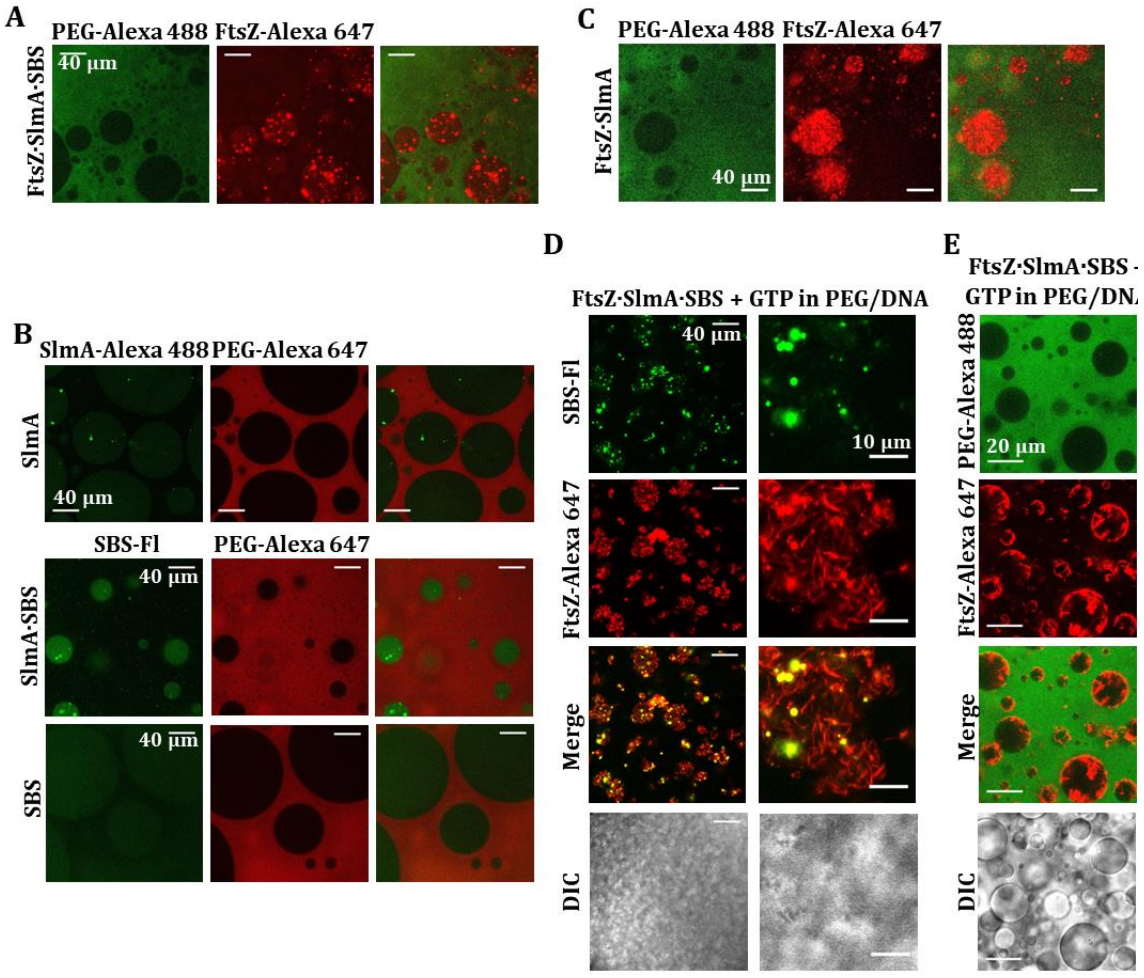


**Figure 1.15. Distribution of different elements in the PEG/DNA LLPS system and fiber formation upon addition of GTP to FtsZ·SlmA·SBS condensates.** Representative confocal images showing the distribution of FtsZ·SlmA·SBS (A), SlmA, SBS and SlmA·SBS (B) and FtsZ·SlmA (C). (D and E) Assembly of FtsZ fibers upon GTP addition (2 mM) to FtsZ·SlmA·SBS using different labels. FtsZ, SlmA and SBS concentrations were 12, 5 and 1 µM, respectively. All experiments were performed in working buffer. In (C) the brightness of the images was enhanced (50%).

To reproduce charged and uncharged cellular compartments, FtsZ·SlmA·SBS condensates were also reconstituted in microfluidics-based microdroplets stabilized by the *E. coli* lipid mixture containing the PEG/DNA LLPS system (**Figure 1.16A**). Production of microdroplets with PEG/DNA and FtsZ was achieved by including the protein in the stream containing PEG, the other aqueous stream containing the unspecific DNA crowder and, when required, GTP. Generated microdroplets were of similar size as those previously produced with the PEG/dextran mixture, and the distribution of both phases among them was homogeneous (**Figure 1.16B**). Simultaneous encapsulation of FtsZ and SlmA·SBS showed FtsZ·SlmA·SBS condensates located mostly at the lipid interface of the microdroplets (**Figure 1.16C**), as with the PEG/dextran LLPS system. In the presence of GTP, fibers of FtsZ decorated by labeled SBS, presumably in complex with SlmA, were observed mainly in the DNA, and a large fraction of the protein and of the SBS located at the lipids (**Figure 1.16D**), similar to that found in the absence of SlmA·SBS (**Figure 1.16B**).

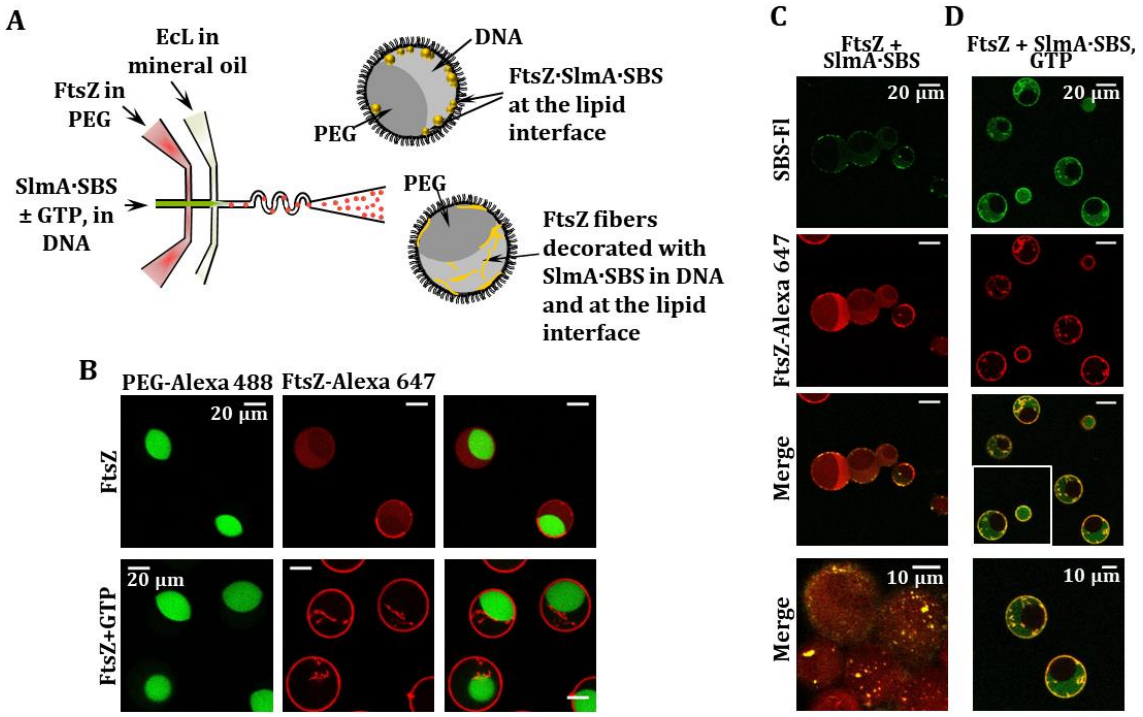


**Figure 1.16. Microfluidic encapsulation of FtsZ ± SlmA·SBS in the PEG/DNA LLPS system inside microdroplets and GTP-induced FtsZ fiber formation.** (A) Scheme of the encapsulation procedure followed for the PEG/DNA LLPS system and illustration, on the right, of the distribution of species within the encapsulated LLPS system. (B) Microdroplets with FtsZ (12 µM) in the absence and presence of 1 mM GTP. (C, D) Representative confocal images of the microdroplets stabilized by the *E. coli* lipid mixture containing the biphasic PEG/DNA mixture and the FtsZ·SlmA·SBS complex without and with 1 mM GTP, respectively. Last image in (C) focuses in the lipid interface to show the high density of condensates. Images at the bottom are an independent image at higher magnification (C) or a magnification of the indicated region in the merged image (D). Encapsulations were conducted in working buffer.

These results show that the formation of biomolecular condensates by FtsZ and SlmA division proteins occurs not only in the presence of inert crowding agents but also in the presence of negatively charged ones mimicking the high nucleic acid content of the bacterial cytoplasm. Moreover, as in the PEG/dextran system, accumulation of the components in one of the phases, in this case the DNA-rich one, resulted in asymmetrical distribution of the condensates in the open LLPS system and, when encapsulated in the microdroplets, condensates were principally assembled at the membrane boundary.

# DISCUSSION

In eukaryotes, formation of membrane-less dynamic macromolecular condensates resulting from biologically regulated liquid–liquid phase separation is a recently discovered regulatory mechanism for spatiotemporal organization of essential intracellular processes. Here, we have shown that FtsZ reversibly forms condensates in the presence of SlmA, a nucleoid occlusion effector of division site selection, in complex with its specific SlmA-binding sites on the chromosome (SBS), and that these condensates are consistent with crowding-driven phase-separated droplets. FtsZ·SlmA·SBS condensates, in which FtsZ remains active for polymerization, were also found in cell-like crowded phase-separated systems revealing their preferential partition into one of the phases, and its accumulation at lipid surfaces of microdroplets generated by microfluidics.

The condensates found here are markedly different from the membrane-free compartments described in prokaryotes, prior to the work shown in this chapter, mostly involved in diverse metabolic pathways (Holthuis and Ungermann, 2013). Carboxysomes and Pdu and Eut microcompartments are examples of confined structural entities that consist of multiprotein complexes encased in a porous protein shell, thus allowing the limited exchange of substrates and reaction products with the surroundings (Holthuis and Ungermann, 2013, Cheng et al., 2008, Parsons et al., 2010, Kerfeld et al., 2018, Yeates et al., 2008). In contrast, FtsZ-rich condensates only require a discrete number of components to be assembled and none of the molecules involved seem to provide a capsid encircling the whole structure, as they capture externally added protein.

The combined action of macromolecular crowding and specific multivalent protein–protein and protein–nucleic acid interactions is the molecular driver of

FtsZ·SlmA·SBS condensation. Excluded volume effects in crowded solutions nonspecifically enhance macromolecular reactions, favoring macromolecular compaction and association (Rivas et al., 2004). The expected magnitude of these effects is much more pronounced in the case of fibrous or large protein assemblies as the biomolecular condensates (Banani et al., 2017, Woodruff et al., 2017, Hernandez-Vega et al., 2017, Rivas and Minton, 2016, Ferrone and Rotter, 2004, Hatters et al., 2002) which is consistent with our findings for the division proteins. All of the crowders tested here induce the formation of FtsZ·SlmA·SBS condensates, and condensation correlates with crowder concentration and hence with volume exclusion effects. Notably, the abundance and size of the condensates seem to be dramatically enhanced at high concentrations of DNA, probably due to the additional exclusion provoked by electrostatic repulsion among DNA, FtsZ, and the SBS sequences, all negatively charged at the working pH. Large effects arising from high concentrations of unspecific DNA on FtsZ assembly and organization have been described before (Monterroso et al., 2016a).

Weak transient interactions between multivalent proteins are known to drive liquid–liquid phase separation. Indeed, most biomolecular condensates described consist of various molecules containing multiple homo- or hetero-association elements, such as nucleic acids, usually RNA, and proteins harboring various domains of interaction (Banani et al., 2017, Shin and Brangwynne, 2017, Alberti, 2017). Multivalency is clearly present in the FtsZ·SlmA·SBS complexes (Schumacher, 2017). Thus, FtsZ forms discrete oligomers in the absence of GTP (Rivas et al., 2000), their size and number significantly enhanced by crowding (Rivas et al., 2001), and the nucleic acid sequence anchors, in dilute solution, a dimer of dimers of SlmA (Cabre et al., 2015, Tonthat et al., 2013). The interaction of FtsZ with SlmA and with the SBS is required for liquid droplet formation, in line with previous observations that nucleic acids favor this type of structure (Banani et al., 2017, Lin et al., 2015, Patel et al., 2015). The concentrations of these three elements and ionic strength are also among the factors influencing condensation, as they modulate their mutual recognition.

The presence of unstructured regions in proteins also seems to promote condensation, and a number of intrinsically disordered proteins can form on their own, under crowding conditions *in vitro* and *in vivo*, liquid droplets that evolve toward solid aggregates in certain cases (Hernandez-Vega et al., 2017, Lin et al., 2015, Patel et al., 2015, Ambadipudi et al., 2017, Molliex et al., 2015). There was no reported evidence of crowding-induced condensation of FtsZ by itself, at the time the work presented in this chapter was conducted. It could not be discarded

though that, since FtsZ self-association can be finely tuned by solution conditions, certain combination of such conditions could lead to condensation, a possibility confirmed by research performed afterwards (see chapter 2). It still remains to be determined if other FtsZ partners can elicit phase separation as we have observed in the presence of SlmA and its cognate SBS sequences.

Probably the most notable results derived from the reconstitution of FtsZ·SlmA·SBS complexes in phase-separated systems are the marked partition of these condensates in DNA-rich phases and the observed tendency of the condensates to concentrate at or nearby the lipid boundary when encapsulated inside microdroplets. Although it was initially proposed that disassembly of FtsZ filaments by SlmA would occur in the nucleoid (Mannik and Bailey, 2015, Bernhardt and de Boer, 2005), different models suggest the antagonist activity hampering FtsZ ring formation falls at the membrane (Mannik and Bailey, 2015, Du and Lutkenhaus, 2014, Tonthat et al., 2013). One possibility is that many SlmA molecules are brought close to the membrane through transertion (coupled translation and membrane insertion) of proteins encoded by sequences near the SBS (Tonthat et al., 2013). This would be reminiscent of the proposed mechanism by which Noc protein functions as a nucleoid occlusion protein in *Bacillus subtilis*. By binding to the cytoplasmic membrane with an amphipathic helix, Noc physically connects the nucleoid to the membrane and crowds out FtsZ from those areas even if there is no evidence that Noc and FtsZ directly interact (Adams et al., 2015). Moreover, in that study, molecular crowding was invoked to explain exclusion of active FtsZ from non-midcell positions, which is conceptually similar to what we propose. Research conducted after the work presented in this chapter showed that, like Noc, SlmA also binds to the membrane, although it only recruits SBS sequences to that location in the presence of FtsZ (see chapter 3).

**Figure 1.17** illustrates the potential biological implications of our findings. In predivisional cells prior to chromosome segregation (stage 1), oligomers of SlmA are bound to their specific DNA target sequences over most of the nucleoid. These SlmA·SBS complexes recruit a portion of the cellular FtsZ, forming condensates in the crowded cytoplasm that cover most of the nucleoid, but which are biased toward the cell poles as the Ter macrodomains migrate to midcell (Bernhardt and de Boer, 2005, Espeli et al., 2012). The local concentration of the three elements in these condensates would be increased, likely enhancing their mutual recognition. Additionally, the nucleoprotein condensates may further accumulate in transient microenvironments resulting from crowding-induced phase separation in the cytoplasm. Condensation into liquid droplets may aid in the localization of the

elements in the vicinity of the membrane, where SlmA would compete with the membrane-anchoring proteins for FtsZ binding (Du and Lutkenhaus, 2014), and reinforce the inhibition of FtsZ fiber formation by other systems operating at the membrane (Rowlett and Margolin, 2015).

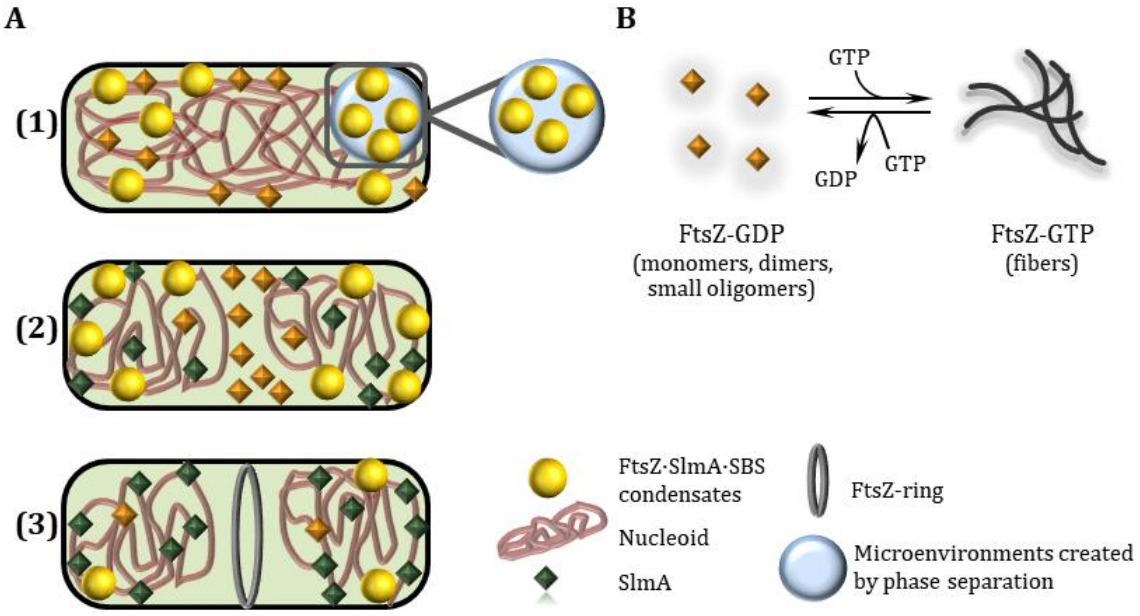


**Figure 1.17. Scheme of the hypothetical influence of FtsZ·SlmA·SBS condensation on the action of SlmA over FtsZ in bacterial division.** (A) Under predivision conditions (1), SlmA·SBS may partially recruit FtsZ forming FtsZ·SlmA·SBS condensates, which may accumulate in transient microenvironments. Condensation into liquid droplets may aid in FtsZ·SlmA·SBS localization nearby the membrane. (2) Under division conditions, the amount of SlmA at midcell decreases and other elements would compete for the interaction with FtsZ that would leave the condensates and, (3) in the presence of GTP, would form a membrane-anchored FtsZ ring. In non-central regions, FtsZ would still be under the control of SlmA, which protects the chromosomes from scission by aberrant division ring formation. (B) Scheme of the self-association of FtsZ. In its GDP form, FtsZ is found as an ensemble of species of small size. GTP binding induces its assembly into fibers that disassemble upon depletion of the nucleotide by FtsZ GTPase activity.

After chromosome segregation begins and the midcell division site becomes available (stage 2), the migration of most of the nucleoid toward the poles and the localization of the Ter macrodomains to midcell decrease the amount of SlmA there (Cho et al., 2011). The Ter macrodomains and associated MatP protein then help to recruit ZapB and ZapA to the division site, where they form a large FtsZ-independent structure that helps to recruit FtsZ at the correct time during the cell cycle (Buss et al., 2017). We postulate that this ZapB·ZapA·FtsZ complex, along with the FtsZ membrane anchors ZipA and FtsA, attracts additional FtsZ away from the FtsZ·SlmA·SBS complexes and, in the presence of GTP, forms a membrane-

anchored FtsZ ring (stage 3). In regions distal from midcell, SlmA would still sequester FtsZ in condensates, serving to protect the segregated chromosomes from scission by aberrant division ring formation in newborn cells.

The condensates of FtsZ and SlmA are dynamic, allowing the incorporation of additional protein, the rapid evolution of the integrated FtsZ toward filaments in the presence of GTP, and its recruitment back into the liquid droplets upon GTP depletion. The dynamism and reversibility are hallmarks of liquid droplets, and they appear to be particularly appropriate for the role of SlmA as a spatiotemporal regulator of the formation of FtsZ filaments. Enhancement of the mutual interactions between the two proteins and the target SBS by their local accumulation within these condensates would ensure that, although SlmA·SBS does not completely block FtsZ assembly, the fibers eventually formed under its control are smaller and rapidly disassemble to condense again into FtsZ·SlmA·SBS liquid droplets. FtsZ within these condensates would remain active for assembly when and where required and indeed, super-resolution fluorescence imaging *in vivo* has provided evidence of non-ring FtsZ persisting as patches that may act as precursors for its reassembly, also suggested to be involved in the formation of mobile complexes by recruitment of other binding partners (Rowlett and Margolin, 2014).

The ability of FtsZ within the nucleoprotein condensates to form fibers can be explained as follows. According to Du and Lutkenhaus (Du and Lutkenhaus, 2014), SlmA accesses FtsZ by binding to its C-terminus, and then severs FtsZ filaments by also binding to the core region of FtsZ. One could imagine that many SlmA molecules may not be always able to achieve both interaction steps, and only interact with the FtsZ C-terminus. This would not block FtsZ polymerization. Moreover, if the interaction between FtsZ and SlmA·SBS depends upon the multivalency of the FtsZ C-terminus as proposed (Schumacher and Zeng, 2016), then as FtsZ filaments become shorter, they will be less likely to stay bound by SlmA·SBS. This in turn might result in some limited reassembly of FtsZ fibers, keeping them in a shortened equilibrium state. All this agrees with the fact that SlmA does not result in total disassembly of FtsZ filaments but only reduces their lifetime, as shown in (Cabre et al., 2015). FtsZ mutants D86N and K190V (in the core domain) and K380M (at the C-terminus) still form filaments when bound to SlmA, indicating that the loss of one charged residue in the target is enough to prevent SlmA from breaking FtsZ fibers. Given that formation of the FtsZ·SlmA·SBS condensates seems to be facilitated by interactions between the negatively charged FtsZ, positively charged SlmA, and negatively charged SBS, it is not

surprising that changing a charged residue in FtsZ might have a large impact on the system.

Some of the next steps in understanding the potential role of the condensates we describe in this study will be to detect these condensates *in vivo* and to determine the effects of other FtsZ-binding proteins such as FtsA, ZipA, and MinC on the condensates *in vitro*. It is intriguing that when SlmA is overproduced, FtsZ-GFP is recruited to nucleoids (Bernhardt and de Boer, 2005), but no high-resolution study has been done to determine whether there is a detectable phase separation in *E. coli* cells. Future work with mutants of FtsZ and other cell division proteins *in vitro* will be necessary to expand and refine our findings. On a broader level, our experimental approach can be extended to other systems undergoing liquid-phase condensation to tackle the molecular mechanisms governing these processes in reconstituted cytomimetic systems with controlled composition.

# CHAPTER 2

# Assembly of bacterial cell division protein FtsZ into dynamic biomolecular condensates

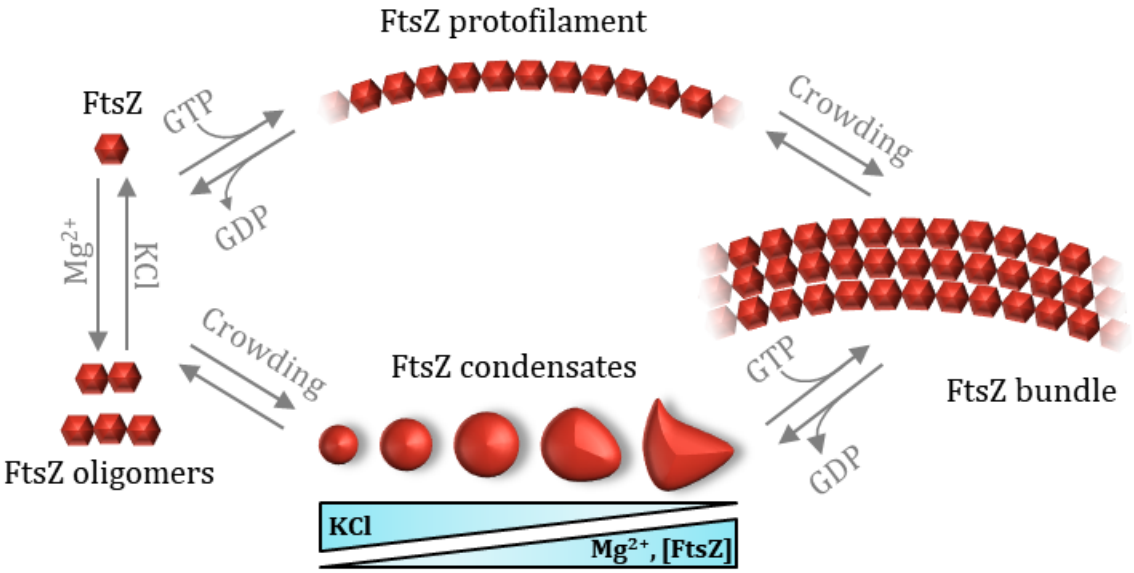


Biomolecular condensation through phase separation may be a novel mechanism to regulate bacterial processes, including cell division. Previous work described in chapter 1 revealed that FtsZ, a protein essential for cytokinesis in most bacteria, forms biomolecular condensates with SlmA, a protein that protects the chromosome from damage inflicted by the division machinery in *Escherichia coli*. The absence of condensates composed solely of FtsZ under the conditions used in that study suggested this mechanism was restricted to nucleoid occlusion by SlmA or to bacteria containing this protein. Here we report that FtsZ alone, under physiologically relevant conditions, can demix into condensates in bulk and when encapsulated in synthetic cell-like systems generated by microfluidics. Condensate assembly depends on FtsZ being in the GDP-bound state and on conditions mimicking the crowded environment of the cytoplasm that promote its oligomerization. Condensates are dynamic and reversibly convert into filaments upon GTP addition. Notably, FtsZ lacking its C-terminal disordered region, a structural element likely to favor biomolecular condensation, also forms condensates, albeit less efficiently. The inherent tendency of FtsZ to form condensates susceptible to modulation by physiological factors, including binding partners, suggests that such mechanisms may play a more general role in bacterial division than initially envisioned.

# RESULTS

## GDP bound FtsZ forms micrometer-sized condensates in crowding conditions

We tested the ability of FtsZ to form biomolecular condensates on its own by exploring conditions known to impact its oligomerization tendency, such as magnesium, protein and salt concentrations, and macromolecular crowding. Confocal images of FtsZ labeled with Alexa 488 (FtsZ-Alexa 488) showed that, at 100 mM KCl, 10 mM $Mg^{2+}$ and in the presence of dextran, Ficoll or PEG as crowders, the protein (5 μM) formed round structures that resembled biomolecular condensates (**Figure 2.1A**). Turbidity measurements on these samples further confirmed the formation of higher order structures in the presence of crowding agents (**Figure 2.1B**), with absorbance values in the absence of crowders virtually zero (0.002 ± 0.002 with 16 μM FtsZ). The observed turbidity trend was compatible with the existence of a threshold protein concentration above which condensates would start forming. Analysis of the data rendered values for this saturation concentration, $c_{sat}$, of 1.3 ± 0.2 μM, 3 ± 1 μM and 3.8 ± 0.1 μM in dextran, Ficoll and PEG, respectively (**Figure 2.1B**). This concentration threshold has been recently established as an additional criterion for identifying phase separation phenomena yielding condensation (Shin and Brangwynne, 2017, Peng and Weber, 2019).

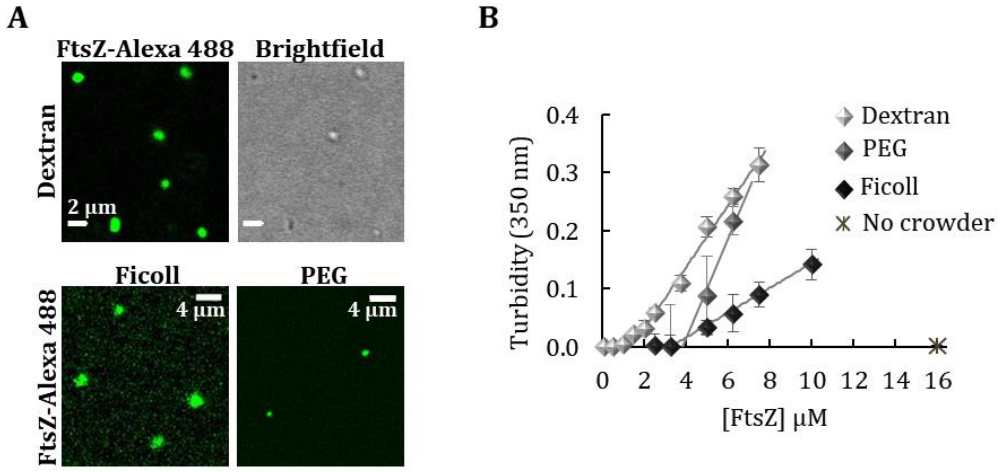


**Figure 2.1. FtsZ forms condensates.** (A) Confocal microscopy and transmitted images of condensates of FtsZ (5 μM) in different crowders. (B) Dependence of the turbidity signal of wild-type FtsZ on protein concentration. Lines correspond to a linear model fit to the data. Dextran 500 and Ficoll 70 concentrations were 200 g/l, and PEG 8 was 75 g/l. All experiments in 50 mM Tris-HCl pH 7.5, 100 mM KCl, 10 mM $MgCl_2$. In (B) data are the average of at least 3 independent experiments ± SD.

Thorough characterization in the presence of dextran showed that the size, shape and abundance of the FtsZ condensates depended on the salt, magnesium and protein concentration. Under the above mentioned $Mg^{2+}$ and KCl conditions, and up to 5 µM FtsZ, a population of mostly round structures resembling condensates was observed by confocal microscopy (**Figures 2.1A and 2.2A**). The size distribution of the condensates increased with protein concentration (**Figure 2.2B**). Accordingly, the turbidity values also increased with protein concentration

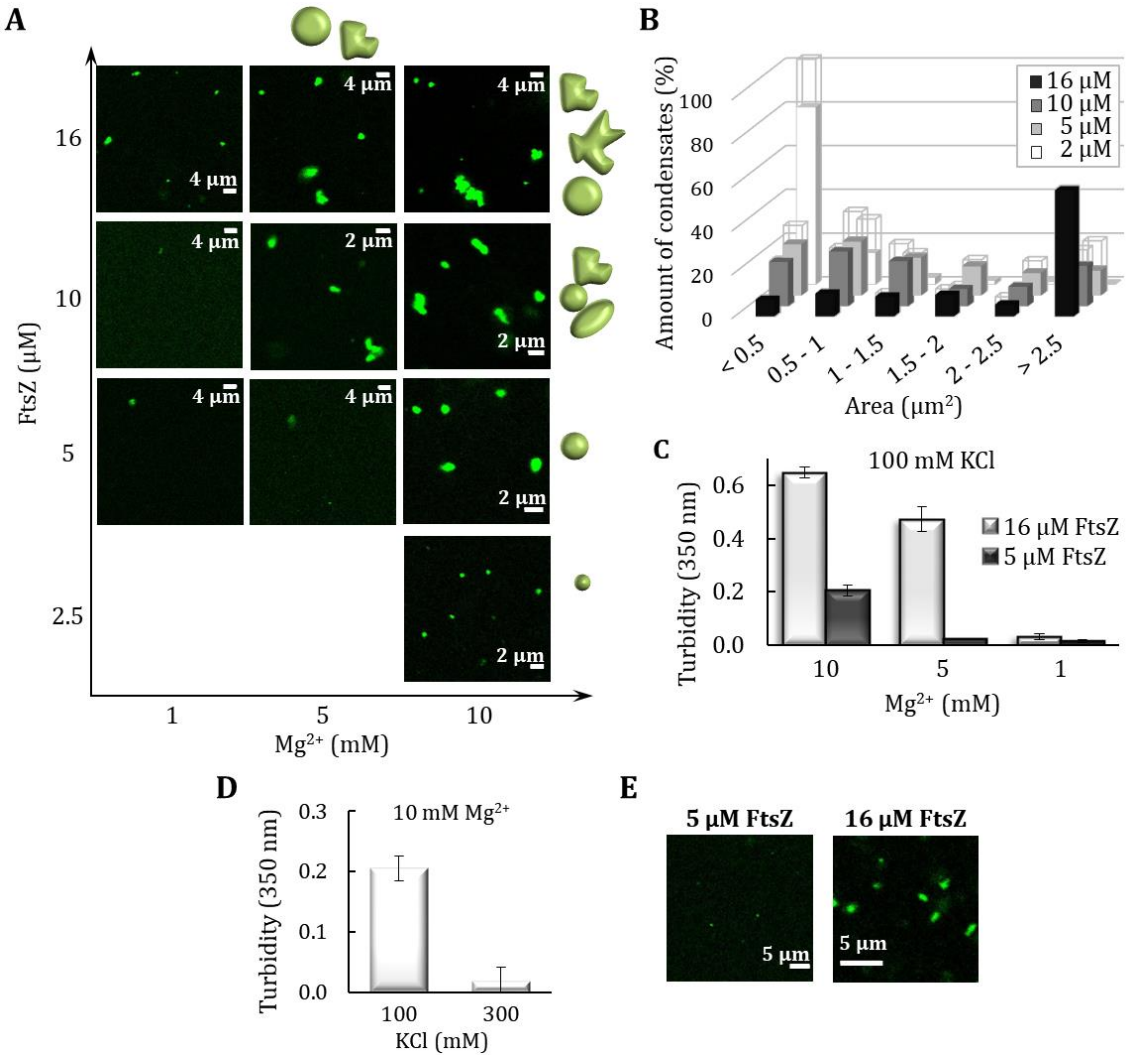


**Figure 2.2. Dependence of the formation of FtsZ arrangements with magnesium, protein and KCl concentration in dextran.** (A) Representative confocal images of the structures formed by FtsZ, with FtsZ-Alexa 488 as a tracer, at the specified magnesium and protein concentrations. (B) Size distribution of condensates at various FtsZ concentrations (in ascending order, n = 124, 99, 80 and 106 particles). Errors, depicted as open sections of the bars, correspond to SD from 3 (2 and 5 µM FtsZ) or 2 (10 and 16 µM FtsZ) independent images. (C) Variation in the turbidity signal of FtsZ with magnesium at two FtsZ concentrations. (D) Variation in the turbidity signal of FtsZ (5 µM) with KCl concentration. Data in (C) and (D) are the average of at least 3 independent experiments ± SD. (E) Structures formed by FtsZ with 300 mM KCl and 10 mM magnesium, at the specified FtsZ concentrations. In all cases, dextran was 200 g/l and buffer was 50 mM Tris-HCl pH 7.5, 100 mM KCl, 10 mM $MgCl_2$ unless otherwise stated.

(**Figure 2.1B**). At high protein concentrations, we found a progressive appearance of irregular FtsZ assemblies of large size at the expense of the smaller and more regular structures (**Figure 2.2A**). Regarding the effect of $Mg^{2+}$, lowering its concentration to 1–5 mM significantly reduced the number of structures, except if protein concentration was tripled to 16 μM, as determined through confocal microscopy and turbidity measurements (**Figure 2.2A and C**). Lastly, an increase in salt to 300 mM KCl resulted in low turbidity values, consistent with scarce and very small structures, even with 10 mM $Mg^{2+}$ (**Figure 2.2D and E**). Only at high protein concentrations was a significant population of arrangements of variable shape apparent (**Figure 2.2E, right**). These results are in line with our previous study on FtsZ·SlmA·SBS biomolecular condensates (chapter 1), at 1 mM $Mg^{2+}$, where FtsZ alone was homogeneously dispersed. Condensation in the presence of Ficoll followed the same trend with KCl and $Mg^{2+}$ concentration as that described with dextran (**Figure 2.3**).

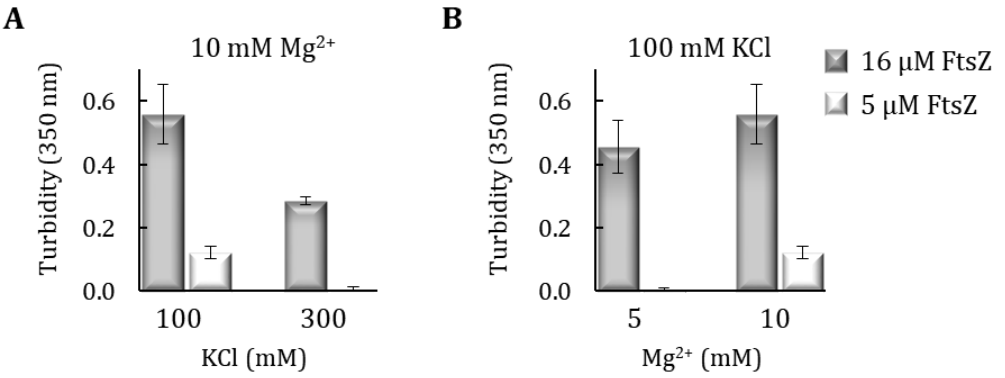


**Figure 2.3. Formation of FtsZ condensates in Ficoll under different conditions.** Variation in the turbidity signal of FtsZ with KCl (A) and magnesium concentrations (B). Data are the average of at least 3 independent experiments ± SD. In all cases, buffer was 50 mM Tris-HCl pH 7.5 and Ficoll 250 g/l at the specified KCl and $MgCl_2$ concentrations.

These experiments show the formation of FtsZ round structures, above a saturation concentration of protein, under salt and ionic strength conditions rendering sufficient multivalency through the promotion of the protein monomers self-association. Regulation of the assembly of these defined micrometer-sized arrangements by ion concentrations and salt suggests an implication of electrostatic forces in their formation, without excluding other possible types of interactions. Selected conditions for further characterization were those where round structures compatible with biomolecular condensates prevailed, 5 μM FtsZ and 200 g/l dextran with 100 mM KCl and 10 mM $MgCl_2$ (working buffer[2]).

[2] Working buffer: 50 mM Tris-HCl pH 7.5, 100 mM KCl, 10 mM $MgCl_2$.

### Condensation of FtsZ lacking the unstructured C-terminal region is less efficient

Unstructured domains of proteins have been implicated as important contributors to biomolecular condensation. To evaluate the impact of such domains on the formation of the condensate-like arrangements described above, we investigated the mutant FtsZΔ315-383 (FtsZΔ$_{Cter}$), which contains the globular domain of FtsZ but lacks the unstructured C-terminal flexible linker as well as the conserved C-terminal peptide known to bind other cell division proteins (Ortiz et al., 2016). We found that this mutant FtsZ retained the ability to form condensates in crowded solutions (**Figure 2.4A**). Interestingly, these condensates in the images

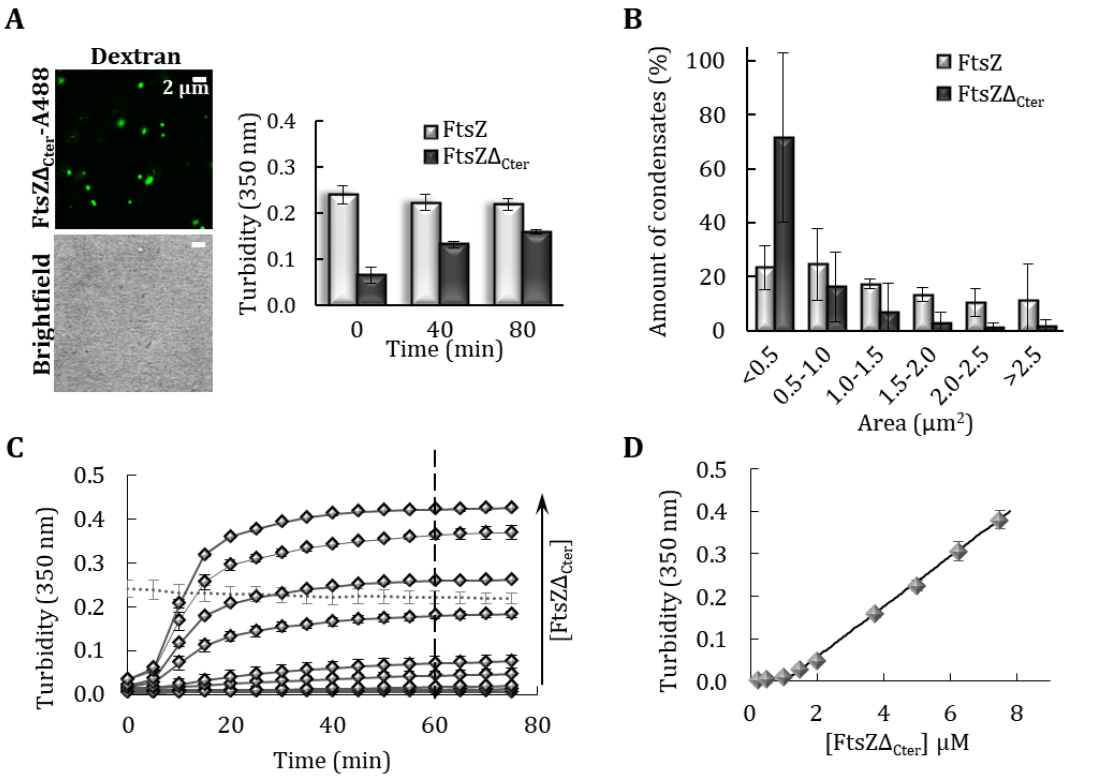


**Figure 2.4. FtsZΔ$_{Cter}$ forms condensates less efficiently.** (A) Confocal microscopy and transmitted images of condensates formed by the FtsZ mutant, FtsZΔ$_{Cter}$, in dextran. On the right, changes in the turbidity signal of the FtsZ mutant condensates over time, with those of wild-type FtsZ shown as reference. (B) Size distribution of FtsZ (n = 99 particles) and FtsZΔ$_{Cter}$ condensates (n = 238 particles) in the presence of dextran. Errors correspond to SD from 3 (FtsZ) or 6 (FtsZΔ$_{Cter}$) independent images. (C) Evolution with time of the turbidity signal of mutant FtsZ at different concentrations of the protein. From bottom to top: 0.1, 0.25, 0.5, 1, 1.5, 2, 3.8, 5, 6.3 and 7.5 µM. Four independent experiments were performed, from which the average of 2 (simultaneously measured) ± SD are shown as representative of the whole set. The dotted line corresponds to the turbidity signal of wild-type FtsZ, averaged from at least 3 independent experiments ± SD, shown as a reference. (D) Dependence of the turbidity signal of FtsZΔ$_{Cter}$ on protein concentration. Symbols are data at equilibrium, average of 4 independent experiments ± SD, extracted from those at the time point indicated in (C) with a dashed line. Solid line corresponds to a linear model fit to the data. Except when specified, FtsZ and FtsZΔ$_{Cter}$ concentrations were 5 µM. All experiments were in working buffer with 200 g/l dextran.

were substantially smaller than those formed by the wild-type protein when visualized at short times after their formation, also reflected in the different size distribution of the condensates of both proteins at the same concentration (**Figure 2.4B**). This observation is compatible with the lower turbidity values measured for the mutant protein after mixing with the crowder. While the turbidity values remained constant for at least 80 min in the case of the wild-type FtsZ, those for the mutant noticeably increased within this same time interval, suggesting that the condensation process is slower (**Figures 2.4A and 2.4C**). Notably, evaluation of the dependence with mutant concentration of the turbidity signal at equilibrium rendered a $c_{sat}$ value similar to that of wild-type, 1.1 ± 0.2 μM (**Figure 2.4D**). Analysis of this mutant by analytical ultracentrifugation showed that it retains the ability to form oligomers in solution (**Figure 2.5**), which would provide the multivalent states that typically favor formation of condensates. Together, this evidence suggests that the unstructured domain of FtsZ may not be strictly required to mediate its assembly as it did not preclude the formation of these structures, but the delay in condensation indicates it probably has a role in enhancing the overall process.

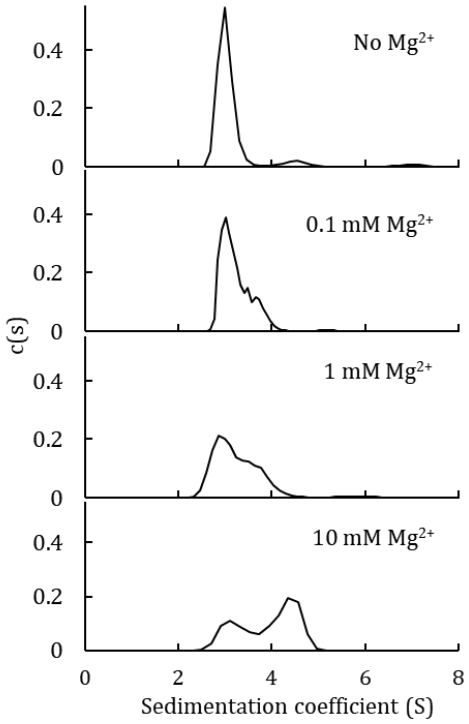


**Figure 2.5. Effect of magnesium on the self-association of FtsZΔ$_{Cter}$ as determined by analytical ultracentrifugation.** Shown are sedimentation coefficient distributions of the mutant (15 μM) in 50 mM Tris-HCl pH 7.5, 300 mM KCl, with the specified magnesium concentrations.

## FtsZ condensates are dynamic, reversible and evolve into filaments in the presence of GTP

Next, we asked whether the round FtsZ structures resembling molecular condensates were dynamic and reversible. To this end, we followed four different approaches: incorporation of added FtsZ on preformed condensates, evolution of condensates over time, GTP-triggered polymerization of FtsZ from condensates and subsequent reassembly into condensates upon GTP depletion, and dissociation of condensates by salt shift. First, we performed capture experiments using two separate pools of FtsZ labeled with spectrally different dyes, and similarly to that described in chapter 1 and for other condensates (Woodruff et al., 2017). We found that FtsZ-Alexa 488 readily incorporated into preformed condensates containing

FtsZ labeled with Alexa 647 (FtsZ-Alexa 647) as a tracer, suggesting that the population of FtsZ within the condensates is dynamic. Images show the initial and final states and the stepwise diffusion of the added protein into the condensates (**Figure 2.6A**). Capture experiments using the reverse dyes yielded the same result (**Figure 2.6B**). Likewise, FtsZΔ$_{Cter}$ condensates displayed dynamic behavior following the same approach (**Figure 2.6C**).

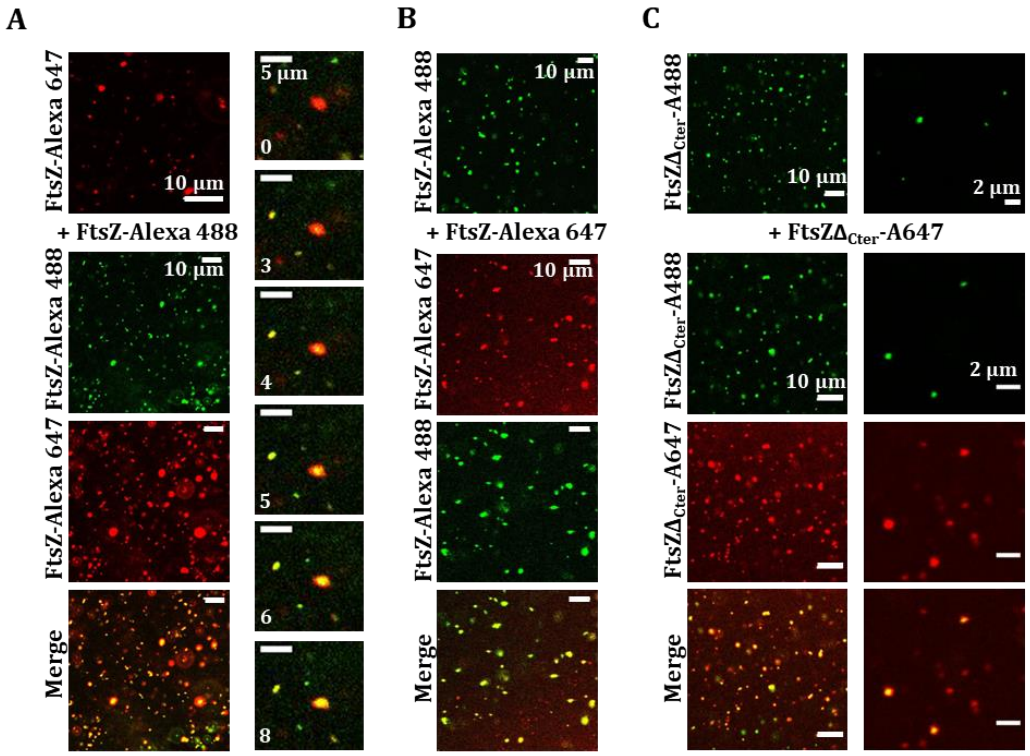


**Figure 2.6. FtsZ condensates are dynamic.** (A) Representative confocal microscopy images showing the initial and final states after addition of FtsZ-Alexa 488 into FtsZ condensates with FtsZ-Alexa 647 as a tracer and, in the right, stepwise diffusion at the times indicated in seconds and (B) initial and final states after addition of FtsZ-Alexa 647 into FtsZ condensates with FtsZ-Alexa 488 as a tracer (C) Images showing the initial and final states after addition of FtsZΔ$_{Cter}$-A647 into mutant condensates with FtsZΔ$_{Cter}$-A488 as a tracer. FtsZ and mutant concentrations were 5 µM. All experiments were conducted in working buffer with 200 g/l dextran.

We also monitored the evolution of FtsZ condensates over time. We found a clear shift of the condensate size distribution toward larger values over a 4 h time course (**Figure 2.7A and B**). Growth of the condensates may be the result of fusion, Ostwald ripening, which seems to be a property of cytoskeletal proteins (Wiegand and Hyman, 2020), or a combination of both. Capture experiments conducted on these grown condensates revealed they remain dynamic in terms of protein incorporation (**Figure 2.7C**).

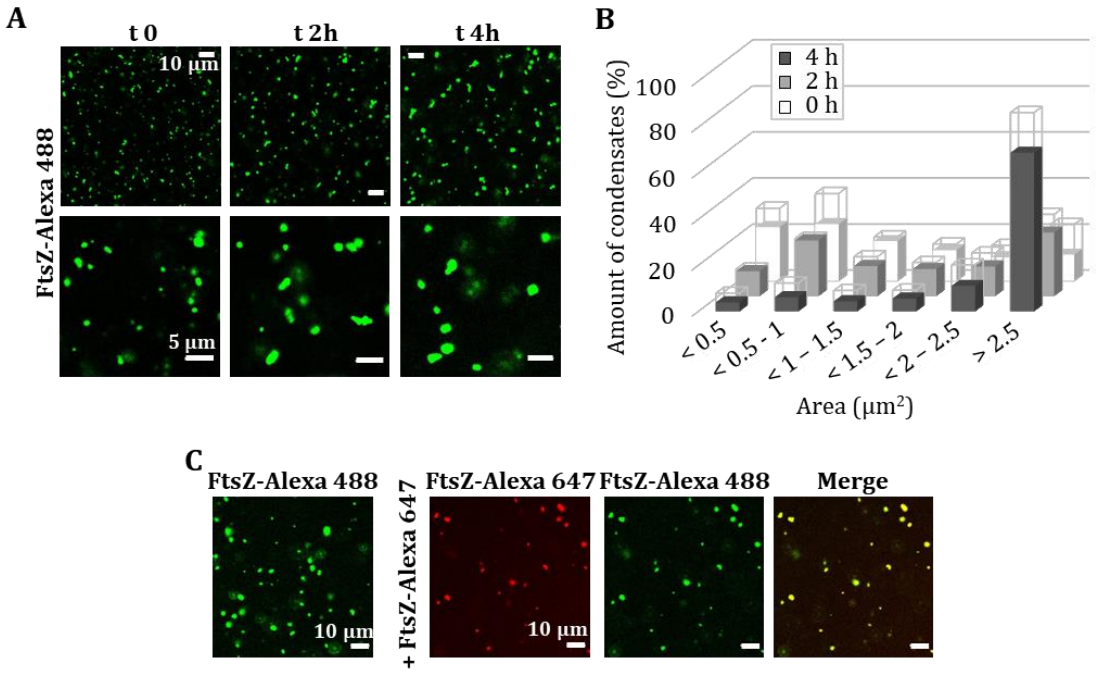


**Figure 2.7. FtsZ condensates grow with time.** (A) Images of FtsZ condensates with time, and (B) corresponding distribution of sizes (n = 99, 157 and 206 particles for 0, 2 and 4 h, respectively). Errors, depicted as open sections of the bars, correspond to SD from 2 (2 h) or 3 (0 and 4 h) independent images. (C) Images showing the dynamism of FtsZ condensates after 4 h incubation. Initial and final states after addition of FtsZ-Alexa 647 into FtsZ condensates with FtsZ-Alexa 488 as a tracer. FtsZ concentration was 5 µM. All experiments were conducted in working buffer with 200 g/l dextran.

Next, we tested the responsiveness of the FtsZ condensates to GTP, which is well known to induce FtsZ polymer formation and is a hallmark of its functionality *in vivo*. Confocal images showed that addition of GTP strongly induced the polymerization of FtsZ that seemed to occur with a concomitant reduction in the number and/or size of the condensates, although both structures coexisted during the time window monitored (**Figure 2.8A**). Turbidity measurements showed a significant decrease in the signal arising from the condensates shortly after GTP addition (**Figures 2.8B and C**). Moreover, measurements with condensates formed using Ficoll as crowding agent exhibited the same behavior (inset in **Figure 2.8C**). This, together with the incipient polymer formation observed in the images taken at short times, strongly suggests that the polymers originate from the condensates. Had polymerization exclusively come from the unassembled protein coexisting with condensates, we would have detected an increase in turbidity instead of the strong decrease observed. In addition, the turbidity signal slightly decreased with time up to a point, dependent on the nucleotide concentration, above which it gradually recovered, reaching a value close to that in the absence of GTP (**Figures 2.8B**). This behavior is consistent with the characteristic

dissociation of the FtsZ polymers due to GTP exhaustion (Mukherjee and Lutkenhaus, 1998). Interestingly, the round condensates after four hours also exhibited conversion into the typical GTP-triggered FtsZ polymers, as monitored by confocal microscopy (**Figure 2.8D**).

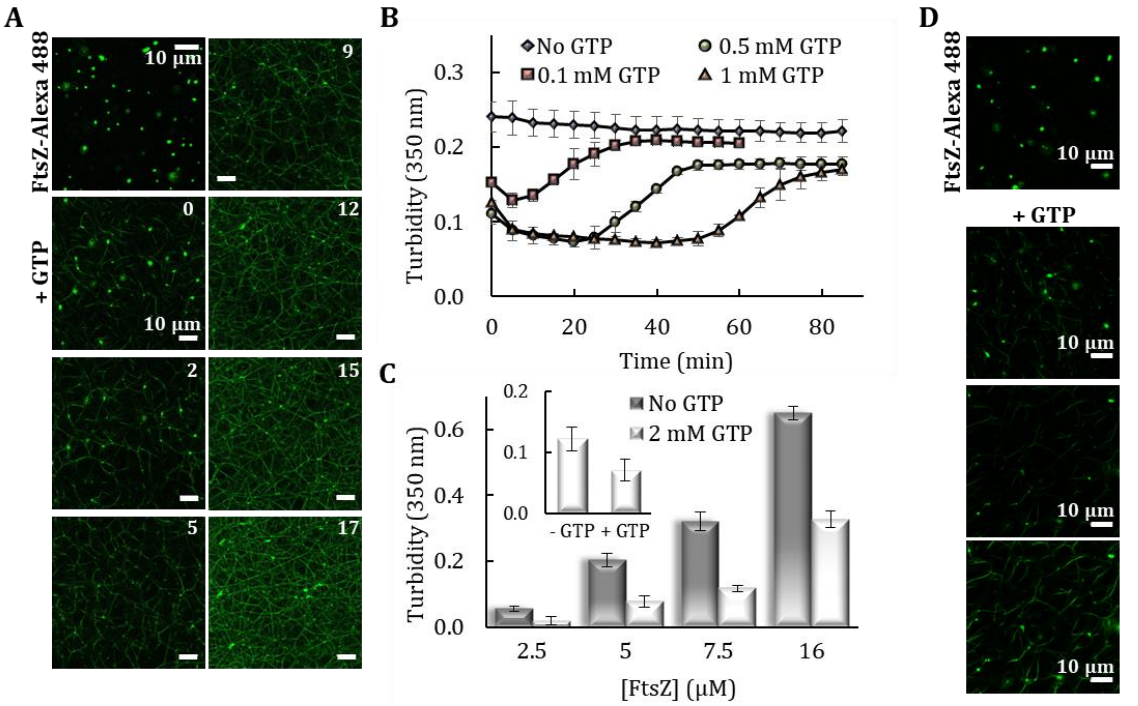


**Figure 2.8. FtsZ within the condensates remains active for polymerization.** (A) Representative images of FtsZ condensates before polymerization and evolution after GTP (0.5 mM) addition at the indicated times, in minutes. All images of the time lapse correspond to a single field. (B) Variation in the turbidity signal of FtsZ upon triggering polymerization by addition of the specified GTP concentrations. Evolution of the signal in the absence of GTP is shown for reference. (C) Effect of GTP addition on the turbidity signal of FtsZ in dextran at different concentrations of the protein. Inset shows the effect of 0.5 mM GTP addition on the turbidity signal of FtsZ in 250 g/l Ficoll. Data in (B) and (C) are the average of at least 3 independent experiments ± SD. The "no GTP" statement refers to samples where no GTP was added (i.e., FtsZ-GDP). (D) Representative confocal images of FtsZ condensates, incubated 4 h, before and after addition of GTP (0.5 mM). The bottom image was obtained by enhancing the brightness (44%) of the one above it (correction applied uniformly to the whole image, using Microsoft PowerPoint) to better appreciate the polymerization of FtsZ into filaments. All experiments were in working buffer with 200 g/l dextran, except inset in (C), and 5 µM or the specified FtsZ concentrations.

Lastly, the reversible nature of FtsZ condensates was assessed by measuring the ability of the protein to assemble into polymers, after addition of 0.1 mM GTP to condensates formed under the working conditions, and back to condensates upon GTP depletion. As shown by confocal microscopy, upon depolymerization the protein formed condensates similar to those before nucleotide addition (**Figure**

**2.9A**). Accordingly, and as observed in the presence of other GTP concentrations, the initial decrease in the turbidity signal was followed by a recovery (**Figure 2.8B**). Further evidence of the reversibility of FtsZ condensates was obtained by inducing a salt shift on condensates formed at these working conditions (i.e., 100 mM KCl). The increase up to 300 mM KCl showed a dramatic reduction in the size and number of condensates, as observed by confocal microscopy (**Figure 2.9B**) accompanied by a drop in the turbidity signal values, matching those of the condensates originally formed at this higher salt concentration (**Figure 2.9C**).

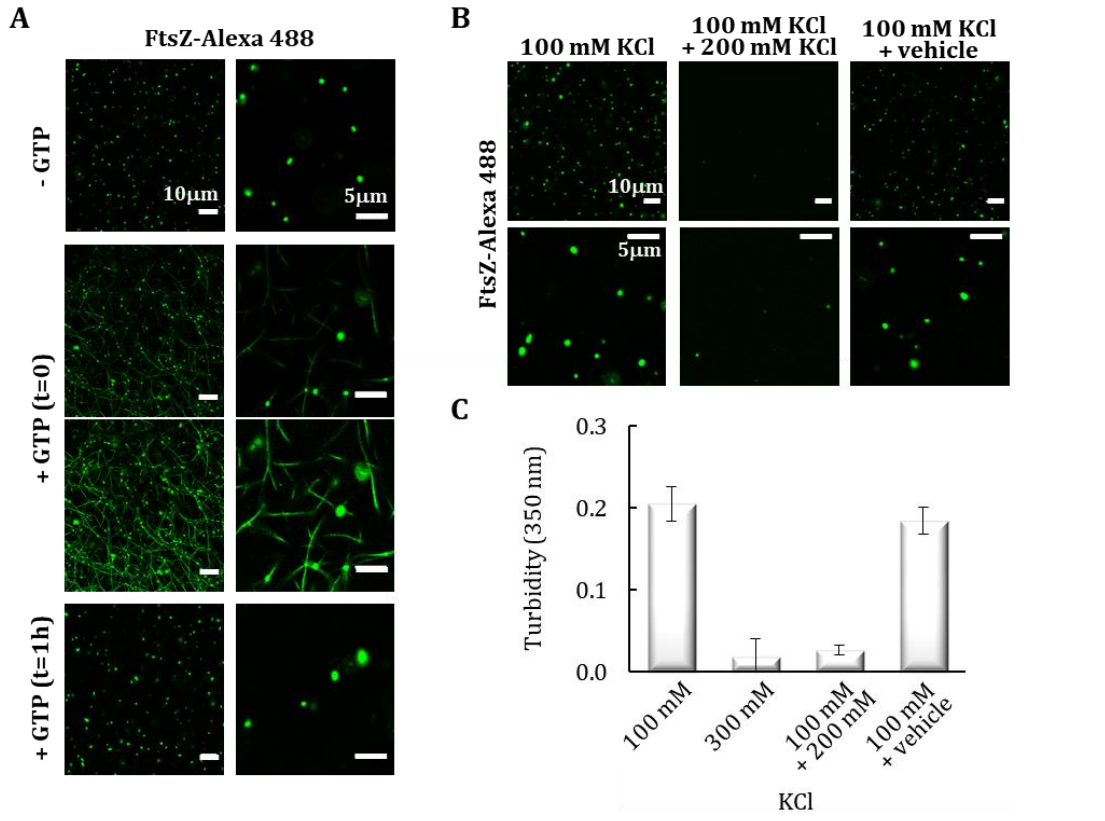


**Figure 2.9. FtsZ condensates are reversible**. (A) Confocal images showing the conversion of FtsZ condensates into GTP-triggered polymers and back. Immediately after addition of GTP (0.1 mM, t = 0), polymers are observed. For GTP and time zero, images within the same column are the identical field, with the images below obtained by enhancing the brightness (40%, left; 60%, right) of the ones above (correction applied uniformly to the whole image, using Microsoft PowerPoint) to better appreciate the polymerization of FtsZ. (B) Images showing FtsZ condensates and their dissociation by addition of KCl up to 300 mM. Images on the far right show the effect of the addition of vehicle instead (the same volume of water without KCl) to account for possible dilution effects (7%). (C) Turbidity values corresponding to the samples in (B). The turbidity of a sample directly prepared in 300 mM KCl is shown for comparison. All experiments were in working buffer, with 200 g/l dextran and 5 µM FtsZ.

### Reconstitution of FtsZ condensates in cytomimetic microdroplets

To determine whether FtsZ condensates could also be formed in a confined cell-like system, we used microfluidics to encapsulate the protein (**Figure 2.10**). Confocal microscopy images of FtsZ, containing FtsZ-Alexa 488 as a tracer, encapsulated in microdroplets stabilized by an *E. coli* lipid mixture boundary, indicated the presence of condensates in the z-sections of the microdroplets with no apparent preference for the lumen or the lipid interface. The presence of these structures was more obvious in the maximal projection of the images (far right in **Figure 2.10A**) that evidenced their presence in all microdroplets. No background signal was observed in the lumen, while a strong fluorescence demarcating the lipid boundary was found.

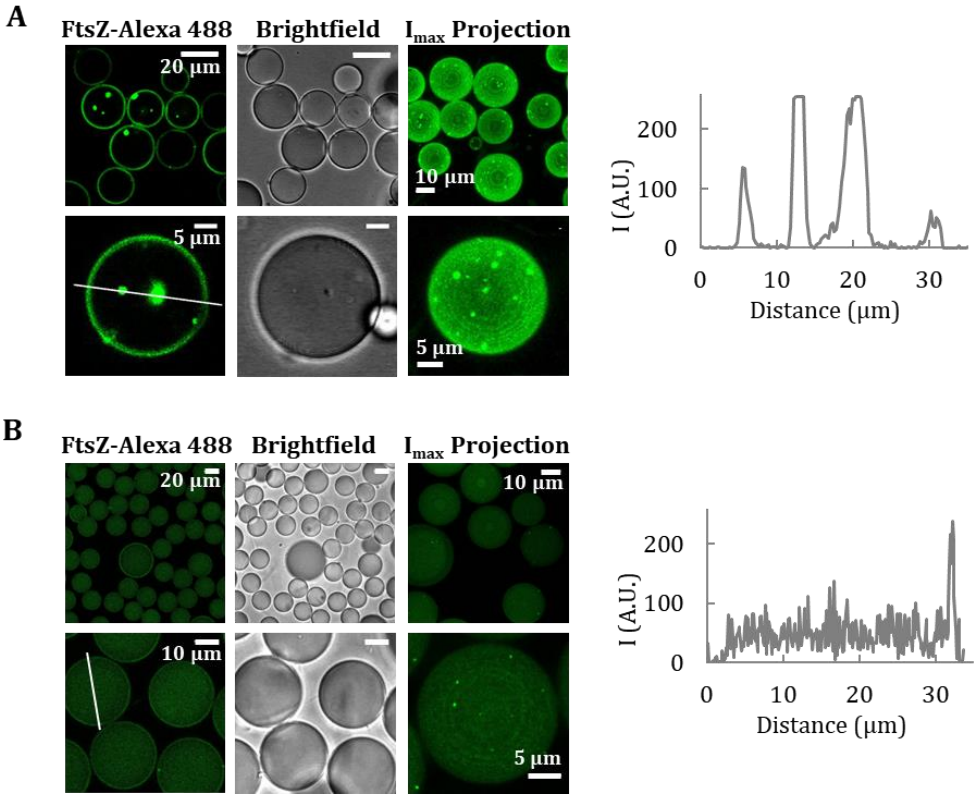


**Figure 2.10. FtsZ condensates are also formed in confined cell-like systems.** (A) Confocal microscopy images of microfluidics microdroplets stabilized by *E. coli* lipids and containing the condensates. 100% of the microdroplets examined (n = 40) contained condensates. Experiments were with 5 µM FtsZ in working buffer with 200 g/l dextran. (B) Encapsulation under experimental conditions not promoting FtsZ condensation in bulk: 12 µM FtsZ in 50 mM Tris-HCl, pH 7.5, 1 mM $MgCl_2$, 300 mM KCl and 150 g/l dextran. 58% of the microdroplets (n = 40) contained condensates. The third column of images for (A) and (B) are maximum intensity projections corresponding to different fields. To the right of (A) and (B) are intensity profiles of the green channel obtained across the lines drawn in the respective images.

Encapsulation of FtsZ under conditions that discourage bulk formation of condensates or any other detectable structures (300 mM KCl, 1 mM $MgCl_2$, 150 g/l dextran) showed scarce and very small condensates in the z-sections of 58% of the microdroplets tested, which were more obvious in the maximal projection and mostly near the membrane (**Figure 2.10B**). It should be noted that the percentage of microdroplets containing condensates under these conditions might be underestimated by the inability to detect condensates smaller than the resolution of confocal microscopy. Under these conditions, the protein remained homogeneously distributed within the lumen, in good agreement with previous reports showing FtsZ encapsulated under similar conditions (Mellouli et al., 2013, Sobrinos-Sanguino et al., 2017a).

These experiments confirm that condensates are still assembled when FtsZ is encapsulated under conditions favoring their formation in bulk. Moreover, incipient condensate formation was also apparent when the protein was encapsulated in conditions under which no condensates were detected by confocal microscopy or turbidity, strongly suggesting that confinement and/or the lipid membrane, directly or indirectly, influence their formation.

# DISCUSSION

Here we show that purified FtsZ protein forms reversible structures compatible with biomolecular condensates, observed under conditions resembling the physiological ones both in bulk solutions and when reconstituted in cytomimetic platforms. These structures are mostly reservoirs of material that have exceeded their solubility in the phase outside the condensate. Their assembly, disassembly, abundance, and coexistence (when the protein concentration is increased to high levels) with irregular clusters are all influenced by crowding and other chemical conditions that affect oligomerization of GDP-bound FtsZ (**Figure 2.11A**). This behavior is probably derived from the well-known self-association properties of this protein, which provide the multivalent states that typically favor formation of condensates. The present work emphasizes the key role of GDP in the formation of FtsZ condensates, different from that in other NTP-bound proteins such as DEAD-box ATPases where ATP hydrolysis promotes disassembly of the condensates (Hondele et al., 2019).

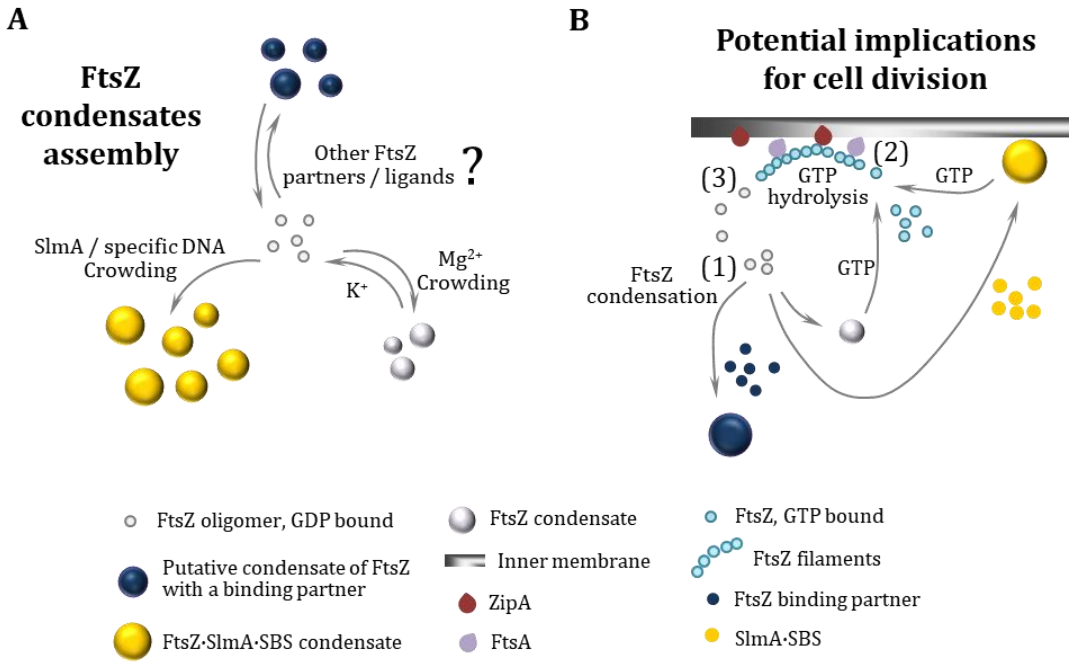


**Figure 2.11. Formation of FtsZ biomolecular condensates and potential role in bacterial cell division regulation.** (A) FtsZ condensate assembly is disfavored by $K^+$, favored by crowding and $Mg^{2+}$ and strongly promoted by the SlmA·SBS nucleoprotein complex. It is possible that condensation is also positively or negatively regulated by additional binding partners or by natural or synthetic ligands of FtsZ. (B) In the cell, FtsZ oligomers could form condensates on their own or together with the nucleoid occlusion factor SlmA (FtsZ·SlmA complexes tend to locate at the cellular membrane as described in chapter 1), and possibly also with other division regulators (1). In the presence of GTP, FtsZ would leave the condensates and associate into filaments attached to the bacterial membrane through the natural anchors, ZipA and FtsA (2). GTP hydrolysis would lead to GDP-bound FtsZ subunits within the filaments, and a loss of their longitudinal interactions would result in the release of FtsZ (3). The released FtsZ would be able to reassemble into homotypic or heterotypic dynamic condensates, contributing to the spatiotemporal regulation of bacterial cell division.

FtsZ within the condensates remained responsive to ligands, only forming filaments upon addition of GTP. This GTP-dependent shuttling of FtsZ between condensate and polymer states was also observed in our previous study of FtsZ·SlmA complexes (chapter 1), which showed that when mixed with the DNA-binding SlmA protein under crowding conditions, FtsZ formed condensates capable of reversible evolution to polymers in the presence of GTP. Condensation seemed more favored in that case, as such structures were observed under a substantially wider range of conditions in which FtsZ on its own was not able to form condensates. This relative promiscuity could be explained by the higher multivalency conferred on the system by the presence of SlmA, a dimer that binds in pairs to a specific SBS site on DNA (Cabre et al., 2015), while also establishing contacts with the C-terminal tail and the folded domain of FtsZ (Du and Lutkenhaus, 2014).

Protein condensate formation is usually associated with regions of low sequence complexity (Banani et al., 2017) and, indeed, FtsZ contains an unstructured segment (Gardner et al., 2013). The mutant FtsZ, deprived of this region, shows condensation possibly related to the multivalency emerging from its oligomerization interfaces. Nonetheless, this mutant displays slower condensation than wild-type FtsZ, which might be a result of differences in their dynamics and/or topology. Along these lines, GTP-induced filaments of FtsZ mutants from different bacterial species lacking the C-terminal peptide and/or the linker exhibited morphological alterations and slower polymerization rates (Buske and Levin, 2013). Also, as here with FtsZ, examples can be found where condensation is observed for folded domains, with disordered regions playing a modulatory role (Wang et al., 2019, Kroschwald et al., 2018, Riback et al., 2017, Oltrogge et al., 2020).

We observed formation of FtsZ condensates in confined cell like environments that included crowding and a membrane boundary. The use of such synthetic systems with controlled composition simplifies the interpretation of condensation compared with *in vivo* studies and, in the particular case of bacteria, circumvents technical obstacles due to their small size. Our encapsulation studies indicate that fully formed FtsZ condensates do not show a preference for the membrane, although it seems that the membrane could participate in the condensation of FtsZ, as shown by the small emerging structures at the lipid surface under bulk non-condensation conditions. This is compatible with either an increase in size of sub-micrometer condensates already present in solution, providing a surface for nucleation (Snead and Gladfelter, 2019), and/or further enhancement of their formation by confinement within the microdroplet. Interestingly, FtsZ·SlmA·SBS nucleoprotein condensates do accumulate at the lipid boundary as described in chapter 1, which we found to interact with membranes (chapter 3).

How might biomolecular condensation of FtsZ be relevant *in vivo*? Under certain conditions, cellular FtsZ oligomers might assemble into condensates, either alone or combined with any of FtsZ's multiple binding partners (**Figure 2.11B**). Condensate formation would be modulated to some extent by weak, transient electrostatic interactions with the environment, as nucleic acids are abundant and most proteins in *E. coli* are polyanions at intracellular pH (Spitzer and Poolman, 2009). As condensation enables dynamic spatial localization of cellular processes, condensates containing FtsZ might be favored during a particular phase of the cell cycle, perhaps used as a cytoplasmic storage form, or as a response to stresses (see below). For instance, the local accumulation of a higher number of molecules provided by condensation could permit more rapid pre-assembly with key protein

partners or ligands than by depending on successive recruitment of cell division proteins in the cytoplasm or on the cytoplasmic membrane. In the presence of GTP, FtsZ would exit the condensates and associate into mobile complexes of filaments attached to the bacterial membrane through the natural anchor proteins, ZipA and FtsA (Rowlett and Margolin, 2014, Baranova et al., 2020, Yang et al., 2017). GTP hydrolysis would increase the amount of FtsZ subunits bound to GDP within the filaments, with the associated loss in their longitudinal interactions and subsequent release of FtsZ (Du and Lutkenhaus, 2019), now available for a new condensation cycle. Curiously enough, the elusive ultrastructure of the *E. coli* Z-ring, only recently revealed through high resolution imaging, shows loosely associated clusters of FtsZ molecules of round appearance (Du and Lutkenhaus, 2019, Lyu et al., 2016). Further work will be required to ascertain the interplay of the FtsZ condensates identified here or of other putative heterotypic condensates involving this protein with the division ring.

The biomolecular condensation of purified FtsZ demonstrated here adds to the growing number of examples of this type of behavior by bacterial proteins. Despite initial doubts raised by the lower frequency of intrinsically disordered regions in bacterial proteomes, very recent research suggests that biomolecular condensation is an organizational principle that also operates in these microorganisms (Azaldegui et al., 2021). As an alternative to the membranous organelles of eukaryotes, such condensates distributed within the bacterial cytoplasm might contribute to the spatial regulation of various metabolic reactions, a role once attributed almost exclusively to the bacterial membrane envelope. In particular, condensates might form preferentially under stress conditions. Interestingly, it was recently reported that late stationary phase *E. coli* assemble protein aggregates at their cell poles containing FtsZ and other proteins; these “regrowth delay bodies” dissolve once growth is resumed, suggesting that they are dynamic (Yu et al., 2019). Such bodies may consist of multiple proteins that tend to form condensates under certain stress conditions such as starvation, desiccation and persister states (Laskowska and Kuczynska-Wisnik, 2020). It is noteworthy that cells in such states are likely deficient in GTP, a situation that as suggested by our results, could contribute to the formation of FtsZ condensates. Given that FtsZ is considered a promising target in the quest for new antibiotics (Kusuma et al., 2019), and that cells in the persister state are particularly resistant to antibiotics (Fisher et al., 2017), understanding how FtsZ forms condensates and where and when such condensates might form in cells may provide additional clues to fight against antimicrobial resistance.

# CHAPTER 3

# The nucleoid occlusion protein SlmA binds to lipid membranes

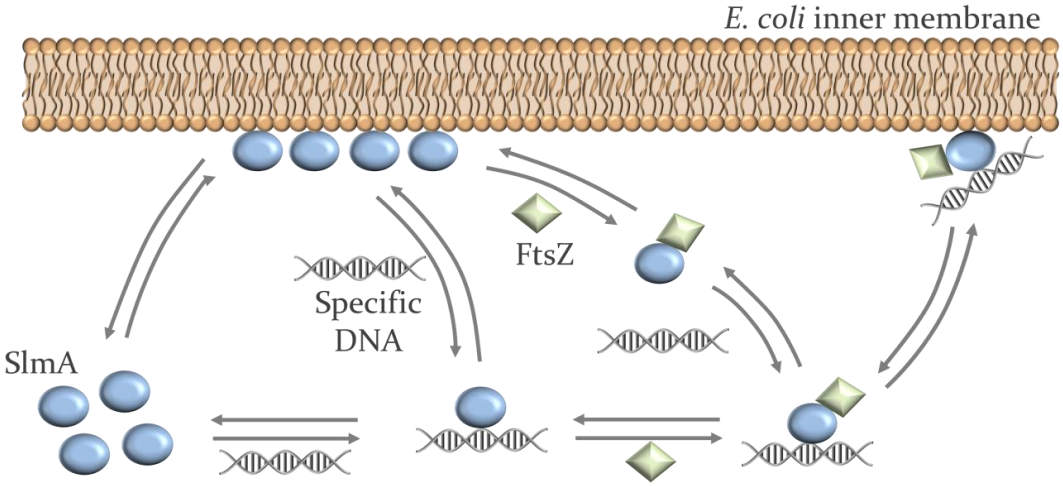


Protection of the chromosome from scission by the division machinery during cytokinesis is critical for bacterial survival and fitness. This is achieved by nucleoid occlusion, which, in conjunction with other mechanisms, ensures formation of the division ring at midcell. In *Escherichia coli*, this mechanism is mediated by SlmA, a specific DNA-binding protein that antagonizes assembly of the central division protein FtsZ into a productive ring in the vicinity of the chromosome. Here, we provide evidence supporting direct interaction of SlmA with lipid membranes, tuned by its binding partners FtsZ and SlmA binding sites (SBS) on chromosomal DNA. Reconstitutions in minimal membrane systems that mimic cellular environments show that SlmA binds to lipid-coated microbeads or locates at the edge of microfluidic-generated microdroplets, inside which the protein is encapsulated. DNA fragments containing SBS sequences do not seem to be recruited to the membrane by SlmA but instead compete with SlmA's ability to bind lipids. The interaction of SlmA with FtsZ modulates this behavior, ultimately triggering membrane localization of the SBS sequences alongside the two proteins. The ability of SlmA to bind lipids uncovered in this work extends the interaction network of this multivalent regulator beyond its well-known protein and nucleic acid recognition, which may have implications in the overall spatiotemporal control of division ring assembly.

# RESULTS

## SlmA binds to biomimetic lipid membranes

To determine if purified SlmA could directly bind lipids, we followed a previously applied strategy involving microbeads coated with a lipid mixture matching the composition of the *E. coli* inner membrane (Martos et al., 2012b). Titrations of SlmA labeled with Alexa Fluor 488 (SlmA-Alexa 488) with increasing concentration of the lipid-coated microbeads, in working buffer[3] with 300 mM KCl, showed that a significant and gradually higher fraction of the protein pelleted alongside the microbeads (**Figure. 3.1A**). Because the precise mode of binding of

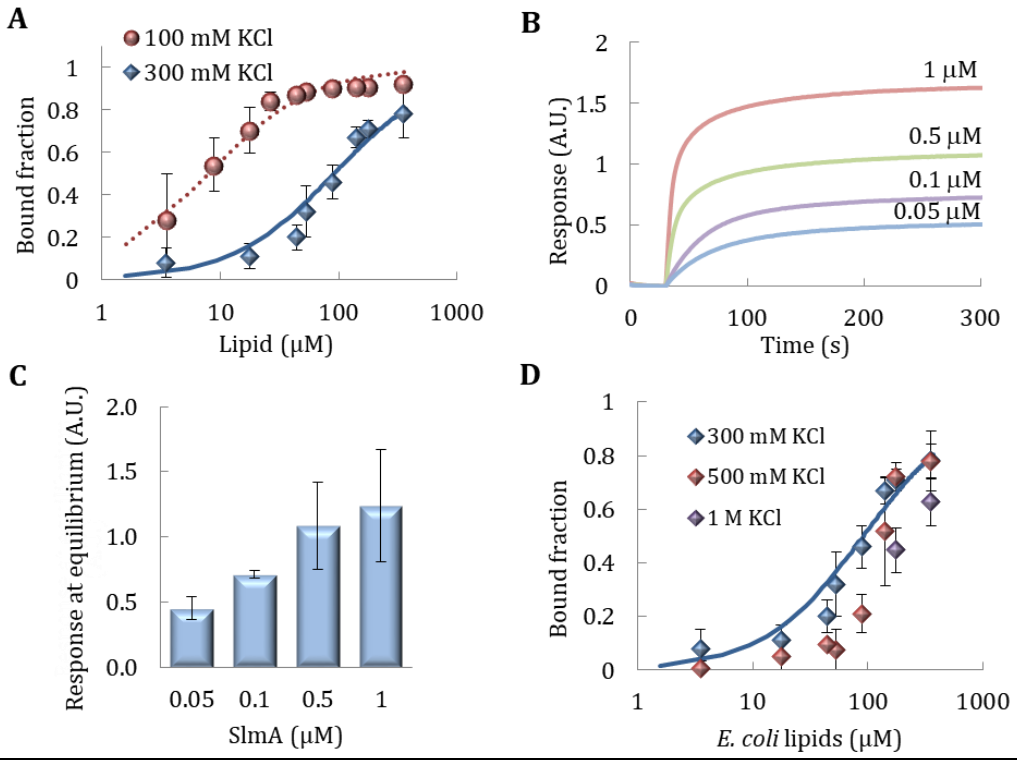


**Figure 3.1. Interaction of SlmA with *E. coli* lipids.** (A) Fraction of SlmA bound to microbeads coated with the *E. coli* lipid mixture as a function of the accessible lipid concentration in working buffer at 100 and 300 mM KCl. Solid line represents the fit of the model indicated in the main text to the experimental data, with $c_{50}$ = 91 ± 15 μM. Dotted line corresponds to a simulation, using the same model and $c_{50}$ = 8 μM. (B) Representative profiles obtained by biolayer interferometry of the binding of SlmA to *E. coli* lipids at the indicated protein concentrations and (C) variation of the response at equilibrium with SlmA concentration. (D) Effect of KCl concentrations above 300 mM on binding to *E. coli* lipids as a function of the accessible lipid concentration. Experiments in working buffer with 300 mM KCl unless otherwise specified. Data are the average of 3 (A and D) or at least 2 (B and C) independent experiments ± SD.

[3] Working buffer: 50 mM Tris-HCl pH 7.5, 5 mM $MgCl_2$.

SlmA is not known, and proteins usually interact with lipids in a multivalent manner, an empirical model was fit to this binding curve to obtain an apparent affinity value, as typically done for protein-lipid interactions (Zhao and Lappalainen, 2012). Analysis of the binding curve obtained using a Langmuir isotherm, with no assumption about the stoichiometry of the interaction, rendered binding of the 50% of total amount of protein at a lipid concentration ($c_{50}$) of 91 ± 15 μM. Binding of SlmA to lipid membranes was independently confirmed by using biolayer interferometry (**Figure 3.1B**). Addition of protein to tips coated with the *E. coli* lipid mixture showed a concentration-dependent rise in the signal, as expected for binding (**Figure 3.1C**).

SlmA, with SlmA-Alexa 488 as a tracer, was subsequently encapsulated inside microdroplets generated by microfluidics stabilized by the *E. coli* lipid mixture. At 300 mM KCl, part of the protein was found at the edges of the microdroplets, with a significant fraction homogeneously distributed in the lumen, as observed in the intensity profiles obtained across the droplets (**Figure 3.2A**). This result further evidences the tendency of the protein to interact with lipid surfaces.

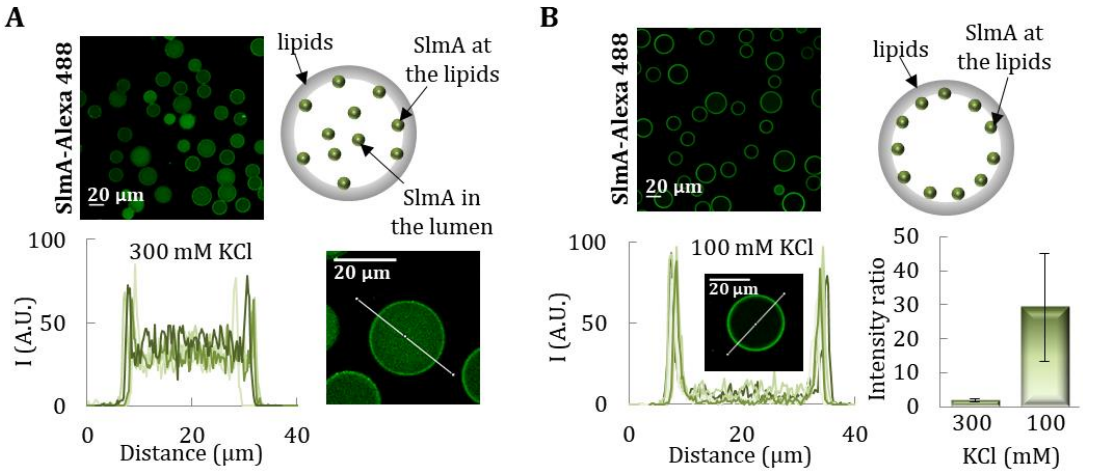


**Figure 3.2. Encapsulation of SlmA inside microfluidics microdroplets stabilized by the *E. coli* lipid mixture**. Confocal images of encapsualted SlmA in working buffer with 300 mM KCl (A) or 100 mM KCl (B), with schematics illustrating the distribution of SlmA within the microdroplets (right), and intensity profiles of 5 different microdroplets corresponding to the green channel, obtained along the line as drawn in the images. The ratios of the intensity at the membrane to that at the lumen, corresponding to the average ± SD, are also shown (n = 5, 300 mM KCl; n = 15, 100 mM KCl). The concentration of SlmA was 5 μM (with 1 μM tracer). Brightness was enhanced (40%) in all images.

Next, the impact of ionic strength on SlmA binding to lipid membranes was studied. Increasing the concentration of KCl to 500 mM and even 1 M had a minor impact on protein binding in the experiments with lipid-coated microbeads with

respect to that determined at 300 mM KCl (**Figure 3.1D**). Interestingly, decreasing the concentration of KCl to 100 mM resulted in a remarkable shift of the binding curve toward lipid concentrations around an order of magnitude lower (**Figure 3.1A**). This large effect on SlmA binding was also detected in microfluidics encapsulation experiments. At this salt concentration (100 mM), virtually all SlmA was localized at the lipid monolayer of the microdroplets, according to the intensity profiles retrieved (**Figure 3.2B**). This protein localization pattern was analogous to that when encapsulated inside giant vesicles (**Figure 3.3**), obtained by off-chip conversion of microdroplets through the acquisition of a second lipid layer using an adapted droplet transfer method. The presence of a crowder inside the microdroplets, required for the generation of giant unilamellar vesicles, did not modify the protein distribution under these encapsulation conditions (**Figure 3.3**).

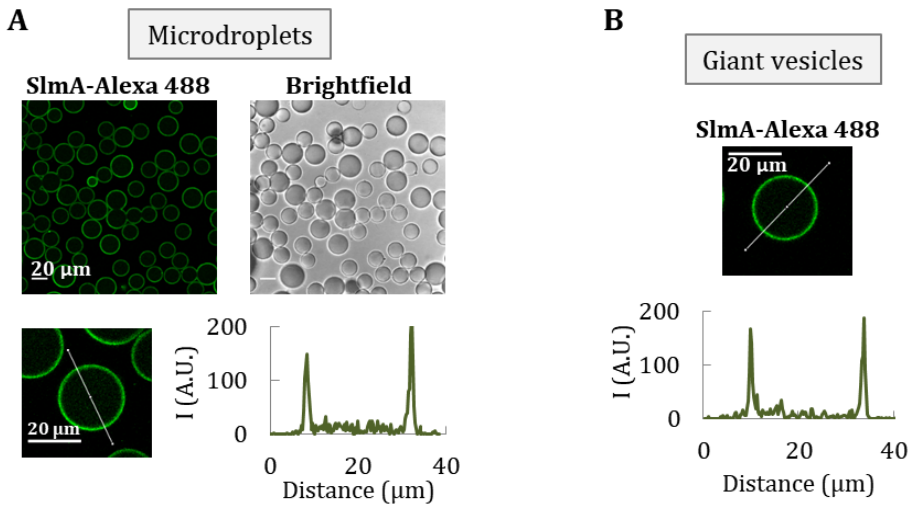


**Figure 3.3. Encapsulation of SlmA inside microdroplets and vesicles.** Encapsulation of SlmA inside microfluidic microdroplets stabilized by the *E. coli* lipid mixture (A) and vesicles formed from them (B). In working buffer with 100 mM KCl and 150 g/l Ficoll. Total SlmA concentration is 5 µM (with 1 µM tracer). Intensity profiles correspond to the signal of the green channel obtained along the line depicted in the images. Brightness enhanced (20%) in all images.

The ability of SlmA to bind to lipid membranes composed solely of neutral lipids was also tested through assays using microbeads coated with phosphatidylcholine (PC) (**Figure 3.4A**). Significant interaction was also found in this case and, at 300 mM KCl, the binding curve was equivalent within error to that determined with the *E. coli* lipid mixture under the same conditions. As with those, binding to PC was relatively insensitive to salt in the 300 mM to 1 M range, whereas at 100 mM KCl, the interaction was strongly favored (**Figure 3.4B and C**). This suggests that hydrophobic interactions play a role in the lipid recognition by SlmA.

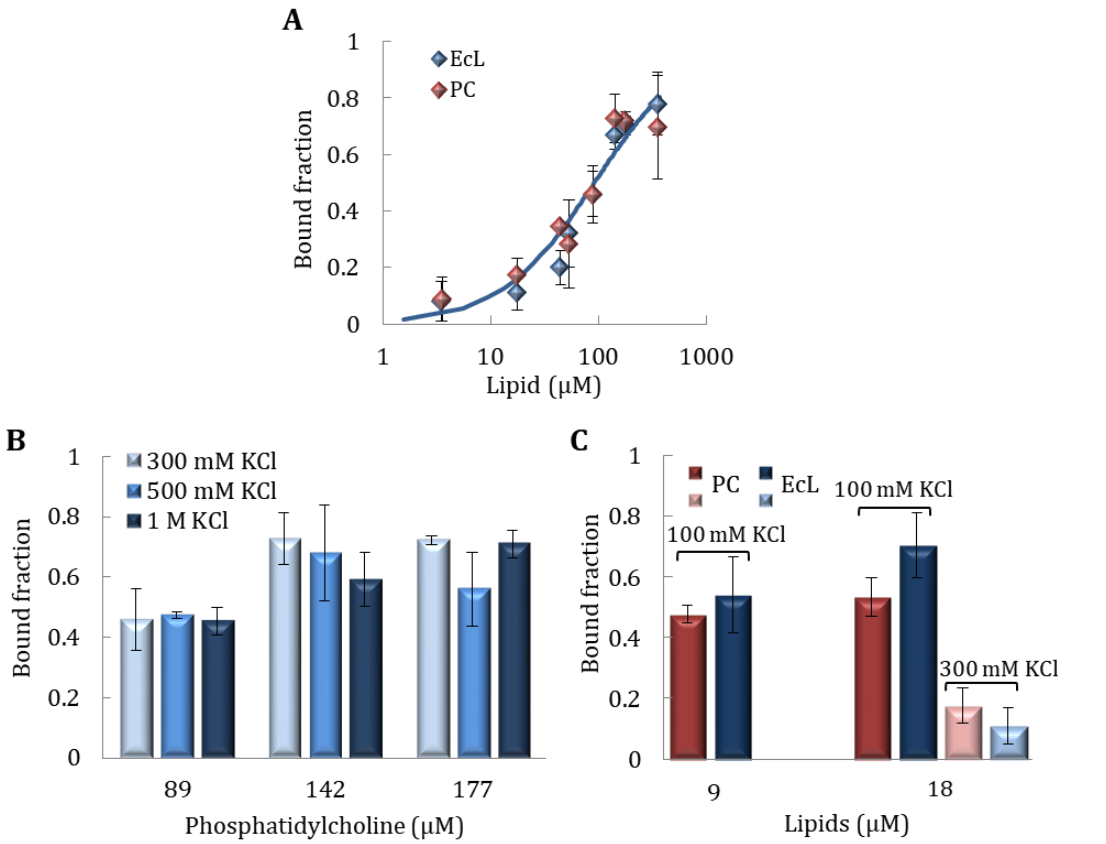


**Figure 3.4. Fraction of SlmA bound to microbeads coated with different lipids.** (A) Fractions of SlmA bound to microbeads coated with the *E. coli* lipid mixture or with PC as a function of the accessible lipid concentration in working buffer with 300 mM KCl. Solid line represents the fit of the model indicated in the main text to the experimental data. (B) Effect of KCl on binding to phosphatidylcholine (PC) as a function of the accessible lipid concentration, in working buffer. (C) Comparison between both lipids at two different concentrations in working buffer at 100 and 300 mM KCl. In all experiments, the concentration of SlmA-Alexa 488 was 250 nM and data are the averages from 3 (EcL) or 2 (PC) independent experiments ± SD.

From all these experiments, it can be concluded that SlmA binds to lipid membranes when reconstituted in cell-mimetic systems. Evolution of the apparent affinity of the interaction with salt follows a mixed trend, being strongly enhanced at low concentrations but weakly affected above a certain threshold. Moreover, hydrophobic forces also seem to contribute to the overall interaction scheme.

### Specific SBS sequences compete with lipid membranes for binding to SlmA

Next, we evaluated the impact of the SBS sequences specifically recognized by SlmA on the interaction of the protein with the membrane. To this end, we coencapsulated SlmA, with SlmA-Alexa 488 as a tracer, and a double-stranded SBS sequence containing a single SlmA binding site, labeled with Alexa Fluor 647 (SBS-

Alexa 647), inside microfluidics microdroplets stabilized by the *E. coli* lipid mixture. Under all conditions assayed, the signal arising from the red-labeled DNA evidenced its homogeneous distribution inside the microdroplets, with the intensity in the profiles dropping to basal levels at the lipid boundary (**Figure 3.5 and 3.6**). SlmA, in turn, partitioned between the lumen and the membrane to a greater or lesser extent depending on the SBS and salt concentration. At 300 mM KCl, the signal corresponding to SlmA at the edges of the microdroplets was similar to that in the lumen (**Figure 3.5**), in contrast with the slightly higher relative signal observed at the membrane in the absence of the SBS (cf. **Figures 3.2A and 3.5**). This suggests competition between the SBS and the membrane for binding to SlmA.

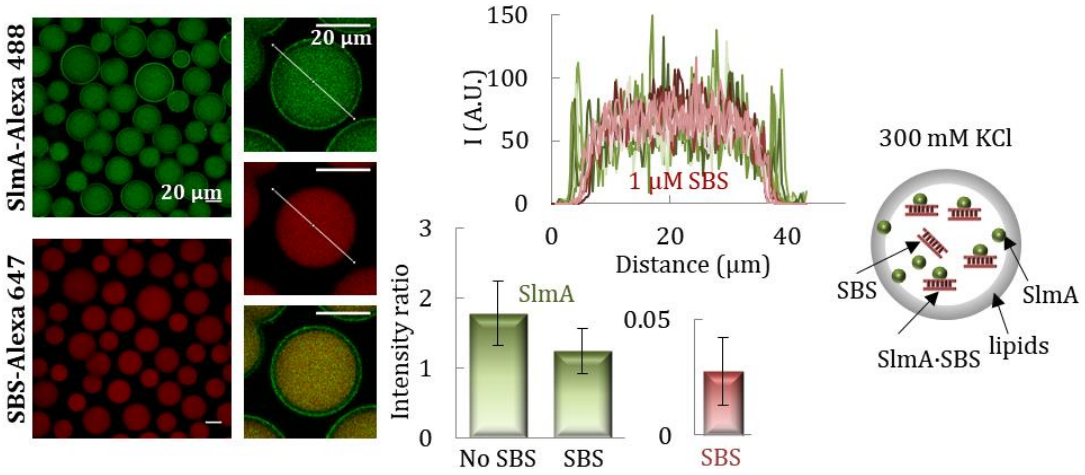


**Figure 3.5. Encapsulation of SlmA and SBS in microfluidics microdroplets stabilized by the *E. coli* lipid mixture at 300 mM KCl**. Shown are representative confocal microscopy images of the microdroplets in the green and red channels, including merged image of a single microdroplet, and intensity profiles corresponding to 5 different microdroplets, obtained along the line as drawn in the images, in each channel. The ratios of the intensity at the membrane to that at the lumen, corresponding to the average ± SD, are also shown, together with those of SlmA encapsulated alone under the same buffer conditions for comparison. The concentration of SlmA was 5 µM, with 1 µM tracer. The concentrations of SBS tracer was 1 µM. Scheme illustrating the distribution of SlmA and SBS within the microdroplets is shown. Encapsulation was performed in working buffer with 300 mM KCl. Brightness was enhanced in all images (20%).

Competition was more obvious in the experiments conducted at 100 mM KCl, in which two different SBS concentrations were tested. At 1 µM SBS, part of the protein dislodged from the lipid boundary (**Figure 3.6, left**) compared with the high levels of SlmA at this location in the absence of SBS (**Figure 3.2B**), shifting toward the lumen of the microdroplets. Accordingly, the intensity in the green channel in that region of the droplet significantly increased, overlapping with the signal corresponding to the red-labeled SBS (**Figure 3.6, left**). SlmA detachment

from the membrane was subtler at 0.4 μM SBS (**Figure 3.6, right**), which is compatible with a concentration-dependent competition between the two types of ligands for the protein. There was no evidence of recruitment of the SBS to the lipid membrane, even when the complex was already formed in solution before encapsulation, despite the significant fraction of SlmA remaining at the edge of the microdroplets, further supporting the competition between both ligands.

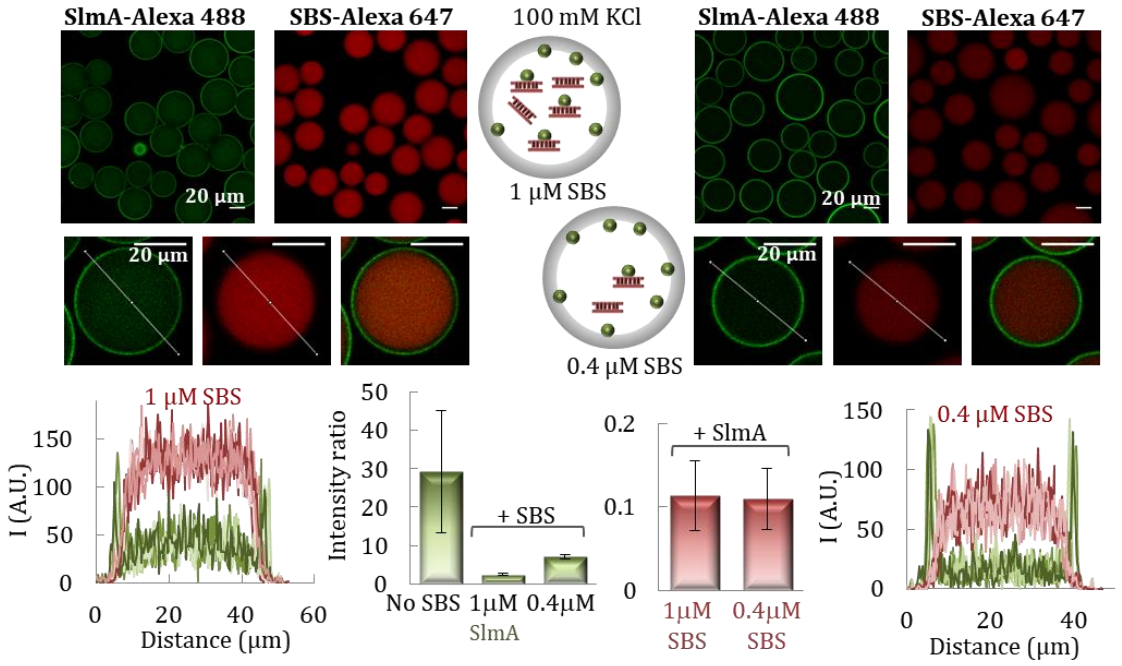


**Figure 3.6. Encapsulation of SlmA and SBS in microfluidics microdroplets stabilized by the *E. coli* lipid mixture at 100 mM KCl**. Representative confocal microscopy images of the microdroplets in the green and red channels. Merged images of single microdroplets, and intensity profiles corresponding to 5 different microdroplets, obtained along the line as drawn in the images, in each channel are shown. The ratios of the intensity at the membrane to that at the lumen, corresponding to the average ± SD, are also shown, together with those of SlmA encapsulated alone under the same buffer conditions for comparison. The concentration of SlmA was 5 μM, with 1 μM tracer. The concentrations of SBS tracer was 1 μM (left) or 0.4 μM (right). Schematics illustrating the distribution of SlmA and SBS within the microdroplets are shown. Encapsulations were conducted in working buffer with 100 mM KCl.

We also studied the impact of SBS-containing DNA on lipid binding by SlmA through fluorescence anisotropy measurements on samples with fluorescein-labeled SBS (SBS-Fl), unlabeled SlmA, and increasing concentrations of *E. coli* lipid-coated microbeads after pelleting the microbeads by centrifugation (**Figure 3.7**). The concentrations of SBS and SlmA in these experiments were kept constant. As expected, in the absence of lipids, the anisotropy of free SBS-containing DNA increased upon addition of SlmA (Cabre et al., 2015). Inclusion of lipid-coated

microbeads resulted in a reduction in the retrieved anisotropy that was dependent on lipid concentration, both at 100 and at 300 mM KCl (**Figure 3.7**). This is compatible with a release of the protein from the nucleoprotein complex upon lipid recognition, in good agreement with that observed in the microdroplet assays. The total intensity measured for the labeled SBS after microbead sedimentation in these experiments was largely independent of the concentration of microbeads, providing additional evidence of a lack of ternary complexes involving both DNA and lipids.

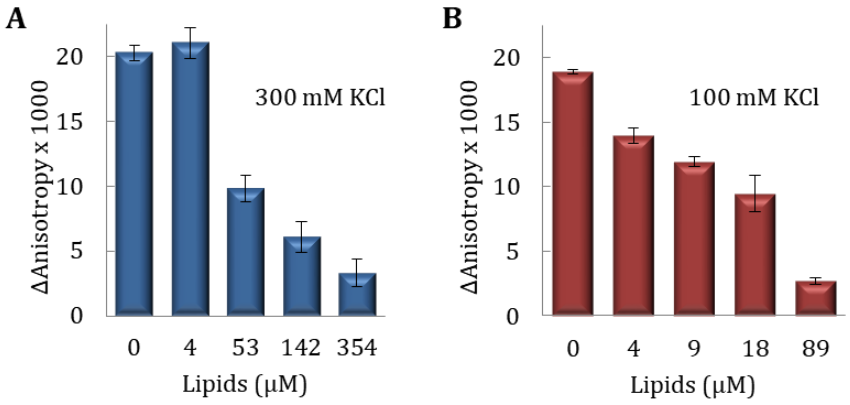


**Figure 3.7. Competition between SBS and lipids for SlmA binding.** Shown is the enhancement of fluorescence anisotropy in the presence of SlmA with respect to the value for the free SBS-Fl, as a function of the concentration of accessible lipids coating microbeads, in working buffer with the specified KCl concentrations. The concentrations of SlmA were 250 nM (A) and 125 nM (B), and that of SBS-Fl was 62.5 nM. Anisotropy was measured after microbead pelleting. Data are the averages from 3 independent experiments ± SDs.

### FtsZ promotes the recruitment of SBS to the membrane by SlmA

The direct recognition of FtsZ, favored by SBS binding, is central to the interaction network of SlmA. To determine the effect of FtsZ on the binding of SlmA to the membrane, we simultaneously encapsulated both proteins inside microdroplets stabilized by the *E. coli* lipid mixture in working buffer with 100 mM KCl (**Figure 3.8A**). The inclusion of FtsZ resulted in a significant shift of a fraction of SlmA from its typical location at the membrane (cf. **Figure 3.2B**) to the lumen of the microdroplet, presumably due to the interaction between the two proteins. Indeed, the intensity signals of SlmA-Alexa 488 and of FtsZ labeled with Alexa Fluor 647 (FtsZ-Alexa 647) overlapped both inside the microdroplet and at the lipid boundary, reflecting an analogous distribution pattern (**Figure 3.8A**). Encapsulation of FtsZ alone showed that although most of the protein remained in the lumen, part of it was also found at the lipid interface (**Figure 3.8B**). This is

consistent with the previously described low tendency of FtsZ to bind to microbeads coated with *E. coli* lipids under these buffer conditions (Sobrinos-Sanguino et al., 2017b).

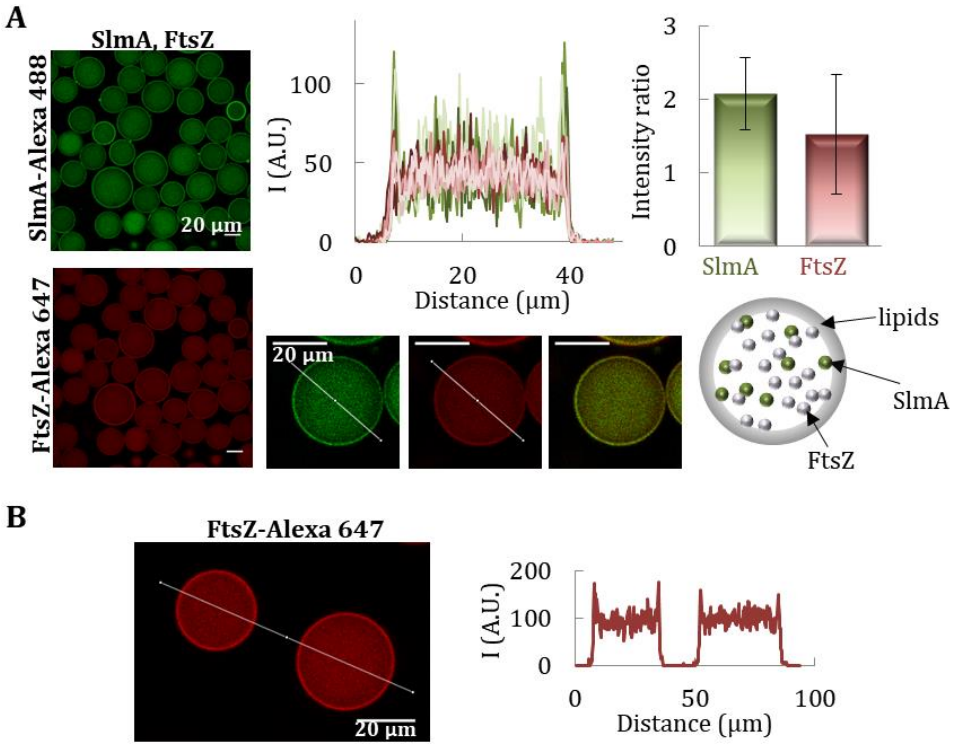


**Figure 3.8. Encapsulation of FtsZ ± SlmA inside microdroplets stabilized by the *E. coli* lipid mixture.** (A) Representative confocal images are shown with intensity profiles in the green and red channels corresponding to 5 different microdroplets, obtained along the lines depicted in the images, including the merged image of a single microdroplet. The ratios of the intensity at the membrane to that at the lumen, corresponding to the averages ± SDs, are also shown. A schematic illustrating the distribution of the two elements in the microdroplets is shown. The concentrations of SlmA and FtsZ were 5 and 12 µM, respectively, with 1 µM tracers, in working buffer with 100 mM KCl. (B) Representative confocal images of FtsZ inside microfluidics microdroplets stabilized by the *E. coli* lipid mixture. Total FtsZ concentration was 12 µM (with 1 µM tracer), in working buffer with 100 mM KCl. Intensity profile corresponds to the signal of the red channel obtained along the line depicted in the image. In (A), the brightness of the images was enhanced (20%).

Given the effect of FtsZ on the interaction of SlmA with lipids, we proceeded to characterize its impact on the competition observed between the membrane and the SBS sequences for the protein. For this purpose, the SBS sequence was encapsulated alongside the two proteins in working buffer with 100 mM KCl, and their distribution was assessed by including SlmA-Alexa 488 and one of the other two elements coupled to a red dye as tracers (**Figure 3.9**). In the two types of experiments, SlmA clearly accumulated at the lipid membrane, with a certain amount remaining in the lumen. The presence of SlmA at nonmembrane regions

was higher than when it was the sole species encapsulated (cf. **Figure 3.9 and 3.2B**) but somewhat lower than when coencapsulated with only one of its partners (**Figures 3.6 and 3.8A**). Images with SBS-Alexa 647 in the presence of FtsZ and SlmA revealed a shift of the DNA toward the lipid boundary, with the consequent appearance of a peak in the red intensity at this location (**Figure 3.9A**). Parallel experiments with FtsZ-Alexa 647 as the secondary fluorescent element revealed its localization both in the lumen and at the lipid boundary, without an obvious preference for any of those locations (**Figure 3.9B**).

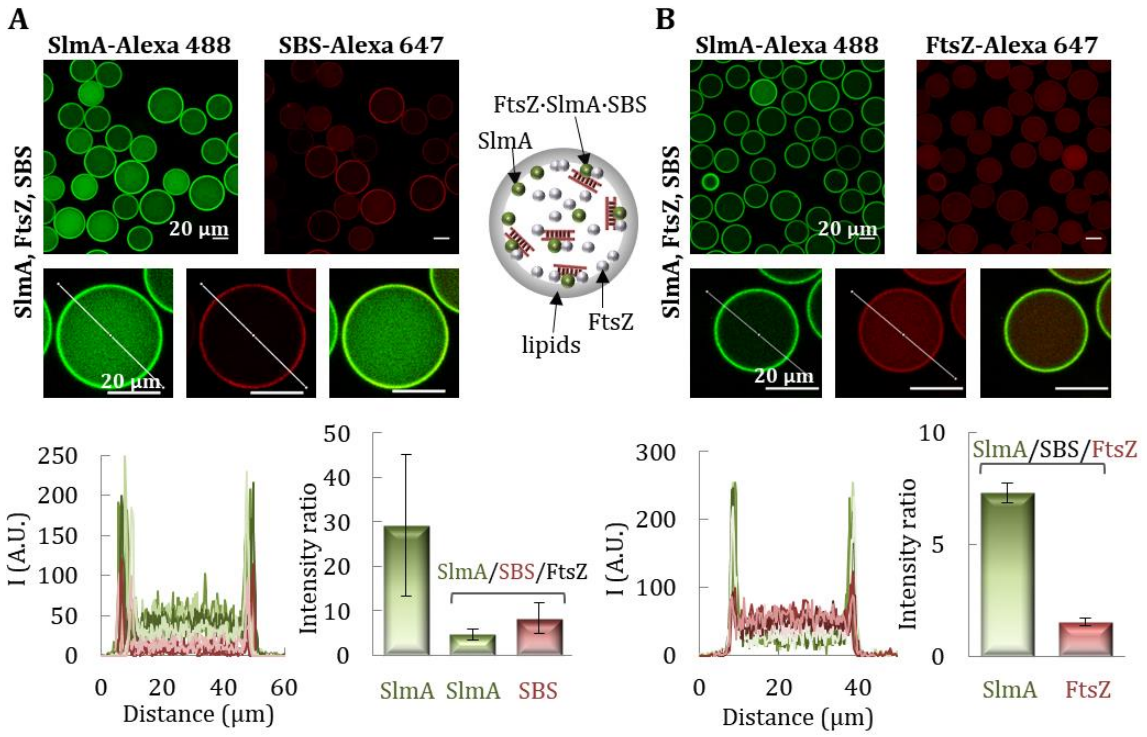


**Figure 3.9. Encapsulation of SlmA and SBS in the presence of FtsZ.** (A and B) Encapsulation of SlmA, FtsZ, and SBS inside microdroplets stabilized by the *E. coli* lipid mixture in working buffer with 100 mM KCl. Shown are representative confocal images and intensity profiles of 5 different microdroplets in the green and red channels obtained across the line depicted in the images, including merged images of single microdroplets. The ratios of the intensity at the membrane to that at the lumen, corresponding to the averages ± SDs, are also shown, together with those of SlmA encapsulated alone under the same buffer conditions, for comparison in panel (A). SlmA, FtsZ, and SBS concentrations were 5 µM, 12 µM, and 1 µM, respectively. Tracers amounts (1 µM) of SlmA and SBS (A) or FtsZ (B) were used. A schematic illustrating the distribution of the three elements in the microdroplets is shown. In (A), the brightness of the images was enhanced (45%).

We also used *E. coli* lipid-coated microbead assays to confirm the recruitment of the SBS to the lipids in the presence of SlmA and FtsZ. Incubation of fluorescein-labeled SBS with microbeads in the presence of both SlmA and FtsZ, followed by centrifugation, led to a decrease in the fluorescence signal compatible with

sedimentation of the DNA together with the beads (**Figure 3.10**). At constant lipid concentration, the amount of bound DNA increased with its total concentration, in an experiment in which the molar ratio of SBS to SlmA to FtsZ was kept at 1:5:12 (**Figure 3.10A**). Titrations at different concentrations of FtsZ, while maintaining constant those of SBS-Fl, SlmA, and the microbeads, showed an increase in the fraction of SBS recruited to the lipids in parallel with the increase in FtsZ concentration (**Figure 3.10B**). All these experiments indicate that in the presence of FtsZ, SlmA is capable of recruiting the SBS to the membrane.

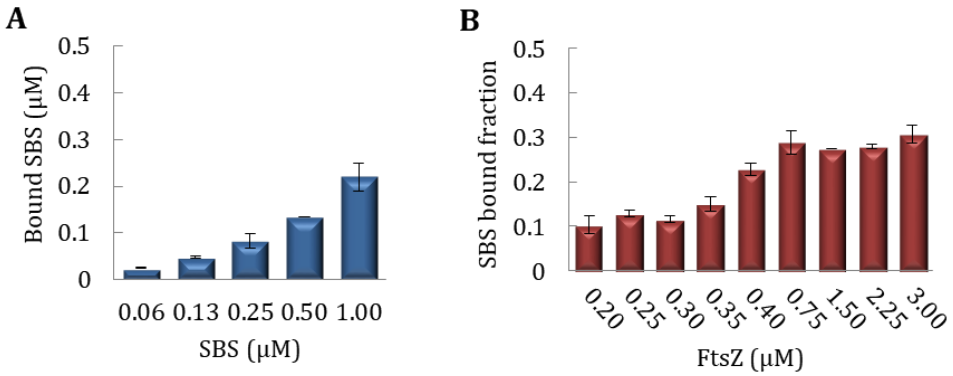


**Figure 3.10. Interaction of SlmA·SBS with lipids in the presence of FtsZ.** (A) Variation of the concentration of SBS bound to microbeads coated with *E. coli* lipids with its total concentration, in the presence of SlmA and FtsZ. SBS was labeled with fluorescein. In all samples, the SBS/SlmA/FtsZ molar ratio was 1:5:12. (B) Variation of the fraction of SBS bound to microbeads coated with *E. coli* lipids with the concentration of FtsZ. SBS was labeled with fluorescein, and its concentration was 0.125 μM and that of SlmA was 0.5 μM. Negligible binding was obtained at and below 0.1 μM FtsZ. The concentration of lipids was 266 μM. All experiments were in working buffer with 100 mM KCl. Data are the averages from 3 independent experiments ± SDs.

# DISCUSSION

The work presented here shows that the nucleoid occlusion factor SlmA, a protein that specifically targets DNA sequences and engages in complex multivalent interactions with FtsZ, displays membrane binding activity as well. The specific DNA sequence, SBS, has a competing role in this interaction scheme, releasing SlmA from the lipids upon formation of the nucleoprotein complex. FtsZ somehow counteracts this competition and, in its presence, the three elements (FtsZ, SlmA, and the SBS) gather at the lipid membrane (**Figure 3.11A**).

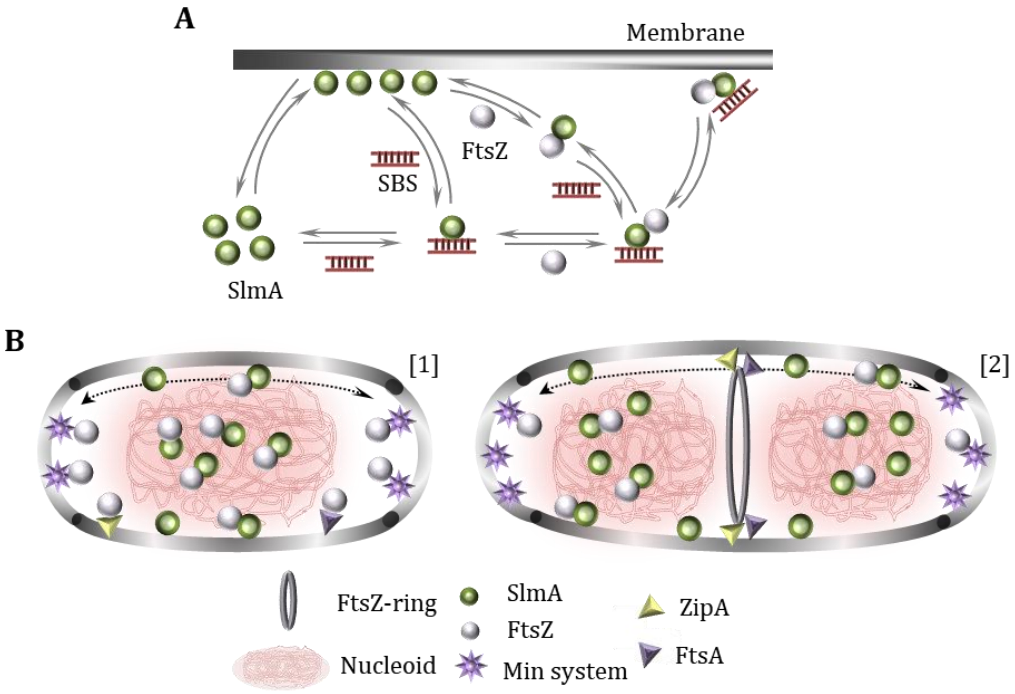


**Figure 3.11. Scheme of the interactions between SlmA, SBS, the membrane, and FtsZ and hypothetical relation with bacterial division stages.** (A) SlmA binds to SBS sequences or the membrane in a competitive fashion. The nucleoprotein complexes of SlmA interact with FtsZ, as result of which the two proteins and the DNA gather at the membrane. In the absence of SBS, FtsZ partially dislodges SlmA from the membrane. The partition of SlmA and its complexes at the membrane seems to depend on conditions such as ionic strength and on the relative concentrations of the participating factors (SlmA, FtsZ, SBS sequences, and lipids). (B) Under nondividing conditions (1), SlmA interacts with either the membrane or the SBS sequences within the nucleoid. SlmA and SBS form complexes that may localize at the membrane only upon interaction with FtsZ. Here, additional FtsZ subunits are anchored through their interaction with FtsA and ZipA. The joint action of the Min system and nucleoid occlusion prevents FtsZ ring formation all over the cell. SlmA modulates the oscillation of the Min waves, perhaps when bound to the membrane. (2) Under division conditions, the chromosomes segregate, pulling SlmA and leaving a SlmA free region at midcell where FtsZ, free from the action of the antagonists, now is able to form an FtsZ ring anchored to the membrane by FtsA and ZipA. In noncentral regions, the chromosomes are still protected from aberrant division by SlmA arresting the formation of a ring, and the Min system inhibits its assembly at the poles.

According to our reconstitution experiments, SlmA binds to *E. coli* lipid minimal membranes (consisting of two kinds of negatively charged lipids and a neutral one) and similarly to model membranes with a single neutral lipid (PC), strongly suggesting that hydrophobic interactions contribute to SlmA lipid binding. This is consistent with the mild impact of salt variations in the 300 mM to 1 M KCl concentration range and with the presence of large hydrophobic regions in SlmA (Tonthat et al., 2011). The strong enhancement of membrane binding at 100 mM KCl, however, points toward a direct or indirect influence of electrostatic forces as

well. Because this effect is observed for both *E. coli* lipids and PC, despite their different net charges, it is possible that it arises from modifications in the oligomerization state of the protein itself, its conformation, or the kind of assemblies it might form upon binding to the membrane surface. Sedimentation velocity experiments rule out alterations in the oligomeric state of the protein prior to lipid binding, as the protein profiles retrieved within the 100 to 500 mM KCl interval (**Figure 3.12**) virtually overlap those corresponding to the dimeric species previously described at 300 mM KCl (Cabre et al., 2015). The formation of higher-order SlmA assemblies once on the membrane, promoted by low salt, remains as a possible explanation for the enhanced binding avidity, which would emerge from several transient, probably weak, contacts between SlmA molecules at high local density and the lipid surface. This kind of multivalent interaction appears recurrently in the SlmA interaction network (Schumacher, 2017). Thus, SlmA targets two low-affinity sites within an FtsZ monomer (Du and Lutkenhaus, 2014), and stabilization of the overall complexes is achieved through contacts with multiple FtsZ subunits (Du et al., 2015) arranged in filaments in the presence of GTP or in shorter oligomers in its absence. Multivalent interactions in the FtsZ-SlmA-SBS complexes are also one of the factors behind their observed tendency to reversibly assemble into dynamic biomolecular condensates under crowding conditions described in chapter 1.

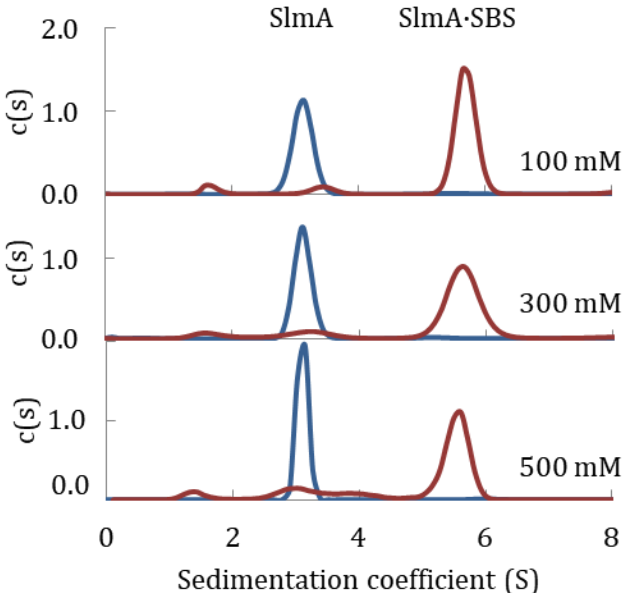


**Figure 3.12. Effect of KCl on SlmA and SlmA·SBS complexes as determined by sedimentation velocity.** Typical sedimentation coefficient distributions of SlmA (5 μM) without and with SBS (1 μM) in working buffer with the specified KCl concentrations. The ~3 S and ~6 S single species are compatible with the SlmA dimer and the 4:1 complex formed by SlmA with the DNA, respectively, previously reported (Cabre et al., 2015).

The interaction of SlmA with the membrane is modulated by its other natural ligands, FtsZ and the SBS sites, in different ways depending on whether only one of them or both are present (**Figure 3.11A**). Individually, FtsZ and the SBS exhibit a competitive behavior, partially dislodging SlmA from the lipid surface. This behavior radically changes when both of them are present and, under

these circumstances, the FtsZ-SlmA-SBS complexes tend to accumulate at the membrane. Competition between SBS sequences and lipids for SlmA could reflect the existence of a common binding site but also a change in the relative orientation, conformation, or stoichiometry induced by each ligand that would preclude recognition by the other. Indeed, SBS interaction with SlmA is known to alter the stoichiometry of the protein, which is otherwise dimeric, in a salt-independent manner (**Figure 3.12**). This is thought to occur with two SlmA dimers in very close proximity and in a highly conserved binding orientation, although not through direct interaction with each other (Cabre et al., 2015, Tonthat et al., 2013). Moreover, SBS-induced conformational changes in SlmA have been also described, such as those stabilizing the flexible DNA-binding domain and the binding pocket into which the C-terminal tail of FtsZ gets inserted (Schumacher and Zeng, 2016).

It is not obvious why FtsZ is necessary for the simultaneous localization of SlmA and SBS sites at the membrane, but different hypotheses can be formulated. For example, FtsZ may unmask the membrane binding region within SlmA if partially/totally occluded in the SlmA-SBS complexes or induce structural changes more compatible with simultaneous binding of both DNA and membranes. Alternatively, or additionally, the higher multivalency obtained through the interaction with FtsZ may endow the overall complex with properties favoring membrane localization. Further experiments using longer DNAs with a single or multiple SBS sites at different distances, mutants of the two proteins, and GTP to induce FtsZ polymers may help to understand the competitive or synergic effects described here.

Although FtsZ has its specific anchoring proteins, namely, FtsA and ZipA in *E. coli* (Haeusser and Margolin, 2016, Ortiz et al., 2016), the interaction with SlmA and the SBS may also aid in membrane localization of FtsZ, an essential early step in cell division (**Figure 3.11B**). Assembly of these FtsZ units would be under the control of the antagonist, in line with the general thought that to be effective, the negative regulation of FtsZ assembly by SlmA should be exerted not only in the cytoplasm but also next to the membrane (Mannik and Bailey, 2015, Schumacher, 2017). Inhibition of FtsZ polymerization is obviously crucial to counteract FtsZ ring formation prior to the start of cell division, but it is still required at other times to prevent aberrant ring formation by the majority of cellular FtsZ that is present outside the central ring (Margolin, 2020). Furthermore, as nonring FtsZ seems to form oligomers transiently attached to the membrane (Margolin, 2020, Walker et al., 2020), inhibition at this location becomes crucial and the cell has developed a robust mechanism based on the action of the Min system. Our results

support the idea that SlmA likely acts coordinately with this system at the membrane. Indeed, it was recently proposed that SlmA can modulate the frequency of oscillation of the Min waves, perhaps participating in a conformational change of MinE that determines its interaction with the bacterial membrane (Shen et al., 2020). Considering our results, it is reasonable to think that besides this putative conformational effect, direct binding of SlmA to the membrane may modify, and in turn may be modified by, the interaction of MinE and the other division components. As neither SlmA nor the Min system uses a sequestration mechanism to inactivate FtsZ polymerization, but instead only shorten the polymers (Cabre et al., 2015, Tonthat et al., 2013, Hernandez-Rocamora et al., 2013), these FtsZ subunits will be available for productive assembly at midcell when required for division (**Figure 3.11B**). The anchoring proteins ZipA and FtsA will aid in releasing FtsZ from these antagonists because they compete for a common target within FtsZ, its C-terminal tail (Ortiz et al., 2016).

Membrane recognition has been also reported for the *B. subtilis* nucleoid occlusion protein Noc, and the concomitant recruitment of DNA seems to be at the heart of the mechanism by which this antagonist blocks aberrant FtsZ ring assembly at noncentral sites (Adams et al., 2015). Specific interaction with the DNA generates protein clusters that enhance the otherwise low membrane binding tendency of this protein, and exclusion of other divisome proteins by Noc-DNA-membrane complexes locally inhibits division ring assembly. The occurrence of Noc binding sites all over the chromosome except for the Ter macrodomain spatially regulates the formation of the complexes, favoring FtsZ ring assembly at midcell. SlmA may follow a similar mechanism, although in this case, the protein and its specific DNA do not gather at the membrane unless FtsZ is present. Participation of additional proteins in the simultaneous binding of DNA and membranes by Noc cannot be fully excluded in the *in vivo* study reported, but without evidence of interaction with the antagonist, FtsZ does not seem the most obvious candidate (Wu and Errington, 2012).

Dual recognition of DNA and membranes also seems to be important for the function of other bacterial proteins, some of which participate in the regulation of cell division. For example, the peripheral membrane protein MinD, which binds to membranes in an ATP-dependent manner, has been also found to bind DNA, suggesting that it could be involved in the overall mechanism of chromosome segregation in addition to its well-known role in the control of division ring positioning (Di Ventura et al., 2013). Other bacterial proteins interacting both with

membrane surfaces and with DNA sequences include SeqA protein, which sequesters replication origins, the proline utilization A flavoprotein (PutA), and RecA, the SOS repair system regulator (Dame et al., 2011, Zhang et al., 2004, Krishna and Vandesande, 1990). Research conducted before the work presented in this chapter showed that the DNA-binding protein MatP, a positive regulator of FtsZ ring assembly that acts indirectly on FtsZ through several FtsZ-binding proteins, also binds to lipid membranes (chapter 4), which may modulate the interplay between chromosome segregation regulation and division site selection by this protein.

Despite recent progress, some of the mechanisms underlying the function of SlmA in cell division still remain enigmatic, reflecting the plasticity of this multivalent factor. The interaction of SlmA with lipid layers introduces another type of binding partner in the pattern of interactions of this protein, and importantly, it provides an additional surface potentially available for the spatial regulation of its function, the inner membrane. These new features and the refined interplay with the other partners and local organizers of the function of this protein, principally the nucleoid and FtsZ, should allow advances in the understanding of the function of this key regulator.

# CHAPTER 4

# The bacterial DNA-binding protein MatP involved in linking the nucleoid terminal domain to the divisome at midcell interacts with lipid membranes

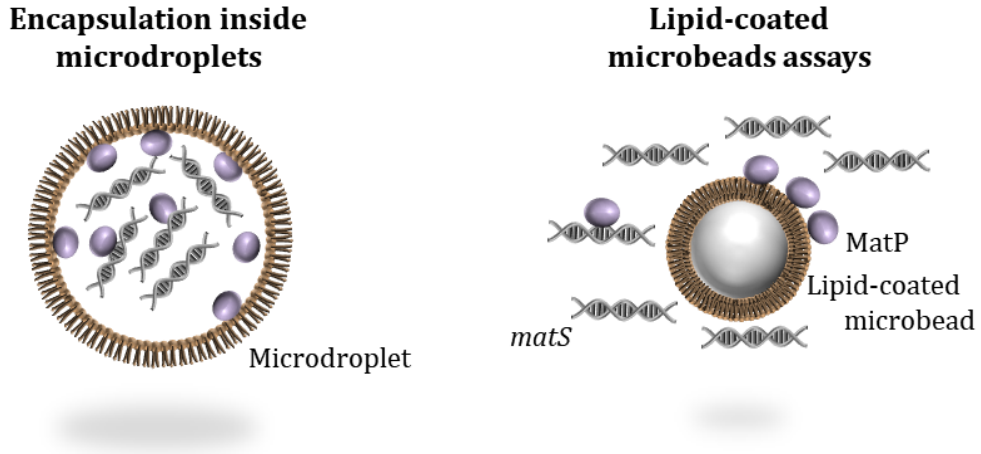


Division ring formation at midcell is controlled by various mechanisms in *Escherichia coli*, one of them being the linkage between the chromosomal Ter macrodomain and the Z-ring mediated by MatP, a DNA-binding protein that organizes this macrodomain and contributes to the prevention of premature chromosome segregation. Here we show that, when encapsulated inside vesicles and microdroplets generated by microfluidics, MatP accumulates at phospholipid bilayers and monolayers matching the lipid composition in the *E. coli* inner membrane. MatP binding to lipids was independently confirmed using lipid-coated microbeads and biolayer interferometry assays, which suggested that the recognition is mainly hydrophobic. Interaction of MatP with the lipid membranes also occurs in the presence of the DNA sequences specifically targeted by the protein, but there is no evidence of ternary membrane/protein/DNA complexes. Consistent with these results, our collaborators found that, during cell division, just before splitting the daughter cells, MatP seems to localize close to the cytoplasmic membrane, suggesting that this protein might interact with lipids. We propose that the association of MatP with lipids may modulate its spatiotemporal localization and its recognition of other ligands.

# RESULTS

## MatP accumulates at the lipid boundaries of microdroplets and vesicles

With the aim of investigating whether MatP had lipid affinity, we encapsulated the protein in working buffer[4] using microfluidics-based technology, inside microdroplets as cell mimic systems surrounded by a lipid boundary resembling that of the *E. coli* inner membrane. MatP (with a trace amount of MatP-Alexa 488) was included in one of the aqueous streams, the other one being buffer. Microdroplets were formed when the aqueous solutions met the continuous phase, constituted by the *E. coli* lipids dispersed in mineral oil, at the production junction of the microchip. Interestingly, according to the confocal microscopy images of the samples, MatP was mostly located at the lipid interface inside the microdroplets, as reflected by the intensity profiles (**Figure 4.1A**). Interaction of the protein with lipids was also found when the solution encapsulated inside microdroplets contained crowding agents like Ficoll or dextran together with MatP (**Figure 4.2A and B**). Encapsulation of free Alexa 488 dye (**Figure. 4.2C**) or of labeled proteins that do not significantly interact with lipids (see, for example, (Sobrinos-Sanguino et al., 2017a)) allowed the discarding of artifactual binding triggered by the dye and/or the encapsulation method.

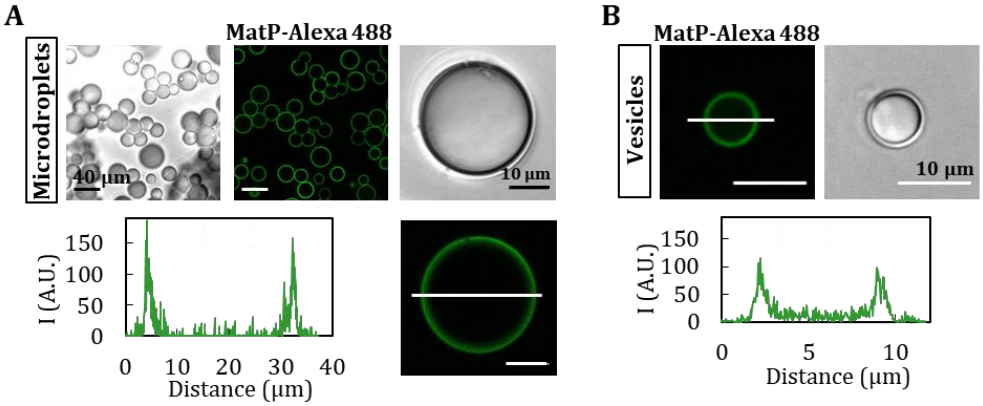


**Figure 4.1. Microfluidic encapsulation of MatP inside microdroplets stabilized by the *E. coli* lipid mixture and GUVs formed from them.** (A) Representative confocal and transmitted images of the microdroplets containing MatP (3.5 µM), and intensity profile corresponding to the green channel (1 µM MatP-Alexa 488), obtained across the line as drawn in the image. (B) Shown are representative confocal and transmitted images of GUVs and an intensity profile corresponding to the green channel (MatP-Alexa 488), obtained across the line as drawn in the image. Vesicles contained 150 g/l Ficoll. Encapsulations were conducted in working buffer.

[4] Working buffer: 50 mM Tris-HCl pH 7.5, 300 mM KCl, and 5 mM $MgCl_2$.

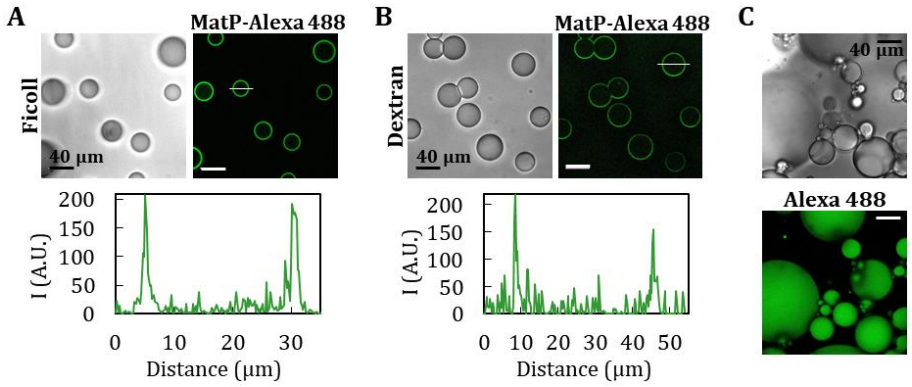


**Figure 4.2. Microdroplets generated by microfluidics containing crowding agents and encapsulation of free dye.** MatP (3.5 µM, with a trace 1 µM MatP-Alexa488) with 150 g/l Ficoll (A) or dextran (B) in working buffer. Intensity profiles below correspond to the green channel, obtained across the line drawn in the image. (C) Representative images of microdroplets generated by manual bulk emulsion, as previously described (Mellouli et al., 2013), with free 1 µM Alexa Fluor 488 dye in working buffer. The brightness of the images corresponding to the green channel was enhanced (30%).

After this observation, we wanted to study whether MatP interaction with the lipids also occurred when the lipid boundary was a bilayer, which provides a better cell-like system, instead of the monolayer surrounding the microdroplets. For this purpose, the microdroplets obtained by microfluidics were converted into GUVs, using a procedure based on the droplet transfer method (Carrara et al., 2012), as previously described (Sobrinos-Sanguino et al., 2017a). The droplets acquired the bilayer upon transition from an oil phase to an aqueous solution through an interface coated with oriented lipids. The crowding agent Ficoll was encapsulated alongside with MatP, and the osmolarity of the outer solution was adjusted by addition of sucrose to render an osmolarity ~25 mOsmol/Kg above the encapsulated solution to improve vesicle integrity and yield. Confocal images of the samples and the corresponding intensity profiles showed that green-labeled MatP also bound to the lipid bilayer at the edge of the GUVs (**Figure 4.1B**). Binding to lipids also occurred when MatP was externally added to GUVs (**Figure 4.3**).

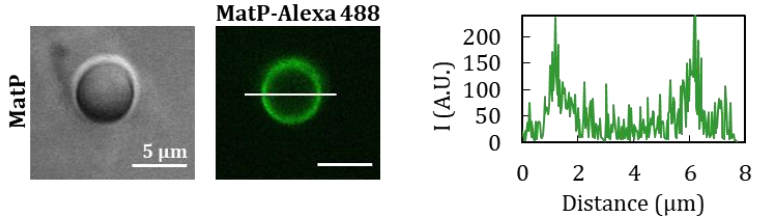


**Figure 4.3. Binding of MatP to the external surface of *E. coli* lipid vesicles.** Representative confocal and transmitted images of GUVs generated from microfluidics droplets containing 150 g/l Ficoll in working buffer after external addition of MatP (5 µM) with a trace amount of MatP-Alexa 488. Intensity profile on the right corresponds to the green channel, obtained across the line drawn in the image.

These results showed that the division protein MatP interacts with lipid monolayers or bilayers resembling the composition of the *E. coli* inner membrane when encapsulated inside micrometer-size cytomimetic containers.

### MatP binds to *E. coli* lipid bilayers at submicromolar concentrations mainly through hydrophobic interactions

To quantify the interaction of MatP with lipid membranes, biolayer interferometry assays were conducted using biosensor tips coated with the *E. coli* lipid mixture. Addition of the protein resulted in a shift in the incident light directed through the biosensor, indicative of binding (**Figure 4.4A**). A dose-response curve obtained by varying the concentration of MatP showed that, above 10 nM, the biosensor signal associated with binding increases with protein concentration, reaching saturation at around 1 µM MatP (**Figure 4.4A and B**).

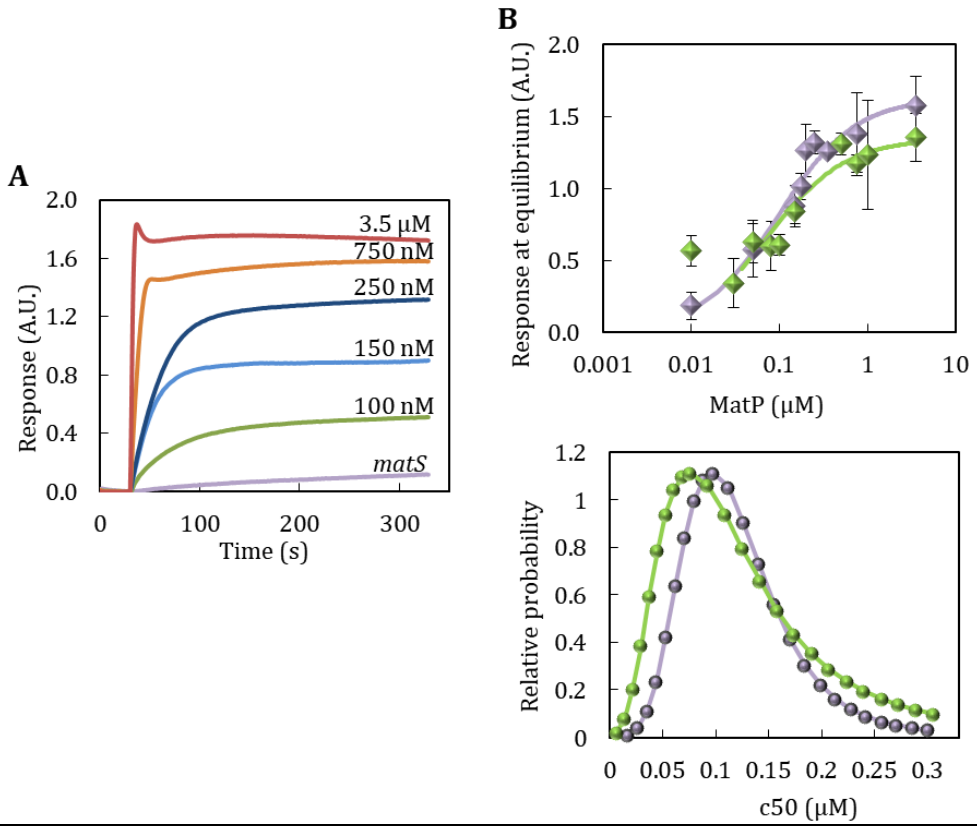


**Figure 4.4. Binding of MatP ± *matS* to *E. coli* lipids by biolayer interferometry.** (A) Representative profiles of the binding of MatP at the indicated concentrations obtained by biolayer interferometry. The profile for *matS* is shown for comparison. (B) Dose-response curves obtained as a function of the concentration of MatP in the absence (violet) and presence of 1 µM *matS* (green). Solid lines are the best fit of the model explained in the main text to the data, rendering the following parameter values: $c_{50}$ = 0.097 µM and *ymax* = 1.6 (MatP), $c_{50}$ = 0.076 µM and *ymax* = 1.3 (MatP in the presence of *matS*). Below, Probability distribution of $c_{50}$ for the binding of MatP to *E. coli* lipids. Dependence of the relative probability of a given value of $c_{50}$ calculated from a Fisher F-test for equality of variances. Color code as in (B). All experiments were conducted in working buffer.

Analysis with a Langmuir adsorption equation (**Figure 4.4B**), with no assumption about the mechanism or stoichiometry of the binding, rendered a $c_{50}$ value of 0.097 µM, corresponding to the concentration of MatP at which half of the maximum response signal was observed.

The binding of MatP to lipids was also ascertained through cosedimentation assays using microbeads coated with the *E. coli* lipid mixture and MatP-Alexa 488. Significant depletion of the protein was observed after incubation with the beads and centrifugation, and the amount of protein bound increased with its concentration at a constant lipid concentration (**Figures 4.5A**). Observation of the microbeads after incubation with the green-labeled protein by confocal microscopy confirmed the interaction (**Figure 4.5B**). The binding isotherm obtained by plotting the concentration of protein bound to the beads against the concentration of free protein was analyzed, as in the biolayer interferometry experiments, using the empirical Langmuir model (**Figure 4.5A**). This analysis rendered a $c_{50}$ of 0.065 µM, close to the midpoint of the response curve obtained by biolayer interferometry. Therefore, these two kinds of binding assays further supported the interaction of MatP with lipids, showing that it occurs at submicromolar concentrations of the protein.

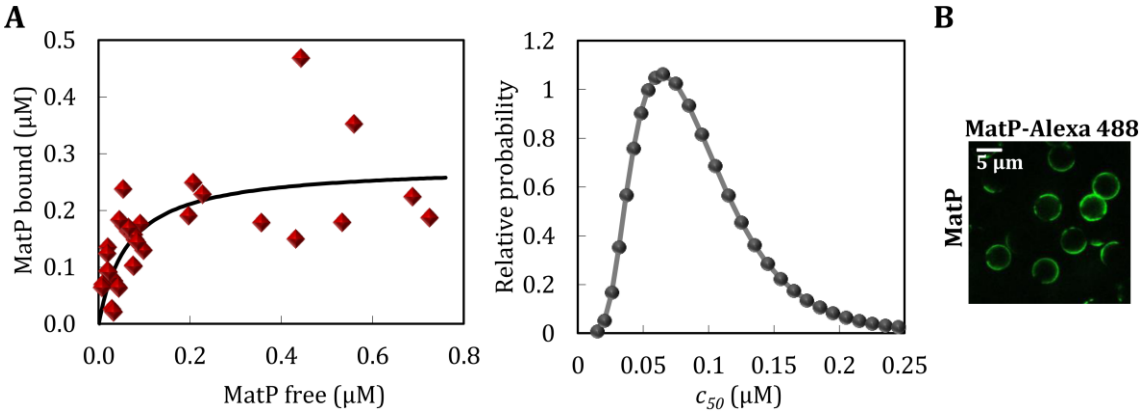


**Figure 4.5. Binding of MatP to microbeads coated with *E. coli* lipids bilayers.** (A) MatP binding to *E. coli* lipid-coated microbeads plotted as a function of the concentration of free MatP is shown in the left. Symbols represent the data, and the solid line represents the best fit according to the model explained in the main text rendering the parameter values $c_{50}$ = 0.065 µM and *ymax* = 0.280 µM. The concentration of the beads is 35 g/l (62 µM accessible lipid). MatP was labeled with Alexa 488. On the right, the dependence of the relative probability of a given value of $c_{50}$ calculated from a Fisher F-test for equality of variances is shown. (B) Representative confocal images of microbeads coated with the *E. coli* lipid mixture after external addition of MatP-Alexa 488. All experiments in working buffer.

To determine the nature of the interactions of MatP with lipids, the biolayer interferometry assays were repeated at lower and higher KCl concentrations: 50 and 500 mM (**Figure 4.6A**). No significant difference in the binding profile was observed at either salt concentration with respect to that obtained in working buffer (300 mM KCl), except for a slight shift toward lower concentration values at 50 mM KCl. These results were further confirmed using lipid-coated microbeads showing MatP-bound fractions of 0.879 ± 0.003, 0.79 ± 0.06, and 0.79 ± 0.05 at 50, 300, and 500 mM KCl, respectively. This relatively insensitive response to changes in ionic strength rules out a major contribution of electrostatic interactions in the recognition of lipids by MatP. The fact that MatP also binds to bilayers of phosphatidylcholine (PC), a neutral lipid, further supports this conclusion, pointing toward hydrophobic interactions as the most likely driving force of lipid recognition by this protein (**Figure 4.6B**).

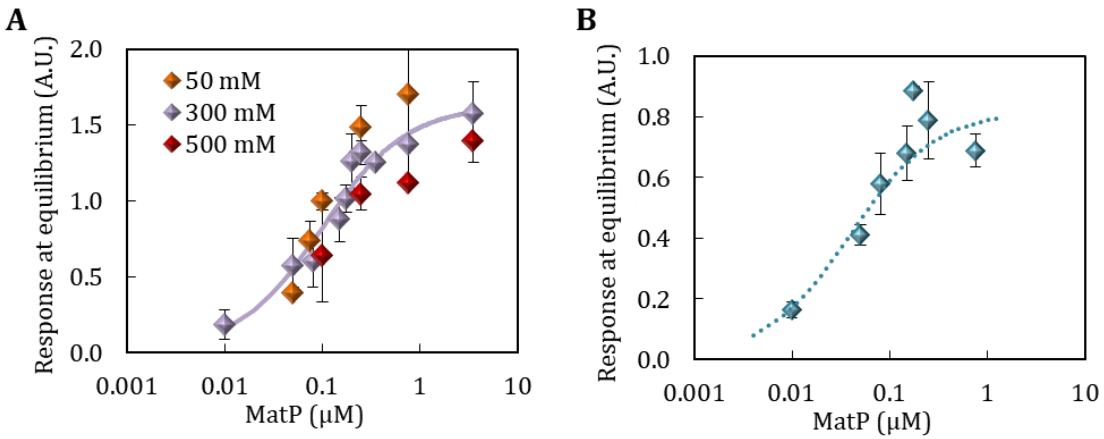


**Figure 4.6. Binding of MatP to EcL at different ionic strengths and to PC by biolayer interferometry.** (A) Dose-response curves obtained as a function of the concentration of MatP with the indicated KCl concentrations. The solid line is the best fit of the model explained in the main text to the data at 300 mM KCl (B) Dose-response curve of MatP binding to PC as a function of the concentration of MatP. Symbols are the data ± SD. Dotted line is only meant to guide the eye. Experiments were performed in working buffer.

### MatP does not recruit *matS* to the membrane

As MatP is a DNA-binding protein, we asked if it was still able to bind to the *E. coli* lipids in the presence of oligonucleotides containing its specific binding sequence, *matS*. To approach this question, we first characterized the protein/DNA complexes in the working buffer used to study MatP binding to lipids. Fluorescence anisotropy binding titrations showed that, in working buffer, purified MatP binds to fluorescein labeled *matS* (Mercier et al., 2008) with high affinity in the

nanomolar concentration range (**Figure 4.7A**). To propose suitable models for the analysis of the binding isotherm, the stoichiometry of the MatP·*matS* complex and the oligomerization state of MatP were studied by sedimentation velocity and SEC-MALS (**Figure 4.7B**). Both *matS* and MatP sedimented as single species with 2.3S and 2.1S, respectively, compatible with the double stranded *matS* sequence and a dimer of the protein (Durand et al., 2012), respectively, as confirmed by light scattering (inset in **Figure 4.7B**). The association state of MatP was insensitive to its concentration in the 0.5-9 μM range (2.3S and 2.0S, respectively). When both MatP and *matS* were present, sedimentation velocity profiles showed the appearance of a 3.5S peak, corresponding to the nucleoprotein complex, that increased from 52% to 89% with increasing concentrations of MatP at the expense of the free DNA species at ~2S. SEC-MALS experiments indicated that this complex contained two monomers of MatP and one molecule of *matS*, in good agreement with previous analysis (Durand et al., 2012). Interestingly, no intermediate or higher order complexes were observed when 1.5:1 or 5:1 protein (monomer): DNA ratios were studied. Analysis of the anisotropy binding isotherm assuming, hence, a model in which one dimer of the protein binds to the DNA forming a single complex, according to the stoichiometries obtained by SV and SEC-MALS, rendered a $K_d$ for the interaction of 15 ± 2 nM, in dimer units ($\Delta G$ = 10.7 ± 0.1 kcal/mol, for the dissociation reaction).

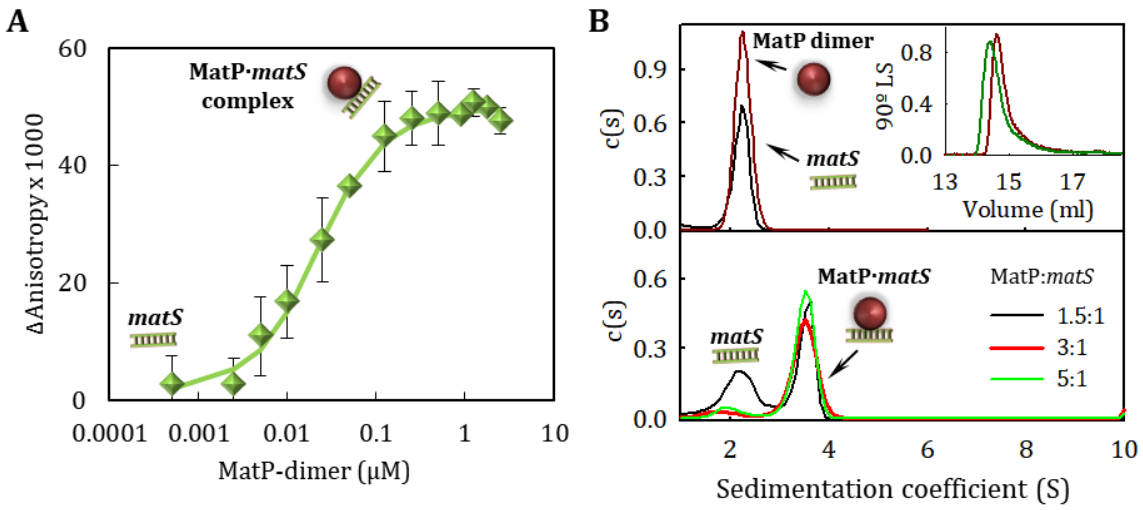


**Figure 4.7. Characterization of MatP·*matS* complexes in solution.** (A) Fluorescence anisotropy binding titrations of fluorescein labeled *matS* (10 nM) with MatP. Symbols are the average of five individual replicates ± SD. Solid line indicates the fit of the specified model. (B) SV profiles of MatP (3 μM) and *matS* (0.6 μM) and, below, of the nucleoprotein complex at the specified ratios. Inset, SEC-MALS profiles of MatP without (red) and with *matS* (green). Determined masses were (35 ± 1) · $10^3$ and (46 ± 1) · $10^3$, respectively. All experiments in working buffer.

We next encapsulated MatP along with *matS* inside cell-like containers to analyze the influence of the oligonucleotide on MatP interaction with the lipids. Encapsulation of MatP (with a trace amount of MatP-Alexa 488) and *matS*-Alexa 647 showed that the location of MatP, almost exclusively at the lipid boundary of the microdroplets or GUVs, was not altered by the presence of *matS*, while the DNA, in turn, remained homogeneously distributed in their lumen (**Figure 4.8**). Remarkably, the intensity profiles showed a drop of the *matS* red signal at the edges of the vesicle, where the green signal corresponding to MatP reaches its maximum. This strongly suggests that MatP at the membrane is not bound to the DNA. The concentrations of MatP and *matS* in these experiments were well above their $K_d$ of interaction, and we used a protein (monomer) molar excess relative to the DNA concentration above 2-fold to ensure formation of the 2:1 complex previously characterized in solution (described above). The same results were found either by including MatP and *matS* in two independent streams, triggering complex formation shortly before encapsulation, or by encapsulating the preformed complex (i.e., MatP and *matS* together in the two streams). Additional experiments in which the fluorescein-labeled *matS* used in the fluorescence anisotropy binding titrations and unlabeled MatP were encapsulated showed, again, that the DNA remained in the lumen of the microdroplets (**Figure 4.9A**). The images obtained in this case were indistinguishable from those corresponding to the encapsulation of fluorescein-labeled *matS* alone (**Figure 4.9B**). These

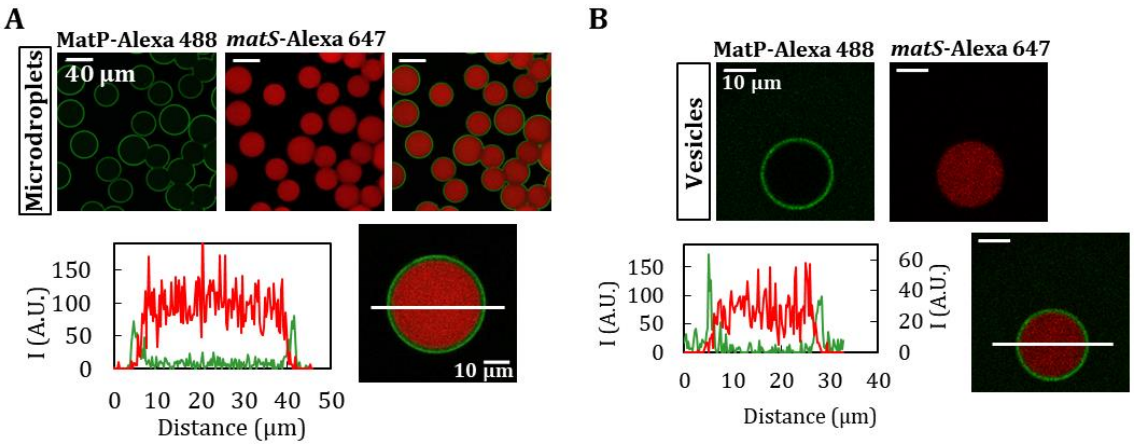


**Figure 4.8. Microfluidic encapsulation of MatP and *matS* inside microdroplets and GUVs formed from them.** (A and B) Representative confocal images of microdroplets and GUVs, respectively, stabilized by the *E. coli* lipid mixture containing MatP and *matS* in working buffer, and intensity profiles below. Profiles correspond to the green (1 µM MatP-Alexa 488) and red (1 µM *matS*-Alexa 647) channels, obtained across the line as drawn in the images. The concentrations of MatP and *matS* were 3.5 and 1.4 µM, respectively. Vesicles also contained 150 g/l Ficoll.

experiments evidenced that MatP still binds to the lipid monolayers or bilayers of microdroplets and GUVs in the presence of *matS*, although there was no sign of concomitant DNA recruitment to the lipid edge.

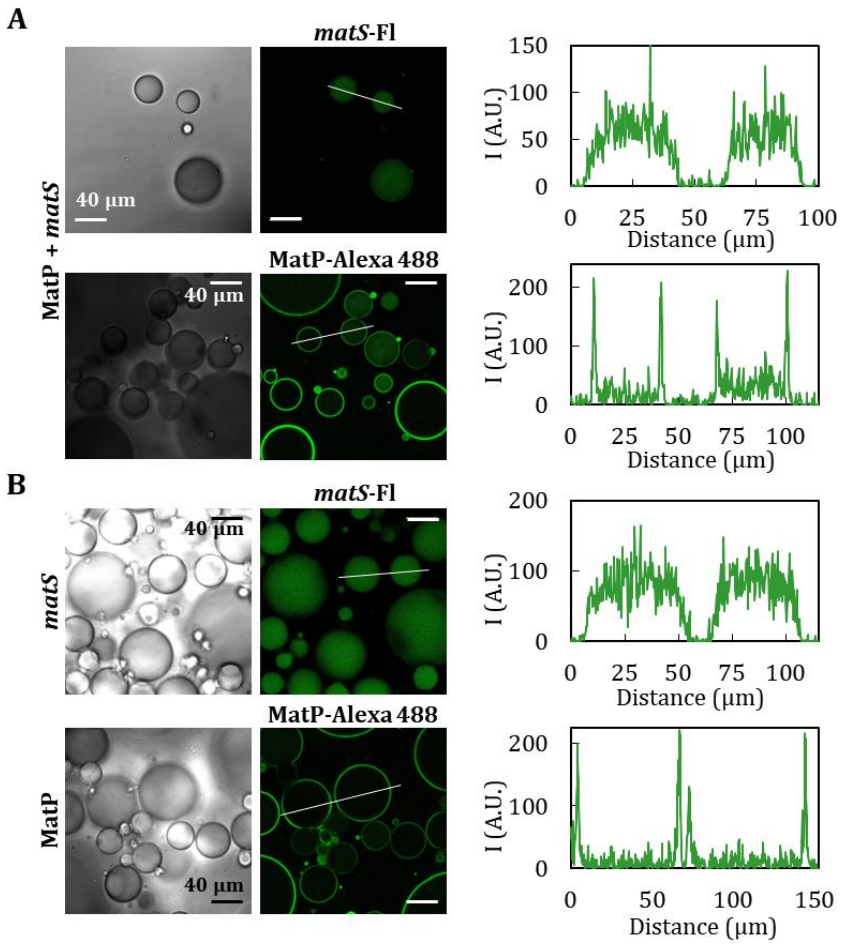


**Figure 4.9. Representative confocal and transmitted images of microdroplets generated by manual bulk emulsion using different combinations of labeled MatP and *matS*.** (A) MatP and *matS* with either labeled *matS* (2.5 µM MatP and 1 µM *matS*, top) or labeled MatP (1.7 µM MatP and 0.8 µM *matS*, bottom). (B) *matS* (1.4 µM, top) and MatP (1.7 µM, bottom). Intensity profiles on the right correspond to the green channel, obtained across the line drawn in the images. All experiments in working buffer.

Next, we probed the influence of *matS* on the binding of MatP to lipids using microbeads coated with the *E. coli* lipid mixture and through biolayer interferometry. Addition of 0.1 to 1 µM unlabeled *matS* prior to or after incubation of MatP with the microbeads did not significantly modify the fraction of MatP-Alexa 488 bound with respect to that in the absence of *matS* (**Figure 4.10A**). Parallel experiments using fluorescein-labeled *matS* and unlabeled MatP showed that the DNA did not bind to the lipids together with MatP (**Figure 4.10A**), in good agreement with the images of the complex encapsulated inside lipid vesicles or

microdroplets. Biolayer interferometry assays conducted to measure the binding of MatP in the presence of a constant 1 µM concentration of *matS* rendered isotherms of binding superimposable, within error, with those obtained in the absence of *matS* (**Figure 4.4B ;** $c_{50}$ = 0.076 µM), and no significant interaction with the lipids was detected for *matS* alone (**Figure 4.4A**). The signal of binding of MatP (150 nM) to the lipids showed a decreasing trend with *matS* concentration (**Figure 4.10B**), more obvious at high concentration, which suggests competition between the lipids and the DNA for binding to the protein. No such effect was observed under conditions under which the interaction between MatP and *matS* is greatly hindered while still allowing significant binding of MatP to the lipids (500 mM KCl, 150 nM MatP (**Figure 4.10B**)), implying the alleged competition observed at lower salt concentrations would arise from the interaction between MatP and *matS*.

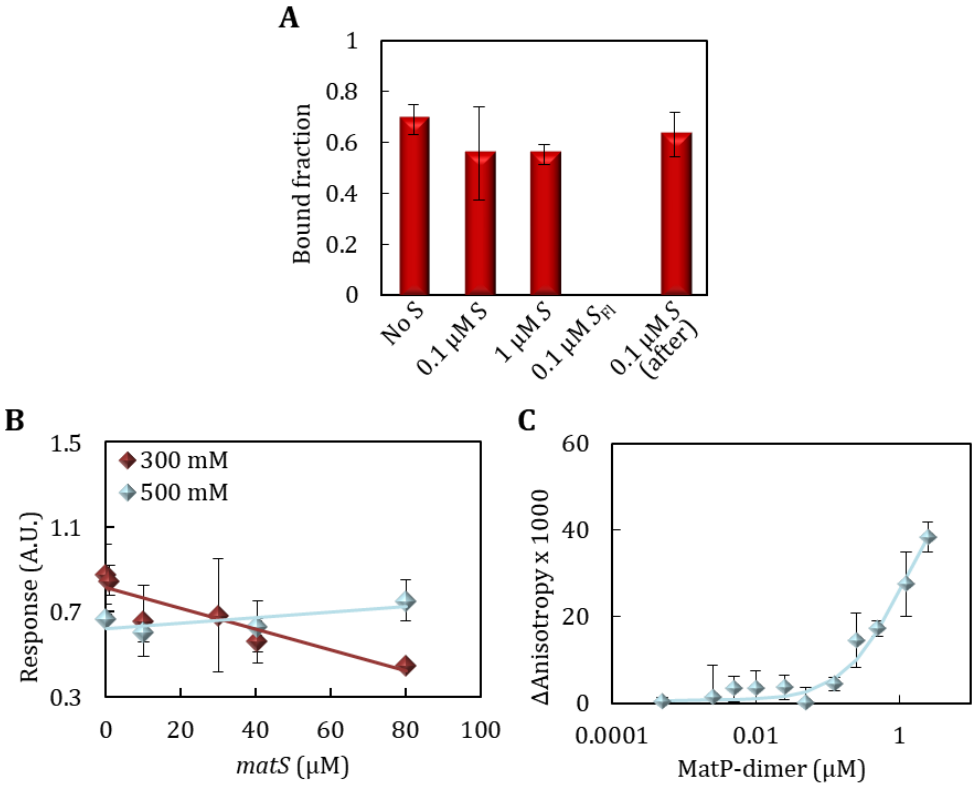


**Figure 4.10. Binding of MatP to lipids in the presence of *matS*.** (A) Effect of *matS* on MatP binding to lipid-coated beads (30 g/l, 53 µM accessible lipid). The MatP concentration in all measurements was 0.25 µM. Unless otherwise stated, the labeled species was MatP-Alexa 488. S and $S_{Fl}$ represent *matS* and *matS* labeled with fluorescein, respectively. For the measurement corresponding to the bar on the far right, *matS* was added to MatP already bound to the lipid. (B) The binding of 0.15 µM MatP to EcL with increasing concentrations of *matS* was monitored by biolayer interferometry. Solid lines are only intended to guide the eye. (C) Fluorescence anisotropy binding titrations of 10 nM *matS*-Fl with MatP at 500 mM KCl. Solid line indicates the fit of the specified model described above in experiments at 300 mM KCl. Symbols are the average of 3 individual replicates ± SD. All experiments in working buffer at the specified KCl concentration.

Competition between *matS* and the membrane for binding to MatP was also observed by fluorescence anisotropy. The formation of complexes of fluorescein-labeled *matS* with MatP led to an increase in the anisotropy with respect to that of free *matS*-Fl (**Figure 4.11**). Incubation of MatP/*matS*-Fl complexes with lipid-coated microbeads and subsequent centrifugation to sediment the beads resulted in a concentration-dependent decrease in the anisotropy value compared to that in the absence of lipids (**Figure 4.11**). At sufficiently high lipid concentration, anisotropy reached values close to that of the free *matS*, compatible with total dissociation of the protein from the DNA because of lipid competition. The fluorescence intensity remained unchanged across the titration, as expected for competition between the lipids and *matS*, rather than recruitment of the latter to the lipids concomitantly with the protein.

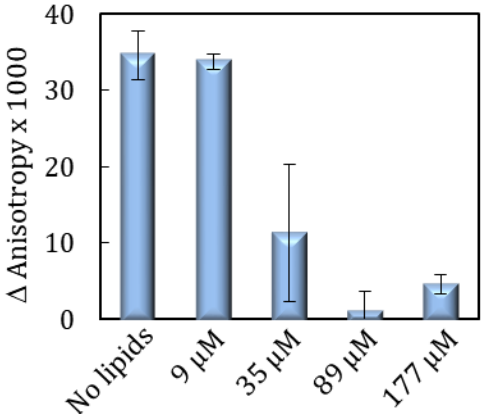


**Figure 4.11. Fluorescence anisotropy-based competition between lipids and DNA for MatP.** Shown is the anisotropy change of *matS*-Fl (50 nM) in the presence of MatP (100 nM) in working buffer as a function of the concentration of accessible lipid coating microbeads.

Further interpretation of these competition experiments and of the results obtained with encapsulated MatP/*matS* complex (see above) by direct comparison of the affinity values determined is not straightforward. While a thermodynamic binding constant was attained for the MatP/*matS* complex through precise determinations of its stoichiometry, only apparent affinity constants could be determined for the interaction of MatP with lipids, given the unknown stoichiometry in this case. Besides, the self-association of the protein should also be taken into account in the interaction scheme, and the amount of MatP bound to *matS* or to the membrane in each situation would depend both on the relative affinities of the protein for the two ligands and on their concentrations. For example, encapsulated MatP finds a concentration of *matS* that is probably too low to reach competition in the presence of an excess of lipid, like that within the boundary, which may explain why the protein is shifted toward the lipid surface despite the presence of *matS*.

Taken together, these experiments show that *matS* and the lipids compete for binding to MatP instead of forming ternary complexes, not necessarily implying overlap between the lipid and nucleic acid binding regions of the protein.

# DISCUSSION

Here we have found that the protein of the Ter linkage MatP interacts with membranes matching the lipid composition of the *E. coli* inner membrane, as shown by encapsulation in cell-like containers, cosedimentation with lipid-coated microbeads, and biolayer interferometry assays. Although MatP presents dual recognition of lipids and nucleic acid sequences, we have not found any indication supporting the formation of ternary complexes, strongly suggesting that both types of ligands may be mutually exclusive.

The interaction of MatP with the membrane seems to be driven by hydrophobic rather than electrostatic forces, given the minor impact of salt variations and the tendency of the protein to recognize neutral lipids. An interaction of an electrostatic nature could have been expected, as the *E. coli* lipid mixture contains negatively charged phospholipids (phosphatidylglycerol and cardiolipin (Raetz and Dowhan, 1990)), while given its high pI, MatP would be positively charged at neutral pH. However, our experiments rule out a major contribution of this kind of interactions, suggesting in turn that the recognition could be the result of hydrophobic protein-lipid contacts. A domain of MatP that may be involved in this type of binding is the C-terminal coiled coil, previously suggested to be responsible for tetramerization (Dupaigne et al., 2012). This domain is away from the N-terminal modules (the four-helix bundle and the RHH) specifically targeting the *matS* sequences. Lipid binding through the coiled-coil domain or any other region of MatP outside the DNA-binding domains would not be incompatible with the lack of DNA recruitment to the membrane. Indeed, overlap between the lipids and DNA-binding sites is only one of the possible explanations for this finding—not even the most probable one—in view of the mainly hydrophobic interaction with lipids and the charged nature of the DNA-binding modules. Other possible scenarios leading to the same experimental observation would involve lipid-induced changes in the association state, orientation, and/or conformation of MatP hampering DNA-binding or some sort of steric hindrance between the two ligands, precluding their simultaneous recognition. Further studies will be required to determine the precise elements within MatP structure responsible for the interaction with lipids.

Membrane binding of MatP may serve to sequester the protein from the chromosome under conditions in which its positive regulation of Z-ring formation is no longer required and even might obstruct the function of proteins like FtsK.

FtsK is needed for the deconcatenation of sister chromosomes and helps to segregate the termini into each daughter cell (Galli et al., 2017, Stouf et al., 2013). FtsK, part of the divisome (Yu et al., 1998), is one of the fastest DNA translocases (Lowe et al., 2008). Membrane binding of MatP released by FtsK during this relatively short time interval might function to prevent rebinding to the *matS* sites close to the *dif* site. We propose that competition between *matS* and lipid for MatP assists in the segregation of the *dif* region by FtsK during the last step of septum closure (**Figure 4.10**). Then, MatP would be subsequently released from the

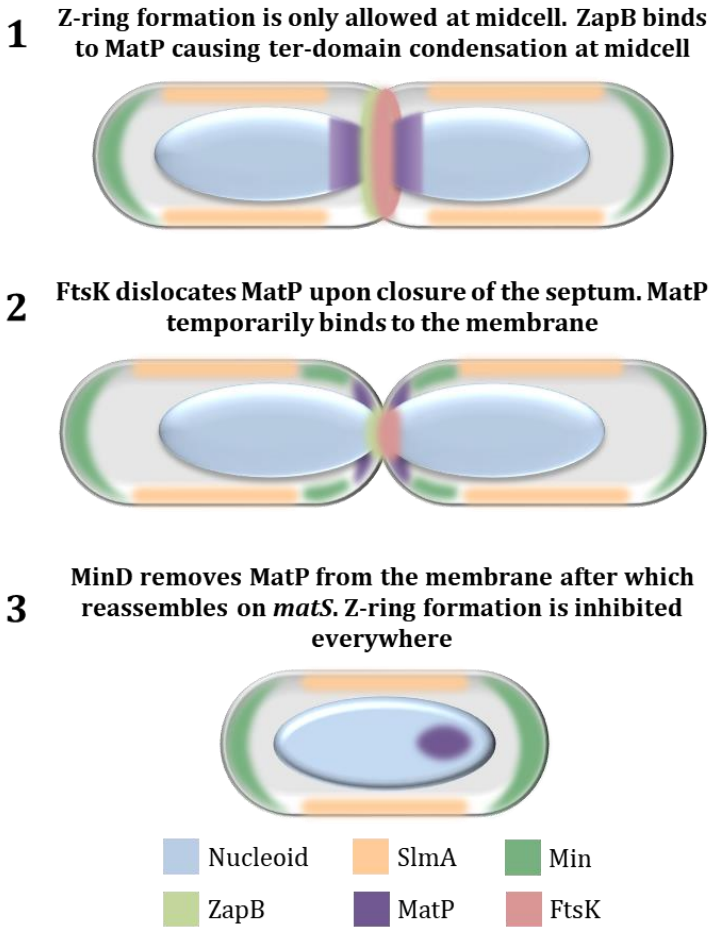


**Figure 4.12. Hypothetical model of the MatP dissociation from the *matS* sites and its binding to the cytoplasmic membrane.** In step 1, ZapB is binding MatP at midcell, causing the 23 *matS* sites to cluster and ensuring that the terminus remains at midcell. Z-ring formation is inhibited at the old poles by the Min system and in the cylindrical part of the cell close to the bulk of the nucleoid, but not in the Ter domain, by the nucleoid occlusion protein SlmA. The orange bar indicates the nucleoid occlusion by SlmA, not the binding of SlmA to the nucleoid. In step 2, the nucleoids are segregating and MatP is pulled away from ZapB. At the same time, the terminus is bound by FtsK that displaces MatP from *matS* sites by translocation of the DNA near the terminus, which allows final segregation of the nucleoids into the daughter cells. In step 3, MinD removes MatP from the membrane, after which it reassembles on *matS*. Z-ring formation is inhibited everywhere by the Min system and the nucleoid occlusion protein SlmA.

membrane to bind again the *matS* sites. A possibility is that, as part of the oscillation of the Min system between the old poles and the newly formed septum before daughter cells have separated (Juarez and Margolin, 2010), detachment from the membrane might be assisted by MinD, known to displace proteins from the membrane surface of the new poles (Lee et al., 2016, Ramm et al., 2018). Testing this hypothesis may be the subject of future research on this system.

Recent studies have revealed that, like MatP, other proteins binding to the bacterial chromosome are also able to interact with lipid membranes. Examples of these proteins are the nucleoid occlusion protein Noc from *Bacillus subtilis* (Adams et al., 2015), a negative modulator of Z-ring assembly, SeqA from *E. coli*, a protein involved in the sequestration of replication origins (Dame et al., 2011), the proline utilization flavoprotein PutA (Zhang et al., 2004), and the SOS repair system regulator RecA (Krishna and Vandesande, 1990). Along the same line, the nucleoprotein complexes of SlmA, the factor counteracting Z-ring formation around the chromosome in *E. coli*, seem to be brought close to the membrane (Mannik and Bailey, 2015, Du and Lutkenhaus, 2014, Tonthat et al., 2013), possibly through transertional linkages (Tonthat et al., 2013), biomolecular condensation (chapter 1) and/or by direct interaction with the lipid membrane (chapter 3). Conversely, well-known membrane-associated proteins like MinD from the Min system (Rowlett and Margolin, 2015) have also been shown to interact, in a non-sequence-specific manner, with chromosomal DNA (Di Ventura et al., 2013).

The main difference between the dual recognition of lipids and DNA by MatP and the other site selection proteins (Noc (Adams et al., 2015) and MinD (Rowlett and Margolin, 2015)) is that the latter can simultaneously bind DNA and lipids. Furthermore, in the particular case of Noc, binding to DNA activates the subsequent interaction with the membrane (Adams et al., 2015). The precise mode of recognition may serve the function of each regulator and may be related to the structural elements involved in membrane binding—amphipathic helixes in the case of MinD (Rowlett and Margolin, 2015) and Noc (Adams et al., 2015)—which we have not found in MatP by using AMPhipaseek software (Sapay et al., 2006). In bacillary bacteria, DNA-membrane interactions are proposed to aid in the localization of the bacterial cell center, where the strength of these interactions decreases and Z-ring assembly is favored (Rabinovitch et al., 2003). According to this, by bridging the chromosome and the membrane, negative regulators of division ring formation such as Noc would exclude FtsZ from noncentral areas, biasing FtsZ assembly to the midcell (Adams et al., 2015). In contrast, physical connection of the chromosome with the membrane through MatP could interfere

with its positive regulation of FtsZ assembly that contributes to division ring positioning. In the last step of binary fission that requires deconcatenation of sister chromosomes and closure of the septum, the presence of MatP might not be beneficial any longer. Therefore, it may be displaced to the membrane to prevent immediate rebinding to the domain, which would happen otherwise given its high affinity for these sites.

Other *E. coli* proteins have been reported to interact with membrane and DNA in a mutually exclusive way, as seems to be the case of MatP. One of these proteins is PutA, which interacts with the membrane primarily through hydrophobic contacts (Zhang et al., 2004) and contains a DNA-binding RHH domain involved in dimerization (Larson et al., 2006), similarly to MatP (Dupaigne et al., 2012). To explain the incompatibility of simultaneous DNA and membrane binding, the formation of multimeric complexes has been suggested, implying the membrane binding domain could be constrained in these complexes and, likewise, membrane-bound protein would constrain the DNA-binding domain, hindering its recognition (Larson et al., 2006). In the case of the protein RecA, the domains for the interaction with DNA and lipids are located on different sides of the protein, which upon membrane interaction, forms polymeric structures, preventing its association with the chromosome (Rajendram et al., 2015). In both cases, membrane binding in the presence of ligands is reversible, implying protein-membrane associations are in equilibrium with the protein/DNA complex, which was also observed in the MatP competition experiments we report here. It remains to be determined whether the binding partners of MatP may also tune its interaction with both DNA and membrane.

Since its identification, the function of MatP and its modulation in the context of division have been traditionally linked to its specific binding to DNA sequences within the Ter macrodomain or to its interaction with other proteins such as ZapB. Our findings strongly suggest that, in addition to protein-nucleic acid and protein-protein interactions, protein-lipid recognition should also be taken into account in the analysis of the function of MatP. Further work will be required to elucidate the precise mechanisms of these protein-membrane interactions and the factors influencing them.

# Concluding Remarks

# CONCLUDING REMARKS

In the first part of this thesis, the ability of FtsZ to form phase-separated condensates in the presence and absence of its nucleoid-associated inhibitor SlmA in crowded cell-like media was discovered and characterized.

- FtsZ, in the absence of GTP, reversibly assembles into structures upon interaction with SBS-bound SlmA in cell-like crowding conditions, consistent with crowding-driven phase-separated biomolecular condensates. These condensates constitute dynamic entities in which FtsZ maintains its GTP-dependent assembly/disassembly properties. Compartmentalization mimicked through model LLPS systems affects the distribution and localization of condensates that were principally found in the non-PEG phase and, when encapsulated inside microfluidic-based microdroplets, they preferentially accumulate at lipid surfaces.

- FtsZ, under conditions that promote protein oligomerization, reversibly forms biomolecular condensates that are dynamic and evolve toward fibers in the presence of GTP. However, this range of conditions is narrower (but still physiological) than that found when SBS-bound SlmA is present and, under some circumstances, condensates coexist with irregular structures. Biomolecular condensation of FtsZ also occurs when encapsulated in cytomimetic containers with incipient formation in conditions under which no condensates were detected in bulk.

- The FtsZ mutant lacking the unstructured flexible linker and the C-terminal peptide ($FtsZ\Delta_{Cter}$) is still able to form condensates in the absence of SlmA. Nevertheless, at short times these condensates were smaller compared to those formed by wild-type FtsZ and the condensation process was found to be slower. Altogether, the results show that the globular domain of FtsZ is enough to drive phase separation, but the C-terminal region probably enhances the overall process.

In the second part, the interaction of the DNA-binding proteins SlmA and MatP with lipids uncovered during their reconstitution in biomimetic membranes is analyzed following an orthogonal approach involving reconstitution in different minimal membrane systems.

- SlmA binds to lipid membranes, being electrostatic and hydrophobic forces involved in the interaction. While specific SBS sequences compete with the lipids for binding to SlmA, the presence of FtsZ promotes their recruitment to the membrane by SlmA.

- MatP binds to lipid membranes at submicromolar concentrations, mainly through hydrophobic interactions and, when encapsulated inside cell-like containers, MatP accumulates at the lipid boundaries of microdroplets and vesicles. Besides, MatP does not recruit *matS* to the membrane, instead, *matS* and the lipids compete for binding to MatP.

# Future Perspectives

# FUTURE PERSPECTIVES

This thesis reports the formation of phase-separated biomolecular condensates by the central division protein FtsZ, greatly promoted by its nucleoid-associated inhibitor SlmA, as well as the ability of the DNA-binding proteins SlmA and MatP to interact with lipid membranes modulated by their binding partners. Both results, point out the possible existence of novel mechanisms which may play important roles in the regulation of the localization and activity of these proteins within the intracellular space. However, further research on the condensation of bacterial division elements and the interaction of SlmA and MatP with lipid membranes seems to be necessary to unravel their implications in bacterial division. Likewise, the knowledge derived from this research could add up to the efforts for the reconstitution of a minimal divisome, a milestone in the grand challenge for the generation of synthetic cells. Besides, the uncovered behavior of the division elements studied in this thesis may serve as a starting point for the search of new antimicrobials targeting the division process. All things considered, the studies presented in this thesis could be continued following different investigation lines.

**In-depth analysis of the biomolecular condensates formed by FtsZ.** Given the complexity of the intracellular space and of biomolecular condensates, especially those involving multiple elements, and the variety of biological processes in which they can be implied, additional studies should be conducted. It would be interesting to determine if other FtsZ division partners can enhance, like SlmA, the assembly of this protein into biomolecular condensates, behave as client macromolecules partitioning inside already formed FtsZ condensates or being excluded from them. Besides, the observed tendency of FtsZ·SlmA·SBS condensates to localize at the lipid boundary (when encapsulated inside microdroplets) or to accumulate in the DNA-enriched phase (when reconstituted in the LLPS system) suggests a possible role of the *E. coli* inner membrane and the nucleoid, respectively, in biomolecular condensation that deserves a closer examination. Further reconstitution of FtsZ condensates using different minimal membrane systems and/ or models mimicking the bacterial nucleoid could shed light on these aspects. In addition, evaluation of the effect of other physiological relevant factors, apart from the already studied in this thesis, such as the presence of anions like glutamate, recently reported to favor the formation of bacterial condensates (Harami et al., 2020) would provide valuable information. Finally, experiments

using super-resolution technologies would help to detect, and subsequently analyze, FtsZ biomolecular condensates *in vivo*.

**Reconstitution of the whole Ter linkage.** The Ter linkage reinforces the formation of the Z-ring at midcell by connecting it with the ter portion of the bacterial nucleoid. This is achieved through a multiprotein network formed by ZapA that binds to FtsZ and ZapB which, in turn, interacts also with MatP bound to the ter region of the chromosome. In this thesis it is initiated the reconstitution of the Ter linkage with the reconstitution of MatP in biomimetic membranes. Future studies including ZapB, ZapA and FtsZ could help to understand the role of the interaction of MatP with lipid membranes and provide new details about the Ter linkage.

**Studies on nucleoid occlusion in combination with other Z-ring positioning mechanisms.** Since nucleoid occlusion acts inside the cell in conjunction with other regulatory systems, it would be interesting to continue the reconstitution initiated here in combination with the other two known positioning mechanisms, the Ter linkage and the Min system.

- **Reconstitution of nucleoid occlusion with the Ter linkage.** A simultaneous reconstitution in cell-like environments of these two opposite mechanisms could provide valuable information on the regulation of Z-ring formation. Interestingly, it has been reported that ZapA, known to stabilize FtsZ polymers and promote bundling of FtsZ filaments *in vitro*, is able to reverse the inhibitory effect of the Min system protein MinC on FtsZ assembly (Rowlett and Margolin, 2015). Therefore, it would be interesting to explore if ZapA could have a similar effect on the negative regulation exerted by the nucleoprotein complexes of SlmA. In this sense, the impact of the presence of ZapA on the interaction of SBS-bound SlmA with FtsZ may be assessed as well as the effect on its inhibitory action over FtsZ polymers. Ultimately, studies on the interplay between ZapA and FtsZ·SlmA·SBS condensates could be very informative.

- **Reconstitution of nucleoid occlusion with the Min system.** Both nucleoid occlusion and the Min system are negative regulatory mechanisms that prevent Z-ring formation at aberrant locations. Interestingly, it has been reported that SlmA could be involved in the modulation of Min oscillations (Shen et al., 2020). Reconstitution of both systems in cell-like environments could help to elucidate how biomolecular condensation and the newly identified interaction of SlmA with lipid membranes could be affected or impact the Min system.

Hence, the combined analysis of these three regulatory systems in cell-like environments mimicking those found inside the bacteria could help to understand how division-site selection occurs in the cell.

**Generation of synthetic cells.** The reconstitution of a minimal division machinery is a pursued goal in the long-term efforts to generate a synthetic cell. However, the reconstitution of such machinery not only requires a set of elements to produce the constricting force, but also the presence of dedicated molecular mechanisms for division-site selection. In this regard, the uncovered behavior of the division elements reported in this thesis could help in the development of minimal modules to spatiotemporally organize the assembly of a minimal divisome.

**Exploration of new antibiotics.** Finally, the formation of biomolecular condensates by FtsZ, largely promoted by its nucleoid-associated inhibitor SlmA, may be essential for cell fitness. In fact, the formation of biomolecular condensates by FtsZ may be related to the regrowth delay bodies observed in non-growing late stationary phase bacteria. These reversible membrane-less structures where FtsZ accumulates have been associated with antibiotic tolerance (Yu et al., 2019). Thus, studies to evaluate the effect of drug candidates targeting these biomolecular condensates in cell-like environments could serve to identify new antibiotics, as it has been proposed for condensates related to other diseases (Wheeler, 2020).

# PUBLICATIONS

# PUBLICATIONS DERIVED FROM THIS THESIS

The work presented in this thesis has been published in the articles referenced below. Chapters corresponding to the "Results" section are partially reproduced as published.

1. Miguel Ángel Robles-Ramos[1], Silvia Zorrilla[1], Carlos Alfonso, William Margolin, Germán Rivas and Begoña Monterroso. 2021. Assembly of bacterial cell division protein FtsZ into dynamic biomolecular condensates. Biochim Biophys Acta Mol Cell Res. 2021 Feb 11;1868(5):118986. [1]These authors contributed equally to this work.

2. Miguel Ángel Robles-Ramos, William Margolin, Marta Sobrinos-Sanguino, Carlos Alfonso, Germán Rivas, Begoña Monterroso and Silvia Zorrilla. 2020. The nucleoid occlusion protein SlmA binds to lipid membranes. mBio. 2020 Sep 1;11(5):e02094-20. Editor's Pick Research Article.

3. Begoña Monterroso, Silvia Zorrilla, Marta Sobrinos-Sanguino, Miguel Á. Robles-Ramos, Marina López-Álvarez, William Margolin, Christine D Keating, and Germán Rivas. 2019. Bacterial FtsZ protein forms phase-separated condensates with its nucleoid-associated inhibitor SlmA. EMBO Rep. 2019 Jan;20(1): e45946. Highlighted publication in SBE-Magazine.

4. Begoña Monterroso, Silvia Zorrilla, Marta Sobrinos-Sanguino, Miguel Ángel Robles-Ramos, Carlos Alfonso, Bill Söderström, Nils Y. Meiresonne, Jolanda Verheul, Tanneke den Blaauwen, and Germán Rivas. 2019. The bacterial DNA-binding protein MatP involved in linking the nucleoid terminal domain to the divisome at midcell interacts with lipid membranes. mBio. 2019 May-Jun; 10(3): e00376-19.

# OTHER PUBLICATIONS

1. Silvia Zorrilla, Begoña Monterroso, Miguel-Ángel Robles-Ramos, William Margolin and Germán Rivas. 2021. FtsZ Interactions and biomolecular condensates as potential targets for new antibiotics. Antibiotics 2021, 10(3), 254.

2. Begoña Monterroso, Miguel Ángel Robles-Ramos, Silvia Zorrilla and Germán Rivas. 2021. Reconstituting bacterial cell division assemblies in crowded, phase-separated media. Methods Enzymol. 2021;646:19-49.

# REFERENCES

# REFERENCES

Adams, D. W., Wu, L. J. & Errington, J. 2015. Nucleoid occlusion protein Noc recruits DNA to the bacterial cell membrane. *Embo Journal,* 34**,** 491-501.

Ahijado-Guzmán, R., Gómez-Puertas, P., Alvarez-Puebla, R. A., Rivas, G. & Liz-Marzán, L. M. 2012. Surface-enhanced raman scattering-based detection of the interactions between the essential cell division FtsZ protein and bacterial membrane elements. *ACS Nano,* 6**,** 7514-7520.

Alberti, S. 2017. Phase separation in biology. *Current Biology,* 27**,** R1097-R1102.

Alberti, S. & Dormann, D. 2019. Liquid–liquid phase separation in disease. *Annual Review of Genetics,* 53**,** 171-194.

Alberti, S., Gladfelter, A. & Mittag, T. 2019. Considerations and challenges in studying liquid-liquid phase separation and biomolecular condensates. *Cell,* 176**,** 419-434.

Albertsson, P. Å. 1986. *Partition of cell particles and macromolecules: Separation and purification of biomolecules, cell organelles, membranes, and cells in aqueous polymer two-phase systems and their use in biochemical analysis and biotechnology*, Third edition. New York : Wiley, 1986.

Ambadipudi, S., Biernat, J., Riedel, D., Mandelkow, E. & Zweckstetter, M. 2017. Liquid-liquid phase separation of the microtubule-binding repeats of the Alzheimer-related protein Tau. *Nature Communications,* 8**,** 13.

André, A. a. M. & Spruijt, E. 2020. Liquid–liquid phase separation in crowded environments. *International Journal of Molecular Sciences,* 21**,** 5908.

Ausländer, S., Ausländer, D. & Fussenegger, M. 2017. Synthetic biology—the synthesis of biology. *Angewandte Chemie International Edition,* 56**,** 6396-6419.

Azaldegui, C. A., Vecchiarelli, A. G. & Biteen, J. S. 2021. The emergence of phase separation as an organizing principle in bacteria. *Biophysical Journal,* 120**,** 1123-1138.

Bailey, M. W., Bisicchia, P., Warren, B. T., Sherratt, D. J. & Mannik, J. 2014. Evidence for divisome localization mechanisms independent of the Min system and SlmA in *Escherichia coli*. *Plos Genetics,* 10**,** 13.

Banani, S. F., Lee, H. O., Hyman, A. A. & Rosen, M. K. 2017. Biomolecular condensates: Organizers of cellular biochemistry. *Nature Reviews Molecular Cell Biology,* 18**,** 285-298.

Banani, S. F., Rice, A. M., Peeples, W. B., Lin, Y., Jain, S., Parker, R. & Rosen, M. K. 2016. Compositional control of phase-separated cellular bodies. *Cell,* 166**,** 651-663.

Baranova, N., Radler, P., Hernandez-Rocamora, V. M., Alfonso, C., Lopez-Pelegrin, M., Rivas, G., Vollmer, W. & Loose, M. 2020. Diffusion and capture permits dynamic coupling between treadmilling FtsZ filaments and cell division proteins. *Nature Microbiology,* 5**,** 407-417.

Beckett, D. 2011. Measurement and analysis of equilibrium binding titrations: A beginner's guide. *Methods Enzymol,* 488**,** 1-16.

Bernhardt, T. G. & De Boer, P. a. J. 2005. SlmA, a nucleoid-associated, FtsZ binding protein required for blocking septal ring assembly over chromosomes in *E coli*. *Molecular Cell,* 18**,** 555-564.

Biswas, N., Ichikawa, M., Datta, A., Sato, Y. T., Yanagisawa, M. & Yoshikawa, K. 2012. Phase separation in crowded micro-spheroids: DNA-PEG system. *Chemical Physics Letters,* 539**,** 157-162.

Boeynaems, S., Alberti, S., Fawzi, N. L., Mittag, T., Polymenidou, M., Rousseau, F., Schymkowitz, J., Shorter, J., Wolozin, B., Van Den Bosch, L., Tompa, P. & Fuxreiter, M. 2018. Protein phase separation: A new phase in cell biology. *Trends in Cell Biology,* 28**,** 420-435.

Brangwynne, C. P., Eckmann, C. R., Courson, D. S., Rybarska, A., Hoege, C., Gharakhani, J., Jülicher, F. & Hyman, A. A. 2009. Germline P granules are liquid droplets that localize by controlled dissolution/condensation. *Science,* 324**,** 1729-1732.

Buske, P. J. & Levin, P. A. 2013. A flexible C-terminal linker is required for proper FtsZ assembly *in vitro* and cytokinetic ring formation *in vivo*. *Molecular Microbiology,* 89**,** 249-263.

Buss, J., Coltharp, C., Shtengel, G., Yang, X. X., Hess, H. & Xiao, J. 2015. A multi-layered protein network stabilizes the *Escherichia coli* FtsZ-ring and modulates constriction dynamics. *Plos Genetics,* 11**,** 24.

Buss, J. A., Peters, N. T., Xiao, J. & Bernhardt, T. G. 2017. ZapA and ZapB form an FtsZ-independent structure at midcell. *Molecular Microbiology,* 104**,** 652-663.

Cabre, E. J., Monterroso, B., Alfonso, C., Sanchez-Gorostiaga, A., Reija, B., Jimenez, M., Vicente, M., Zorrilla, S. & Rivas, G. 2015. The nucleoid occlusion SlmA protein accelerates the disassembly of the FtsZ protein polymers without affecting their GTPase Activity. *Plos One,* 10**,** 21.

Cacace, D. N., Rowland, A. T., Stapleton, J. J., Dewey, D. C. & Keating, C. D. 2015. Aqueous emulsion droplets stabilized by lipid vesicles as microcompartments for biomimetic mineralization. *Langmuir,* 31**,** 11329-11338.

Carrara, P., Stano, P. & Luisi, P. L. 2012. Giant vesicles "colonies": A model for primitive cell communities. *Chembiochem,* 13**,** 1497-1502.

Cheng, S. Q., Liu, Y., Crowley, C. S., Yeates, T. O. & Bobik, T. A. 2008. Bacterial microcompartments: Their properties and paradoxes. *Bioessays,* 30**,** 1084-1095.

Cho, H. B., Mcmanus, H. R., Dove, S. L. & Bernhardt, T. G. 2011. Nucleoid occlusion factor SlmA is a DNA-activated FtsZ polymerization antagonist. *Proceedings of the National Academy of Sciences of the United States of America,* 108**,** 3773-3778.

Coltharp, C., Buss, J., Plumer, T. M. & Xiao, J. 2016. Defining the rate-limiting processes of bacterial cytokinesis. *Proceedings of the National Academy of Sciences,* 113**,** E1044-E1053.

Cordell, S. C., Robinson, E. J. H. & Löwe, J. 2003. Crystal structure of the SOS cell division inhibitor SulA and in complex with FtsZ. *Proceedings of the National Academy of Sciences,* 100**,** 7889-7894.

Cunha, S., Woldringh, C. L. & Odijk, T. 2001. Polymer-mediated compaction and internal dynamics of isolated *Escherichia coli* nucleoids. *Journal of Structural Biology,* 136**,** 53-66.

Dame, R. T., Kalmykowa, O. J. & Grainger, D. C. 2011. Chromosomal macrodomains and associated proteins: Implications for DNA organization and replication in gram negative bacteria. *Plos Genetics,* 7**,** 5.

De Pereda, J. M., Leynadier, D., Evangelio, J. A., Chacón, P. & Andreu, J. M. 1996. Tubulin secondary structure analysis, limited proteolysis sites, and homology to FtsZ. *Biochemistry,* 35**,** 14203-14215.

De Vries, R. 2010. DNA condensation in bacteria: Interplay between macromolecular crowding and nucleoid proteins. *Biochimie,* 92**,** 1715-1721.

Den Blaauwen, T., Hamoen, L. W. & Levin, P. A. 2017. The divisome at 25: The road ahead. *Curr Opin Microbiol,* 36**,** 85-94.

Dewachter, L., Verstraeten, N., Fauvart, M. & Michiels, J. 2018. An integrative view of cell cycle control in *Escherichia coli*. *FEMS Microbiology Reviews,* 42**,** 116-136.

Di Ventura, B., Knecht, B., Andreas, H., Godinez, W. J., Fritsche, M., Rohr, K., Nickel, W., Heermann, D. W. & Sourjik, V. 2013. Chromosome segregation by the *Escherichia coli* Min system. *Molecular Systems Biology,* 9**,** 12.

Dominak, L. M., Gundermann, E. L. & Keating, C. D. 2010. Microcompartmentation in artificial cells: pH-induced conformational changes alter protein localization. *Langmuir,* 26**,** 5697-5705.

Du, S. S. & Lutkenhaus, J. 2014. SlmA antagonism of FtsZ assembly employs a two-pronged mechanism like MinCD. *Plos Genetics,* 10**,** 17.

Du, S. S. & Lutkenhaus, J. 2019. At the heart of bacterial cytokinesis: The Z ring. *Trends in Microbiology,* 27**,** 781-791.

Du, S. S., Park, K. T. & Lutkenhaus, J. 2015. Oligomerization of FtsZ converts the FtsZ tail motif (conserved carboxy-terminal peptide) into a multivalent ligand with high avidity for partners ZipA and SlmA. *Molecular Microbiology,* 95**,** 173-188.

Dupaigne, P., Tonthat, N. K., Espeli, O., Whitfill, T., Boccard, F. & Schumacher, M. A. 2012. Molecular basis for a protein-mediated DNA-bridging mechanism that functions in condensation of the *E. coli* chromosome. *Molecular Cell,* 48**,** 560-571.

Durand, D., De La Sierra-Gallay, I. L., Brooks, M. A., Thompson, A. W., Lazar, N., Lisboa, J., Van Tilbeurgh, H. & Quevillon-Cheruel, S. 2012. Expression, purification and preliminary structural analysis of *Escherichia coli* MatP in complex with the *matS* DNA site. *Acta Crystallographica Section F-Structural Biology Communications,* 68**,** 638-643.

Ellis, R. J. 2001. Macromolecular crowding: Obvious but underappreciated. *Trends in Biochemical Sciences,* 26**,** 597-604.

Erickson, H. P., Anderson, D. E. & Osawa, M. 2010. FtsZ in bacterial cytokinesis: Cytoskeleton and force generator all in one. *Microbiology and Molecular Biology Reviews,* 74**,** 504-528.

Espeli, O., Borne, R., Dupaigne, P., Thiel, A., Gigant, E., Mercier, R. & Boccard, F. 2012. A MatP-divisome interaction coordinates chromosome segregation with cell division in *E. coli*. *Embo Journal,* 31**,** 3198-3211.

Espeli, O., Mercier, R. & Boccard, F. 2008. DNA dynamics vary according to macrodomain topography in the *E. coli* chromosome. *Molecular Microbiology,* 68**,** 1418-1427.

Ferrone, F. A. & Rotter, M. A. 2004. Crowding and the polymerization of sickle hemoglobin. *Journal of Molecular Recognition,* 17**,** 497-504.

Fisher, R. A., Gollan, B. & Helaine, S. 2017. Persistent bacterial infections and persister cells. *Nature Reviews Microbiology,* 15**,** 453-464.

Folta-Stogniew, E. & Williams, K. R. 1999. Determination of molecular masses of proteins in solution: Implementation of an HPLC size exclusion chromatography and laser light scattering service in a core laboratory. *Journal of biomolecular techniques : JBT,* 10**,** 51-63.

Galli, E., Midonet, C., Paly, E. & Barre, F. X. 2017. Fast growth conditions uncouple the final stages of chromosome segregation and cell division in *Escherichia coli*. *Plos Genetics,* 13**,** 21.

Gardner, K., Moore, D. A. & Erickson, H. P. 2013. The C-terminal linker of *Escherichia coli* FtsZ functions as an intrinsically disordered peptide. *Molecular Microbiology,* 89**,** 264-275.

Gonzalez, J. M., Jimenez, M., Velez, M., Mingorance, J., Andreu, J. M., Vicente, M. & Rivas, G. 2003. Essential cell division protein FtsZ assembles into one monomer-thick ribbons under conditions resembling the crowded intracellular environment. *Journal of Biological Chemistry,* 278**,** 37664-37671.

González, J. M., Vélez, M., Jiménez, M., Alfonso, C., Schuck, P., Mingorance, J., Vicente, M., Minton, A. P. & Rivas, G. 2005. Cooperative behavior of *Escherichia coli* cell-division protein FtsZ assembly involves the preferential cyclization of long single-stranded fibrils. *Proceedings of the National Academy of Sciences,* 102**,** 1895-1900.

Haeusser, D. P. & Margolin, W. 2016. Splitsville: Structural and functional insights into the dynamic bacterial Z ring. *Nature Reviews Microbiology,* 14**,** 305-319.

Harami, G. M., Kovács, Z. J., Pancsa, R., Pálinkás, J., Baráth, V., Tárnok, K., Málnási-Csizmadia, A. & Kovács, M. 2020. Phase separation by ssDNA binding protein controlled via protein-protein and protein-DNA interactions. *Proceedings of the National Academy of Sciences,* 117**,** 26206-26217.

Hatters, D. M., Minton, A. P. & Howlett, G. J. 2002. Macromolecular crowding accelerates amyloid formation by human apolipoprotein C-II. *Journal of Biological Chemistry,* 277**,** 7824-7830.

Hernandez-Rocamora, V. M., Garcia-Montanes, C., Reija, B., Monterroso, B., Margolin, W., Alfonso, C., Zorrilla, S. & Rivas, G. 2013. MinC protein shortens FtsZ protofilaments by preferentially interacting with gdp-bound subunits. *Journal of Biological Chemistry,* 288**,** 24625-24635.

Hernandez-Vega, A., Braun, M., Scharrel, L., Jahnel, M., Wegmann, S., Hyman, B. T., Alberti, S., Diez, S. & Hyman, A. A. 2017. Local nucleation of microtubule bundles through Tubulin concentration into a condensed Tau phase. *Cell Reports,* 20**,** 2304-2312.

Holthuis, J. C. M. & Ungermann, C. 2013. Cellular microcompartments constitute general suborganellar functional units in cells. *Biological Chemistry,* 394**,** 151-161.

Hondele, M., Sachdev, R., Heinrich, S., Wang, J., Vallotton, P., Fontoura, B. M. A. & Weis, K. 2019. DEAD-box ATPases are global regulators of phase-separated organelles. *Nature,* 573**,** 144-+.

Howlett, G. J., Minton, A. P. & Rivas, G. 2006. Analytical ultracentrifugation for the study of protein association and assembly. *Current Opinion in Chemical Biology,* 10**,** 430-436.

Hu, Z. & Lutkenhaus, J. 1999. Topological regulation of cell division in *Escherichia coli* involves rapid pole to pole oscillation of the division inhibitor MinC under the control of MinD and MinE. *Molecular Microbiology,* 34**,** 82-90.

Huang, K.-H., Durand-Heredia, J. & Janakiraman, A. 2013. FtsZ ring stability: Of bundles, tubules, crosslinks, and curves. *Journal of Bacteriology,* 195**,** 1859-1868.

Hurley, K. A., Santos, T. M. A., Nepomuceno, G. M., Huynh, V., Shaw, J. T. & Weibel, D. B. 2016. Targeting the bacterial division protein FtsZ. *Journal of Medicinal Chemistry,* 59**,** 6975-6998.

Hürtgen, D., Härtel, T., Murray, S. M., Sourjik, V. & Schwille, P. 2019. Functional modules of minimal cell division for synthetic biology. *Advanced Biosystems,* 3**,** 1800315.

Hyman, A. A., Weber, C. A. & Jülicher, F. 2014. Liquid-liquid phase separation in biology. *Annual Review of Cell and Developmental Biology,* 30**,** 39-58.

Jain, A. & Vale, R. D. 2017. RNA phase transitions in repeat expansion disorders. *Nature,* 546**,** 243-247.

Juarez, J. R. & Margolin, W. 2010. Changes in the Min oscillation pattern before and after cell birth. *Journal of Bacteriology,* 192**,** 4134-4142.

Keating, C. D. 2012. Aqueous phase separation as a possible route to compartmentalization of biological molecules. *Accounts of Chemical Research,* 45**,** 2114-2124.

Kerfeld, C. A., Aussignargues, C., Zarzycki, J., Cai, F. & Sutter, M. 2018. Bacterial microcompartments. *Nature Reviews Microbiology,* 16**,** 277-290.

Koga, S., Williams, D. S., Perriman, A. W. & Mann, S. 2011. Peptide–nucleotide microdroplets as a step towards a membrane-free protocell model. *Nature Chemistry,* 3**,** 720-724.

Kretschmer, S. & Schwille, P. 2016. Pattern formation on membranes and its role in bacterial cell division. *Current Opinion in Cell Biology,* 38**,** 52-59.

Krishna, P. & Vandesande, J. H. 1990. Interaction of RecA protein with acidic phospholipids inhibits DNA-binding activity of RecA. *Journal of Bacteriology,* 172**,** 6452-6458.

Kroschwald, S., Munder, M. C., Maharana, S., Franzmann, T. M., Richter, D., Ruer, M., Hyman, A. A. & Alberti, S. 2018. Different material states of Pub1 condensates define distinct modes of stress adaptation and recovery. *Cell Reports,* 23**,** 3327-3339.

Kusuma, K. D., Payne, M., Ung, A. T., Bottomley, A. L. & Harry, E. J. 2019. FtsZ as an antibacterial target: Status and guidelines for progressing this avenue. *Acs Infectious Diseases,* 5**,** 1279-1294.

Larson, J. D., Jenkins, J. L., Schuermann, J. P., Zhou, Y. Z., Becker, D. F. & Tanner, J. J. 2006. Crystal structures of the DNA-binding domain of *Escherichia coli* proline utilization A flavoprotein and analysis of the role of Lys9 in DNA recognition. *Protein Science,* 15**,** 2630-2641.

Laskowska, E. & Kuczynska-Wisnik, D. 2020. New insight into the mechanisms protecting bacteria during desiccation. *Current Genetics,* 66**,** 313-318.

Laue, T. M., Shah, B.D., Ridgeway, T.M., Pelletier, S.L. 1992. *Computer-aided interpretation of analytical sedimentation data for proteins. In Analytical Ultracentrifugation in Biochemistry and Polymer Science (S. E. Harding and A. J. Rowe, ed.),* Cambridge, UK: Royal Society of Chemistry.

Lee, H. L., Chiang, I. C., Liang, S. Y., Lee, D. Y., Chang, G. D., Wang, K. Y., Lin, S. Y. & Shih, Y. L. 2016. Quantitative proteomics analysis reveals the Min system of *Escherichia coli* modulates reversible protein association with the inner membrane. *Molecular & Cellular Proteomics,* 15**,** 1572-1583.

Leung, A. K. W., Lucile White, E., Ross, L. J., Reynolds, R. C., Devito, J. A. & Borhani, D. W. 2004. Structure of *Mycobacterium tuberculosis* FtsZ Reveals Unexpected, G Protein-like Conformational Switches. *Journal of Molecular Biology,* 342**,** 953-970.

Lin, Y., Protter, D. S. W., Rosen, M. K. & Parker, R. 2015. Formation and maturation of phase-separated liquid droplets by RNA-binding proteins. *Molecular Cell,* 60**,** 208-219.

Lioy, V. S., Cournac, A., Marbouty, M., Duigou, S., Mozziconacci, J., Espeli, O., Boccard, F. & Koszul, R. 2018. Multiscale structuring of the *E. coli* chromosome by nucleoid-associated and condensin proteins. *Cell,* 172**,** 771-783.

Löwe, J. 1998. Crystal structure determination of FtsZ from *Methanococcus jannaschii*. *Journal of Structural Biology,* 124**,** 235-243.

Lowe, J., Ellonen, A., Allen, M. D., Atkinson, C., Sherratt, D. J. & Grainge, I. 2008. Molecular mechanism of sequence-directed DNA loading and translocation by FtsK. *Molecular Cell,* 31**,** 498-509.

Lutkenhaus, J., Pichoff, S. & Du, S. 2012. Bacterial cytokinesis: From Z ring to divisome. *Cytoskeleton,* 69**,** 778-790.

Lyu, Z. X., Coltharp, C., Yang, X. X. & Xiao, J. 2016. Influence of FtsZ GTPase activity and concentration on nanoscale Z-ring structure *in vivo* revealed by three-dimensional superresolution imaging. *Biopolymers,* 105**,** 725-734.

Mannik, J. & Bailey, M. W. 2015. Spatial coordination between chromosomes and cell division proteins in *Escherichia coli*. *Frontiers in Microbiology,* 6**,** 8.

Männik, J., Wu, F., Hol, F. J. H., Bisicchia, P., Sherratt, D. J., Keymer, J. E. & Dekker, C. 2012. Robustness and accuracy of cell division in *Escherichia coli* in diverse cell shapes. *Proceedings of the National Academy of Sciences,* 109**,** 6957-6962.

Margolin, W. 2020. Bacterial division: Journey to the center of the cell. *Current Biology,* 30**,** R114-R116.

Martos, A., Jiménez, M., Rivas, G. & Schwille, P. 2012a. Towards a bottom-up reconstitution of bacterial cell division. *Trends in Cell Biology,* 22**,** 634-643.

Martos, A., Monterroso, B., Zorrilla, S., Reija, B., Alfonso, C., Mingorance, J., Rivas, G. & Jimenez, M. 2012b. Isolation, characterization and lipid-binding properties of the recalcitrant FtsA division protein from *Escherichia coli*. *Plos One,* 7**,** 6.

Martos, A., Raso, A., Jimenez, M., Petrasek, Z., Rivas, G. & Schwille, P. 2015. FtsZ polymers tethered to the membrane by ZipA are susceptible to spatial regulation by Min waves. *Biophysical Journal,* 108**,** 2371-2383.

Meinhardt, H. & Boer, P. a. J. D. 2001. Pattern formation in *Escherichia coli*: A model for the pole-to-pole oscillations of Min proteins and the localization of the division site. *Proceedings of the National Academy of Sciences,* 98**,** 14202-14207.

Mellouli, S., Monterroso, B., Vutukuri, H. R., Te Brinke, E., Chokkalingam, V., Rivas, G. & Huck, W. T. S. 2013. Self-organization of the bacterial cell-division protein FtsZ in confined environments. *Soft Matter,* 9**,** 10493-10500.

Mercier, R., Petit, M. A., Schbath, S., Robin, S., El Karoui, M., Boccard, F. & Espeli, O. 2008. The MatP/*matS* site-specific system organizes the terminus region of the *E. coli* chromosome into a macrodomain. *Cell,* 135**,** 475-485.

Minton, A. P. 1990. Holobiochemistry: The effect of local environment upon the equilibria and rates of biochemical reactions. *International Journal of Biochemistry,* 22**,** 1063-1067.

Minton, A. P. 2000. Implications of macromolecular crowding for protein assembly. *Current Opinion in Structural Biology,* 10**,** 34-39.

Minton, A. P. 2001. The influence of macromolecular crowding and macromolecular confinement on biochemical reactions in physiological media. *Journal of Biological Chemistry,* 276**,** 10577-10580.

Molliex, A., Temirov, J., Lee, J., Coughlin, M., Kanagaraj, A. P., Kim, H. J., Mittag, T. & Taylor, J. P. 2015. Phase separation by low complexity domains promotes stress granule assembly and drives pathological fibrillization. *Cell,* 163**,** 123-133.

Monterroso, B., Reija, B., Jimenez, M., Zorrilla, S. & Rivas, G. 2016a. Charged molecules modulate the volume exclusion effects exerted by crowders on FtsZ polymerization. *Plos One,* 11**,** 14.

Monterroso, B., Robles-Ramos, M. Á., Zorrilla, S. & Rivas, G. 2021. Reconstituting bacterial cell division assemblies in crowded, phase-separated media. *In:* KEATING, C. D. (ed.) *Methods in Enzymology.* Academic Press.

Monterroso, B., Zorrilla, S., Sobrinos-Sanguino, M., Keating, C. D. & Rivas, G. 2016b. Microenvironments created by liquid-liquid phase transition control the dynamic distribution of bacterial division FtsZ protein. *Scientific Reports,* 6**,** 13.

Mukherjee, A. & Lutkenhaus, J. 1998. Dynamic assembly of FtsZ regulated by GTP hydrolysis. *Embo Journal,* 17**,** 462-469.

Niki, H., Yamaichi, Y. & Hiraga, S. 2000. Dynamic organization of chromosomal DNA in *Escherichia coli*. *Genes Dev,* 14**,** 212-23.

Nolivos, S., Upton, A. L., Badrinarayanan, A., Muller, J., Zawadzka, K., Wiktor, J., Gill, A., Arciszewska, L., Nicolas, E. & Sherratt, D. 2016. MatP regulates the coordinated action of topoisomerase IV and MukBEF in chromosome segregation. *Nature Communications,* 7**,** 12.

Nollert, P., Kiefer, H. & Jähnig, F. 1995. Lipid vesicle adsorption versus formation of planar bilayers on solid surfaces. *Biophys J,* 69**,** 1447-55.

Oliva, M. A., Cordell, S. C. & Löwe, J. 2004. Structural insights into FtsZ protofilament formation. *Nature Structural & Molecular Biology,* 11**,** 1243-1250.

Oltrogge, L. M., Chaijarasphong, T., Chen, A. W., Bolin, E. R., Marqusee, S. & Savage, D. F. 2020. Multivalent interactions between CsoS2 and Rubisco mediate alpha-carboxysome formation. *Nature Structural & Molecular Biology,* 27**,** 281-287.

Ortiz, C., Natale, P., Cueto, L. & Vicente, M. 2016. The keepers of the ring: Regulators of FtsZ assembly. *Fems Microbiology Reviews,* 40**,** 57-67.

Osawa, M., Anderson, D. E. & Erickson, H. P. 2009. Curved FtsZ protofilaments generate bending forces on liposome membranes. *The EMBO Journal,* 28**,** 3476-3484.

Parsons, J. B., Frank, S., Bhella, D., Liang, M. Z., Prentice, M. B., Mulvihill, D. P. & Warren, M. J. 2010. Synthesis of empty bacterial microcompartments, directed organelle protein incorporation, and evidence of filament-associated organelle movement. *Molecular Cell,* 38**,** 305-315.

Patel, A., Lee, H. O., Jawerth, L., Maharana, S., Jahnel, M., Hein, M. Y., Stoynov, S., Mahamid, J., Saha, S., Franzmann, T. M., Pozniakovski, A., Poser, I., Maghelli, N., Royer, L. A., Weigert, M., Myers, E. W., Grill, S., Drechsel, D., Hyman, A. A. & Alberti, S. 2015. A liquid-to-solid phase transition of the ALS protein FUS accelerated by disease mutation. *Cell,* 162**,** 1066-1077.

Pelletier, J., Halvorsen, K., Ha, B. Y., Paparcone, R., Sandler, S. J., Woldringh, C. L., Wong, W. P. & Jun, S. 2012. Physical manipulation of the *Escherichia coli* chromosome reveals its soft nature. *Proceedings of the National Academy of Sciences of the United States of America,* 109**,** E2649-E2656.

Peng, A. & Weber, S. C. 2019. Evidence for and against Liquid-Liquid Phase Separation in the Nucleus. *Non-Coding Rna,* 5**,** 14.

Pichoff, S. & Lutkenhaus, J. 2002. Unique and overlapping roles for ZipA and FtsA in septal ring assembly in *Escherichia coli*. *The EMBO Journal,* 21**,** 685-693.

Pollard, T. D. 2010. A guide to simple and informative binding assays. *Mol Biol Cell,* 21**,** 4061-7.

Popp, D., Iwasa, M., Narita, A., Erickson, H. P. & Maeda, Y. 2009. FtsZ condensates: An *in vitro* electron microscopy study. *Biopolymers,* 91**,** 340-350.

Rabinovitch, A., Zaritsky, A. & Feingold, M. 2003. DNA-membrane interactions can localize bacterial cell center. *Journal of Theoretical Biology,* 225**,** 493-496.

Raetz, C. R. H. & Dowhan, W. 1990. Biosynthesis and function of phospholipids in *Escherichia coli*. *Journal of Biological Chemistry,* 265**,** 1235-1238.

Rajendram, M., Zhang, L. L., Reynolds, B. J., Auer, G. K., Tuson, H. H., Ngo, K. V., Cox, M. M., Yethiraj, A., Cui, Q. & Weibel, D. B. 2015. Anionic phospholipids stabilize RecA filament bundles in *Escherichia coli*. *Molecular Cell,* 60**,** 374-384.

Ramm, B., Glock, P., Mucksch, J., Blumhardt, P., Garcia-Soriano, D. A., Heymann, M. & Schwille, P. 2018. The MinDE system is a generic spatial cue for membrane protein distribution *in vitro*. *Nature Communications,* 9**,** 16.

Riback, J. A., Katanski, C. D., Kear-Scott, J. L., Pilipenko, E. V., Rojek, A. E., Sosnick, T. R. & Drummond, D. A. 2017. Stress-triggered phase separation is an adaptive, evolutionarily tuned response. *Cell,* 168**,** 1028-1040.

Rico, A. I., Krupka, M. & Vicente, M. 2013. In the beginning, *Escherichia coli* assembled the proto-ring: An initial phase of division. *Journal of Biological Chemistry,* 288**,** 20830-20836.

Rippe, K. 1997. Analysis of protein-DNA binding at equilibrium. *BIF futura,* 12**,** 20-26.

Rivas, G., Fernandez, J. A. & Minton, A. P. 2001. Direct observation of the enhancement of noncooperative protein self-assembly by macromolecular crowding: Indefinite linear self-association of bacterial cell division protein FtsZ. *Proceedings of the National Academy of Sciences of the United States of America,* 98**,** 3150-3155.

Rivas, G., Ferrone, F. & Herzfeld, J. 2004. Life in a crowded world. Workshop on the Biological Implications of Macromolecular Crowding. *EMBO Reports,* 5**,** 23-27.

Rivas, G., Lopez, A., Mingorance, J., Ferrandiz, M. J., Zorrilla, S., Minton, A. P., Vicente, M. & Andreu, J. M. 2000. Magnesium-induced linear self-association of the FtsZ bacterial cell division protein monomer - The primary steps for FtsZ assembly. *Journal of Biological Chemistry,* 275**,** 11740-11749.

Rivas, G. & Minton, A. 2022. Influence of nonspecific interactions on protein associations: Implications for biochemistry *in vivo*. *Annual Review of Biochemistry,* 91**,** 321-351.

Rivas, G. & Minton, A. P. 2016. Macromolecular crowding *in vitro*, *in vivo*, and in between. *Trends in Biochemical Sciences,* 41**,** 970-981.

Rivas, G., Vogel, S. K. & Schwille, P. 2014. Reconstitution of cytoskeletal protein assemblies for large-scale membrane transformation. *Curr Opin Chem Biol,* 22**,** 18-26.

Rodrigues, C. D. & Harry, E. J. 2012. The Min system and nucleoid occlusion are not required for identifying the division site in *Bacillus subtilis* but ensure its efficient utilization. *PLoS Genet,* 8**,** e1002561.

Romberg, L. & Levin, P. A. 2003. Assembly dynamics of the bacterial cell division protein FtsZ: Poised at the edge of stability. *Annual Review of Microbiology,* 57**,** 125-154.

Rowlett, V. W. & Margolin, W. 2013. The bacterial Min system. *Current Biology,* 23**,** R553-R556.

Rowlett, V. W. & Margolin, W. 2014. 3D-SIM super-resolution of FtsZ and its membrane tethers in *Escherichia coli* cells. *Biophysical Journal,* 107**,** L17-L20.

Rowlett, V. W. & Margolin, W. 2015. The Min system and other nucleoid-independent regulators of Z ring positioning. *Frontiers in Microbiology,* 6**,** 10.

Royer, C. A. & Beechem, J. M. 1992. Numerical analysis of binding data: Advantages, practical aspects, and implications. *Methods Enzymol,* 210**,** 481-505.

Royer, C. A. & Scarlata, S. F. 2008. Fluorescence approaches to quantifying biomolecular interactions. *In:* BRAND, L. & JOHNSON, M. L. (eds.) *Fluorescence Spectroscopy.* San Diego: Elsevier Academic Press Inc.

Royer, C. A., Smith, W. R. & Beechem, J. M. 1990. Analysis of binding in macromolecular complexes: A generalized numerical approach. *Anal Biochem,* 191**,** 287-94.

Salvarelli, E., Krupka, M., Rivas, G., Vicente, M. & Mingorance, J. 2011. Independence between GTPase active sites in the *Escherichia coli* cell division protein FtsZ. *FEBS Letters,* 585**,** 3880-3883.

Sapay, N., Guermeur, Y. & Deleage, G. 2006. Prediction of amphipathic in-plane membrane anchors in monotopic proteins using a SVM classifier. *Bmc Bioinformatics,* 7**,** 11.

Scheffers, D.-J., De Wit, J. G., Den Blaauwen, T. & Driessen, A. J. M. 2002. GTP hydrolysis of cell division protein FtsZ: Evidence that the active site is formed by the association of monomers. *Biochemistry,* 41**,** 521-529.

Schuck, P. 2000. Size-distribution analysis of macromolecules by sedimentation velocity ultracentrifugation and Lamm equation modeling. *Biophysical Journal,* 78**,** 1606-1619.

Schumacher, M. A. 2017. Bacterial nucleoid occlusion: Multiple mechanisms for preventing chromosome bisection during cell division. *In:* LOWE, J. & AMOS, L. A. (eds.) *Prokaryotic Cytoskeletons: Filamentous Protein Polymers Active in the Cytoplasm of Bacterial and Archaeal Cells.* New York: Springer.

Schumacher, M. A. & Zeng, W. J. 2016. Structures of the nucleoid occlusion protein SlmA bound to DNA and the C-terminal domain of the cytoskeletal protein FtsZ. *Proceedings of the National Academy of Sciences of the United States of America,* 113**,** 4988-4993.

Schwille, P., Spatz, J., Landfester, K., Bodenschatz, E., Herminghaus, S., Sourjik, V., Erb, T. J., Bastiaens, P., Lipowsky, R., Hyman, A., Dabrock, P., Baret, J. C., Vidakovic-Koch, T., Bieling, P., Dimova, R., Mutschler, H., Robinson, T., Tang, T. D., Wegner, S. & Sundmacher, K. 2018. MaxSynBio: Avenues towards creating cells from the bottom up. *Angew Chem Int Ed Engl,* 57**,** 13382-13392.

Shen, J. P., Chang, Y. R. & Chou, C. F. 2020. Frequency modulation of the Min-protein oscillator by nucleoid-associated factors in *Escherichia coli*. *Biochemical and Biophysical Research Communications,* 525**,** 857-862.

Shin, Y. & Brangwynne, C. P. 2017. Liquid phase condensation in cell physiology and disease. *Science,* 357**,** 7.

Silber, N., Matos De Opitz, C. L., Mayer, C. & Sass, P. 2020. Cell division protein FtsZ: From structure and mechanism to antibiotic target. *Future Microbiology,* 15**,** 801-831.

Small, E. & Addinall, S. G. 2003. Dynamic FtsZ polymerization is sensitive to the GTP to GDP ratio and can be maintained at steady state using a GTP-regeneration system. *Microbiology,* 149**,** 2235-2242.

Snead, W. T. & Gladfelter, A. S. 2019. The control centers of biomolecular phase separation: How membrane surfaces, PTMs, and active processes regulate condensation. *Molecular Cell,* 76**,** 295-305.

Sobrinos-Sanguino, M., Zorrilla, S., Keating, C. D., Monterroso, B. & Rivas, G. 2017a. Encapsulation of a compartmentalized cytoplasm mimic within a lipid membrane by microfluidics. *Chemical Communications,* 53**,** 4775-4778.

Sobrinos-Sanguino, M., Zorrilla, S., Monterroso, B., Minton, A. P. & Rivas, G. 2017b. Nucleotide and receptor density modulate binding of bacterial division FtsZ protein to ZipA containing lipid-coated microbeads. *Scientific Reports,* 7**,** 9.

Söderström, B. & Daley, D. O. 2017. The bacterial divisome: More than a ring? *Current Genetics,* 63**,** 161-164.

Sokolova, E., Spruijt, E., Hansen, M. M. K., Dubuc, E., Groen, J., Chokkalingam, V., Piruska, A., Heus, H. A. & Huck, W. T. S. 2013. Enhanced transcription rates in membrane-free protocells formed by coacervation of cell lysate. *Proceedings of the National Academy of Sciences,* 110**,** 11692-11697.

Spitzer, J. & Poolman, B. 2009. The role of biomacromolecular crowding, ionic strength, and physicochemical gradients in the complexities of life's emergence. *Microbiology and Molecular Biology Reviews,* 73**,** 371-+.

Stouf, M., Meile, J. C. & Cornet, F. 2013. FtsK actively segregates sister chromosomes in *Escherichia coli*. *Proceedings of the National Academy of Sciences of the United States of America,* 110**,** 11157-11162.

Strulson, C. A., Molden, R. C., Keating, C. D. & Bevilacqua, P. C. 2012. RNA catalysis through compartmentalization. *Nature Chemistry,* 4**,** 941-946.

Theberge, A. B., Courtois, F., Schaerli, Y., Fischlechner, M., Abell, C., Hollfelder, F. & Huck, W. T. S. 2010. Microdroplets in microfluidics: An evolving platform for discoveries in chemistry and biology. *Angewandte Chemie International Edition,* 49**,** 5846-5868.

Tonthat, N. K., Arold, S. T., Pickering, B. F., Van Dyke, M. W., Liang, S. D., Lu, Y., Beuria, T. K., Margolin, W. & Schumacher, M. A. 2011. Molecular mechanism by which the nucleoid occlusion factor, SImA, keeps cytokinesis in check. *Embo Journal,* 30**,** 154-164.

Tonthat, N. K., Milam, S. L., Chinnam, N., Whitfill, T., Margolin, W. & Schumacher, M. A. 2013. SlmA forms a higher-order structure on DNA that inhibits cytokinetic Z-ring formation over the nucleoid. *Proceedings of the National Academy of Sciences of the United States of America,* 110**,** 10586-10591.

Torre, P., Keating, C. D. & Mansy, S. S. 2014. Multiphase water-in-oil emulsion droplets for cell-free transcription–translation. *Langmuir,* 30**,** 5695-5699.

Valens, M., Penaud, S., Rossignol, M., Cornet, F. & Boccard, F. 2004. Macrodomain organization of the *Escherichia coli* chromosome. *The EMBO Journal,* 23**,** 4330-4341.

Vendeville, A., Larivière, D. & Fourmentin, E. 2011. An inventory of the bacterial macromolecular components and their spatial organization. *FEMS Microbiol Rev,* 35**,** 395-414.

Walker, B. E., Mannik, J. & Mannik, J. 2020. Transient membrane-linked FtsZ assemblies precede Z-ring formation in *Escherichia coli*. *Current Biology,* 30**,** 499-508.

Walter, H. & Brooks, D. E. 1995. Phase separation in cytoplasm, due to macromolecular crowding, is the basis for microcompartmentation. *FEBS Letters,* 361**,** 135-139.

Wang, H., Yan, X., Aigner, H., Bracher, A., Nguyen, N. D., Hee, W. Y., Long, B. M., Price, G. D., Hartl, F. U. & Hayer-Hartl, M. 2019. Rubisco condensate formation by CcmM in beta-carboxysome biogenesis. *Nature,* 566**,** 131-+.

Wang, J., Choi, J.-M., Holehouse, A. S., Lee, H. O., Zhang, X., Jahnel, M., Maharana, S., Lemaitre, R., Pozniakovsky, A., Drechsel, D., Poser, I., Pappu, R. V., Alberti, S. & Hyman, A. A. 2018. A molecular grammar governing the driving forces for phase separation of prion-like RNA binding proteins. *Cell,* 174**,** 688-699.e16.

Wheeler, R. J. 2020. Therapeutics—how to treat phase separation-associated diseases. *Emerging Topics in Life Sciences,* 4**,** 331-342.

Wiegand, T. & Hyman, A. A. 2020. Drops and fibers - how biomolecular condensates and cytoskeletal filaments influence each other. *Emerging Topics in Life Sciences,* 4**,** 247-261.

Woldringh, C. L., Mulder, E., Huls, P. G. & Vischer, N. 1991. Toporegulation of bacterial division according to the nucleoid occlusion model. *Research in Microbiology,* 142**,** 309-320.

Woldringh, C. L., Mulder, E., Valkenburg, J. a. C., Wientjes, F. B., Zaritsky, A. & Nanninga, N. 1990. Role of the nucleoid in the toporegulation of division. *Research in Microbiology,* 141**,** 39-49.

Woodruff, J. B., Gomes, B. F., Widlund, P. O., Mahamid, J., Honigmann, A. & Hyman, A. A. 2017. The centrosome is a selective condensate that nucleates microtubules by concentrating tubulin. *Cell,* 169**,** 1066-1077.

Wu, L. J. & Errington, J. 2004. Coordination of cell division and chromosome segregation by a nucleoid occlusion protein in *Bacillus subtilis*. *Cell,* 117**,** 915-925.

Wu, L. J. & Errington, J. 2012. Nucleoid occlusion and bacterial cell division. *Nature Reviews Microbiology,* 10**,** 8-12.

Yang, X. X., Lyu, Z. X., Miguel, A., Mcquillen, R., Huang, K. C. & Xiao, J. 2017. GTPase activity-coupled treadmilling of the bacterial tubulin FtsZ organizes septal cell wall synthesis. *Science,* 355**,** 744-747.

Yeates, T. O., Kerfeld, C. A., Heinhorst, S., Cannon, G. C. & Shively, J. M. 2008. Protein-based organelles in bacteria: Carboxysomes and related microcompartments. *Nature Reviews Microbiology,* 6**,** 681-691.

Yu, J., Liu, Y., Yin, H. & Chang, Z. 2019. Regrowth-delay body as a bacterial subcellular structure marking multidrug-tolerant persisters. *Cell discovery,* 5**,** 1-15.

Yu, X.-C. & Margolin, W. 1997. $Ca^{2+}$-mediated GTP-dependent dynamic assembly of bacterial cell division protein FtsZ into asters and polymer networks *in vitro*. *The EMBO Journal,* 16**,** 5455-5463.

Yu, X. C., Tran, A. H., Sun, Q. & Margolin, W. 1998. Localization of cell division protein FtsK to the *Escherichia coli* septum and identification of a potential N-terminal targeting domain. *Journal of Bacteriology,* 180**,** 1296-1304.

Zaslavsky, B. Y. 1994. *Aqueous two-phase partitioning: Physical chemistry and bioanalytical applications*, CRC press.

Zaslavsky, B. Y., Miheeva, L. M., Mestechkina, N. M., Pogorelov, V. M. & Rogozhin, S. V. 1978. General rule of partition behaviour of cells and soluble substances in aqueous two-phase polymeric systems. *FEBS Letters,* 94**,** 77-80.

Zhang, W. M., Zhou, Y. Z. & Becker, D. F. 2004. Regulation of PutA-membrane associations by flavin adenine dinucleotide reduction. *Biochemistry,* 43**,** 13165-13174.

Zhao, H. & Lappalainen, P. 2012. A simple guide to biochemical approaches for analyzing protein–lipid interactions. *Molecular Biology of the Cell,* 23**,** 2823-2830.

Zhou, H.-X. 2008. Effect of mixed macromolecular crowding agents on protein folding. *Proteins: Structure, Function, and Bioinformatics,* 72**,** 1109-1113.

Zorrilla, S., Monterroso, B., Robles-Ramos, M., Margolin, W. & Rivas, G. 2021. FtsZ interactions and biomolecular condensates as potential targets for new antibiotics. *Antibiotics (Basel),* 10**,** 204.